# Precision Machine Design for the Semiconductor Equipment Manufacturing Industry

by

Matthew James Van Doren

B.S., The University of Texas at Austin (1990)

M.S., The University of Texas at Austin (1992)

Submitted to the Department of Mechanical Engineering
in partial fulfillment of the requirements for the degree of

Doctor of Philosophy in Mechanical Engineering

at the

MASSACHUSETTS INSTITUTE OF TECHNOLOGY

May 1995

© Massachusetts Institute of Technology 1995
All rights reserved.

Signature of Author.....
Department of Mechanical Engineering
May 10, 1995

Certified by.....
Alexander Slocum
Associate Professor
Thesis Supervisor

Accepted by .....
Ain A. Sonin
Chairman, Departmental Committee on Graduate Studies

MASSACHUSETTS INSTITUTE
OF TECHNOLOGY

AUG 31 1995

ARCHIVES

# Precision Machine Design for the Semiconductor Equipment Manufacturing Industry

by
Matthew James Van Doren

Submitted to the Department of Mechanical Engineering
on May 10, 1995 in partial fulfillment of the
requirements for the degree of
Doctor of Philosophy in Mechanical Engineering

## Abstract

Since the development of the integrated circuit in 1958, the semiconductor industry has seen rapid advances in process technology. Even today, semiconductor manufacturers must decrease device size and increase product complexity just to stay competitive in the world market place. The economics and clean environment required for production put severe demands on semiconductor process tools. Furthermore, design reviews of semiconductor manufacturing equipment have revealed serious flaws in the design of many of these systems.

This thesis presents a design methodology that is meant for the mechanical design community in the semiconductor equipment manufacturing industry. Examinations of mechanical design practices and design requirements by the author in this area indicate that equipment design could benefit significantly from a new design methodology based on technologies from the machine tool, instrument, and optics design communities. This thesis contains contributions in several areas. First, the research develops a set of numerical error modeling tools to identify, quantify, and minimize position, velocity, and force transmission errors in the design of mechanical systems. Second, the research establishes a set of deterministic mechanical design rules that can be used in creating system-level designs that meet functional requirements for throughput, cleanliness, reliability, repeatability, and machine footprint.

In parallel with the development of the design methodology, the author designed the structural and wafer handling portions of an actual semiconductor process tool. The error modeling techniques and mechanical design rules are further illustrated through their application to this design problem. The design process is described from initiation to prototyping and testing of the system. Test data from the prototype verified the ability of the new design approach to satisfy positioning and repeatability requirements in an actual system. These data also correlated well with predictions made by the error modeling techniques discussed in the thesis.

Thesis Supervisor: Alexander H. Slocum
Title: Associate Professor

## Acknowledgments

The author wishes to briefly acknowledge some of the people who contributed to the completion of this thesis. First, Prof. Alex Slocum was instrumental in obtaining the corporate sponsorship that allowed this research to be performed. As my advisor and the chairman of my thesis committee, Prof. Slocum provided a frenetic yet stimulating research environment. The other members of my thesis committee, Prof. David Trumper, Prof. Ernest Rabinowicz, and Prof. Nam Suh provided numerous comments that helped direct the course of this research. The Track Systems Division of Silicon Valley Group, Inc. in San Jose, California provided the author with a wonderful opportunity to design a significant portion of a complex manufacturing system. Many engineers at SVG who were involved in the Accipiter project contributed to this research both directly and indirectly.

Additionally, I would like to thank my parents for encouraging my curiosity and creativity. Without them I surely would never have reached this point. Next, I must thank the one person who helped me the most, Sara Milanowski. Her unending encouragement and understanding were invaluable. Finally, I must acknowledge Lucy who had the unusual fortune to watch me write most of this thesis. She showed amazing patient in the, at first unnerving and eventually adorable, habit of staring at me as I worked.

Matthew J. Van Doren
Massachusetts Institute of Technology
May 1995

# Contents

**Precision Machine Design for the Semiconductor Equipment Manufacturing Industry** 3

Abstract 3

Acknowledgments 5

**Contents** 7

**List of Figures** 13

**List of Tables** 19

**Chapter 1: Introduction and Thesis Overview** 21

1.1 Introduction 21

1.2 The Semiconductor Industry 22

1.2.1 Automation in Semiconductor Production Facilities 22

1.2.2 The Need for a Precision Machine Design Methodology 26

1.2.3 Historical Perspective 28

1.2.4 Functional Requirements of the Semiconductor Equipment Industry 28

1.3 Precision Machine Design for the Semiconductor Equipment Industry 29

1.4 Thesis Contributions 32

1.5 Thesis Structure 36

**Chapter 2: Machine Design Methodologies and Their Application to the Semiconductor Equipment Industry** 39

2.1 Introduction 39

2.2 Previous Work on Precision Machine Design Methodologies 40

2.2.1 Design Theory 40

2.2.1.1 Axiomatic Design 40

2.2.1.2 The Design Process 42

2.2.1.3 The Analytical Hierarchy Procedure 43

2.2.1.4 Robust Design 44

2.2.2 Deterministic Design 44
2.2.3 Kinematic Couplings 45
2.2.4 Error Modeling in Machine Design 46
2.2.4.1 Displacement Error Modeling 46
2.2.4.1.1 Displacement Error Modeling in Machine Tools and CMMs 47
2.2.4.1.2 Displacement Error Modeling in Robotics 48
2.2.4.2 Velocity and Force Transmission Error Modeling 50
2.2.5 Mechanical Design in Cleanrooms 50
2.3 A Precision Machine Design Methodology for Semiconductor Process Equipment 52
2.3.1 Error Modeling 52
2.3.2 Mechanical Design Rules 54
2.4 Summary 57
**Chapter 3: Error Modeling in Precision Machines 59**
3.1 Introduction 59
3.2 The Displacement Error Model 60
3.2.1 Homogeneous Transforms 62
3.2.2 Construction of the Displacement Error Model 64
3.2.3 Assignment of Coordinate Frames 69
3.2.3.1 Denavit and Hartenberg Parameters 70
3.2.3.2 The Center of Compliance Method 72
3.2.4 Error Sources 73
3.2.4.1 Geometric Errors 73
3.2.4.2 Mechanical Errors 74
3.2.4.3 Control System Errors 74
3.2.4.4 Dynamic Errors 75
3.2.4.5 Thermal Errors 75
3.2.5 Inclusion of Error Sources in the Error Model 75
3.2.6 The Use of Displacement Error Models in Complex Systems 77
3.2.7 Case Study: Displacement Error Modeling in a Process Tool 80
3.2.7.1 The Machine Frame 81
3.2.7.2 The Wafer Handling Robot 83

3.2.7.3 Frame and Robot Error Sources 86
3.2.7.4 The Example System's Displacement Error Model 88
3.2.7.5 Repeatability Test Data for the Prototype Wafer Handling Robot 93
3.3 Error Modeling for Velocity and Force Transmission 93
3.3.1 Mathematical Background 94
3.3.2 Errors in Velocity Transmission 95
3.3.3 Errors in Force Transmission 96
3.3.4 Case Study: Velocity Error Modeling in a Process Tool 97
3.4 Summary 102

**Chapter 4: Supporting Elements of the Precision Machine Design Methodology 103**

4.1 Introduction 103
4.2 Deterministic Design 104
4.2.1 Case Study: Use of Kinematic Couplings in a Machine Frame 107
4.2.2 Case Study: Use of a Kinematic Coupling in a Wafer Handling Robot 110
4.3 Elastic Averaging 111
4.3.1 Elastic Averaging vs. Deterministic Design 111
4.3.2 Case Study: Use of Rolling Element Bearings in a Wafer Handling Robot 112
4.4 Reduction of the Effects of Rotational Errors 117
4.4.1 Abbe Errors 118
4.4.2 Case Study: A Wafer Gripping and Centering Mechanism 118
4.5 Static and Dynamic Structural Deformations 121
4.5.1 Static Effects 121
4.5.2 Dynamic Effects 122
4.5.3 Case Study: The Structural Frame of a Process Tool 125
4.5.4 Case Study: The Design of a Ballscrew Support Structure 128
4.6 Control and Mechanical System Integration 132
4.6.1 Control Systems in Cleanroom Robots 132
4.6.2 Case Study: Control System Development for a Wafer Handling Robot 135
4.6.2.1 Wafer Handling Robot Control System Simulations 143
4.6.2.2 Wafer Handling Robot Prototype Control System Experimental Results 156
4.7 Cleanroom Equipment Design Considerations 164

4.7.1 Cleanrooms 165
4.7.2 Mechanical Guidelines for Minimizing Wafer Contamination 166
4.7.3 Case Study: The Clean Design of a Wafer Handling Robot 167
4.8 Summary 168

**Chapter 5: Summary and Conclusions 171**
5.1 Introduction 171
5.2 Summary of the Precision Machine Design Methodology for Semiconductor Manufacturing Equipment 171
5.3 Other Technologies for Ultra-Clean Wafer Handling 174
5.4 Future Areas of Research in Precision Machine Design for Semiconductor Manufacture 175

**Appendix A: Precision Machine Design Applied to a Photoresist Processing System 177**
A.1 Introduction 177
A.2 The Photoresist Application Process 178
A.3 The 90 Series Photoresist Processing System 179
A.4 The Design of a New Photoresist Processing System: The Accipiter Project 184
A.5 The Conceptual Design Stage of the Accipiter Project 187
A.5.1 Conceptual Design of the Machine Configuration 188
A.5.1.1 Machine Concepts 190
A.5.1.2 Selection of the Machine Concept Layout 196
A.5.2 Conceptual Design of the Machine Frame 198
A.5.3 Conceptual Design of the Wafer Handling Robot 203
A.5.3.1 Development of Design Concepts 205
A.5.3.2 Selection of the Design Concept 220
A.5.4 Conceptual Design of the Wafer Gripping and Centering Mechanism 222
A.6 Embodiment and Detailed Design of the Accipiter Project 228
A.6.1 The Machine Frame Embodiment Design 229
A.6.2 The Wafer Handling Robot Embodiment Design 230
A.7 The Finished Design 239
A.8 The Prototype Wafer Handling Robot and Test Frame 240
A.9 Summary 246

**Appendix B: Error Modeling Case Study Data** 247
B.1 Introduction 247
B.2 Displacement Error Model 247
B.3 Velocity Error Model 254
B.4 Positioning Repeatability Test Data for the Prototype Wafer Handling Robot 255
**Appendix C: Finite Element Analysis Results for Machine Frame** 259
C.1 Introduction 259
C.2 The 90 Series Frame 259
C.3 The Accipiter Frame 260
**Appendix D: Trajectory Generation and Control System Simulation Software** 261
D.1 Introduction 261
D.2 Trajectory Generation Source Code 261
D.3 Dynamic Simulation Source Code 272
**Appendix E: AHP Selection Matrices** 281
E.1 Introduction 281
E.2 Selection Matrices 281
E.2.1 Machine Layout 281
E.2.2 Machine Structure 284
E.2.3 Wafer Handling Robot 287
E.2.4 Wafer Gripper 289
**References** 293
**Vita** 303

# List of Figures

Figure 1.1 Time history of acceleration levels of a human casually setting a loaded cassette down on a hard surface (from [Slocum '93B]). 24

Figure 1.2 Time history of acceleration levels of a robot setting a loaded cassette down on a hard surface (from [Slocum '93B]). 24

Figure 1.3 Bay and chase fab configuration. 25

Figure 1.4 Trial #1 offers superior repeatability and inferior accuracy while trial #2 offers better accuracy and inferior repeatability. 31

Figure 1.5 Finalized Accipiter machine concept. 34

Figure 1.6 Deterministically designed machine frame. 35

Figure 1.7 Deterministically designed wafer handling robot. 35

Figure 3.1 Example coordinate frames. 64

Figure 3.2 Definition of differential errors. 66

Figure 3.3 Isometric view of new SVG photoresist processing system. 80

Figure 3.4 Coordinate frame assignments for the machine frame. 82

Figure 3.5 Wafer handling robot with coordinate frame assignments. 84

Figure 3.6 Beginning, intermediate, and final positions for the trajectory used to generate error plots. 89

Figure 3.7 Total end effector errors plotted for the trajectory shown in Figure 3.6. 90

Figure 3.8 Repeatability-related end effector errors for the trajectory shown in Figure 3.6. 90

Figure 3.9 Straight-line trajectory used for process module access. 91

Figure 3.10 Total end effector errors plotted for a typical straight-line trajectory used for process module access. 92

Figure 3.11 Repeatability-related end effector errors plotted for a typical straight-line trajectory used for process module access. 92

Figure 3.12 Condition number of Jacobian matrix for the trajectory shown in Figure 3.6. 98
Figure 3.13 Velocity error gains for base revolute joint for the trajectory shown in Figure 3.6. 99
Figure 3.14 Velocity error gains for elbow joint for the trajectory shown in Figure 3.6. 100
Figure 3.15 Condition number of Jacobian matrix for straight-line trajectory shown in Figure 3.9. 100
Figure 3.16 Velocity error gains for base revolute joint for straight-line trajectory. 101
Figure 3.17 Velocity error gains for elbow joint for straight-line trajectory. 101
Figure 4.1 Three groove deterministically designed kinematic coupling. 105
Figure 4.2 Straight groove and gothic arch groove. 106
Figure 4.3 Process tool with kinematically coupled process modules and end stations. 108
Figure 4.4 Machine frame showing locations for groove portions of kinematic couplings. 108
Figure 4.5 Kinematic coupling ball shown at left and groove at right. 109
Figure 4.6 Wafer handling robot body detached from carriage at kinematic coupling. 110
Figure 4.7 Locations in the wafer handling robot where rolling element bearings are used. 113
Figure 4.8 Cutaway view of a crossed roller bearing. 113
Figure 4.9 Motion of crossed rollers. 114
Figure 4.10 Elbow joint using crossed roller bearings. 115
Figure 4.11 Circular arch linear guide with recirculating ball bearing blocks. 116
Figure 4.12 Linear guides used in telescoping vertical axis. 117
Figure 4.13 Fork-type gripper showing Abbe error caused by bearing offset. 119
Figure 4.14 Tongue-type gripper with very small Abbe error. 120
Figure 4.15 Frame design for SVG 90 Series photoresist processing system. 126
Figure 4.16 Machine frame with structural damping added. 127
Figure 4.17 Shear damped beam. 128

Figure 4.18 Fully collapsed telescoping vertical axis shown at left with ball nut structural support at right. 129
Figure 4.19 Time history of acceleration amplitude from vibration of ballscrew before addition of damping material. 130
Figure 4.20 Time history of acceleration amplitude from vibration of ballscrew after addition of damping material. 131
Figure 4.21 Power spectral density of ballscrew vibration before addition of damping material (130 Hz bandwidth measurement). 131
Figure 4.22 Power spectral density of ballscrew vibration after addition of damping material (130 Hz bandwidth measurement). 132
Figure 4.23 Schematic representation of wafer handling robot. 136
Figure 4.24 Inertial properties for 3 DOF, planar manipulator. 140
Figure 4.25 Individual joint responses to simultaneous steps inputs to each joint for (i) fully nonlinear system in the left column and (ii) a linearized system in the right column. 145
Figure 4.26 End effector and joint trajectories for typical straight line move into a process module. 146
Figure 4.27 Actual joint trajectories for typical trajectory. 147
Figure 4.28 Following errors for typical trajectory. 148
Figure 4.29 Following errors when feedforward acceleration is used for typical trajectory. 149
Figure 4.30 Interactive (disturbance) torques for each joint for typical trajectory. 150
Figure 4.31 End effector and joint trajectories for high speed straight line move. 151
Figure 4.32 Actual joint trajectories for high speed trajectory. 152
Figure 4.33 Following errors for high speed trajectory. 153
Figure 4.34 Following errors when feedforward acceleration is used for high speed trajectory. 154
Figure 4.35 Interactive (disturbance) torques for each joint for high speed trajectory. 155
Figure 4.36 Commanded trajectory for the robot's linear carriage. 157
Figure 4.37 Actual trajectory for the robot's linear carriage. 158

Figure 4.38 Following errors for the robot's linear carriage. 158
Figure 4.39 Commanded trajectory for the robot's telescoping axis. 159
Figure 4.40 Actual trajectory for the robot's telescoping axis. 159
Figure 4.41 Following errors for the robot's telescoping axis. 160
Figure 4.42 Commanded trajectory for the robot's proximal revolute joint. 160
Figure 4.43 Actual trajectory for the robot's proximal revolute joint. 161
Figure 4.44 Following errors for the robot's proximal revolute joint. 161
Figure 4.45 Commanded trajectory for the robot's distal revolute joint. 162
Figure 4.46 Actual trajectory for the robot's distal revolute joint. 162
Figure 4.47 Following errors for the robot's distal revolute joint. 163
Figure 4.48 Power spectral density for accelerometer placed on gripper housing for constant speed distal revolute move. 164
Figure A.1 Top view of the 90 Series photoresist processing system. 180
Figure A.2 Process modules from 90 Series Track. Spin module at left, chill plate center, and vapor prime (hot plate) at right. 181
Figure A.3 Shuttle arm for wafer handling in 90 Series. Fully retracted arm shown at left and arm insertion calibration shown at right. 182
Figure A.4 Silo machine concept with kinematically coupled layers. 190
Figure A.5 Vertical section of the silo concept showing air flow and modules. 191
Figure A.6 Top view of single layer in the silo concept. 192
Figure A.7 Two thirds scale wooden model of the silo concept (with an extra layer). 193
Figure A.8 Vertical box machine concept. 194
Figure A.9 Wall-mounted machine concept. 194
Figure A.10 Semicircular machine concept. 195
Figure A.11 Traditional horizontal machine concept. 195
Figure A.12 Rectangular configuration with modular frame concept. 196
Figure A.13 Traditional rectangular machine configuration. 197
Figure A.14 Concept for perforated vertical wall with suction to prevent dirty boundary later development. 197

Figure A.15 Wooden model of a machine tool type track base with integral kinematic couplings. 199
Figure A.16 Box-type substructure concept with central I-beam for bending stiffness. 199
Figure A.17 Modular machine substructure concept with central tube for bending and torsional stiffness. 200
Figure A.18 Early version of final machine frame design. 201
Figure A.19 Refined concept for final machine frame design with central spine for torsional and bending stiffness. 202
Figure A.20 Central spine for final machine frame design. 202
Figure A.21 Early concepts for dual grippers mounted on a wafer handling robot. 206
Figure A.22 Horizontal linear drive concepts - ballscrew, belt drive, and linear motor. 208
Figure A.23 Vertical (or distal) linear drive concepts - telescoping shuttle, simple shuttle, and piston. 209
Figure A.24 Harmonic drive gear reducer. 210
Figure A.25 Wafer handler concept with linear final joint and a fixed tower. 212
Figure A.26 Wafer handler concept with dual output revolute joints and a fixed mast. 213
Figure A.27 Handler concept with two concentric revolute joints and a fixed mast. 213
Figure A.28 Kinematically redundant wafer handler concept. 214
Figure A.29 Handler concept with linear motion produced by three coupled revolute joints. 215
Figure A.30 Out-of-plane coupled straight line motion handler concept. 217
Figure A.31 Initial telescoping handler concept. 218
Figure A.32 Diving tower handler concept with two revolute joints. 219
Figure A.33 Telescoping handler concept derived from concepts shown in Figure A.31 and Figure A.32. 220
Figure A.34 Geometric parameters required to determine alley width and handler reach into process modules. 221
Figure A.35 Process geometric module constraints. 223
Figure A.36 Cassette geometric constraints. 224
Figure A.37 Vertical process module constraints. 224

Figure A.38 Early vacuum gripper concept. 226
Figure A.39 Passive gripper concept. 226
Figure A.40 Early fork gripper concept with edge contact on wafer. 227
Figure A 41 Fork gripper concept. 227
Figure A.42 Tongue gripper concept. 228
Figure A.43 Machine frame. 229
Figure A.44 Wafer handling robot. 230
Figure A.45 Wafer handling robot with fully extended and fully retracted telescoping axis. 231
Figure A.46 Side view of fork grippers and upper arm assembly. 232
Figure A.47 Top view of fork grippers and arm assembly. 233
Figure A.48 Finished fork gripper design. 233
Figure A.49 Finished tongue gripper design. 234
Figure A.50 Side view of the fully collapsed telescoping axis. 235
Figure A.51 Fully extended telescoping axis. (Shown without linear bearings.) 236
Figure A.52 End view of the horizontal carriage. 238
Figure A.53 Finalized machine concept. 240
Figure A.54 Prototype wafer handling robot next to test frame. 241
Figure A.55 Prototype fork grippers and arm assembly in test fixture. 241
Figure A.56 Telescoping ballscrew and motor parts. 242
Figure A.57 Stages in the assembly of the prototype telescoping axis. 242
Figure A.58 Prototype wafer handling robot partially disassembled in test frame. 243
Figure A.59 Prototype wafer handling robot with telescoping axis in fully retracted and fully extended configurations. 244
Figure A.60 Robot body detached from horizontal carriage at kinematic coupling being lifted out of carriage with a manual crane. 245
Figure A.61 Prototype wafer handling robot executing straight-line motion. 245
Figure C.1 90 Series frame loaded under torsion. 259
Figure C.2 Spine of the Accipiter frame loaded under torsion. 260
Figure C.3 Rear portion of Accipiter frame with normal loads on top of structure. 260

# List of Tables

Table 3.1 Denavit and Hartenberg Parameters for Wafer Handling Robot _____ 85
Table 4.1 Control system parameters for wafer handling robot. _____ 142
Table B.1 Wafer Handler Displacement Error Gains _____ 247
Table B.2 Individual Axis Errors and End Effector Equivalent Errors _____ 249
Table B.3 Total End Effector Errors _____ 250
Table B.4 Machine Frame Displacement Error Gains. _____ 251
Table B.5 Individual Axis Errors and End Point Equivalent Errors. _____ 252
Table B.6 Total End Effector Errors. _____ 253
Table B.7 Table of Velocity Error Gains _____ 254
Table B.8 Table of Velocity Error Gains _____ 255
Table B.9 Table of Velocity Error Gains _____ 255
Table B.10 Table of Horizontal Carriage Repeatability Data _____ 256
Table B.11 Table of Telescoping Axis Repeatability Data _____ 256
Table B.12 Table of Proximal Revolute Joint Repeatability Data _____ 257
Table B.13 Table of X-direction Robot Repeatability Data _____ 257
Table B.14 Table of Y-direction Robot Repeatability Data _____ 258
Table E.1 Machine Layout Selection Matrix _____ 281
Table E.2 Machine Frame Selection Matrix _____ 284
Table E.3 Wafer Handler Selection Matrix _____ 287
Table E.4 Wafer Gripper Selection Matrix _____ 289

# Chapter 1: Introduction and Thesis Overview

## 1.1 Introduction

Semiconductor manufacturing is a worldwide industry that now impacts even the most mundane tasks in everyday life. The products of this industry are found not only in the high tech computer and other electronic goods with which semiconductors have been traditionally associated, but also in common household appliances and children's toys. Consequently, this industry is large and growing. Many of the key battles in the international war of economic competitiveness are fought in this industry. According to a forecast by World Semiconductor Trade Statistics, Inc., which was released by the Semiconductor Industry Association, the worldwide semiconductor industry was projected to reach $87.8 billion by the end of 1994 and $103.4 billion by the end of 1996[1]. The American market is expected to reach $32.5 billion followed closely by the Japanese market at an expected value of $31 billion in 1996. Europe and Asia make up the remainder of the world market projected at $18.5 and $21.4 billion respectively.

The semiconductor equipment industry produces the process tools that are used in the complex manufacture of semiconductors. These tools rely heavily upon automation for the movement of wafers[2] through these production systems. A number of different sources have identified various performance and reliability problems in the design of this equipment as related to the movement of wafers. Accordingly, this thesis presents a precision machine design methodology to increase performance and reliability of process tools through the use of analytical and deterministic design tools. This new methodology combines existing technologies from other fields to address design complexities unique to cleanroom manufacturing.

---

[1] *Solid State Technology*, March 1994, p. 16.

[2] Typically many chips, called die, are produced on a single silicon wafer.

## 1.2 The Semiconductor Industry

Currently, state-of-the-art manufacturers of semiconductors can produce characteristic line widths of 0.35 μm. By the year 2001, these sizes are expected to reach 0.18 μm[3]. As a rule of thumb, a dust particle five to ten times smaller than this characteristic size can create a killer defect in an integrated circuit (IC)[4] rendering it useless. As a result, semiconductors must be manufactured in hyper-clean environments. These cleanliness requirements have serious implications for the equipment design engineer.

### 1.2.1 Automation in Semiconductor Production Facilities

The economics of building cleanrooms, filling them with the required process tools, the high valued-added nature of semiconductors, and intense worldwide competition combine to create an environment where semiconductor manufacturing facilities (fabs) are expected to operate nearly continuously. As a result, high levels of equipment reliability and throughput are important to the success of these manufacturing operations. Process technology defines a manufacturer's capabilities; however, the supporting automation may determine whether or not the manufacturer can compete successfully.

Several sources have documented the need for automation in semiconductor fabs. Jacobsen, Harper and Bailey, and Lovell, et al. have discussed the need for automating production of semiconductors [Jacobson '89], [Harper '84], [Lovell '90]. Also, SEMATECH[5] has created a roadmap for automated material handling systems in semiconductor manufacture [SEMATECH '93].

To illustrate the levels of performance often expected in semiconductor manufacture, it is worthy to briefly consider the design of the wafer transfer robot that is discussed in depth later in the thesis. This robot is expected to transfer one wafer every

---

[3] *Semiconductor International*, January 1995, p. 47.

[4] Dynamic Random Access Memory (DRAM), Application Specific Integrated Circuits (ASICs), and microprocessors are examples of the types of semiconductors commonly manufactured worldwide.

[5] SEMATECH is a consortium of large U.S. semiconductor manufacturers.

six seconds. The process tool that uses this robot is expected to have approximately 80% availability three shifts a day, seven days a week. With this much operating time, the wafer handling robot could easily see several million cycles of operation every year.

Ideally, wafer handling automation in a semiconductor fab would be virtually invisible. It must be recognized that this material handling automation adds no value to the product. However, to provide the required cleanliness levels and uniform and controlled transfer of wafers throughout the production process, automation is a necessity.

Material handling automation has many benefits when compared with the alternative of using human labor to transfer wafers. The first of these benefits is the ability to automatically control and coordinate the transfer of wafers between and within process tools for maximum throughput. This benefit is essentially the same one that has led to the use of material movement automation in other industries. Additional benefits of using automation in transferring wafers between and within process tools in a cleanroom come in the form of particle generation reduction. First, because a human worker will not be required to physically move wafers, fewer workers may actually be required inside the cleanroom. The mere absence of humans helps to decrease particle generation. A second reduction in particle generation comes from the potentially smooth, controlled, and consistent movement of wafers in cassettes by a robot. Every vibration or rattle experienced by a wafer in a cassette increases the potential for particle generation and migration within the cassette. When programmed with the appropriately smooth trajectories, a robot can easily minimize the peak accelerations seen by wafers in a cassette. Also, an appropriately designed transfer system can provide very smooth landings of a cassette in a load station. Even with skill and patience, a human operator cannot consistently duplicate the smooth set-down of a cassette.

Figure 1.1 and Figure 1.2 demonstrate the benefit of a smooth set-down of a cassette by a robot. These figures show how the human operator may induce much higher vibration levels in the cassette[6]. In the trial depicted in Figure 1.1, a peak amplitude of almost 8 g's ($\cong$ 80 m/s$^2$) of acceleration was experienced by a wafer in the cassette. With

[6] The data in these figures was taken by instrumenting a wafer with an accelerometer in a loaded cassette.

extreme care, the human operator can achieve better results than those shown in Figure 1.1. However, in a working fab, one can hardly expect workers to always use extreme care and patience. Robots on the other hand can repeatably perform smooth set downs. The peak amplitude in Figure 1.2, is about 1.5 g's (15 m/s$^2$). With improved robot design and smoother trajectories, this level can be further reduced by an order of magnitude or more.

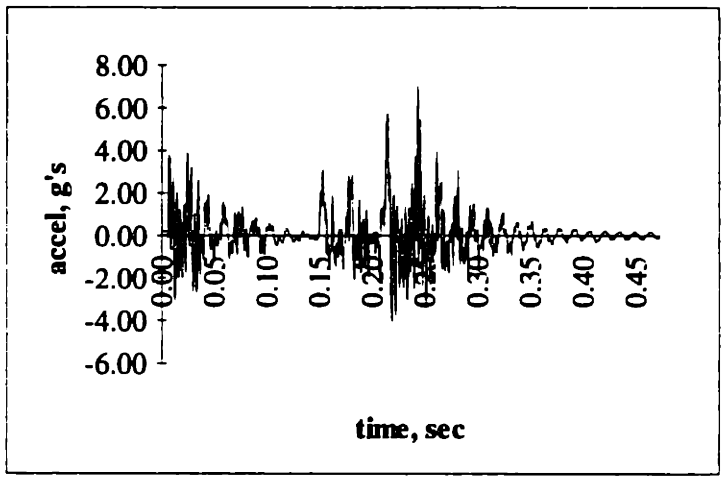


**Figure 1.1** Time history of acceleration levels of a human casually setting a loaded cassette down on a hard surface (from [Slocum '93B]).

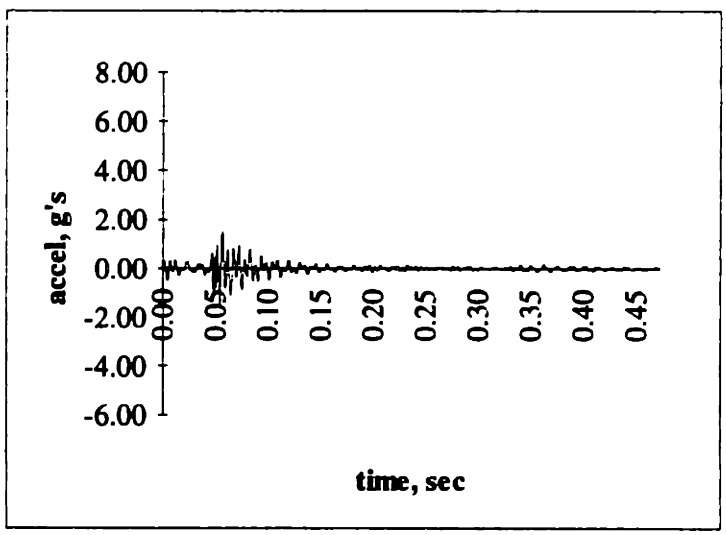


**Figure 1.2** Time history of acceleration levels of a robot setting a loaded cassette down on a hard surface (from [Slocum '93B]).

Several different facility layouts are popular with semiconductor manufacturers. The two most common are *Bay & Chase* and *Ballroom*. The bay and chase layout is shown in Figure 1.3. Each bay may contain a certain type of process, e.g. photolithography. The chase area typically has less stringent cleanliness requirements and is used for service activity. The ballroom configuration is basically a wide open room with manufacturing equipment grouped according to process flow.

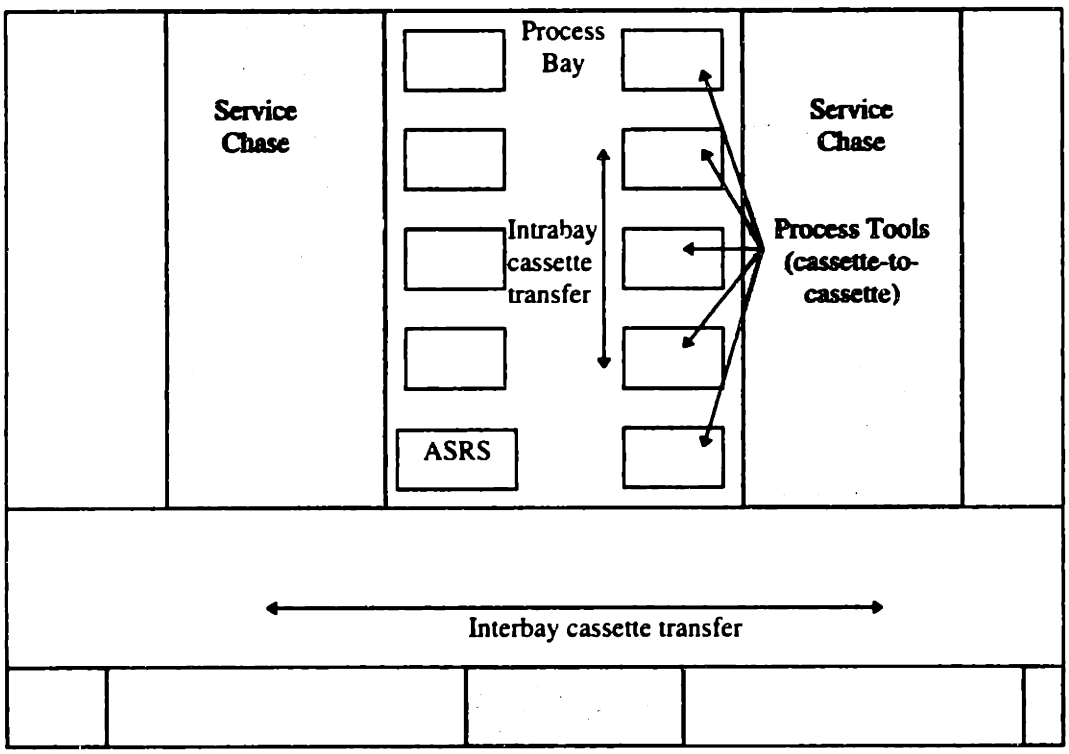


**Figure 1.3** Bay and chase fab configuration.

The automation and material handling systems in semiconductor fabs can be divided into three general areas. Following Tyra, these three areas are called *interbay*, *intrabay*, and *cassette-to-cassette* automation [Tyra '93]. Figure 1.3 shows how these three areas are distributed in a fab. Normally wafers are transferred between process tools in containers called *cassettes*, which usually contain 25 wafers. Interbay automation typically moves cassettes between process bays and automated storage and retrieval (ASRS) locations[7]. Intrabay automation moves cassettes between individual process

[7] These ASRS machines are typically called stockers and are used to balance the flow of wafers through a fab.

tools. Finally, cassette-to-cassette automation refers to all mechanisms that handle individual wafers within process tools.

Automated systems in semiconductor manufacture range from simple one or two degree of freedom (DOF) serial transfer devices to generic six DOF industrial robots retrofitted for cleanroom use. Furthermore, these systems have a wide range of positioning accuracy and repeatability requirements. On the coarse end of the spectrum, the transfer of wafer cassettes might require only .25 mm or even 2.5 mm repeatability. Despite the relative simplicity of achieving these levels of performance, problems exist even with these systems. Cassettes themselves often contribute to this problem. These cassettes lack sufficient alignment features[8]. Additionally, these cassettes are often dimensionally unstable due to their plastic construction and abusive treatment[9]. On the other extreme, the step-and-repeat positioning stages used in photolithography are an example of a truly precision mechanical system. (These positioning stages are an high precision example of cassette-to-cassette automation). In these systems, exposure masks must be accurately aligned with already exposed underlying layers and then the wafer must be moved from site to site for each of the many die on a wafer. These systems may have repeatability on the order of 0.01 μm. Other forms of cassette-to-cassette automation are in the intermediate area of this spectrum with positioning repeatability requirements as small as 0.025 mm.

The precision machine design methodology discussed in this thesis is generally applicable to all three areas of automation.

### 1.2.2 The Need for a Precision Machine Design Methodology

Detailed examinations of a number of "state-of-the-art" semiconductor production equipment manufacturers have led to the recognition of the need for a precision machine design methodology for the semiconductor industry. Participation in SEMATECH sponsored design reviews of five major semiconductor equipment manufacturers and

[8] Kinematic couplings, which are discussed later in the thesis, could easily and inexpensively solve this alignment problem.
[9] Tossing a dirty cassette into a bin for washing might be enough to deform it.

discussions with many engineers and service personnel indicates significant reliability problems exist in U.S. manufactured semiconductor process tools [Slocum '92C], [Slocum '92D], [Slocum '92E], [Slocum '92F], [Slocum '93A], [Slocum '93B]. Many of these problems are directly related to the existing mechanical design practices in the automated wafer and cassette handling mechanisms. For example, the structural design of many semiconductor processing tools lacks the necessary stiffness and integrity to form a proper base for process modules and wafer or cassette handling mechanisms. Observations and simple experimentation made during the design reviews have linked reliability problems manifested as positioning errors and mechanical drift to these inadequate structures.

Mechanisms used in cleanroom automation suffer from a variety of problems. Often position adjustments proliferate throughout a machine to correct for non-repeatable mechanisms and compliant structures. These position adjustments are needed to "set-up" a machine to allow it to successfully complete the required wafer transfers. Unfortunately, these nondeteriministic practices often create systems that are not reliable and require frequent "tweaking" to allow continued operation. Reliability problems are often directly traceable to failures in the wafer handling systems. Frequently, these difficulties are manifested as a lack of robustness; that is, current designs cannot tolerant any variation in their operational parameters.

Further justification for the need for a new design methodology comes from an economic analysis of semiconductor manufacturing. Carnes, using an economic model developed at SEMATECH, has shown that the long term cost of ownership of process tools has a significant impact on the cost of wafer production [Carnes '91]. This economic model shows that the cost of production on a per wafer basis is highly sensitive to throughput, overall tool reliability, as well as the yield of the manufacturing process. Conversely, the initial purchase price of the machine is less important. Economically then, a manufacturer can expect returns on an investment in designing in higher performance, better reliability, and less particle contamination.

### 1.2.3 Historical Perspective

From the invention of the transistor by the American physicists John Bardeen, Walter Brattain, and William Shockley announced in 1948[10] to the development of the first integrated circuit by Jack Kilby of Texas Instruments and Robert Noyce of Fairchild Camera in 1958, the semiconductor industry is one that has seen rapid development. Furthermore, as described by von Hippel, *lead users*[11] in the semiconductor industry have guided the evolution of this industry through their process innovations [von Hippel '88]. The leaders in implementing new technology in this industry have been process scientists. Therefore, it is not surprising that automation, which is frequently considered to be of secondary importance when compared to process technology, suffered in its development. Tyra shows how semiconductor process equipment producers often decide to design their own wafer transfer mechanisms to satisfy the specific requirements of their equipment [Tyra '93]. Although outside manufacturers of wafer handling automation do exist, their products often do not fit the wide variations found in process equipment design.

The rapid development in the semiconductor industry has created a situation where process technology guided machine development and the fast pace and lack of tradition in machine design outstripped mechanical design techniques resulting in non-optimal machines.

### 1.2.4 Functional Requirements of the Semiconductor Equipment Industry

A broad set of functional requirements for the wafer handling automation in semiconductor manufacturing operations has been identified. These requirements follow:

- High reliability
- Clean mechanical design to minimize contamination
- Short cycle times (fast transfers)
- Repeatable positioning of wafers

[10] These three scientists shared the 1956 Nobel prize in physics for their invention.

[11] Lead users are the consumers of the technology. In the semiconductor industry, the manufacturers are the lead users.

- Small footprint.

The importance of the first four requirements should be evident from the discussion of the semiconductor industry thus far. The fifth element, small footprint, is also related to the cleanroom environment. Because cleanrooms tend to be expensive to build and maintain on a floor area basis, semiconductor equipment producers are expected to design and build compact equipment. Frequently, a major criterion for comparing different competitors' designs is the floor space required.

These functional requirements can be used to direct the design process of virtually any wafer handling system in a semiconductor fab.

## 1.3 Precision Machine Design for the Semiconductor Equipment Industry

Based on the need for improvements in the design of the wafer transfer systems in semiconductor fabs described above, this thesis develops a precision machine design methodology for complex multi-station systems. This methodology, which is based on technologies from the machine tool, instrument, and optics design communities, has the potential to meet the needs of the semiconductor industry. The research described in this thesis integrates existing technology in a new and unique way to create a fundamentally new design paradigm that will help redefine the way machines are created for cleanroom use.

Machine design for semiconductor equipment shares many similarities with machine design in other areas such as metal forming. However, cleanroom machines are frequently an order of magnitude more complex than machine tools. For example, a typical CNC machine tool might have three to five controlled axes of motion. The photoresist processing system discussed later in this thesis has in excess of 35 controlled degrees of freedom. Additionally, this machine must be designed to function ultra-reliably in a Class 1 cleanroom for nearly continuous operation. As if this were not enough, the machine must also achieve high levels of throughput and occupy a minimum

amount of floor space. This photoresist processing system is representative of processing equipment in the semiconductor industry.

A survey of the research literature in machine design, such as the one conducted for this thesis, reveals a vast resource of machine tool-related work. Semiconductor machine design, on the other hand, is startlingly underrepresented. Relatively few papers have been published on the subject of semiconductor equipment and automation design. Those few papers that are found usually originate in the industrial sector and typically discuss a particular company's attempts at creating a cleanroom robot or automation system. (See the discussion in Chapter 2 on semiconductor machine design.) There is no discussion of a design methodology for cleanroom machine design[12]. A large body of research dealing with semiconductor process technology does exist. However, good machine design is also critical to the success of this industry. And so, this thesis will make a fundamental contribution to the emerging field of Precision Machine Design for semiconductor manufacturing equipment.

Deterministic design is a concept that is central to this thesis. Determinism is a design philosophy that states that precision machines follow cause and effect relationships and with care and patience these relationships can be modeled and controlled to give the desired results. This philosophy may seem obvious at first, but variations in machine performance are often ascribed to random effects that are not random at all. When a deterministic design technique is implemented properly, an error model can be used to predict machine performance based on component performance. Because positioning problems can be identified before the machine is built, the design cycle can be dramatically shortened.

Typically, machine structures used in this industry are very light and compliant. To accommodate the mechanical drift inherent in these machines, large numbers of mechanical positioning adjustments are added to the wafer handling mechanisms and process modules. Field service personnel must set-up machines and then continually adjust them to keep the wafer positioning systems operating properly. To correct these

[12] At least, none that this author has been able to find.

problems, it is proposed that a mechanically rigid frame with highly repeatable, deterministically designed kinematic couplings be used to create a system that does not contain the overly compliant structures and accompanying mechanical drift encountered in existing designs.

Although this thesis draws upon concepts that have been developed in the area traditionally called *Precision Engineering* and used in the machine tool, instrument, and optics design communities, this research does not advocate relying on absolute open loop accuracy. Rather, this research is concerned with robust, repeatable, and stable mechanisms and structures. The goal is to achieve position repeatability and other performance targets in addition to high reliability. Physical modeling and closed loop control are central to achieving this goal.

Figure 1.4 shows the difference between accuracy and repeatability. Generally, speaking accuracy is more difficult to achieve than repeatability[13]. Additionally, high repeatability is often not accompanied by high accuracy especially in multiple degree of freedom serial manipulators. However, if some external method is available to identify the inaccuracy in a highly repeatable process, that mechanism can often be used with great success.

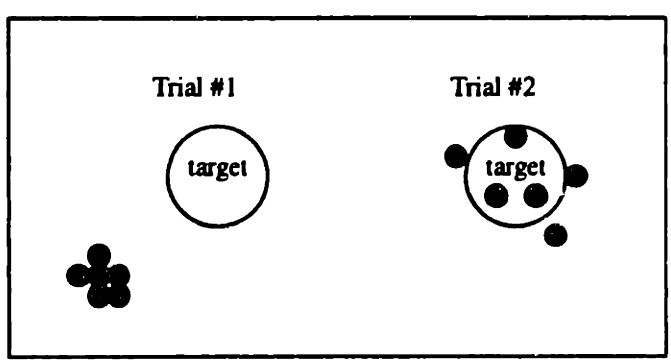


**Figure 1.4** Trial #1 offers superior repeatability and inferior accuracy while trial #2 offers better accuracy and inferior repeatability.

The successful execution of the design methodology presented in this thesis will result in repeatable systems. Typically, a system designed in this manner will require an

[13] According to axiomatic design theory, which is discussed further in Chapter 2, if a design is fully uncoupled, it may be easier to obtain high accuracy than high repeatability [Suh '90].

initial teaching/learning phase in which a repeatable mechanism is taught exactly form where and to where wafers are to be transferred.

## 1.4 Thesis Contributions

This thesis develops a fundamentally new approach for the design of automa ed semiconductor manufacturing equipment. The deterministic approach used here seeks to develop designs where system robustness is increased by superior mechanical design. Designs created with this design methodology will have the following characteristics: Support structures will be sufficiently stiff to provide a rigid base for the attachment of wafer handling mechanisms and process modules. For example, machine frames currently made from many bolted square steel tubes can be replaced with weldments. The weldment can then have all necessary reference surfaces machined directly into the frame. Process modules and wafer handling mechanisms can then be deterministically mounted to the rigid machine frame, thereby eliminating reliability-degrading position adjustments. The design of the wafer handling mechanisms will be guided by the same deterministic design philosophy. Lost motion and mechanical drift will be reduced dramatically by choosing robust mechanical and control system components.

The precision machine design methodology is guided by the two primary contributions described in the thesis. First, the research develops a set of numerical error modeling tools to identify, quantify, and – through the use of these tools in the design process – minimize the effects of kinematic errors and sources of non-repeatability in the design of mechanical positioning systems. These errors are not limited purely to static effects; rather, the numerical modeling tools can also include the dynamic system effects that tend to degrade machine performance. Error modeling has been discussed by many researchers previously. However, most of this work is devoted to the metrology effort; that is, quantifying errors of existing machines. A few researchers have addressed the design question for machine tools which usually have six or fewer degrees of freedom. By comparison, this research focuses on the use of error modeling for guiding and coordinating the design of complex semiconductor manufacturing tools, which can be an

order of magnitude more complex than machine tools. Additionally, the error modeling techniques described here include not only displacement error modeling, but also new work on velocity and force transmission error modeling. For the second area of contribution, the research establishes a set of mechanical design rules that may be used in creating system-level designs that meet requirements for repeatability, reliability, minimum cost, maximum maintainability, and manufacturing ease. The application of these design rules is integrated with the numerical error modeling techniques.

Although the contributions described above are generally applicable to a wide variety of mechanical systems, the thesis specifically targets the design of wafer handling subsystems in semiconductor manufacturing equipment. The proper application of the numerical error modeling tools and the accompanying mechanical design rules in the design of these systems will result in equipment that is capable of quickly, repeatably, and reliably moving wafers based on positioning and process cycle requirements through the various process steps used in semiconductor manufacture. Special emphasis is placed on the requirements for short cycle times, high reliability, and mechanical design that minimizes contamination of the clean semiconductor manufacturing environment.

In addition to the error modeling tools and the mechanical design rules presented in the thesis, the design of a unique frame and wafer handling robot for a new photoresist processing system for Silicon Valley Group, Incorporated (SVG) in San Jose, California is described. This photoresist processing system design project is called the Accipiter[14] project and will replace SVG's current flagship system, the 90 Series. The finalized concept for this machine is shown in Figure 1.5. This design demonstrates in detail the application of the precision machine design methodology for semiconductor manufacturing equipment.

[14] An accipiter is a bird of prey that typically has short wings and a long tail.

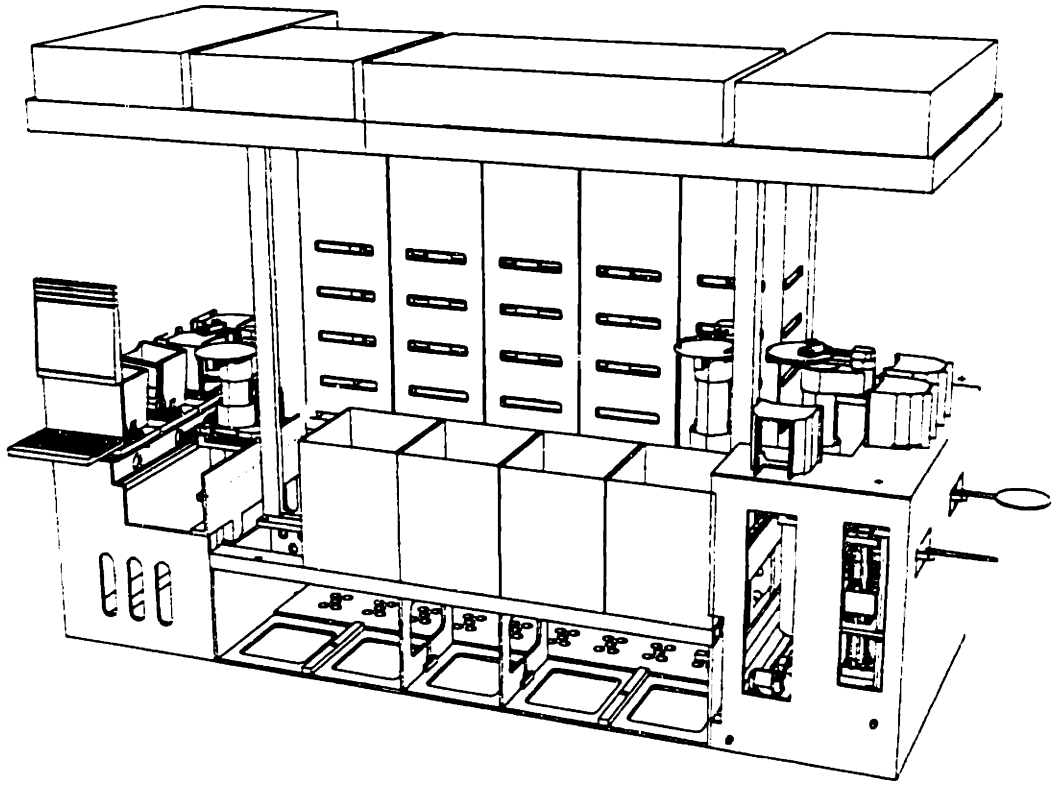

**Figure 1.5** Finalized Accipiter machine concept[15].

The example implementation proceeds from the initial product planning and conceptualization to the detailed system and component design to the actual fabrication and testing of a prototype system. Therefore, the case study shows how these techniques can be used in the conceptual, embodiment, and detail design stages as well as the evaluation of an existing system. The application of the precision machine design methodology focuses on the structural and wafer handling systems. The new structurally rigid machine frame is shown in Figure 1.6. The Accipiter's wafer handling robot, designed as a part of this research project, is shown Figure 1.7 Numerous specific examples of both the numerical error modeling techniques and the application of the mechanical design methodology are used throughout the thesis.

[15] Courtesy of Silicon Valley Group.

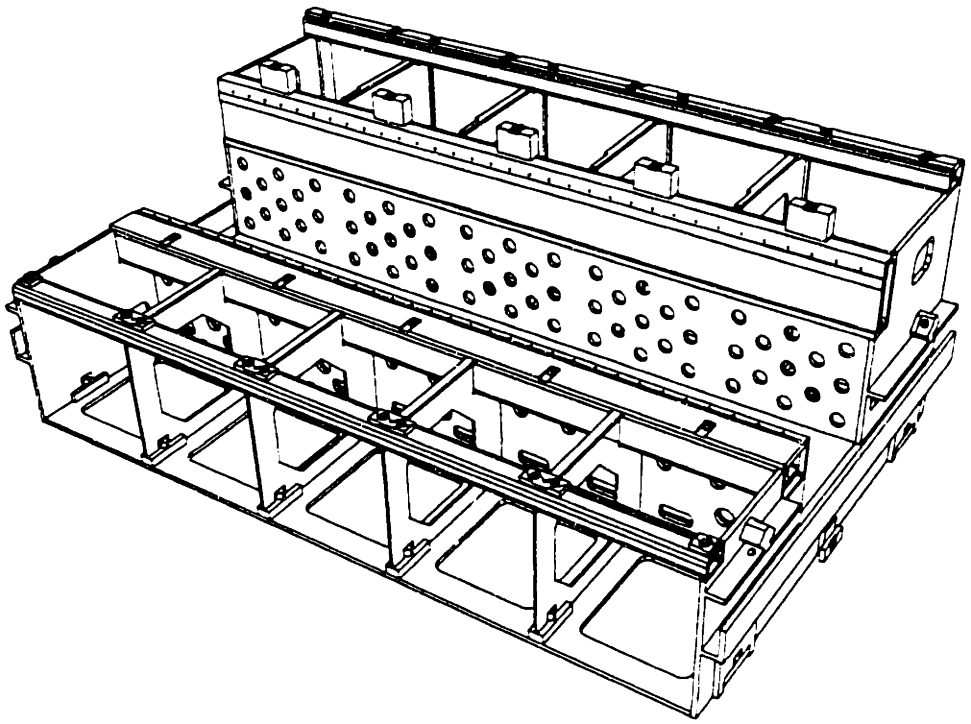

**Figure 1.6** Deterministically designed machine frame[16].

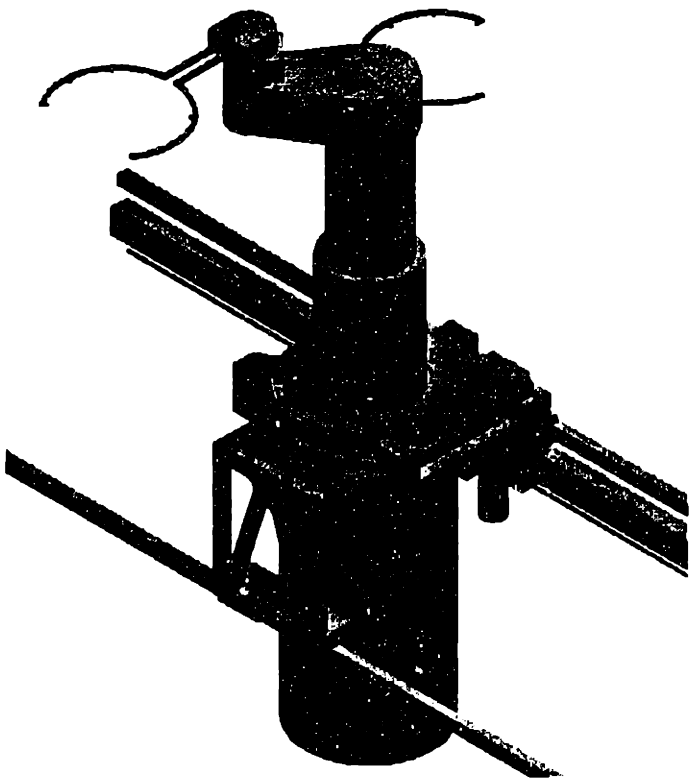

**Figure 1.7** Deterministically designed wafer handling robot.

[16] Courtesy of Silicon Valley Group.

## 1.5 Thesis Structure

This thesis contains two basic parts. Chapters 1 through 4 contain the first portion, which consists of a discussion of the precision design methodology that was briefly described above. These chapters present the development of the analytical design tools and design theory contained in this methodology. The second portion, which is an extended case study illustrating the use of precision machine design in the development of a semiconductor process tool, is contained in Appendix A. It should be noted that the design resulting from the process described in Appendix A is used throughout the thesis to illustrate specific details of the error modeling and mechanical design rules. However, the complete process used to arrive at this design is fully discussed only in the second portion of the thesis.

Chapter 2 begins with a discussion of the work of other researchers in areas related to those in this thesis. Briefly, literature from the following areas is reviewed:

- design theory
- deterministic design
- kinematic couplings[17]
- error modeling in machine design
- mechanical design in cleanrooms.

Having described the work of other researchers, the chapter continues with a more formal and thorough definition of the central topic of this thesis, precision machine design for the semiconductor equipment manufacturing industry. The primary constituents of the precision machine design theory, error modeling and the mechanical design rules, are defined here.

[17] These types of couplings might also be referred to as "deterministic structural couplings." Traditionally, these structural couplings have been called kinematic couplings. This practice has resulted in some instances of misunderstanding because the word "kinematic" is usually associated with the science of motion.

The thesis continues in Chapter 3, with a complete presentation of error modeling in machine design. The chapter begins with a discussion of homogeneous transform based displacement error models. After a presentation of the necessary mathematical background, two methods of assigning coordinate frames in machine structures, the adapted Denavit and Hartenberg approach and the center of compliance approach, are described. Additionally, the chapter contains a discussion of the various sources of errors in machines and how these errors may be included in an error model. Next, the concept of error modeling is extended to include a new quantitative method to include velocity and force transmission effects. The chapter also describes how these error modeling techniques can be used both as design and analysis tools. Finally, Chapter 3 presents a complete working error model for a process tool frame and its integral wafer handling robot.

Chapter 4 follows with a description of the mechanical design rules that complement error modeling in the precision machine design methodology. This chapter contains a discussion of the following areas:

- deterministic design
- elastic averaging
- reduction of the effects of rotational errors
- static and dynamic structural deformations
- control and mechanical system integration
- considerations for cleanroom equipment design.

The ideas discussed in this chapter are illustrated extensively with case studies drawn from the SVG process tool frame and wafer handling robot designs.

Appendix A formally introduces the design project that served as a testbed for the ideas developed by the research and described in this thesis. First, the photoresist application process is described. Next, past designs of photoresist processing equipment are described briefly. Many of the problems with these designs are qualitatively

described. The chapter continues by defining the functional requirements for the design of a new photoresist processing tool. Following the introduction of the design problem, the conceptual design stage is discussed. Alternate designs for the machine layout, the machine structure, the wafer handling robot, and the wafer gripping/centering mechanism are presented and evaluated here. Appendix A continues with a brief presentation of the embodiment and detailed design phase. This chapter also presents the prototype development of the wafer handling robot and a test frame. Test data from the prototype system are presented in case studies in Chapters 3 and 4. The thesis concludes in Chapter 5 with a summary of the precision machine design methodology and a discussion of future trends and new areas of research.

# Chapter 2: Machine Design Methodologies and Their Application to the Semiconductor Equipment Industry

## 2.1 Introduction

Precision machine design is an area that has been evolving and developing for hundreds of years. Indeed, Evans discusses the use of kinematic couplings (*deterministic structural couplings*) as far back as the 1800's [Evans '89]. Machine tools have been common since the industrial revolution occurred in Great Britain in the first half of the 19th century. Industrial robots, developed in the 1960's, were made possible by the advent of modern control theory and the digital computer. The cleanroom manufacturing technology that made digital computers possible has been developing rapidly since the first commercial integrated circuits were marketed in 1959. Technology from all of these areas combines to form the foundation for this research.

This chapter begins with a discussion of the work of other researchers that is related to precision machine design. First, general design theory and design methodology as developed by other researchers are discussed. The chapter continues with an explanation of deterministic design theory developed for applications in machine tool and instrument design. Kinematic couplings, which follow directly from the principles of deterministic design, are also discussed in some detail. Next, the error modeling techniques of various researchers are presented. The discussion of previous work is concluded with a short survey of some of the special design practices required for cleanroom manufacturing equipment. The remainder of the chapter defines the topic of this thesis more formally. The two major components of the precision machine design methodology developed in this research, error modeling and a set of mechanical design rules, are described more thoroughly in preparation for their discussion in Chapters 3 and 4.

## 2.2 Previous Work on Precision Machine Design Methodologies

The field of machine design is a broad one. Technology from different areas must often be drawn together in the course of executing a successful design. It is not surprising, then, that previous research from a variety of fields can contribute to the development of a precision machine design methodology for the semiconductor equipment manufacturing industry as described in this thesis.

### 2.2.1 Design Theory

Engineering design is an area that has long been conducted with an experience-based approach rather than a science-based approach. Successful design efforts often rely heavily upon a particular designer's judgment. Ad hoc solutions are also common in engineering design. These approaches to design are especially commonplace in equipment design. While this kind of approach may result in a working design, it can often be inefficient and may frequently result in failure. A generalized, scientific approach[18] to equipment design, thus, seems to be a desirable goal.

#### 2.2.1.1 Axiomatic Design

Suh has developed an axiomatic approach to engineering design that addresses design as a science [Suh '90]. This design theory centers around two design axioms and the relationship between *functional requirements* and *design parameters*. Functional requirements are the goals of a design; they essentially define the design problem. Design parameters describe the characteristics of a design that satisfy the functional requirements. Suh's design axioms are stated as follows:

1. The Independence Axiom. Maintain the independence of functional requirements.

2. The Information Axiom. Minimize the information content in a design.

[18] A designer's experience may still be an important asset.

On initial inspection, the concise statement of these axioms might lead the casual observer to believe the problem has been over-simplified. However, these axioms can be useful tools in directing the solution of a design problem.

A mathematical representation of the independence axiom helps to clarify its importance and application. Equation 2.1 is a matrix expression for this axiom.

$$\underline{fr} = [A]\underline{dp} \tag{2.1}$$

where $\underline{fr}$ is the vector of functional requirements, $[A]$ is the design matrix, and $\underline{dp}$ is the vector of design parameters. Before Equation 2.1 can be used successfully, the design problem must be formulated quantitatively. That is, the designer must establish the mathematical relationship between a design problem's functional requirements and its design parameters. So, it can be seen that there is no generic set of "design" units attached to Equation 2.1. Rather, the units of that equation are dependent on the particular formulation of a design problem.

When the design matrix is diagonal, the independence axiom is satisfied because a single design parameter satisfies a single functional requirement. This situation represents an *uncoupled* design. A fully populated design matrix indicates a case where the design is *coupled* and the independence of the functional requirements cannot be guaranteed. In the coupled case, a single functional requirement is dependent on multiple design parameters. The designer of this type of system may have difficulty in achieving the desired values of his or her functional requirements since it may not be clear how the design parameters should be adjusted. The third situation that may exist is represented by a triangular matrix where all of the elements either above or below (but, not both) the diagonal are zero. This case is called a *decoupled* design. In this case, the functional requirements can be satisfied if the design parameters are varied in the correct sequence. The designer must start with the functional requirement that is dependent upon only one design parameter. After setting this design parameter, the designer may proceed to the next functional requirement that is dependent on two design parameters, one of which has already been established. The designer can continue in this manner and satisfy each of

the functional requirements by selecting a single design parameter. As a practical matter, most design problems probably first appear to coupled. However, the designer can almost always systematically decouple the design.

The second axiom can be interpreted simply as a requirement to arrive at the design with the minimum complexity that satisfies the functional requirements.

This topic is treated in depth in the literature and so will not be discussed further here. However, the axiomatic approach to design can be a useful tool to guide the design process.

#### 2.2.1.2 The Design Process

Having established a need for a scientific base for equipment design, it is useful to examine the process a designer actually uses to create designs. For this research, the methods of Pahl and Beitz serve as a model [Pahl '88]. These German researchers present a systematic method of design involving four distinct phases:

1. Clarification of the task
2. Conceptual design
3. Embodiment design
4. Detail design.

The first phase is the problem statement. This is the stage where a designer must translate an often broadly and nebulously stated need for a new product or process into a set of viable functional requirements. This stage is the most critical. The designer must accurately gather information and correctly define what is required of the design. The next three stages in the design process involve determining the design parameters that will satisfy the stated functional requirements. In the conceptual design stage, the designer develops solution methods and converts these into alternate design candidates. These alternate designs must be evaluated on the basis of how their design parameters satisfy the functional requirements. Some candidate designs may be eliminated at this point because they fail to fulfill all of the functional requirements. Some means must be

employed to evaluate the remaining designs. In the next stage, embodiment design, the designer develops a layout of the design. This layout is used as a basis to perform technical and economic analysis of the design. Some iteration in the design may be required at this stage depending on the results of the analysis. The final phase is the detailed design stage where the design is converted into the actual documentation, technical drawings, manufacture and assembly directions, etc. that facilitate the manufacture of the object of the design.

#### 2.2.1.3 The Analytical Hierarchy Procedure

The next area of design theory research examined for this thesis deals specifically with the concept selection that occurs at the end of the conceptual design phase. Because design is often performed by a group of engineers, concept selection is frequently an activity where not only must a design be selected but often contentious group dynamics must also be handled effectively. The Analytical Hierarchy Procedure (AHP) developed by Saaty and further refined by Marsh et al. in the Precision Engineering Research Group at MIT is an example of such a method [Marsh '93].

The AHP is a hierarchical process in that multiple levels of criteria are used to evaluate a design. Some high level criteria may be established and further divided into lower levels of criteria. The criteria in the selection method can be thought of as a means to evaluate a concept's design parameters ability to satisfy the functional requirements of the design task. The evaluation is performed by assigning weights to the relative importance of each criterion. Then each design is evaluated numerically on its ability to satisfy each criterion. The multiple levels of criteria allow a design to be evaluated accurately without results becoming skewed by the direct comparison of major criteria and minor criteria as may occur in some other selection methods. The weighting of criteria is performed by rating just one criterion's relative importance to all other criteria at that level in the hierarchy. A consistent matrix of relative importance is then established numerically for all criteria at that level. The final rating of design alternatives is performed at the lowest level of the AHP. Here, designs are evaluated on their ability to satisfy the various criteria. The interested reader should refer to the literature for a

more rigorous definition of the AHP method [Marsh '93]. This method is used to evaluate alternate designs in this thesis as described in Appendices A and E.

#### 2.2.1.4 Robust Design

A final area of interest in the field of design theory is robust design as described by Taguchi and Clausing [Taguchi '90]. A primary tenet of this design philosophy is that quality and robustness are a product of good design rather than on-line control of manufacturing processes. Engineers must create designs that are tolerant both to environmental fluctuations and interactions between the components of the design. Another tenet of robust design is that engineers must constantly work to create designs that can be produced consistently. Taguchi emphasizes creating product quality through good design practices rather than merely trying to keep manufacturing processes within established tolerances. This philosophy is consistent with the ideas in this thesis in that the design process itself is targeted for improvements in achieving higher reliability in the finished product.

### 2.2.2 Deterministic Design

Deterministic design[19] is a simple concept that has already been referred to in the thesis. The concept of determinism is stated very clearly and simply by Donaldson [Donaldson '72]. He states:

> . . . machine tool errors obey cause-and-effect relationships, and do not vary randomly for no reason. Further, the causes are not esoteric and uncontrollable, but can be explained in terms of familiar engineering principles.

This statement seems rather obvious, but the approach developed because of the wide application of statistical methods to systems that are not truly random. Bryan also discusses the philosophy of determinism [Bryan '84], [Bryan '80], [Bryan '81]. His statement of the concept is similar to Donaldson's:

> The basic idea is that machine tools obey cause and effect relationships that are within our ability to understand and control and that there is

[19] This type of design is sometimes called kinematic design, but will be called deterministic design here to avoid confusion.

nothing random or probabilistic about their behavior. Everything happens for a reason and the list of reasons is small enough to manage.

Classical Newtonian physics give a deterministic view of the world. Truly random effects do exist in nature, e.g. Shot noise, Johnson noise, and Brownian motion. Additionally, quantum mechanics gives an essentially probabilistic explanation of nature. Fortunately, for the machine designer, only classical physics are important.

Both Bryan and Donaldson bring the perspective of metrology efforts in highly accurate machine tools. However, the concept of determinism can easily be generalized to any form of machine design. Indeed, echoes of the deterministic design philosophy are heard in Taguchi methods [Taguchi '90].

### 2.2.3 Kinematic Couplings

Kinematic couplings have long been used for fixturing in instrument design. The simple and elegant method of using one contact point to constrain one degree of freedom can result in an extremely useful coupling. Two rigid bodies are located relative to each other very accurately by constraining all six degrees of freedom. Thus, kinematic couplings have six contact points.

Traditionally, kinematic couplings have been used in instrument applications where high accuracy and repeatability are required, but only small loads are encountered. Sherrington and Smith describe a typical instrument application of a kinematic coupling used for relocating small specimens on a stylus roughness measuring instrument [Sherrington '93]. Kinematic coupling are also useful in optics where a lense can be supported without overconstraint deforming the lense and changing its optical properties.

In machine tool applications, fixturing has typically been performed using elastic averaging and extensive overconstraint. This method is capable of withstanding high forces and offers high stiffness, but may not be as easy to set up or as accurate as a kinematic coupling. Additionally, over-constraint in a fixture may deform the workpiece, thereby introducing manufacturing errors in the resulting parts. Slocum has shown how kinematic couplings can be designed to withstand the large forces in machine tool

applications with sufficient stiffness [Slocum '88A]. Additionally, Slocum and Donmez demonstrated experimentally that these couplings can give repeatability on the order of 0.3 μm even under the severe conditions encountered in machine tools [Slocum '88B].

Slocum has also presented a detailed method for the design of kinematic couplings [Slocum '92A], [Slocum '92B]. Coupling configuration and stability are addressed as well as stresses, deflections, and the resulting error motions in the couplings.

Baush and Youcef-Toumi describe in a more general sense how automation can be used in reconfiguring fixturing requirement [Bausch '90]. These researchers use screw theory to analyze a given fixture for full kinematic constraint.

### 2.2.4 Error Modeling in Machine Design

A number of researchers have contributed to the analytical techniques used to evaluate errors in precision machines. Much of the literature deals specifically with the machine tools used in material forming operations. Other pertinent literature comes from the field of robotics. As will be shown in this thesis, many of these techniques can be extended and further developed so that they might be applied to other types of machines.

The error modeling literature can be grouped into several categories. Error modeling can be divided into displacement-level and velocity/force transmission-level analysis. The literature is dominated by the position-level approaches. The researchers who address velocity and force transmission have generally approached the topic with much less depth.

#### 2.2.4.1 Displacement Error Modeling

Within the displacement-level modeling techniques, most of the literature is concerned with analysis of existing machines for metrological [Hocken '77], [Jan '90] and sometimes compensation purposes [Donmez '86]. Few researchers mention the possibility of using error modeling in the design of machines. Also, much of this position-level research is targeted at a specific type of machine. Examples exist for various machine tools [Treib '87], coordinate measuring machines (CMMs) [Teeuwsen

'89], and industrial robots [Eman '87]. The same technique can generally be applied to all of these machines since they can be characterized by open, serial kinematic chains. However, many machine tools have only three linear degrees of freedom (or fewer) that are oriented orthogonally with respect to each other. CMMs may have more degrees of freedom, but still usually have orthogonal linear axes. The approaches for industrial robots are usually more generic since these robots frequently have a combination of revolute and linear axes with a variety of changing orientations [Eman '87],[Vaishnav '87]. An assortment of techniques for characterizing errors in machines is found in the literature. These techniques include analytical geometry [Love '73], screw theory [Ziegert '90], vector representations [Weck '84], and rigid body kinematics using homogeneous transform matrices [Reshetov '88], [Soons '92]. Some researchers have also extended the homogeneous transform matrix method to include the conventions of Denavit and Hartenberg for describing serial kinematic chains [Denavit '55], [Weill '91].

#### 2.2.4.1.1 Displacement Error Modeling in Machine Tools and CMMs

Several of the earliest efforts in quantifying errors in machine tools were concerned specifically with the measurements that are necessary to characterized these errors. Hocken et al. presented a method using laser interferometers to quantify the three dimensional errors present in a CMM [Hocken '77]. These researchers used a set of vectors to describe important geometric features of the CMM and the object to be measured. Infinitesimal rotation matrices were used to account for angular errors. Schultschik was similarly interested in the volumetric accuracy of machines [Schultschik '77]. In this work, vectors and rotation matrices were also used to describe the geometry of a machine tool.

The earliest mention of an *error budget* for a machine tool comes from Donaldson [Donaldson '80]. This research is one of the few examples of previous work that is targeted specifically at the design of machines. Donaldson describes an error model as a means to predict and control the total positioning error in a system. He is primarily concerned with high accuracy machine tools. Although Donaldson describes in some detail the various error sources that are important contributors, he does not discuss the

underlying mathematics needed to represent the geometry of multi-degree of freedom machines.

Several researchers have approached the problem of error modeling in machine tools with the specific purpose of compensating for the errors in an operational machine. Donmez et al. uses a homogeneous transform model based approach that includes geometric and thermally-induced error sources [Donmez '86]. In this research, calibration data are used to create an empirical error model which in turn is used in real time along with temperature sensors to compensate for errors in a turning center. Similarly, Teeuwsen, et al. describes a homogeneous transform model based approach that is used to compensate for geometric errors in a CMM [Teeuwsen '89].

Other researchers have also addressed the displacement error modeling problem in machine tools. For example, Shin and Wei, Soons et al., and Treib all use homogeneous transform based models of machines to describe errors in the machines [Shin '92], [Soons '92], [Treib '87]. Each of these works also uses statistical methods to help characterize the errors in machines.

#### 2.2.4.1.2 Displacement Error Modeling in Robotics

Displacement error modeling in robotics is similar to that in machine tools and CMMs. However, the geometry of robots is generally more diverse than that found in machine tools and CMMs. Paul thoroughly described the use of homogeneous transform matrices to describe the geometry of robots [Paul '81]. He also derived quantities for the derivative of a rotation and translation homogeneous transform (scaling and perspective operations were not included in this discussion because they are not needed to describe the kinematics of mechanisms). Paul's goal was the development of expressions relating end effector velocities and joint velocities in robots. However, the differential transformations he described are also useful for lumping errors in a machine's motion at the base of a coordinate frame in a homogeneous transform model of the machine. This approach is used later in the thesis for displacement error modeling and has been described by several other researchers.

The research presented by Eman et al. is representative of the homogeneous transform model based approach to error modeling in robotics [Eman '87]. In this research, the error contributions within the HTM model are manipulated so that they can be represented separately from the ideal geometric model. Furthermore, the error terms are separated into first and second order effects. This approach is in contrast to that used commonly to describe machine tools where the error terms are simply multiplied together with the other transformations and never explicitly separated [Donmez '86], [Slocum '92A]. Weill and Shani use an approach identical to Eman describing the mathematics of the displacement error model [Weill '91]. Furthermore, these researchers include the additional step of examining the relationship between standard geometric tolerancing and its contribution to the error in the machine. Similar to error modeling in machine tools, error modeling in robotics is targeted primarily at the metrology problem. Although many researchers describe error modeling for analysis of existing machines, few actually demonstrate the use of their techniques on real systems. Veitschegger and Wu are one of the few exceptions; they describe the use of error modeling to refine the geometric description of a PUMA 560 manipulator [Veitschegger '88].

Salisbury and Craig described how the condition number of a robot's Jacobian matrix[20] can be used to determine areas in a robot's work space were error propagation from joints to the end effector increases [Salisbury '82]. As the Jacobian becomes more ill-conditioned, the magnitude of velocity errors propagating to the end effector increases. This effect is discussed in the next section in relation to velocity and force transmission errors in multi-degree of freedom machines. However, Toyama et al. uses a simple approach to generating an error map of a robot's workspace by concentrating displacement error measurements in work space locations where the Jacobian is not well conditioned [Toyama '91].

[20] A robot's Jacobian matrix relates the velocity of each joint to the velocity of the end effector of the manipulator. The Jacobian is a function of a robot's geometry and changes values as the robot changes configurations.

#### 2.2.4.2 Velocity and Force Transmission Error Modeling

Research into velocity and force transmission error modeling has been considerably less popular than displacement error modeling. The techniques that are described in the literature are based on the condition number of the Jacobian matrix discussed above. Normally, the Jacobian matrix is used to relate joint velocities to end effector velocities and so the condition number gives some indication of the errors that propagate from the joints to the end effector. Because the Jacobian can also be used to relate joint torques to end effector forces in a static or quasi-static manner, the same basic technique is used to describe force/torque transmission. A number of researchers, including Chiu, Dubey and Luh, Klien and Blaho, and Van Doren have approached this problem in a similar manner [Chiu '87], [Dubey '88], [Klein '87], [Van Doren '92]. The results of these research efforts give a means to evaluate the relative magnitude of velocity and force/torque transmission errors. In general, these methods are only useful for identifying areas in a robot's workspace that will have larger errors than other regions.

### 2.2.5 Mechanical Design in Cleanrooms

Another area of research that is pertinent to this thesis is the mechanical technologies that are used specifically for robots and other mechanical systems in cleanrooms. Because cleanliness and high reliability are two of the most important functional requirements in cleanroom design, these are the areas that have been emphasized in the literature.

A number of researchers discuss particular implementations of cleanroom robots. Papanek describes the retrofitting of an AdeptOne™ SCARA-type robot for use in a Class 10 cleanroom [Papanek '87]. Some of the mechanical modifications required for this redesign were the application of non-contact labyrinth style seals in the revolute joints and the use of negative gage pressure in the internal cavities of the robot to evacuate any particles generated inside the robot. The arm was also painted with a two component polyurethane paint to reduce particle generation from the exterior surfaces of the robot. In a similar article, Stevens discusses the design of a 4 degree of freedom robot for use in a Class 10 cleanroom [Stevens '87]. This robot also used labyrinth seals in

rotary joints and negative gage pressure in the internal cavities of the robot to control migration of particles out of the manipulator. Additionally, both of these robots made use of internal routing of motor and sensor wires. Stevens also discusses the need to minimize turbulence, which can stir up particles, created by the robot. Roth and Schneider also discuss the design of a cleanroom robot [Roth '93]. These researchers used the following features in their robot: (1) a compact, aerodynamic body to reduce turbulence, (2) sealed rotary axes, (3) negative gage pressure inside the robot, and (4) an epoxy-enamel paint to reduce particle generation on the outer surfaces of the arm. Makino describes several commercially available Japanese cleanroom robots [Makino '90]. He suggests using features similar to those already described with the addition of using liquid magnetic seals in rotary joints. Also, Makino suggests using vacuum grease or fluorine containing grease for lubrication.

The second area of concern for cleanroom mechanical design is reliability. SEMATECH has published several documents dealing specifically with this topic [Dhudshia '93], [SEMATECH '92]. In the "Guidelines for Equipment Reliability," increasing reliability is presented as a continuous process that must be integrated with the life cycle of process equipment [SEMATECH '92]. This document presents a process of establishing reliability goals and requirements and evaluating whether or not these goals are being met starting in the concept and feasibility phase of a design process and continuing in the design phase, prototype development, pilot production, actual operation and production, and finally the phase out of the equipment. In "Design Practices for Higher Equipment Reliability," more specific attention is paid to the design process [Dhudshia '93]. Reliability requirements, parts selection, design simplification, the use of redundancy, protective design techniques, the minimization of external factors on a design, and the use of scheduled maintenance are all discussed in this document.

## 2.3 A Precision Machine Design Methodology for Semiconductor Process Equipment

As discussed in Chapter 1, the precision machine design methodology presented in this thesis gives a deterministic approach to the design of automation systems for semiconductor production equipment. The two primary components of the methodology, error modeling and a set of mechanical design rules, are explained further in the following sections.

### 2.3.1 Error Modeling

The numerical error modeling tools presented here contain elements to quantify the end effector position, velocity tracking, and force transmission characteristics of the mechanical positioning systems in question. The error modeling techniques developed in this thesis are intended for the design of systems and not the analysis of existing equipment The end effector displacement portions of these numerical modeling tools are based on homogeneous transform models of the mechanical positioning systems. This system geometry-based numerical tool, which shares similarities with the error budgets and error analysis used by other researcher mentioned above, makes use of the conventions of Denavit and Hartenberg [Denavit '55] for describing the kinematics of three dimensional mechanical systems. This spatial model of the system is used to generate matrices of error gains that allow a designer to determine the effect of various errors on the end effector of that system. Similarly, Jacobian matrices, which are derived from closed form expressions for the end effector position written in terms of positions of each of the axes in the mechanical system, are used to obtain information about the propagation of velocities and forces from each input in the system to the end effector. The error modeling tools for velocity and force effects result in errors gains (similar to the displacement error modeling tools) unlike the methods of other researchers mentioned above. The combination of the numerical models for quantifying errors in end effector position, velocity, and force outputs form the basis of a design tool that may be used in guiding the design of semiconductor wafer handling systems as well as other mechanical systems.

The position-based part of the numerical error models forms the central portion of the modeling work. The homogeneous transform model of the system is useful in determining the effects of specific errors on the end effector or any other output location that may be of interest. For completeness, the numerical model is complimented with additional information regarding the possible error sources in the system. These errors are categorized as follows:

1. Geometric errors including form, straightness, parallelism, and orthogonality resulting from both manufacturing and maintenance irregularities.

2. Mechanical errors such as backlash and compliance in structures, bearings, transmissions, and actuators.

3. Control system errors including the following: (a) sensor effects such as accuracy, repeatability, hysteresis, and calibration (b) effects from the control algorithm such as possible following errors in trajectory tracking and (c) actuator and transmission effects such as bandwidth and amplifier or actuator saturation.

4. Dynamic errors resulting from rotational imbalance, inertial loading, and various noise sources.

5. Thermally induced errors (in especially sensitive cases) including thermal deformations, warping, and bending induced by differential thermal expansion/contraction caused by temperature gradients in a machine.

Because the primary interest in this thesis is developing repeatable positioning systems by improving the design of both structures and mechanisms, the errors contributing to performance degradation are further subdivided into two categories. These categories are (1) repeatable errors and (2) nonrepeatable errors (but, not random). The first category can be described as errors that lead to absolute position errors at the end point a mechanism. The second category include effects such as mechanical drift, slop due to non-preloaded bearings, hysteresis, and backlash in transmission systems.

The error modeling tools will help designers separate these different effects. Using an error model, the designer can minimize repeatable errors and eliminate nonrepeatable errors as needed to achieve the performance goals of a design.

### 2.3.2 Mechanical Design Rules

The second portion of the research describes mechanical design rules that may be used in conjunction with the error modeling techniques described above to form the basis of this new mechanical design methodology for wafer handling systems in semiconductor manufacturing equipment. The following areas have been identified as important for this type of design:

1. Deterministic design
2. Elastic averaging
3. Reduction of the effects of rotational errors
4. Static and dynamic structural deformation
5. Control and mechanical system integration
6. Considerations for cleanroom equipment design.

These six areas are briefly explained here and are more thoroughly discussed in Chapter 4.

Deterministic design as developed by other researchers was presented in Section 2.2.2. In the context of the design of semiconductor manufacturing equipment, the principles of deterministic design can be used to guide the development of structures, the selection of repeatable and robust attachment methods, and the design of wafer handling systems. To avoid any more repetition of these thoughts, further discussions of deterministic design are delayed until Chapter 4.

Elastic averaging is a complimentary design technique as compared to deterministic methods. This approach to design relies on extensive over-constraint or forced geometric congruence between mechanical parts. This overconstraint should be viewed in contrast to the areas of point contact found in kinematic couplings. Elastic

averaging is a technique that finds wide application in the design of joints and bearings and understanding this principle is important for the machine designer.

The Abbe error principle refers simply to the amplification of angular errors by a moment arm [Bryan '79]. A common example used to describe this principle is the layout of a micrometer and a set of dial calipers. In the micrometer, the measurement occurs along the same axis as the dimension being measured. In a set of dial calipers, the measurement is offset by the length of the jaws. Thus, in the calipers any angular error of the jaws relative to the base results in an Abbe error. In general, the effects of angular errors can and should be minimized by reducing or eliminating moment arms in the design of moving axes in machines. Because of other constraints in a design, it is not always possible to avoid Abbe errors. However, if the designer is aware of the presence and effects of these errors, they can be carefully accounted for in an error model of the system; thereby allowing for the creation of a successful design.

In addition to the design techniques discussed above, the use of sufficiently stiff, well-damped machine structures will greatly benefit the performance of machines used in the semiconductor manufacturing industry. A graphic example of an overly compliant structure was observed while testing a cassette and SMIF pod[21] intrabay transfer robot [Slocum '93A]. The robot performed well and was within it's specified ±0.05 mm repeatability. However, as much as ±0.8 mm of deflection at the end effector was caused by deformations of the cleanroom floor tiles adjacent to the measuring location that resulted from a person shifting his/her weight on the floor. As a result of the testing performed in the cleanroom, a serious concern arose regarding the ability of the system to position payloads accurately and repeatably at a target location in the presence of fab personnel who may be moving around the machines. This problem is a result of the cleanroom floor design and certainly was not within the control of the robot designers. However, the performance of the design is affected by all system components and in this case the floor was a significant contributor to positioning inaccuracies. Other examples of compliant, under damped systems have been observed in cassette handling

[21] Standard Mechanical Interface. A SMIF pod is a completely enclosed box containing a controlled environment used to transfer cassettes of wafers.

mechanisms. Fundamental modes of approximately 4 Hz have been measured and were plainly visible to even the most casual observer [Slocum '92F].

Precision machine design includes not only the mechanical technologies commonly thought of when discussing machine design, but also the design and integration of the control systems used to successfully operate process tools. The mechanical and control systems cannot be viewed independently; an integrated, system-level approach coordinating mechanical and control system design will insure that maximum performance is achieved. The previously mentioned design reviews showed many instances where a simple PID control system was implemented and tuned without any modeling or knowledge of system parameters only after the mechanical system had been designed and built [Slocum '92C], [Slocum '92D], [Slocum '92E], [Slocum '92F]. [Slocum '93A], [Slocum '93B]. In at least one case, this type of approach resulted in additional mechanical design changes that may have been avoided [Slocum '92F].

A number of cleanroom considerations and their effects have already been discussed in Chapter 1. However, from a design stand point two primary concerns must be addressed. First, the machine must be clean and more importantly it must not contaminate the wafers being processed. The cleanliness requirement is especially important for wafer handling automation because these systems repeatedly handle the wafers and can potentially be a large source of contamination. Second, because of the expense of cleanroom floorspace, the manufacturing equipment must be very compact. The requirement for a small footprint has a large impact on how all of the systems in a machine function and are packaged. Typically, a semiconductor manufacturing system contains a large amount of support equipment. Packaging requirements for this equipment can also have a large effect on the design of the machine structural frame. Additionally, the size of wafer handling robots must be minimized. As will be shown later in the thesis, these size requirements can sometimes dramatically effect the system's design.

Another area that will not be considered in depth in this thesis, but deserves some mention, is the effect of temperature within machines, especially those that require high

precision. Thermal effects can cause many types of errors that are often overlooked in the design of a machine [Slocum '92A]. These effects are produced by temperature gradients and/or the varying coefficients of expansion of materials used in a machine. Heat can be introduced into a machine from many sources including electronics, actuators, and even overhead lights and technicians working near a machine. Many of these effects will not be present in a cleanroom because of the temperature control and laminar flow of air. However, other sources may still cause difficulties. Thermal effects probably will not be a serious concern for a material handling system with ±0.025 mm repeatability. However, the effects will certainly be important in a wafer stepper where submicron positioning resolution is required.

## 2.4 Summary

This chapter presented additional background for and a more detailed explanation of the precision machine design methodology. The work of researchers in pertinent areas was discussed briefly. First, design theory and design methodologies of other researchers were presented. Next, deterministic design and kinematic couplings were discussed. Then the error modeling and clean room mechanical design techniques from the literature were discussed. Finally, the chapter described the error modeling and mechanical design techniques developed in this thesis.

# Chapter 3: Error Modeling in Precision Machines

## 3.1 Introduction

Error modeling is the central concept in the precision machine design methodology presented in this thesis. When designing any precision mechanical system composed of revolute and prismatic joints where a tool position or end effector position must be achieved accurately or repeatably, the construction of an error model may be useful. The error model allows the designer to allocate errors in the system such that every component in a machine can be designed to perform as required to achieve the desired accuracy and repeatability. It should be noted that error models are intended to be used both as tools to assist in guiding the design of a system based on required performance and as analysis tools to be used in evaluating the performance of existing systems.

The error model is a design tool that can be used throughout the design process to manage the development of a design. Once a design problem has been properly formulated, geometric error models are useful in defining the geometry of conceptual designs and performing preliminary analysis of a design concept's ability to satisfy the motion-related functional requirements of the problem. After the selection of a concept, the error model can guide the embodiment design phase. In this design stage, the error model provides a means to select components to use in the design and to evaluate their contribution to the performance of the system. Even after the design has been completed, the error model can be used in evaluating the actual performance of a system. If problems are encountered, the error model may prove useful in determining the source of the difficulties and selecting a means to eliminate the problem.

This chapter begins by presenting displacement error modeling. The displacement techniques are based on the work of other researchers, but the techniques have been extended and modified here for the design problems found in semiconductor

manufacturing equipment. First, the mathematical background for the homogeneous transform-based displacement error model is discussed. Next, the chapter introduces the construction of the geometric model for specific systems along with the calculation of *error gains* that quantify the effect of particular errors. Then, sources of errors are categorized and the inclusion of these errors in the error model is explained. The chapter continues with the presentation of a new error modeling technique for the transmission of velocity or force/torque errors to the end point of a mechanism. The mathematical foundation for the velocity/force error model is given along with an explanation for the calculation of error gains. The chapter also contains a discussion of a working error model for a machine frame and integral wafer handling robot from SVG's Accipiter design project to further illustrate error modeling. Data from testing of the wafer handling robot prototype is also included in the error modeling case study.

## 3.2 The Displacement Error Model

Displacement error models have been developed in a variety of forms by different researchers, as was discussed in Chapter 2. Much of this work has been devoted to quantifying errors in machines after they have been designed and built. Also, machine tools are frequently the subject of these other researchers. In metal cutting operations, large loads and temperature effects are often encountered and must be accounted for in an error model. By contrast, the conditions found in semiconductor manufacturing are very different and error modeling must account for these differences. In handling wafers in a cleanroom, no large disturbance forces are encountered. Furthermore, cleanrooms are temperature controlled and wafer handling mechanisms have relatively small power requirements, so little heat is dissipated. Additionally, machine tools typically have six or fewer controlled degrees of freedom. A typical process tool might have an order of magnitude more degrees of freedom.

In this chapter, displacement error modeling is applied specifically to the systems found in semiconductor manufacturing systems. Methods are presented to model the large number of degrees of freedom in a system. Also, the error modeling techniques

discussed here are geared toward achieving the repeatable performance (rather than highly accurate performance) required of most semiconductor wafer handling systems. In this error modeling, sources of nonrepeatability are of primary importance in the displacement error model. Additionally, the system error model can be used to help define the functional requirements of various subsystem designs. For example, the error model can set goals for the maximum allowable deformations in a machine's frame[22]. Furthermore, the system error model will give positioning repeatability requirements for a machine's wafer handling mechanisms based on the total required positioning repeatability and error contributions from other sources. The error model will also help a designer select the method for attaching process modules to a machine frame and determine whether additional positioning adjustments can be avoided.

The actual construction of the error model is composed of two major steps: first, the system geometry and kinematics are defined using homogeneous transform matrices (HTM's), and second, the errors that may be present in each of the joints and links of the system are systematically examined and quantified. The homogeneous transform model of the system geometry is used to create a matrix of error gains or sensitivities that explicitly quantify how errors are magnified and propagate through a machine. Generally, the HTM model can be created in a single stand alone spread sheet. Next, the errors in the system must be appropriately modeled. These errors can be divided into categories such as geometric errors, mechanical errors, control system errors, dynamic errors, and thermally induced errors. Spreadsheets for each type of error can be linked to the HTM model to easily create the complete error model. For example, if bearing and structural compliances are known for a machine, the HTM model can be used to find deformation errors induced by external loading (e.g., from a payload or some disturbance forces) in a machine The matrix of error gains can then be used to find the accumulated effects of all significant errors at the end effector of the system in question.

[22] In this manner, the error model indirectly specifies the required stiffness of the machine frame.

### 3.2.1 Homogeneous Transforms

Homogeneous transforms are 4x4 matrices used to transform position and orientation information in three dimensional space from one coordinate system to another. Equation 3.1 shows the general form of an HTM between the (*i-1*) and (*i*) coordinate frames.

$$ {}^{i-1}T_i = \begin{bmatrix} r_{11} & r_{12} & r_{13} & p_x \\ r_{21} & r_{22} & r_{23} & p_y \\ r_{31} & r_{32} & r_{33} & p_z \\ 0 & 0 & 0 & 1 \end{bmatrix} \tag{3.1} $$

The upper 3x3 portion of the HTM is a rotation matrix between the (*i-1*) and (*i*) frames and the first three elements of the fourth column are the corresponding translations in position. This translation is simply the displacement vector between the origin of coordinate frame (*i-1*) and frame (*i*).

A number of methods exist, such as Euler angles and the unit quaternion, for representing rotation. For this work, simple fixed angles, which are often called roll, pitch, and yaw are used. Equation 3.2 gives the rotation matrix for a rotation about the x axis. Similarly, Equations 3.3 and 3.4 give y and z axis rotation matrices respectively.

$$ R_x = \begin{bmatrix} 1 & 0 & 0 \\ 0 & Cos\theta_x & -Sin\theta_x \\ 0 & Sin\theta_x & Cos\theta_x \end{bmatrix} \tag{3.2} $$

$$ R_y = \begin{bmatrix} Cos\theta_y & 0 & Sin\theta_y \\ 0 & 1 & 0 \\ -Sin\theta_y & 0 & Cos\theta_y \end{bmatrix} \tag{3.3} $$

$$ R_z = \begin{bmatrix} Cos\theta_z & -Sin\theta_z & 0 \\ Sin\theta_z & Cos\theta_z & 0 \\ 0 & 0 & 1 \end{bmatrix} \tag{3.4} $$

Rotations are not vector quantities and the order in which rotations are performed must be properly accounted for when multiplying individual rotation matrices together[23]. Equation 3.5 gives the equivalent rotation matrix for a rotation about the X axis followed by a rotation about the Y axis followed by a rotation about the Z axis.

$$R_{xyz} = \begin{bmatrix} Cos\theta_z Cos\theta_y & Cos\theta_z Sin\theta_y Sin\theta_x - Sin\theta_z Cos\theta_x & Cos\theta_z Sin\theta_y Cos\theta_x + Sin\theta_z Sin\theta_x \\ Sin\theta_z Cos\theta_y & Sin\theta_z Sin\theta_y Sin\theta_x + Cos\theta_z Cos\theta_y & Sin\theta_z Sin\theta_y Cos\theta_x - Cos\theta_z Sin\theta_x \\ -Sin\theta_y & Cos\theta_y Sin\theta_x & Cos\theta_y Cos\theta_x \end{bmatrix} \tag{3.5}$$

Equation 3.5 can be calculated from Equations 3.2, 3.3, and 3.4 by starting with Equation 3.2 (the first operation), premultiplying this by Equation 3.3 (the second operation), and finally premultiplying the result by Equation 3.4.

Adding additional coordinate frames to a serial kinematic chain is a straight forward procedure. As a new frame is added, the HTM from the preceding frame can be derived. Transformations from frames farther back in the chain can be calculated by multiplying multiple HTM's together. For example, Equation 3.6 shows how a transformation from frame $(i\text{-}1)$ to frame $(i+1)$ can be calculated.

$$^{i-1}T_{i+1} = {}^{i-1}T_i \, {}^{i}T_{i+1} \tag{3.6}$$

Figure 3.1 shows how these three reference frames might be located spatially. Multiplying together individual HTM's allows a designer to create a geometric model of virtually any system.

[23] That is, rotations are not commutative.

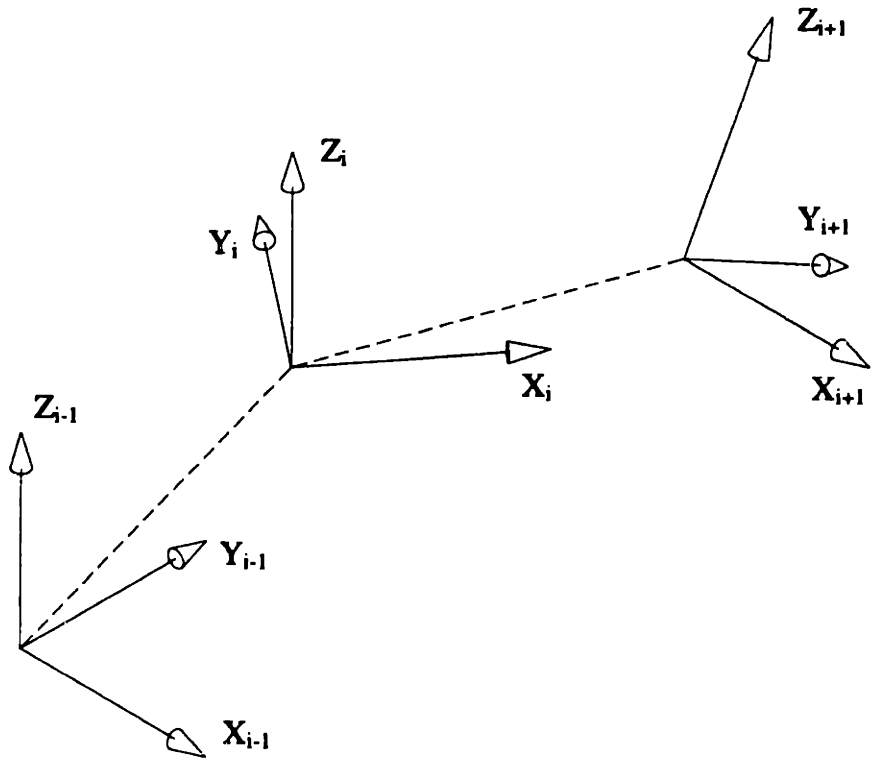


**Figure 3.1** Example coordinate frames.

### 3.2.2 Construction of the Displacement Error Model

The first step in creating a displacement error model of a system is creating a model of the system geometry. For this work, serial kinematic chains, such as the one shown in Figure 3.1, are used to model all aspects of a system's geometry. Equation 3.7 gives the ideal representation of the geometry of a serial chain modeled with $n$ coordinate frames.

$$ {}^{0}T_n = \prod_{i=1}^{n} {}^{i-1}T_i \tag{3.7} $$

In general, both translational errors and rotational errors will be lumped at the base of each successive coordinate frame to represent the errors between the actual and ideal geometry of a system.

Equation 3.8 shows how the actual transformation from frame ($i$-$1$) to frame ($i$) is defined in terms of a differential error, $dT_i$, lumped at the base of coordinate system ($i$).

$$ {}^{i-1}T_i^a = {}^{i-1}T_i + dT_i \tag{3.8} $$

Lumping errors at the base of a coordinate frame follows from Paul's definition of differential translational and rotational operations used in developing robot kinematics [Paul '81]. Equation 3.9 defines the differential error in terms of an error matrix and the transformation matrix.

$$ dT_i = T_i * \delta T_i \tag{3.9} $$

where the error matrix, $\delta T_i$, post multiplies the transformation matrix because the errors are written with respect to the ($i$) frame. Equation 3.10 defines this error matrix in terms of rotational and translational error components.

$$ \delta T_i = \begin{bmatrix} 0 & -\varepsilon_z & \varepsilon_y & \delta_x \\ \varepsilon_z & 0 & -\varepsilon_x & \delta_y \\ -\varepsilon_y & \varepsilon_x & 0 & \delta_z \\ 0 & 0 & 0 & 0 \end{bmatrix} \tag{3.10} $$

where the $\varepsilon$'s are differential rotational errors about the labeled axes and the $\delta$'s are differential translational errors as shown in Figure 3.2. It should be noted that unlike finite rotations, differential rotations are vector quantities and the order of the rotation operation is not important. By substituting Equation 3.9 into Equation 3.8 and performing some simple manipulation, Equation 3.11 can be obtained.

$$ {}^{i-1}T_i^a = {}^{i-1}T_i(I + \delta T_i) \tag{3.11} $$

Equation 3.11 defines the actual transformation in terms of the ideal transformation and any errors that may be present in the system.

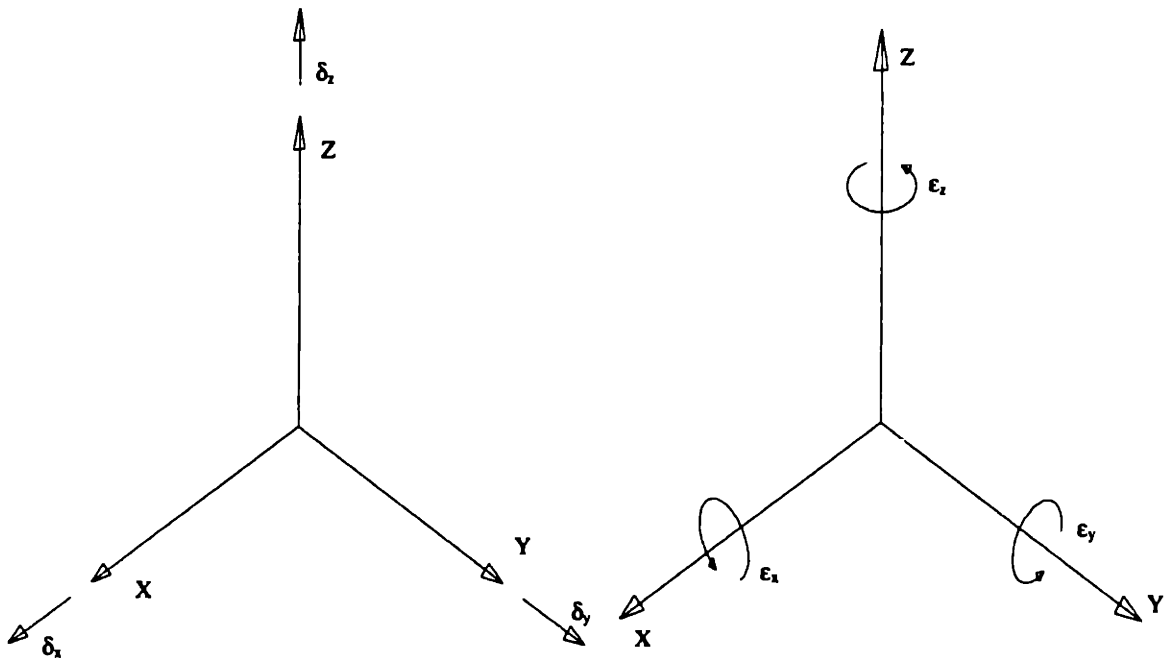


**Figure 3.2** Definition of differential errors.

Now the actual geometric model for a system can be formulated in terms of the ideal transformations and corresponding error matrices as shown in equation 3.12.

$$ {}^{0}T_n^a = \prod_{i=1}^{n} {}^{i-1}T_i * E_i \tag{3.12} $$

where the new error matrices are defined in Equation 3.13, which is the sum of the identity matrix and the matrix in Equation 3.10.

$$ E_i = \begin{bmatrix} 1 & -\varepsilon_z & \varepsilon_y & \delta_x \\ \varepsilon_z & 1 & -\varepsilon_x & \delta_y \\ -\varepsilon_y & \varepsilon_x & 1 & \delta_z \\ 0 & 0 & 0 & 1 \end{bmatrix} \tag{3.13} $$

Interestingly, if small angle approximations are used in the general HTM given in Equation 3.14, the result simplifies to Equation 3.13.

$$E_i = \begin{bmatrix} Cos\varepsilon_z Cos\varepsilon_y & Cos\varepsilon_z Sin\varepsilon_y Sin\varepsilon_x - Sin\varepsilon_z Cos\varepsilon_x & Cos\varepsilon_z Sin\varepsilon_y Cos\varepsilon_x + Sin\varepsilon_z Sin\varepsilon_x & \delta_x \\ Sin\varepsilon_z Cos\varepsilon_y & Sin\varepsilon_z Sin\varepsilon_y Sin\varepsilon_x + Cos\varepsilon_z Cos\varepsilon_y & Sin\varepsilon_z Sin\varepsilon_y Cos\varepsilon_x - Cos\varepsilon_z Sin\varepsilon_x & \delta_y \\ -Sin\varepsilon_y & Cos\varepsilon_y Sin\varepsilon_x & Cos\varepsilon_y Cos\varepsilon_x & \delta_z \\ 0 & 0 & 0 & 1 \end{bmatrix} \tag{3.14}$$

If Equation 3.12 is expanded with explicit terms for each of the errors in the error matrices, a result given by Equation 3.15 is obtained.

$$^0T_n^a = {}^0T_n + \sum_{i=1}^{n} V_i \tag{3.15}$$

where $V_i$ comes from explicit expansion of error terms. This result is the same as that derived by other researchers [Eman '87]. This formulation is useful for metrology purposes, when end point errors are measured and information about individual axes' errors is desired. The explicit nature of the $\sum_{i=1}^{n} V_i$ term gives some means to back out this information (this is by no means a simple problem).

For error modeling in design, the actual geometric model given by Equation 3.12 serves as the basis. After the system geometry has been defined and the appropriate error matrices have been placed at each coordinate frame base, the designer proceeds by calculating error gains for each error in the system. This process is typically performed numerically in a spreadsheet or other convenient mathematics software package. Before calculating the gains it is important to note the following: The gain for a translational error on the translational error in the same direction at the end point is always 1. Similarly, the gain for a rotational error on the rotational error in the same direction at the end point is always 1. Also, a translational error never affects a rotational error at the end point; so, the gain is always 0. Only rotational errors result in error sensitivities other than 1 or 0 when the effects of these errors on translational errors at the end effector are considered. This effect is known as an Abbe error. Detection and avoidance of large Abbe errors is one of the primary benefits of error modeling.

To find the error gains for each rotational error, each joint is treated individually by substituting zero values for all other error terms at that joint and at the other joints. To calculate the error gain for a particular error, a small nominal value is used for the error. With this single error, the difference between the actual end point and the ideal end point is calculated. A rotational error will affect the three translational components of the end point location. The error gain is calculated by dividing the resultant position errors by the nominal rotational error. This gain represents purely the geometric effect of individual errors on the end point position. This process is repeated for each rotational error at each coordinate frame origin[24]. The resulting error gains can then be used as multipliers for the actual errors to find their effect on the end point of the system. Although multiplying the error gains with the actual errors will result in a measure of the total system error, the error gain itself is an important metric for the designer. The magnitude of the error gain gives the designer a measure for the error magnification created by the geometry of a particular system. The designer can often minimize these error gains to reduce the resultant end point error for a given component error in an isolated portion of the system.

As was stated previously, serial kinematic chains are used to model all aspects of a system's geometry. Some systems are not completely serial in nature; however, using a serial chain does not limit the application of the technique. Parallel systems can also be modeled with a serial chain representing each portion of the parallel system. The connection point between individual serial chains within the parallel structure will impose geometric constraints on the system resulting in a more complex model that usually must be treated on an ad hoc basis. (Equation 3.16, below, can be used to determine what these geometric constraints are.) Even if a system is composed only of serial chains, these chains often interact and this interaction must be modeled. As long as each serial chain has the same base reference frame, the interaction can be easily modeled. For example, the point at which a wafer handling robot picks up a wafer from a process module represents an interaction between the geometry used to model the machine frame and process module and the geometry used to model the wafer handling mechanism. If there are no errors in either the robot or the frame, then the transformation from the base

[24] This procedure makes it clear why a spreadsheet is useful to perform these operations automatically.

frame to the robot's end effector, ${}^{0}T_{endeffector}$, and the transformation from the base frame to the process module, ${}^{0}T_{processmod}$, will be identical. In general, there will be errors and a transformation matrix between the end point of the robot and the end point of the process module will represent the difference in the position of the two kinematic chains. Equation 3.16 gives a representation for this intermediate transformation.

$$ {}^{endeffector}T_{processmod} = {}^{0}T^{-1}_{endeffector}\,{}^{0}T_{processmod} \tag{3.16} $$

The upper 3x3 of this intermediate transformation will give the direction cosines for the orientation errors between the robot end effector and the process module. The first three elements of the 4th column will give the translational errors.

### 3.2.3 Assignment of Coordinate Frames

Having established the mathematical foundation for displacement error modeling, the proper formulation of an error model requires that coordinate frames be assigned in appropriate locations. The most direct means to build a displacement error model is to assign a base reference frame at a convenient location in the system, a single coordinate frame for each rigid body in a serial chain, and a final reference frame at the end point of the chain. To account for multiple chains in a single system, the base reference frame should be the same for each chain.

Although the error model can be formulated with virtually any frame assignment, a thoughtful choice will greatly simplify the modeling process. Different approaches may be used for design models and metrology models. A system designer probably will choose to assign coordinate frames in a kinematically convenient manner. Additionally, the designer will assign coordinate frames to facilitate predictive modeling of errors in the system. Conversely, an error model constructed for measuring errors in an existing system will often contain coordinate frames located on parts of a machine where actual measurements can be made. This arrangement of frames allows measured data to be used directly in the analysis error model.

The following two sections present two favored methods for assigning coordinate frames. The first approach is based on the kinematic description for a system originally developed by Denavit and Hartenberg [Denavit '55]. The second approach assigns coordinate frames at the centers of compliance in a machine to ease the assignment of structural deformation-related translational errors at the coordinate frame base.

### 3.2.3.1 Denavit and Hartenberg Parameters

The assignment of coordinate frames in machines with only orthogonal linear axes of motion, as is often the case in machine tools, is straightforward because all frames can be assigned parallel to one another. For systems containing revolute axes, as is often the case in semiconductor processing equipment, the frame assignment procedure can be more complex because the relative orientation of reference frames changes as revolute axes rotate. Denavit and Hartenberg's notation has developed into a standard form for applying homogeneous transforms to serial mechanism. Several, forms of this convention, which differ only in small details, exist and that described by Craig is used in this thesis [Craig '89]. Furthermore, the procedure works with the revolute and prismatic (or translational) *lower pair* joint types. Higher order joints such as cylindrical, planar, spherical, and helical joints can be modeled as combinations of lower pair joints. For example, a cylindrical joint is simply a revolute and a prismatic joint acting about the same axis; a planar joint is simply two orthogonal prismatic joints; a spherical joint is three revolute joints with joint axes intersecting at a point; a helical joint is identical to the cylindrical joint except a constraint relates the linear and rotary motion.

The Denavit and Hartenberg method allows some choice in frame location, but a set of rules governs the assignment procedure so that a kinematically efficient set of frames results. The frames are assigned such that the Z axis points along the joint axis whether it is revolute or prismatic[25]. The frame origin is assigned at the intersection of the common perpendicular between the next distal joint axis and the joint axis in question. Next, the X axis is assigned so that it points along this common perpendicular.

[25] For a linear joint, the Z axis points along the line of motion. For a revolute joint, the Z axis points along the line about which the axis rotates.

Supplementary details can be found in Craig. Psuedo-joints, with no movement, can be also be assigned in a kinematic chain to account for special geometries.

To complete the description of the system geometry, four parameters per joint are assigned. These parameters are commonly called the Denavit and Hartenberg parameters, or simply DH parameters. The twist angle, $\alpha_i$, is the angle between $Z_i$ and $Z_{i+1}$ measured about $X_i$. The link length, $a_i$, is the distance from $Z_i$ to $Z_{i+1}$ measured along $X_i$. The link offset, $d_i$, is the distance from $X_{i-1}$ to $X_i$ measured along $Z_i$ and is the joint displacement for an axis with a prismatic joint. The joint angle, $\theta_i$, is the angle between $X_{i-1}$ and $X_i$ measured about $Z_i$ and is the joint displacement for a revolute axis.

Using the references frames and DH parameters assigned above, the homogeneous transform matrix from frame (*i-1*) to (*i*) can be found simply by applying Equation 3.17.

$$ {}^{i-1}T_i = \begin{bmatrix} Cos\theta_i & -Sin\theta_i & 0 & a_{i-1} \\ Sin\theta_i Cos\alpha_{i-1} & Cos\theta_i Cos\alpha_{i-1} & -Sin\alpha_{i-1} & -Sin\alpha_{i-1} d_i \\ Sin\theta_i & Cos\theta_i Sin\alpha_{i-1} & Cos\alpha_{i-1} & Cos\alpha_{i-1} d_i \\ 0 & 0 & 0 & 1 \end{bmatrix} \qquad (3.17) $$

The homogeneous transform in Equation 3.17 is derived simply by multiplying HTM's for a rotation about the $X_i$ axis ($\alpha_{i-1}$ twist angle), translation along the $X_i$ axis (link length, $a_{i-1}$), rotation about the $Z_i$ axis (joint angle, $\theta_i$), and finally translation along the $Z_i$ axis (link offset, $d_i$).

If the Denavit and Hartenberg approach is used in assigning coordinate frames, the geometric model of the system will be relatively easy to construct because the basic form of the HTM between each frame is already known. In fact, all that is required to change the geometric model is the adjustment of the appropriate DH parameters. This method is straightforward and requires no modification for use in the error modeling design tool described in this thesis.

It should be noted that the use of the DH parameter method for the metrology problem can result in complications as pointed out by several researchers [Hayati '83], [Veitschegger '86]. For metrology purposes, difficulties may arise when consecutive

joints are nearly parallel. In these cases, determining DH parameters from the HTM model can be difficult because of numerical ill conditioning of the matrices. The problem is solved by adding a fifth parameter to nearly parallel joints to account for the small variations in parallelism. This fifth parameter is not required for the design problem where end effector errors are estimated based on nominal DH parameters and errors lumped at each joint.

#### 3.2.3.2 The Center of Compliance Method

If angular errors occur within a system about a point other than the base of a coordinate frame, an Abbe error will result. This would be the case, for example, if a coordinate frame were assigned to one end of a rigid body and rotational errors were occurring about another location within that rigid body. In this case, the translational error components would have to include the resulting Abbe error[26]. These angular errors can come from a variety of sources. Manufacturing errors and thermally induced errors are two possibilities. Structural deformation errors are a third source that may dominate these angular errors.

For systems where compliance-related angular deformations are significant, the error model may be simplified by placing the coordinate frame at the center of compliance for the axis of interest. In this manner, the angular errors created by deformations in the system will not contribute to the translational errors at the local coordinate frame base. Determination of the center of compliance for linear or rotary joints is usually not difficult if only bearing compliances are considered. Other angular errors may still have Abbe error components for which some accounting must be made.

Using the center of compliance method of assigning coordinate frames is usually desirable when loading in the system creates significant deformations that dominate other types of angular errors. Because assigning frames according to the center of compliance method can be a labor intensive undertaking[27], it should only be used where appropriate.

---

[26] Abbe errors occurring between different rigid bodies in a kinematic chain are accounted for by the HTM model of the system geometry.

[27] First, the center of compliance of each frame must be calculated and next, HTM's between frames must formulated according to the system geometry.

In general, the types of systems found in semiconductor manufacturing do not suffer from deformations as the primary source of errors because larger external forces are not encountered. Therefore, for most systems, the convenience of the Denavit and Hartenberg method is preferable. Also, depending on the geometry of a particular system, the Denavit and Hartenberg method of assigning coordinate frames may allow frame assignment at or near the center of compliance.

### 3.2.4 Error Sources

After constructing the geometric model of a system, a designer can continue the predictive displacement error modeling process by including estimates of the various errors that will contribute to the total error at the end point of the system of interest. These errors can be categorized according to the source of the inaccuracy as follows:

1. Geometric
2. Mechanical
3. Control system
4. Dynamic
5. Thermally induced.

Identifying the source or cause of an error is useful in the design process because the designer will be better able to reduce the effects of unwanted errors. Furthermore, the various contributions to total system errors can be analyzed individually using the displacement error model. For the metrology problem, it may also be useful to categorize errors. However, actually determining the contributions of various error sources to system performance requires a careful approach under controlled conditions.

#### 3.2.4.1 Geometric Errors

Geometric errors can generally be described as inaccuracies in the components that make up a system. These errors include form, straightness, parallelism, and orthogonality errors. These types of errors may result from manufacturing, assembly, or even maintenance irregularities. If it were possible to manufacture and assemble

components exactly according to design specifications, geometric errors would be virtually nonexistent. Of course, these errors are unavoidable. A designer must be aware of their sources and magnitudes. Many design parameters such as material choice and manufacturing methods will also affect the existence and magnitudes of geometric errors.

#### 3.2.4.2 Mechanical Errors

Mechanical errors are closely related to geometric errors, but this category includes errors that are dependent on the static or quasi-static mechanical performance of a particular component. Mechanical errors include effects such as deformations due to compliance, backlash, or mechanical hysteresis. Displacement errors caused by compliance in mechanical components are common in structures or structural parts, bearings, and mechanical transmissions. Backlash or hysteresis errors are common in mechanical transmissions[28]. Hysteresis may also be encountered in the performance of particular types of bearings.

#### 3.2.4.3 Control System Errors

Control systems and their associated electronics often contribute significant errors to servo-controlled positioning systems. This category includes contributions from several sources such as a system's sensors, actuators, power amplifiers, and even control algorithm type. Sensor effects include characteristics of particular sensors such as accuracy, repeatability, hysteresis, and calibration (or lack of calibration). Actuators and amplifiers can also contribute to errors depending on their particular operational characteristics. These elements must be selected and sized for the requirements of the system of interest. An improper control algorithm can also cause following errors in trajectory tracking, end point positioning errors, overshoot, and even instabilities in system performance. Unmodeled system dynamics may mean that certain control algorithm types are inappropriate. Also, the proper algorithm can be improperly tuned or may go out of tune because of system changes caused by aging and wear.

[28] Even so-called "zero backlash" transmissions usually contain a small amount of backlash or hysteresis.

#### 3.2.4.4 Dynamic Errors

Dynamic errors refer to the vibrations encountered in virtually all mechanical systems. These types of errors also result from the mechanical construction of a system, i.e. the damping and compliance characteristics of the system as well as the distribution of system inertia. Vibration may result from imbalance of rotating members, inertial loading, and background excitation. The control system may also be a source of dynamic errors in a system. Again, sensors, actuators, amplifiers, and control algorithms can contribute to vibrations induced by the servo loops in a positioning system. An improperly tuned control system may result in unwanted transient responses and system overshoot. Conversely, a sophisticated control system may actually be able to reduce levels of vibration in a system. Chapter 4 contains a more detailed discussion of dynamic effects.

#### 3.2.4.5 Thermal Errors

Thermal errors include thermal deformations, warping, and bending induced by differential thermal expansion or contraction caused by temperature gradients in a machine. Gross changes in the temperature of a machine environment can cause parts with high coefficients of thermal expansion to expand or contract significantly. However, cleanroom manufacturing environments are temperature controlled, so environmental temperature changes are unlikely to cause changes. Temperature gradients caused by heat sources such as actuators or amplifiers are a more likely source of errors. With the levels of repeatability required for wafer positioning in most process tools, thermal effects will not be significant unless a particularly large temperature gradient is introduced into the system. The precision positioning stages used in wafer steppers are one example of process tools where temperature effects are important because of the high degree of precision required.

### 3.2.5 Inclusion of Error Sources in the Error Model

During the design of a machine, complete descriptions of error sources and magnitudes in a particular system cannot be generated. It is necessary to model the system as accurately as is feasible and required given system repeatability goals. Some

error information may be available from past tests or manufacturers' data. Other numerical data may be calculated with finite element methods or analytical models. Still other error data may have to be estimated based on the designer's knowledge of the system and experience dealing with similar systems.

Once error data for all of the individual errors in the system has been generated, the designer must use the error gains calculated from the geometric model of the system to determine the effect of each error on the end point in the system. Finally, the designer must address the question of how each of the equivalent end point errors should be combined to determine the total end point error. Several other researchers have previously addressed this question and the methods described here follow their work [Donaldson '80] [Slocum '92A].

Broadly stated, errors can be categorized in two groups: systematic errors and random errors. Errors categorized as systematic are generally attributed to a well understood source and their direction and magnitude can be easily predicted based on knowledge of the state of the system. Therefore, these errors are easily accounted for in the system error model. For systematic errors, the total error value is found simply by adding up the individual errors as shown in Equation 3.18.

$$\varepsilon_{systematic,tot} = \sum_{i=1}^{N} \varepsilon_{systematic,i} \tag{3.18}$$

Errors categorized as random, on the other hand, are less thoroughly understood. As was discussed in Chapter 2, these errors are not truly random. Rather, the exact cause of the errors has not been established based on the level of system understanding. For random errors, some means must be used to place bounds on the magnitude of the errors. Also, because the temporal and spatial distribution of these errors is not fully known, the frequency characteristics must also be accounted for. Depending on the particular error, different distributions may be used to describe the error. For example, a pure sinusoidal wave form, a Gaussian distribution, or a uniform probability distribution may be appropriate. The magnitude of the error may be described with root-mean-squared

(RMS) values or peak-to-valley (PV) values. The total value of RMS error is found simply by taking the square root of the sum of the squares of the individual errors as shown in Equation 3.19.

$$\varepsilon_{rms,tot} = \left( \frac{\sum_{i=1}^{N} \varepsilon_{rms,i}^{2}}{N} \right)^{1/2} \tag{3.19}$$

For a uniform probability distribution, the RMS value can be related to the PV value by Equation 3.20.

$$\varepsilon_{rms,tot} = \frac{1}{2\sqrt{3}} \left( \sum_{i=1}^{N} PV_i^2 \right)^{1/2} \tag{3.20}$$

Because the error values used in the error modeling process are estimates, some means must be employed to arrive at a reasonable estimate of the total error. For this work in the displacement error model, individual axis contributions to the total end point errors are summed according to both Equation 3.18 and Equation 3.19. The total estimate for the end point error is then taken as the average of the absolute values of the systematic and RMS values. This procedure must, of course, be repeated for each of the six end point error components.

### 3.2.6 The Use of Displacement Error Models in Complex Systems

Although an error model can be a useful design tool for virtually any positioning system, the designer faced with a complex machine comprised of many degrees of freedom and complex structures will especially benefit from its use. In a complex design, total system performance can only be guaranteed if each subsystem performs to its design requirements. The displacement error model gives the designer a tool to guide the design of each subsystem and also to model the interactions between subsystems. For example, the case study detailed in Section 3.2.7 below describes a system containing 19 positioning degrees of freedom in three wafer handling mechanisms and in excess of 200

wafer pick-up/drop-off locations within the machine that these wafer handling mechanisms must access. Only by carefully modeling this system, can the required positioning performance throughout the machine be successfully achieved.

By implementing the error model in a spreadsheet, the designer can easily manage all of the errors present in a complex system. For example, when using DH parameters to describe the geometry of serial positioning systems, only one homogeneous transform model needs to be created. The designer can rapidly create new geometric descriptions of systems by changing the DH parameters for each new system in the existing model. By modeling the system in this fashion, the design process is streamlined and the possibility of making mistakes is reduced. Furthermore, this method of modeling is especially desirable in the conceptual design phase of a project when various alternate designs must be evaluated. The error model can provide important data to the designer about the positioning performance of each candidate design.

Additionally, the supporting structure of the machine may also be a significant factor in the positioning performance of the system. Using the displacement error modeling techniques, the frame of the machine can be modeled. Depending on the structure of this support system, this modeling may be important to guarantee that environmental disturbances, inertial loading, or background excitation does not degrade the positioning performance of the system. Within cleanrooms, it is not uncommon that systems fail to meet positioning requirements, not because of some short coming in the mechanism, but because of large errors induced by an insufficient supporting frame.

Designers of cleanroom systems have an additional benefit from the displacement error modeling method because of the architecture of cleanroom positioning systems. In the cleanroom, systems with revolute joints (especially those near the wafer surface) are desirable because of the particle contamination benefits. That is, revolute joints are much easier to design cleanly because of the ease of sealing when compared to linear joints. Of course, kinematic requirements may still dictate the use of linear joints. However, these can be positioned away from the wafers being transferred. Revolute joints may also be

desirable because of the advantages in packaging space versus reach lengths that can be achieved.

However, the use of revolute joints means that the kinematics of the systems are generally more complex than those of a system made of purely orthogonal linear axes. In cases with orthogonal kinematics, system geometry can be more easily visualized and experienced designers may be able to mitigate the effects of errors in their systems without the use of a formal error model. With increasing numbers of degrees of freedom in a system and the inclusion of revolute joints, it becomes increasingly difficult to perform error modeling by the "seat of your pants." Therefore, in the types of systems commonly found in cleanrooms, the use of displacement error modeling as described in this thesis is even more important.

In Section 3.2.2, it was mentioned that translational (rotational) errors always have an error gain of 1 on the end point translational (rotational) error in the same direction. This statement is quite accurate and for machine tools where axes are almost always orthogonal throughout the geometric model of the system, the matrix of error gains will contain only 1's and 0's for the translational (rotational) on translational (rotational) errors. For systems containing revolute axes, as is common in robots, the situation is somewhat more complicated. As a robot changes configurations, the relative orientation of coordinate frames changes with the changing joint positions. Consequently, a certain translational error in one of the proximal joints of the robot is not always parallel to the same (or any for that matter) axis in the end point reference frame. One can see that the magnitude of the error is unaffected by the relative orientation of the coordinate frames, but to be interpreted meaningfully these errors must be represented in the end point coordinate frame. Therefore, the translational on translational errors and rotational on rotational errors must be multiplied by a rotation matrix that is a function of the system geometry[29] to represent these errors correctly in the end point reference frame. The case study in Section 3.2.7 illustrates this point more graphically.

[29] Multiplication by a rotation matrix does not change the magnitude of the errors, only their distribution among the three linear axes of the end point coordinate frame.

### 3.2.7 Case Study: Displacement Error Modeling in a Process Tool

This section presents the application of the displacement error modeling techniques discussed above to the design of Silicon Valley Group's new photoresist processing system. Figure 3.3 shows the design concept for the entire machine, which uses three wafer handling robots in different locations. In the figure, the left side of the machine is an end station where cassettes of wafers are loaded into and removed from the machine. The right side of the machine is a stepper interface, where wafers are passed to and received from a wafer stepper. The stepper interface also contains cassettes for storage of rejected wafers. The center portion of the machine features hot and chill plates stacked along the backside of the machine. The spin stations for applying photoresist and developing exposed wafers are positioned in the front of the machine.

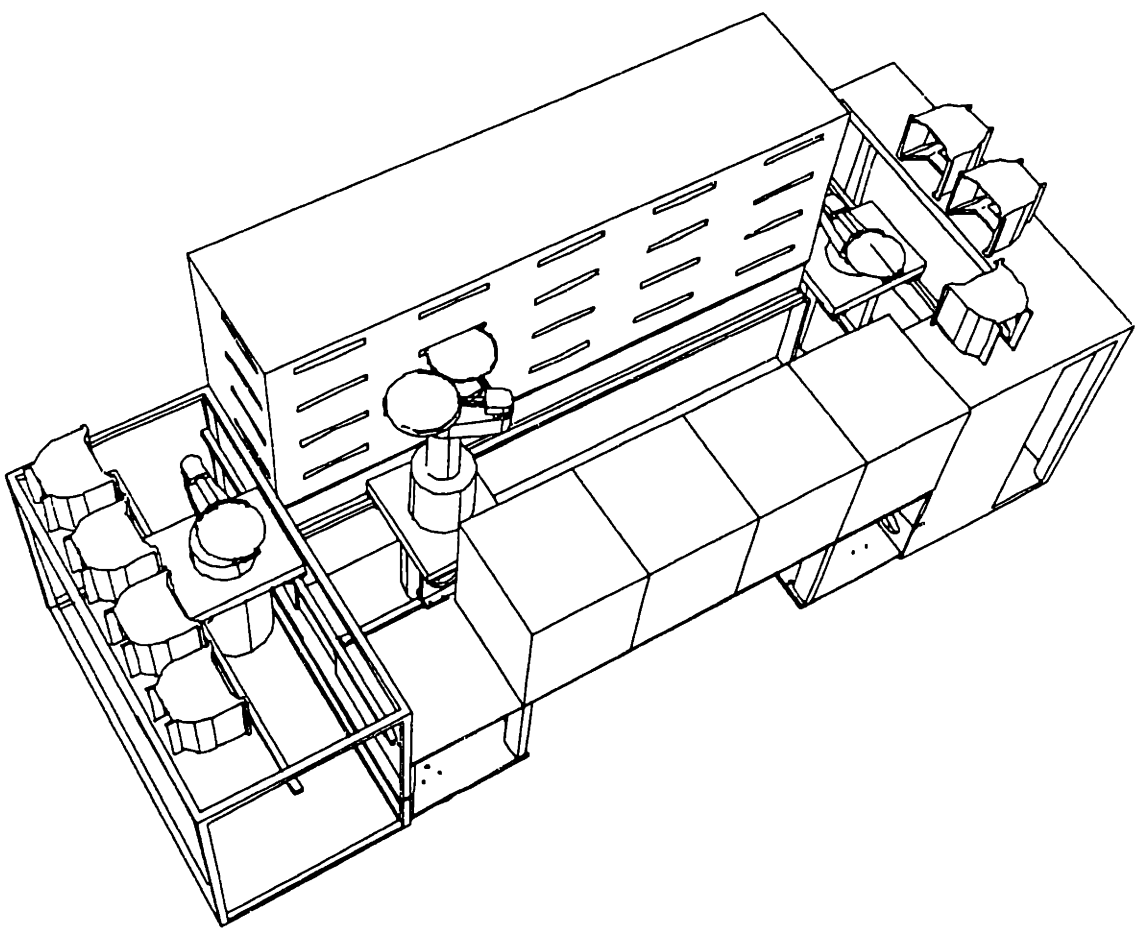

**Figure 3.3** Isometric view of new SVG photoresist processing system[30].

[30] Courtesy of Silicon Valley Group.

Because of the complexity of the machine and the stringent positioning repeatability requirements for wafers loaded into the spin modules, the displacement error model is a crucial element in the design of the system. The error model was used in developing a dramatically new design for the frame of the machine and a new method for attaching the process modules to the machine frame. The design of the wafer handling robot used in the machine was also directed with the displacement error model.

This case study presents the working error model for the newly designed photoresist processing system. The numerical details of this case study are presented in Appendix B. Appendix A of this thesis fully discusses the development of this design and should be referred to for more information.

The error model presented here contains elements for both the machine frame and the wafer handling robot as will be seen in the following sections. Additionally, the final section of the case study, 3.2.7.5, briefly presents results from initial position repeatability testing of the wafer handling robot prototype.

To remain somewhat concise, the following discussion only details the central portion of the machine. The techniques employed for the end station and stepper interface are virtually identical; the only differences in the error model are in the frame geometric model where different displacement offsets are required to describe the geometry of the end station and stepper interface.

#### 3.2.7.1 The Machine Frame

Figure 3.4 shows a schematic representation of the central portion of the machine with the coordinate frames for the structural portion of the error model attached. For the machine frame a serial chain of three coordinate frames is used to model the position of each wafer transfer location. Because there is one wafer transfer location per process module, there are a number of serial chains represented in Figure 3.4. For convenience, the homogeneous transform model of the machine frame is implemented in a spread sheet so that the repetitive nature of the model is easily handled with numerical software.

The base coordinate frame, which is identical to the one used for the wafer handling robot described later, is located in the center of the robot alley at one end of the machine at the height of the lowest wafer transfer level. This reference frame is used to simplify the geometric model used for the wafer handling robot. The second coordinate frame is located at the centroid of the kinematic coupling that connects each process module to the machine frame[31]. The final frame is located at the wafer transfer location within each process module. This arrangement of frames allows all errors associated with the frame to be lumped at the base reference frame and errors associated with the location of the transfer location within the process module to be lumped at the second frame located at the kinematic coupling centroid.

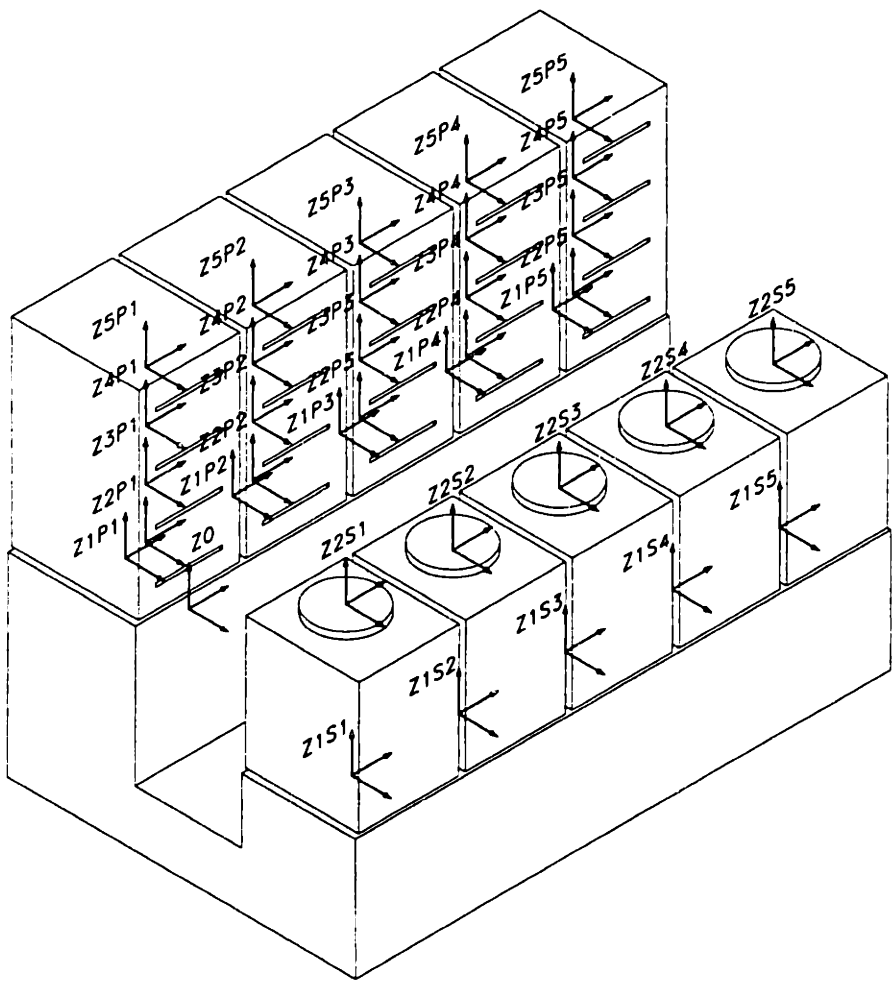


**Figure 3.4** Coordinate frame assignments for the machine frame.

[31] In the rear of the machine, each of the five multi-module stacks is connected to the frame with a single kinematic coupling.

The geometric model of the machine frame is comparatively simple because all of the coordinate frames are parallel to each other. Equation 3.21 gives the form of the HTM between each of these reference frames.

$$ {}^{i-1}T_i = \begin{bmatrix} 1 & 0 & 0 & x \\ 0 & 1 & 0 & y \\ 0 & 0 & 1 & z \\ 0 & 0 & 0 & 1 \end{bmatrix} \tag{3.21} $$

### 3.2.7.2 The Wafer Handling Robot

The coordinate frames for the wafer handling robot, which were assigned using the Denavit and Hartenberg method, are shown in Figure 3.5. In the figure for clarity, the robot is shown displaced along the horizontal axis away from the base reference frame with the vertical axis fully extended. The robot has seven controlled degrees of freedom; five of these control the five joints of the robot and two control the motion of the jaws of each of the two grippers. The jaws of each gripper are mechanically coupled so that they move in and out equal amounts when wafers are being picked up or set down. The first degree of freedom in the system is the long horizontal travel axis that moves the robot along the alley in the machine frame. The next degree of freedom is a revolute one in which the entire vertical column in the robot rotates about its center. The third degree of freedom is the vertical telescoping axis that allows the robot to access process modules at various heights. The final two degrees of freedom are the two revolute elbow joints that rotate independently of each other. The kinematics of the robot are such that the horizontal linear joint, the base revolute joint, and either of the elbow joints can be coordinated so that the robot moves in a straight line into a process module. The small motions of the vertical axis are also used when wafers are being picked up or set down.

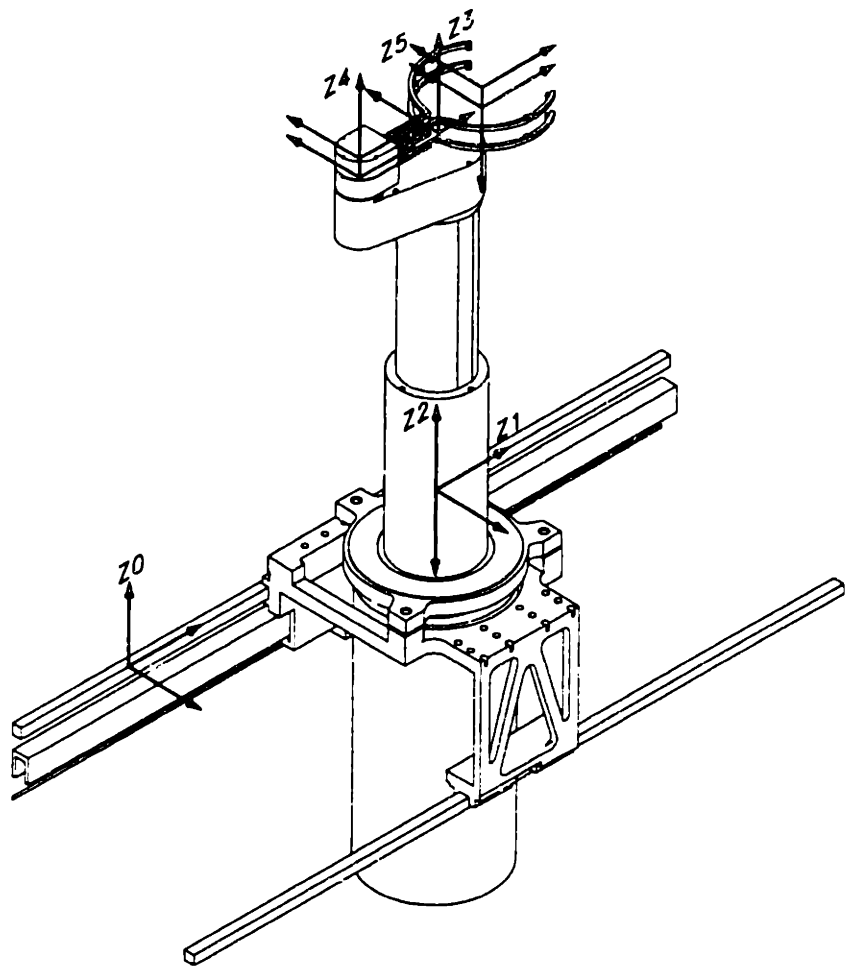


**Figure 3.5** Wafer handling robot with coordinate frame assignments.

The first three coordinate frames are all at the height of the lowest wafer transfer level (the lower gripper) when the vertical axis is fully retracted. The revolute joints in the system are shown at their nominal home locations[32]. Table 3.1 gives the DH parameters for the wafer handling robot. It should also be noted that the fourth and fifth coordinate frames are duplicated to represent both wafer gripper locations. The only difference between the two sets of frames is the presence of a small vertical offset for the upper gripper. By using this split representation, the geometric model can be easily adjusted to represent either the upper or lower gripper configuration.

[32] That is, the joint displacement is zero according to the way the DH parameters are defined.

**Table 3.1** Denavit and Hartenberg Parameters for Wafer Handling Robot

| index | twist angle, deg | link length, in | link offset, in | joint angle, deg |
|---|---|---|---|---|
| i | $\alpha_{i-1}$ | $a_{i-1}$ | $d_i$ | $\theta_i$ |
| 1 | -90° | 0 | $d_1$ | 0° |
| 2 | 90° | 0 | 0 | $\theta_2$ |
| 3 | 0° | 0 | $d_3$ | 90° |
| 4a | 0° | $l_3 = -6.425$ | $d_{4a} = 0.0$ | $\theta_4$ |
| 4b | 0° | $l_3 = -6.425$ | $d_{4b} = 1.378$ | $\theta_4$ |
| 5a | -90° | $l_4 = 9.986$ | $d_5 = 0.0$ | 0 |
| 5b | -90° | $l_4 = 9.986$ | $d_5 = 0.0$ | 0 |

Equations 3.22 to 3.26 give the transform matrices between each of the reference frames as a function of the joint positions. These HTM's form the basis of the geometric model of the wafer handling robot.

$$ {}^{0}T_1 = \begin{bmatrix} 1 & 0 & 0 & 0 \\ 0 & 0 & 1 & d_1 \\ 0 & -1 & 0 & 0 \\ 0 & 0 & 0 & 1 \end{bmatrix} \tag{3.22} $$

$$ {}^{1}T_2 = \begin{bmatrix} Cos\theta_2 & -Sin\theta_2 & 0 & 0 \\ 0 & 0 & -1 & 0 \\ Sin\theta_2 & Cos\theta_2 & 0 & 0 \\ 0 & 0 & 0 & 1 \end{bmatrix} \tag{3.23} $$

$$ {}^{2}T_3 = \begin{bmatrix} 0 & -1 & 0 & 0 \\ 1 & 0 & 0 & 0 \\ 0 & 0 & 1 & d_3 \\ 0 & 0 & 0 & 1 \end{bmatrix} \tag{3.24} $$

$$
{}^{3}T_{4} = \begin{bmatrix} Cos\theta_4 & -Sin\theta_4 & 0 & l_3 \\ Sin\theta_4 & Cos\theta_4 & 0 & 0 \\ 0 & 0 & 1 & d_4 \\ 0 & 0 & 0 & 1 \end{bmatrix} \tag{3.25}
$$

$$
{}^{4}T_{5} = \begin{bmatrix} 1 & 0 & 0 & l_4 \\ 0 & 0 & 1 & 0 \\ 0 & -1 & 0 & 0 \\ 0 & 0 & 0 & 1 \end{bmatrix} \tag{3.26}
$$

Equation 3.27 gives the ideal kinematic model of the wafer handling robot. If no errors were present in the system, the motions of the end effector of the robot could be described exactly using this equation.

$$
{}^{0}T_{5} = \begin{bmatrix} -Sin(\theta_2+\theta_4) & 0 & -Cos(\theta_2+\theta_4) & -l_3Sin\theta_2 - l_4Sin(\theta_2+\theta_4) \\ Cos(\theta_2+\theta_4) & 0 & -Sin(\theta_2+\theta_4) & d_1 + l_3Cos\theta_2 + l_4Cos(\theta_2+\theta_4) \\ 0 & -1 & 0 & d_3 + d_4 \\ 0 & 0 & 0 & 1 \end{bmatrix} \tag{3.27}
$$

The first element of the fourth column gives the location of the end point in the X dimension of the base reference frame. Similarly, the Y end point coordinate is given by the second term of the fifth column and the Z coordinate by the third element. The direction cosines of the upper 3x3 rotation matrix give the orientation of the end effector. In this case because the revolute axes create motions in the horizontal plane, the end effector orientation can easily be seen as the rotation about the base frame Z axis by the sum of the base revolute and the elbow joint rotations.

### 3.2.7.3 Frame and Robot Error Sources

Having created the geometric models of the machine frame and wafer handling robot, the next step is to account for the various errors that are expected to occur in the system. As was described previously, the total system is modeled with two serial chains, one for the machine frame and one for the robot, that interact at the wafer drop off

locations within process modules. In the error modeling process, it is necessary to separately account for errors in the frame and in the robot.

For the frame portion of the displacement error model, the errors in the system are expected to be primarily geometric, mechanical, and dynamic in nature. Because the frame is a rigid structure, there are no control system effects to be accounted for. Additionally, because the environment in which this machine will be used is temperature controlled and there are no large heat sources from systems mounted on the machine frame no thermal effects were accounted for in the error model. This is not to say that there are no thermal effects, but for the level of precision of interest here, which is about ±0.001 inch, these effects are negligible. Significant design work went into minimizing the remaining geometric, mechanical, and dynamic errors in the machine frame. Tables B.5 and B.6 in Appendix B show that the expected values of these errors are quite small. Later portions of the thesis describe in more detail the elements of the frame design that minimize these errors.

The primary source of geometric errors in the machine are expected to come from inaccuracies in the kinematic coupling attachment of the process modules to the machine frame and within the construction of the process module itself. However, as will be discussed later in the thesis, the machine frame and kinematic couplings are designed so that these errors are extremely small. Mechanical errors in the system are expected to come from compliance within the machine frame. Again though, the frame was designed to be very rigid and both internal and external disturbance forces are expected to be quite small. Dynamic errors will come primarily from background vibration sources. However, the frame design includes special structural damping sources to significantly increase its dynamic stiffness; thereby reducing the effects of vibration.

Error sources for the wafer handling robot were categorized in a similar fashion. Errors in the robot are expected to come from geometric, mechanical, dynamic, and control system sources. Because the positioning repeatability of the robot is of greater importance than its absolute accuracy, mechanical errors specifically affecting the repeatability were separated from other errors in the error model. Additionally, control

system errors were also separated for the benefit of the control system design. For the same reasons as were stated for the machine frame, thermal errors were not considered in the displacement error model of the wafer handling robot. Tables B.2 and B.3 in Appendix B give some details of these errors for a representative configuration of the robot. Again later portions of the thesis describe details of the robot design and control system modeling that were employed to mitigate the effects of these errors in the placement of wafers.

Geometric errors in the robot are expected to come primarily from imperfections in the machining of structural parts and the assembly of these parts. Dynamic errors from background excitation and from inertial loading within the wafer handler are also of concern. Because of the extremely light payload[33], the stiff design of the wafer handler, and the addition of damping material where practical, these errors are also not expected to be large[34]. The hysteresis present in the harmonic gear reducers in the revolute joints is expected to be a primary contributor to nonrepeatability in the robot[35]. Manufacturer's data for these transmission elements was used to judge the effects of these nonrepeatabilities. Also, the resolution of the optical encoders in all servo controlled joints will have an important effect on the control system's ability to move the robot with the required repeatability. For this reason, the sensor resolution is also addressed explicitly in the error model[36].

#### 3.2.7.4 The Example System's Displacement Error Model

The displacement error model is actually distributed among three spread sheets. One spread sheet contains the HTM model of the frame, another the HTM model of the robot, and the third contains the error gains and total end point errors for both the frame and the robot. Because of the size of the HTM models, they are not included in Appendix B. However, the construction of these portions of the error model is straightforward using the transformation matrices given above. Appendix B does contain the error gains

---

[33] A 200 mm silicon wafer's mass is just 0.05 kg.

[34] In fact, experiences with the robot prototype showed that vibration of the wafer gripper is not a problem.

[35] Again, initial repeatability testing of the robot prototype showed this to be the case.

[36] The prototype robot controller settles to within a single encoder count of the commanded position for all five servo-controlled axes.

that are calculated from the HTM models and also the calculations for the total system errors. These error gains are shown for a representative configuration in Tables B.1 and B.4. It should be noted that the HTM model of the wafer handling robot is a function of the joint positions of the robot and that shown in the appendix is for a particular configuration. Consequently, as the robot moves its error gains change and the resulting end point errors also change.

To illustrate the effects of the changing error gains on the end point errors of the wafer handling robot as it moves, the error model was used to calculate end point errors over the course of several trajectories. Figure 3.6 shows the first of these trajectories. This trajectory was selected not because the robot will actually be required to move in this fashion, but because the trajectory traverses the entire range of motion of the robot.

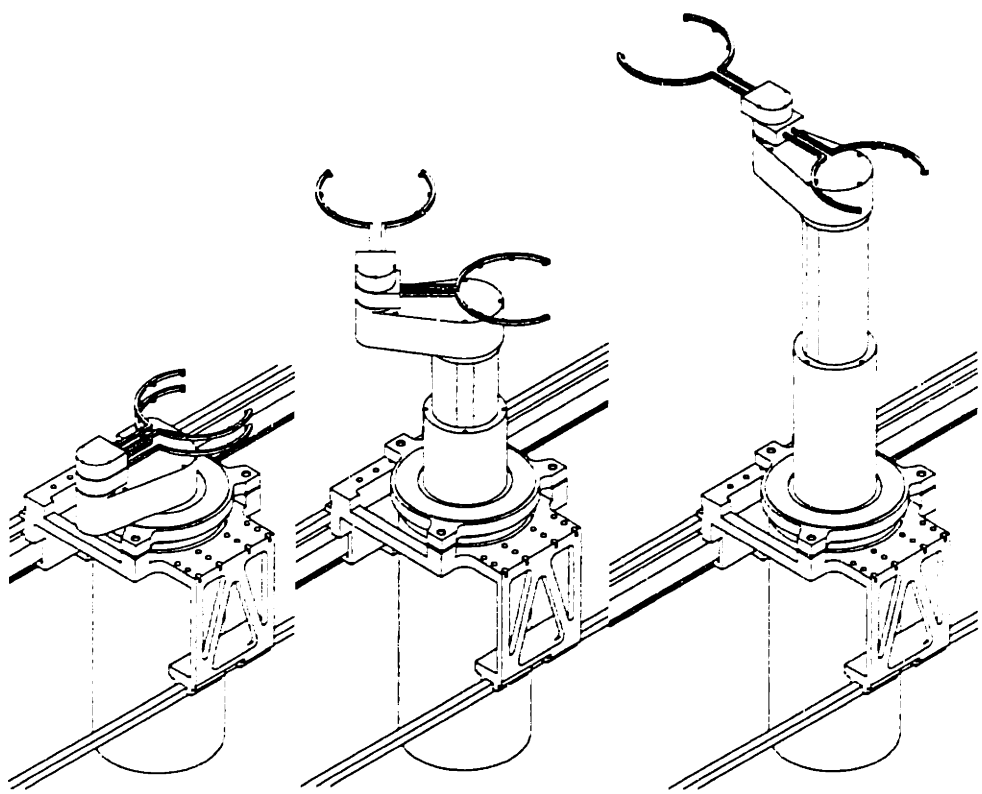

**Figure 3.6** Beginning, intermediate, and final positions for the trajectory used to generate error plots.

Figure 3.7 shows the total end point errors for the wafer handling robot in the three translational directions. The rotational errors are also quite small as can be seen in

Appendix B, but are not plotted here because the translational position of the wafer is more important in the positioning within a process module. Similarly, Figure 3.8 shows the repeatability related errors for the same trajectory.

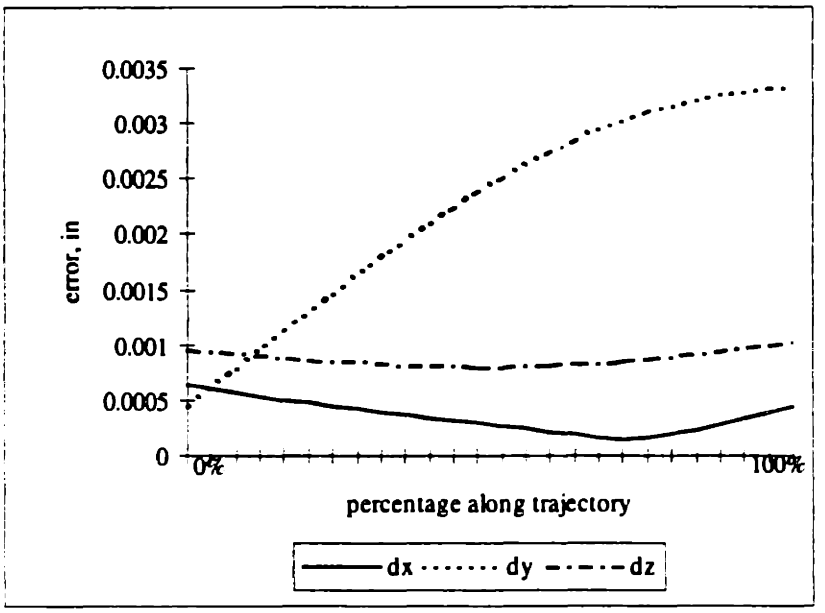


**Figure 3.7** Total end effector errors plotted for the trajectory shown in Figure 3.6.

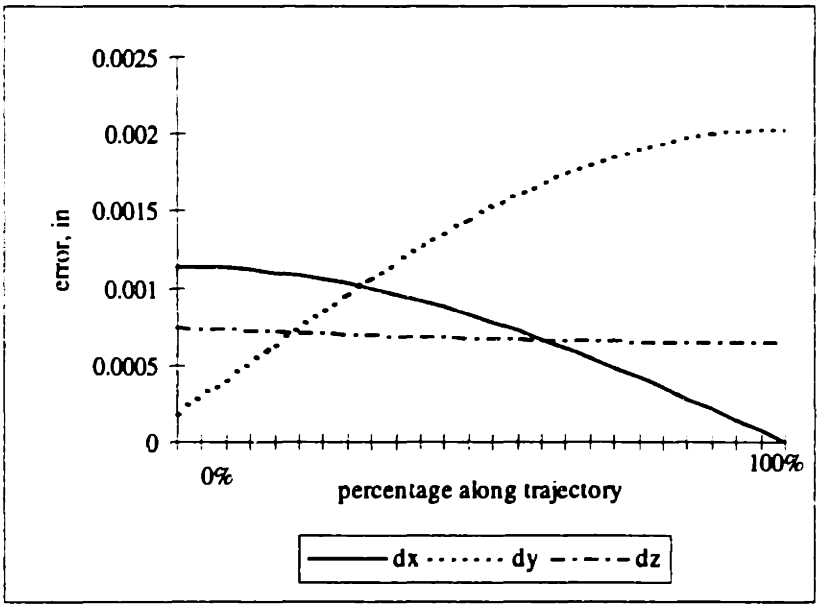


**Figure 3.8** Repeatability-related end effector errors for the trajectory shown in Figure 3.6.

Figure 3.9 shows a straight-line trajectory that is representative of those that will be used by the wafer handling robot to access process modules. It should be noted that while one gripper is moving into a process module, the other elbow joint does not move so that the second gripper remains entirely within the robot's alley in the machine.

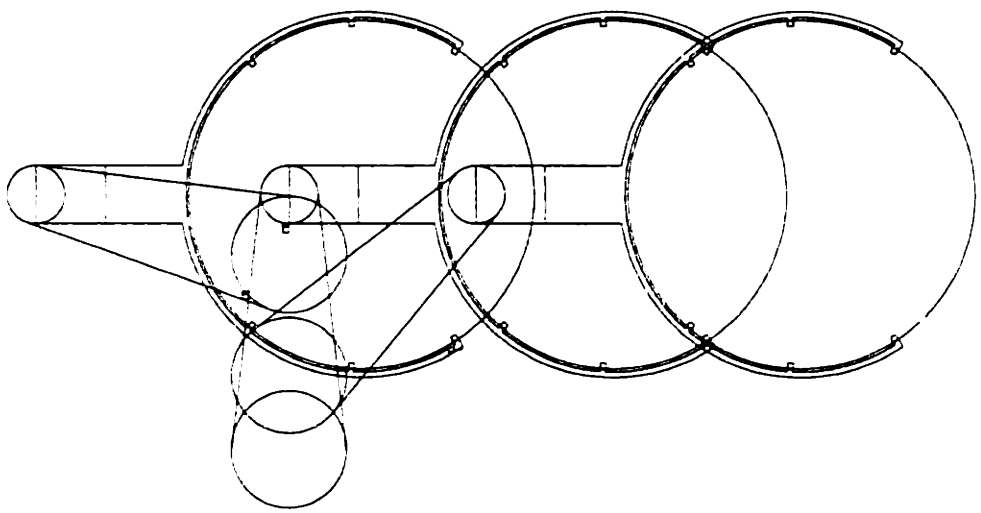

**Figure 3.9** Straight-line trajectory used for process module access.

Figure 3.10 and Figure 3.11 show plots of the total end point translational errors and the repeatability related errors respectively. The trajectory used to generate these plots is the straight-line trajectory shown above with a move segment from the robot's home position to the start point of the straight-line motion prefixed to the straight-line data. This trajectory also does not contain any vertical motion of the robot.

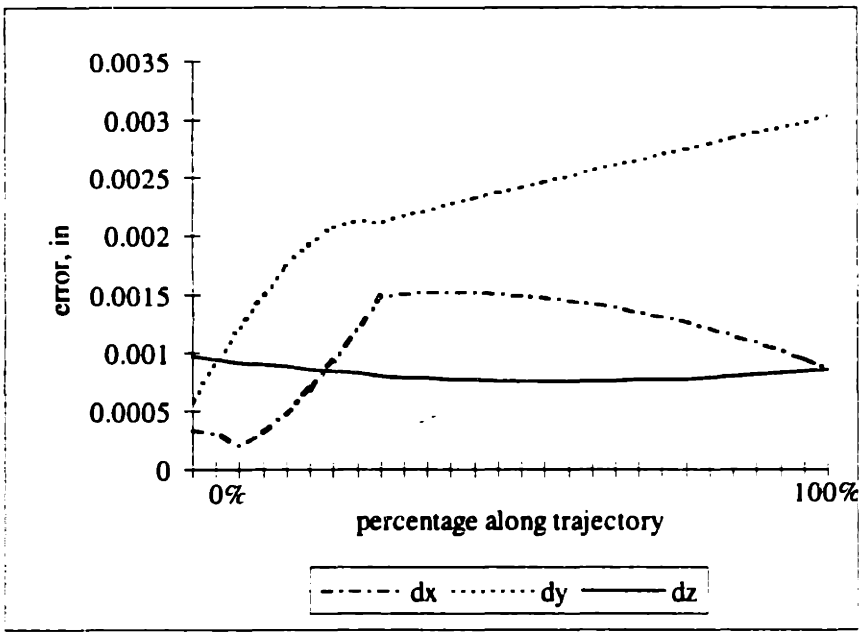


**Figure 3.10** Total end effector errors plotted for a typical straight-line trajectory used for process module access.

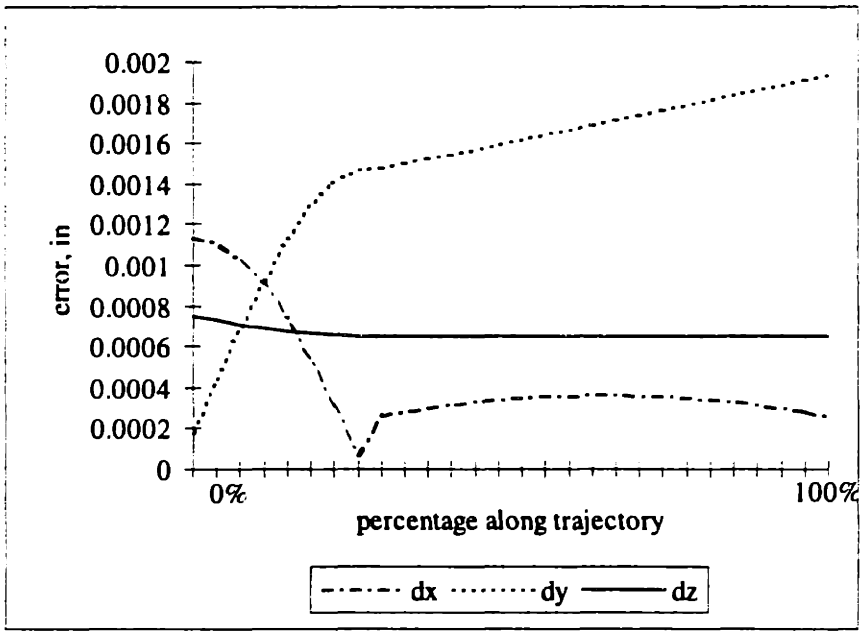


**Figure 3.11** Repeatability-related end effector errors plotted for a typical straight-line trajectory used for process module access.

#### 3.2.7.5 Repeatability Test Data for the Prototype Wafer Handling Robot

Position repeatability testing was performed on the prototype wafer handling robot (discussed in Appendix B). This testing served as preliminary verification that the robot is capable of meeting its positioning goals[37]. Test data are given along with the robot's error model in Appendix B. Measurements on individual axes indicate that both the horizontal carriage and the telescoping axis are repeatable to ±0.0002 inches. Tests for the total system repeatability were performed in orthogonal directions in the horizontal plane by indicating off the gripper housing. These tests showed that the robot is repeatable to ±0.002 inches, which is in close agreement with the predictions of the error model above. As discussed in Chapter 4 the prototype robot controller settled to within a single encoder count for each of the five motion axes. These tests indicate that the hysteresis in the harmonic drive and belt transmission in the revolute axes mentioned above and included in the error model are the primary sources of nonrepeatability in the robot. Additionally, it should be noted that these test data correlate well with the results predicted by the error modeling techniques.

## 3.3 Error Modeling for Velocity and Force Transmission

In addition to the error modeling that can be performed for the displacement performance of a positioning system, it is also possible to perform a similar analysis for the velocity and force transmission characteristics of a system with multiple degrees of freedom. This section of the thesis presents a new approach for error modeling for the velocity and force transmission properties of motion systems modeled as serial chains. This type of error modeling should prove useful in any design problem where the velocity characteristics of the end point of a system must be maintained through a predefined trajectory. The same techniques can be used to model errors in the quasi-static transmission of forces from the individual axes of a system to its end point. This technique might be useful whenever the end point of the system is required to interact with its environment.

[37] Dial indicators with 0.0001 and 0.001 inch resolution were used for this repeatability testing.

### 3.3.1 Mathematical Background

In general, the end point position of a system can be written as a function of its joint positions as shown in Equation 3.28.

$$\underline{x} = f(\underline{\theta}) \tag{3.28}$$

where $\underline{x}$ is a vector of end point positions and $\underline{\theta}$ is a vector of joint positions. This expression is of the same form as the expression for the end point positions derived for the wafer handling robot in Section 3.2.7.2. By differentiating this position expression with respect to time and applying the chain rule, Equation 3.29 can be obtained which relates the end effector velocities to the joint velocities.

$$\dot{\underline{x}} = [J]\dot{\underline{\theta}} \tag{3.29}$$

where $\dot{\underline{x}}$ is a vector of joint velocities, $[J]$ is the Jacobian matrix, and $\dot{\underline{\theta}}$ is a vector of joint velocities. Instantaneously, Equation 3.29 is a linear expression. However, the Jacobian matrix is a function of system geometry including joint positions so the elements that make up the matrix change values as the system moves. The Jacobian can be calculated from Equation 3.28 as shown in Equation 3.30.

$$[J] = \frac{\partial \underline{x}}{\partial \underline{\theta}} \tag{3.30}$$

For simple geometries, the Jacobian can usually be calculated in a straightforward manner. However, for more complex systems such as general six degree of freedom robots, these computations can become more difficult. Many other researchers have examined these types of kinematic problems at great length [Duffy '80] [Craig '89].

For a quasi-static system the principle of virtual work shows that the joint torques or forces are related to the end point torques and/or forces by the transpose of the Jacobian matrix as shown in Equation 3.31.

$$\underline{\tau} = [J]^T \underline{F} \tag{3.31}$$

where $\underline{\tau}$ is the vector of joint forces and $\underline{F}$ is the vector of end point forces[38].

### 3.3.2 Errors in Velocity Transmission

As was mentioned in Chapter 2 the condition number of the Jacobian matrix, which is the ratio of the maximum and minimum singular values, can be used to bound the magnitude of end point velocity or force errors based on the size of the joint velocities or forces [Strang '88] [Salisbury '82]. Equation 3.32 shows how the ratio of the vector norms of the end point error velocities, $\delta \underline{\dot{x}}$, and the end point velocities must be less than the product of the condition number, $\sigma$, and the ratio of the vector norms of the joint error velocities, $\delta \underline{\dot{\theta}}$, and the joint velocities.

$$\frac{\|\delta \underline{\dot{x}}\|}{\|\underline{\dot{x}}\|} \leq \sigma \frac{\|\delta \underline{\dot{\theta}}\|}{\|\underline{\dot{\theta}}\|} \tag{3.32}$$

Note that Equation 3.32 can be written in this manner since the condition number of a matrix and its inverse are identical. The simple interpretation of Equation 3.32 is that as the condition number of the Jacobian becomes larger, it is possible that the end point velocity errors will become larger for a given joint velocity error. It is interesting to note that the condition number can become infinitely large in configurations commonly referred to as singularities. These locations occur at the boundaries of the workspace and sometimes within the workspace. A singularity is a location where the end point loses one or more degrees of freedom and is characterized by a Jacobian matrix that does not have full rank.

This property of the Jacobian's condition number has been well known for sometime and can be used to analyze the workspace of candidate designs. However, a much simpler and much more accurate measure of error transmission properties of the robot can easily be calculated if one simple, but reasonable assumption is made. The

[38] The vectors of joint forces and end point forces can actually contain both forces and torques. For simplicity, the vector quantity will be referred to as forces with the possibility of torques being implicit.

required assumption is that the only nonzero component of the joint error velocity is in the same direction as the joint velocity. This means that the other possible five components of the error velocity must be zero. This assumption is a good one because velocity errors are almost certainly going to come from velocity tracking errors in the control system. Other joint velocity errors would have to come from actual mechanical deformations of the robot's structure and would be very small in magnitude compared to tracking errors.

Having made this assumption, a velocity "error gain" can be determined in a manner similar to the displacement error gain without the need to calculate any vector norms or condition numbers. The velocity error gain will simply be the product of the Jacobian matrix and a small characteristic joint velocity in the appropriate dimension with the result normalized by the characteristic velocity as shown in Equation 3.33.

$$\underline{g}_{vel,i} = ([J]\begin{bmatrix} 0 \\ \dot{\theta}_{char,i} \\ 0 \\ \vdots \\ 0 \end{bmatrix})/\dot{\theta}_{char,i} \tag{3.33}$$

where is the $\underline{g}_{vel,i}$ is the vector of velocity error gains that maps the way a particular joint velocity error will propagate to the end point velocities.

### 3.3.3 Errors in Force Transmission

Because the joint forces in a robot can be related to the end point forces with the transpose of the Jacobian matrix for a quasi-static system, all of the analysis discussed in the previous section can be applied to the force transmission problem. For example, Equation 3.34 shows how the condition number of the transpose of the Jacobian bounds the errors in the end point force produced by a give joint force vector and accompanying error vector.

$$\frac{\|\delta \underline{F}\|}{\|\underline{F}\|} \leq \sigma \frac{\|\delta \underline{\tau}\|}{\|\underline{\tau}\|} \tag{3.34}$$

Error gains for the transmission of joint forces to end point forces can also be calculated in a manner analogous to that for the velocity transmission problem except that the inverse of the transpose of the Jacobian must be used in place of the Jacobian matrix.

It should also be mentioned that these methods for errors in force transmission only apply to a quasi-static system. If any portions of the system are accelerating than at least part of the joint forces will be taken up by inertial forces. Furthermore, frictional forces may be significant even in a system where joints are moving at or near constant velocity, thereby invalidating the relationship used as a basis for the force transmission error modeling. Research in force control methods deals with this area in much more detail.

### 3.3.4 Case Study: Velocity Error Modeling in a Process Tool

This case study presents a velocity error model for the wafer handling robot that has already been discussed. The Jacobian matrix for this robot, which can be derived from the displacement equation discussed in the previous case study, is given in Equation 3.35.

$$J = \begin{bmatrix} 0 & -l_3 Cos\theta_2 - l_4 Cos(\theta_2+\theta_4) & -l_4 Cos(\theta_2+\theta_4) & 0 \\ 1 & -l_3 Sin\theta_2 - l_4 Sin(\theta_2+\theta_4) & -l_4 Sin(\theta_2+\theta_4) & 0 \\ 0 & 1 & 1 & 0 \\ 0 & 0 & 0 & 1 \end{bmatrix} \tag{3.35}$$

Treating only one of the two elbows, the end point velocities of the robot are related to the joint velocities by Equation 3.36.

$$\begin{bmatrix} \dot{x} \\ \dot{y} \\ \dot{\theta} \\ \dot{z} \end{bmatrix} = J \begin{bmatrix} \dot{d}_1 \\ \dot{\theta}_2 \\ \dot{\theta}_4 \\ \dot{d}_3 \end{bmatrix} \tag{3.36}$$

Appendix B contains more numerical data for this case study. The case study also uses the same two sample robot trajectories as did the displacement error model case study presented in Section 3.2.7.

Figure 3.12 shows how the condition number varies across the first of these two trajectories. It is evident that the robot is approaching a singularity as it nears the end of the trajectory. This singularity corresponds to the configuration of the robot where the arm is fully extended perpendicular to the long horizontal axis. When the robot is in this singularity it cannot move in a direction purely perpendicular the horizontal axis. Therefore, this configuration is to be avoided. As is discussed later in the thesis, the length of the upper arm segment was optimized so that the robot is never required to come close to this singularity.

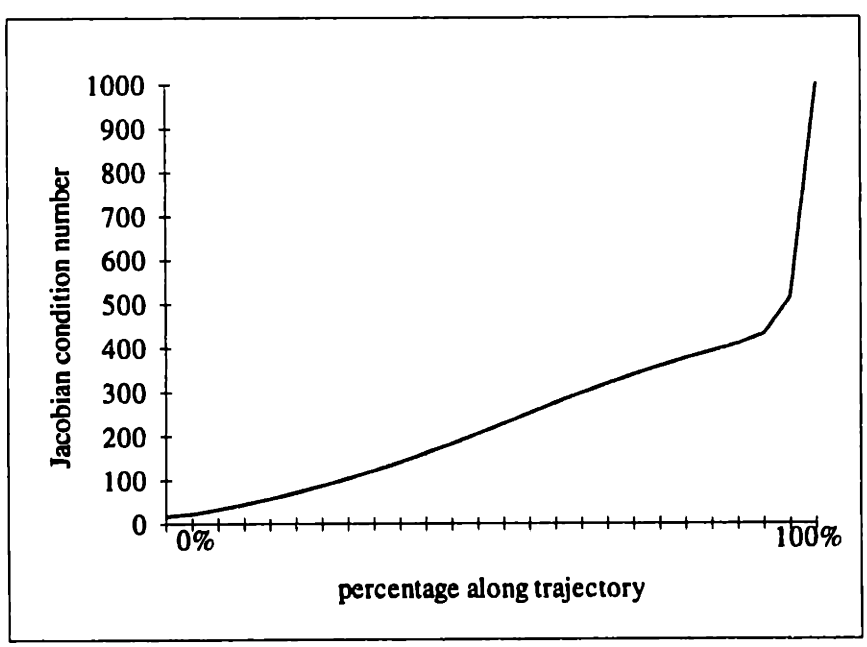


**Figure 3.12** Condition number of Jacobian matrix for the trajectory shown in Figure 3.6.

Because the actual magnitude of the end point velocity errors are dependent on the magnitude of the joint velocity errors, only the error gains are plotted here. Also, this robot is primarily a positioning system, so the actual velocity errors are not significant as long as the positioning repeatability goals are satisfied and the robot does not deviate significantly from its desired trajectory. Figure 3.13 and Figure 3.14 show the velocity error gains for both the base revolute joint and the elbow joint. Because the horizontal axis and the telescoping axis are both linear, they have constant error gains of 1 for velocities in the direction of the joint movement and 0 for all other velocity directions. Also, both of the revolute joints have velocity error gains of 1 for the end effector rotational velocity. Tables B.7, B.8, and B.9 in Appendix B show these gains for a single robot configuration. It should be noted that the translational on translational and rotational on rotational velocity error gains are analogous to the situation observed for the displacement error gains.

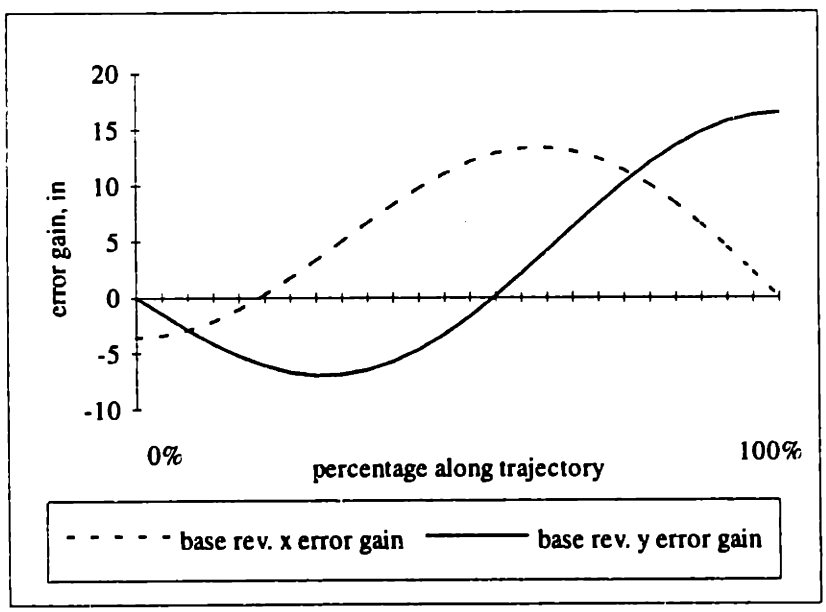


**Figure 3.13** Velocity error gains for base revolute joint for the trajectory shown in Figure 3.6.

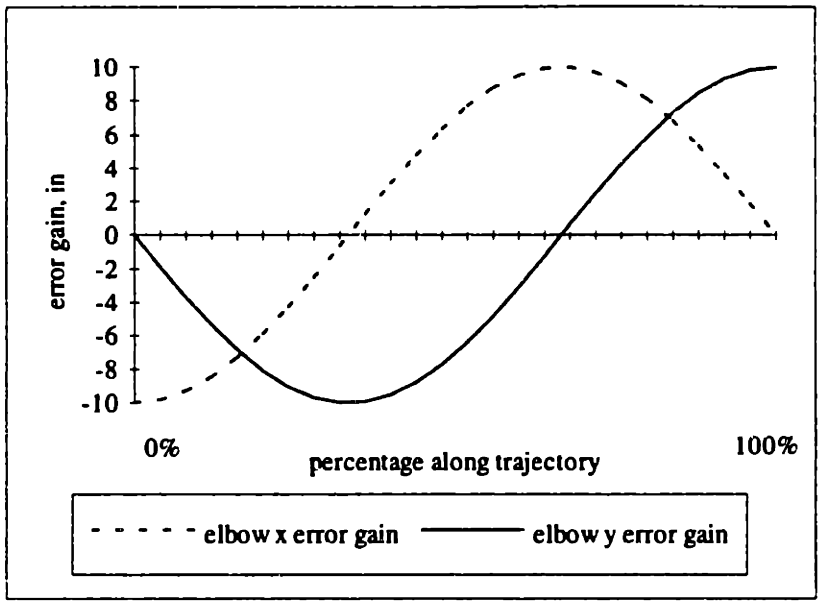


**Figure 3.14** Velocity error gains for elbow joint for the trajectory shown in Figure 3.6.

Figure 3.15 shows the condition number for the typical straight line trajectory. It can be seen from this plot that the robot does not approach any singularities during a typical move.

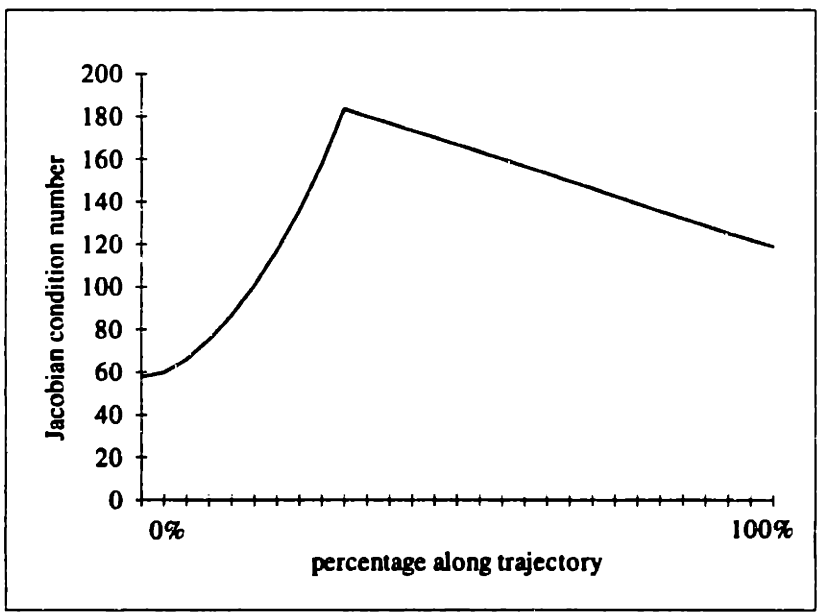


**Figure 3.15** Condition number of Jacobian matrix for straight-line trajectory shown in Figure 3.9.

Figure 3.16 and Figure 3.17 show the velocity error gains for this straight-line trajectory. It is interesting to note that the elbow X-direction velocity error gain is zero for the straight line portion of the trajectory because the gripper remains aligned with the X-axis for this part of the move.

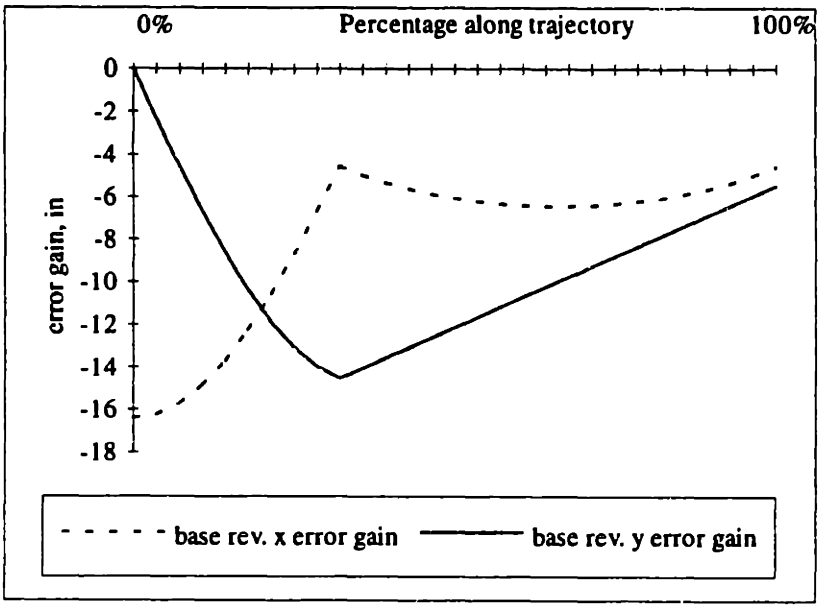


**Figure 3.16** Velocity error gains for base revolute joint for straight-line trajectory.

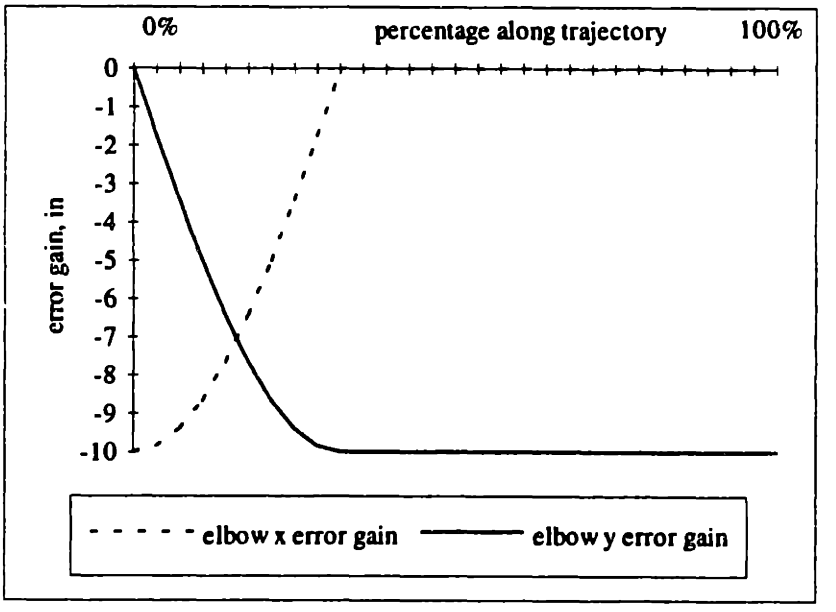


**Figure 3.17** Velocity error gains for elbow joint for straight-line trajectory.

## 3.4 Summary

This chapter presented the error modeling techniques that are tailored for use in directing the design of automation systems in semiconductor processing equipment. These error modeling tools were grouped into two categories: displacement error modeling and velocity and force transmission error modeling. A homogeneous transform based description of a system's geometry was used as a basis for the displacement error model. In this method, translational and rotational errors are lumped at the base of coordinate systems that are in turn attached to each rigid body in a system. The HTM model can be used to calculate error gains that give the sensitivity of end point errors to errors in each coordinate frame in the system. These error gains are used in conjunction with different error sources to assist a designer in selecting the appropriate system geometry as well as individual components such as bearings, power transmissions, and position sensors. The chapter also presented a new method to calculate error gains for the transmission of velocity and force errors to the end point velocity output and force output. These error gains can be used by a designer in a manner similar to the displacement error gains to guide the design process. Additionally, the chapter discussed error models of a wafer handling robot and machine frame to further illustrate the construction of working error models. Positioning repeatability test data from the prototype wafer handling robot, which was presented along with the displacement error model, corresponds well with levels of performance predicted by the error modeling techniques described in this chapter.

# Chapter 4: Supporting Elements of the Precision Machine Design Methodology

## 4.1 Introduction

In addition to the error modeling techniques described in the previous chapter, which form the backbone of the precision machine design methodology presented in this thesis, a number of supporting elements are required to complete the methodology. This chapter continues the explanation of this new design paradigm by developing several areas of importance in the design of semiconductor manufacturing equipment. These areas are as follows:

1. Deterministic design
2. Elastic averaging
3. Reduction of the effects of rotational errors
4. Static and dynamic structural deformations
5. Control and mechanical system integration
6. Considerations for cleanroom equipment design.

In the initial presentation of the precision machine design methodology in Chapter 2, these six areas were explained briefly. This chapter extends this discussion and illustrates the importance of these areas and their application to the design of semiconductor manufacturing equipment with a number of case studies. As was done in Chapter 3, these case studies are based on Silicon Valley Group's Accipiter design project for their new photoresist processing system.

The chapter begins with a discussion of deterministic design and how it was used to identify the need for a rigid machine frame with kinematically coupled process modules in SVG's new machine. The chapter continues with an explanation of elastic

averaging. The use of several types of rolling element bearings in a wafer handling robot further illustrates this principle. Next, the importance of minimizing Abbe errors is discussed and examined in the design of two wafer centering end effectors for the wafer handling robot. Then, the importance of static and dynamic effects in structural design is considered and explained through the design of the machine frame for SVG's new system. Following that, the integration of control system and mechanical design in positioning systems is discussed. A thorough examination of the new wafer handling robot's control system based on dynamic simulation results and trajectory tracking data from the prototype robot is also included. Finally, the chapter presents many of the special requirements placed on semiconductor equipment designs by the cleanroom manufacturing environment. Again the design elements from the Accipiter project are used to illuminate this discussion.

## 4.2 Deterministic Design

Determinism is a philosophy of machine design that simply states that the proper function of a machine will inevitably follow from the proper design of the cause and effect relationships in the machine. Deterministic design, which has also been called kinematic design, usually deals with the design of static couplings between rigid bodies and certain types of bearing arrangements. These principles have traditionally been used in the instrument and optics design communities. However, deterministic design principles also find useful application in the design of machine tools. Furthermore, one of the purposes of this thesis is to advocate the use of these same principles in the design of semiconductor manufacturing equipment.

The deterministic design of kinematic couplings and bearings is based on the simple fact that rigid bodies have six degrees of freedom and each degree of freedom can be restrained by one contact point. Therefore, two rigid bodies can be accurately located relative to one another with six contact points. Any additional contact points would create over-constraint in the system. This over-constraint has at least two effects. First, because any real solid body is not absolutely rigid, the over-constraint may cause

deformation of the body resulting in positioning inaccuracies. Second, the over-constraint creates a nondeterministic system where the position of one rigid body relative to another may not be repeatably maintained. Using this deterministic design technique, both deterministically designed bearings and deterministically designed structural couplings can be created. Figure 4.1 shows an example of a three-groove kinematic coupling.

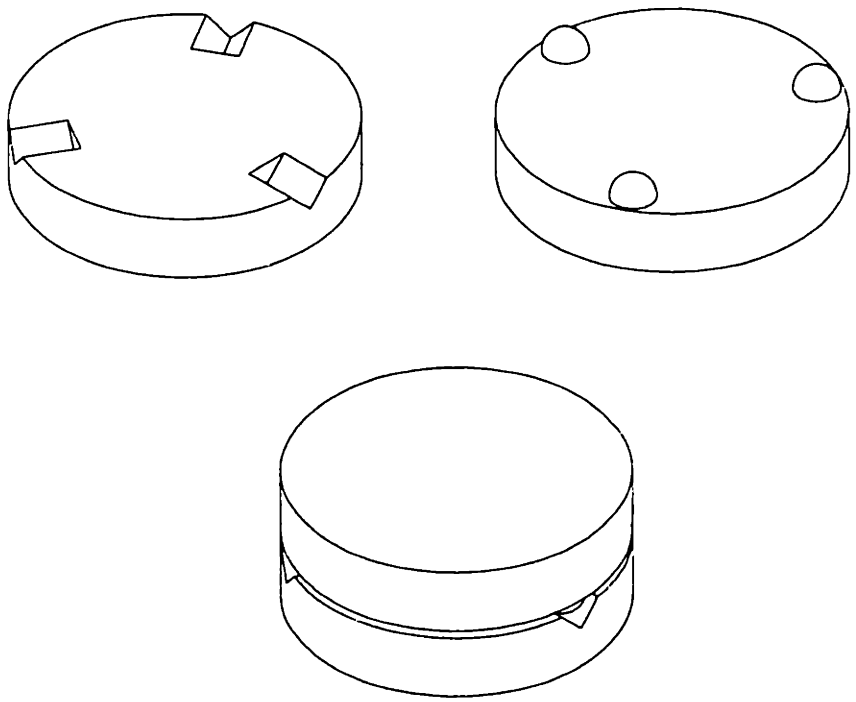

**Figure 4.1** Three groove deterministically designed kinematic coupling.

Deterministically designed kinematic couplings can be readily used anywhere rigid bodies must be repeatably and accurately fixtured relative to each other. For example, in machine tool manufacturing, a part may be fixtured to a pallet incorporating a kinematic coupling. The pallet can then be repeatably attached to various machine tool carriages possessing a matching coupling without fixturing the part again.

Additionally, deterministic bearings can be used when highly precise motion is required. In a deterministic bearing, five degrees of freedom may be restrained, where the sixth degree of freedom is the one supported by the bearing. These types of bearings

typically find application in instrument design where the bearings are not subject to large loads.

Because deterministic design relies on a small number of contact points, large loads are not distributed across large bearing areas. For example, the six contact points in a three-groove structural coupling may be subject to large hertzian contact stresses. However, the point contact is only an approximation because surface imperfections and deformations will create a contact patch. As shown in Figure 4.2, the coupling can be made with a ball in a straight groove or a gothic arch groove. The gothic arch increases the size of the effective contact patch and thereby reduces the stresses that are created on the surfaces of the balls and grooves[39]. By selecting proper materials based on the loads and numbers of fixturing cycles that a coupling will see, highly accurate, repeatable, and long lived couplings can be designed [Slocum '88B]. Materials such as hardened steels and ceramics are good choices for the contact portions of the couplings. Also, the location and orientation of the coupling points must be arranged for maximum stability in the coupling design. Both the stress and stability issues have been addressed in the literature [Slocum '92B].

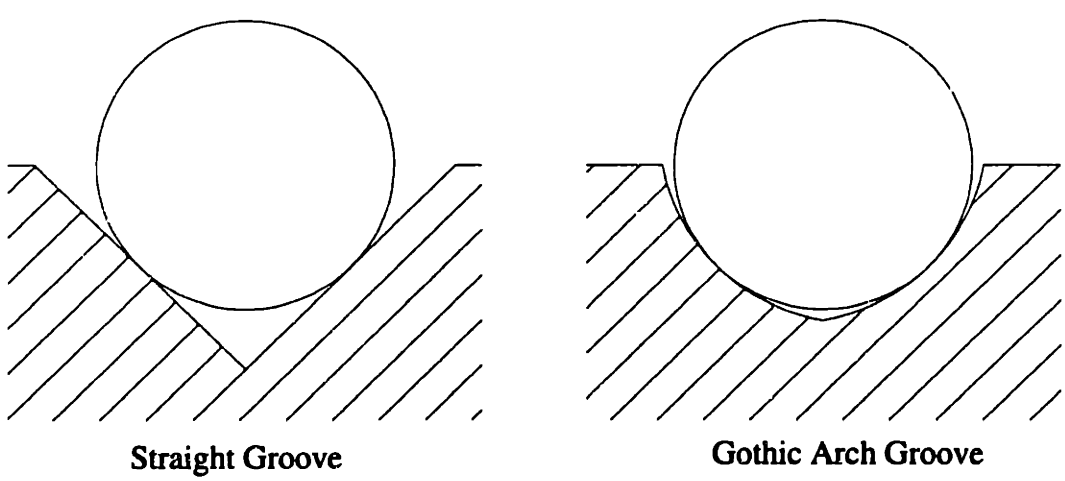


**Figure 4.2** Straight groove and gothic arch groove.

[39] As a rule of thumb, the radius of each half of the gothic arch should be about 1.1 times the radius of the ball used in the coupling. Also, the two halves of the gothic arch should be arranged so that a normal line through the contact points lies at about 45° angle to the plane of the coupling.

As was mentioned in Chapter 1, semiconductor process tools and wafer handling automation have been found to be plagued with nondeterministic designs. The nondeterminism is exhibited in compliant structures, structural couplings with numerous position adjustments, and nonrepeatable mechanisms. One of the primary goals of this research is to eliminate these practices and replace them with more robust, deterministic designs. Because determinism is one of the underlying themes of this thesis, further details and design examples are found in the following case studies in this chapter and in the discussions in Appendix A on the design of SVG's new photoresist processing system.

### 4.2.1 Case Study: Use of Kinematic Couplings in a Machine Frame

As was mentioned previously, one of the goals in the design of SVG's new machine, was a more robust and repeatable wafer handling system. Figure 4.3 shows an isometric view of the new machine including the process modules and end stations. One of the ways that the functional requirements for positioning repeatability and robustness is achieved in the new design is through the use of deterministic mounting of process modules within the rigid machine frame. Because the new frame is designed to be very stiff, reference surfaces can be machined directly into the frame.

The groove portions of the kinematic couplings for each process module (and the end stations) are attached directly to the frame of the machine. Figure 4.4 shows the groove mounting locations in the frame. The process modules, in turn, contain the ball portions of the couplings (as do the end stations). The process modules are assembled on a master fixture, so that they can be mounted directly on the frame after assembly without further set-up. Using the arrangement of kinematic couplings, no additional position adjustments are required in either the frame or the process modules. This mounting method gives a robust, deterministic system. Furthermore, the displacement error models described in Chapter 3 can be used to easy model this assembly method.

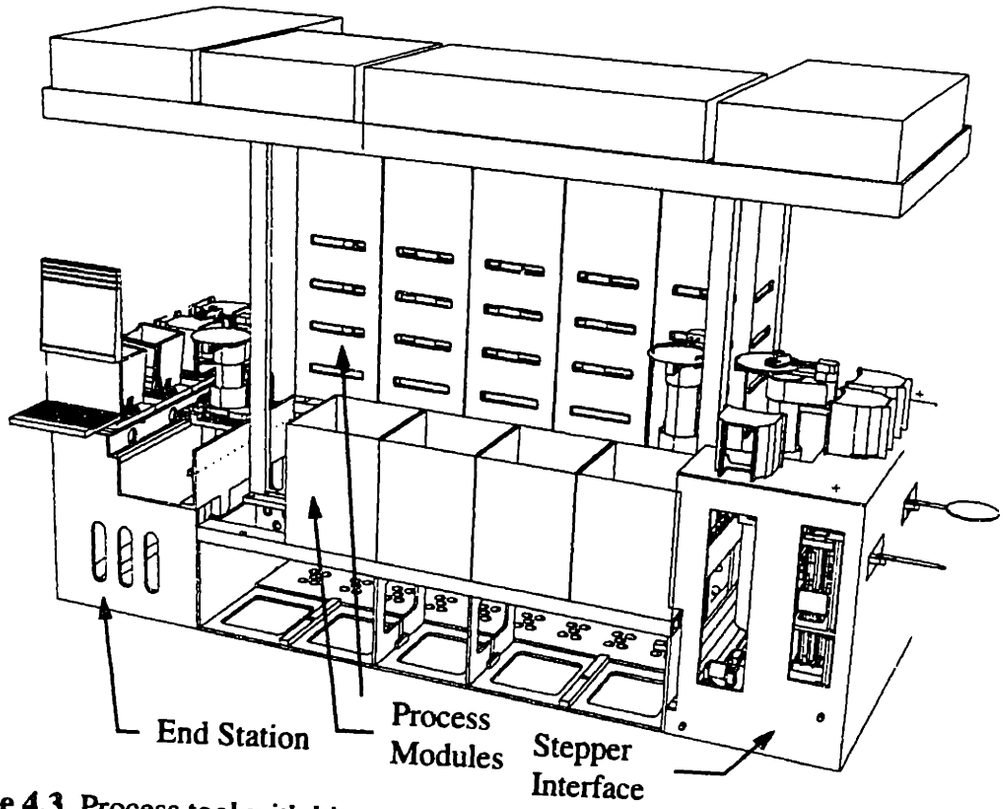


**Figure 4.3** Process tool with kinematically coupled process modules and end stations[40].

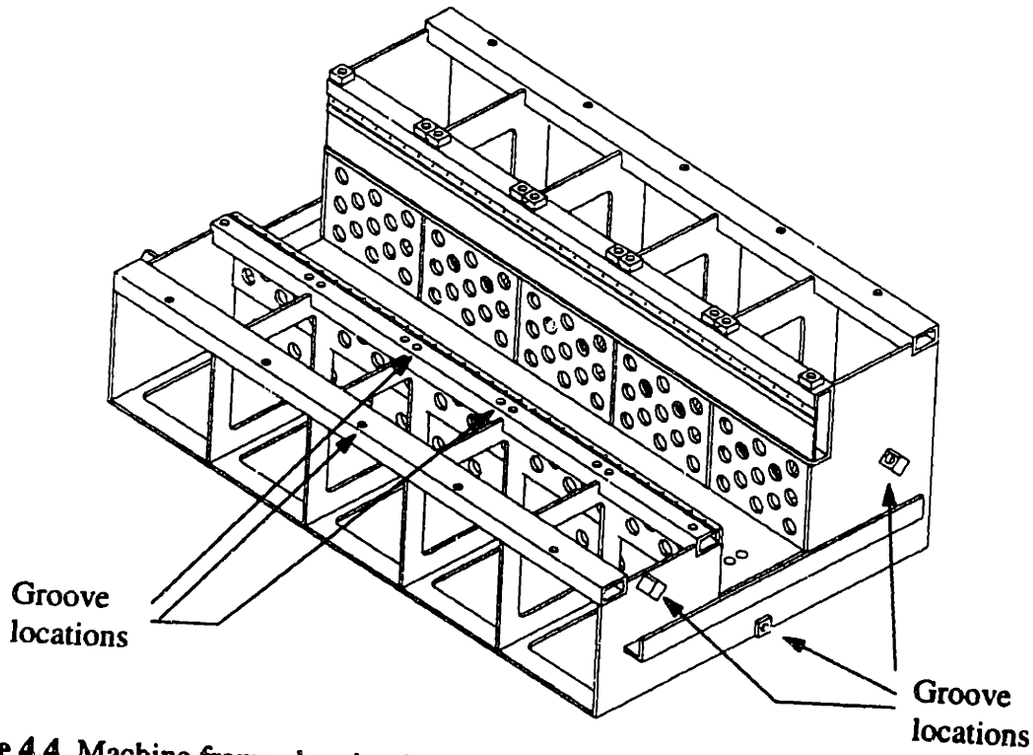


**Figure 4.4** Machine frame showing locations for groove portions of kinematic couplings.

[40] Courtesy of Silicon Valley Group.

Figure 4.5 shows details of the balls and grooves used in the machine frame. To simplify manufacture, a straight groove is used rather than a gothic arch groove. To keep contact stresses low despite the flat walls of the groove, a very large effective radius ball is used. The ball is not spherical; rather, it has a large radiused surface where the ball contacts the groove. The ball and groove pieces are ground from stainless steel and then hardened. Each ball/groove interface is preloaded by using a stack of spring washers on a bolt that passes directly through the center of the ball and groove. The spring washers give a preload force of 150 pounds when they are fully compressed. Spread sheet analysis of the contact stresses in the kinematic coupling with the given ball and groove geometry gives a coupling stiffness of $4.6 \times 10^6$ lbs/in. This analysis also shows that error motions that result from deformations in the coupling are less than a tenth of a micron. For the precision requirements in this frame, static deformations of the coupling will have no effect on the system.

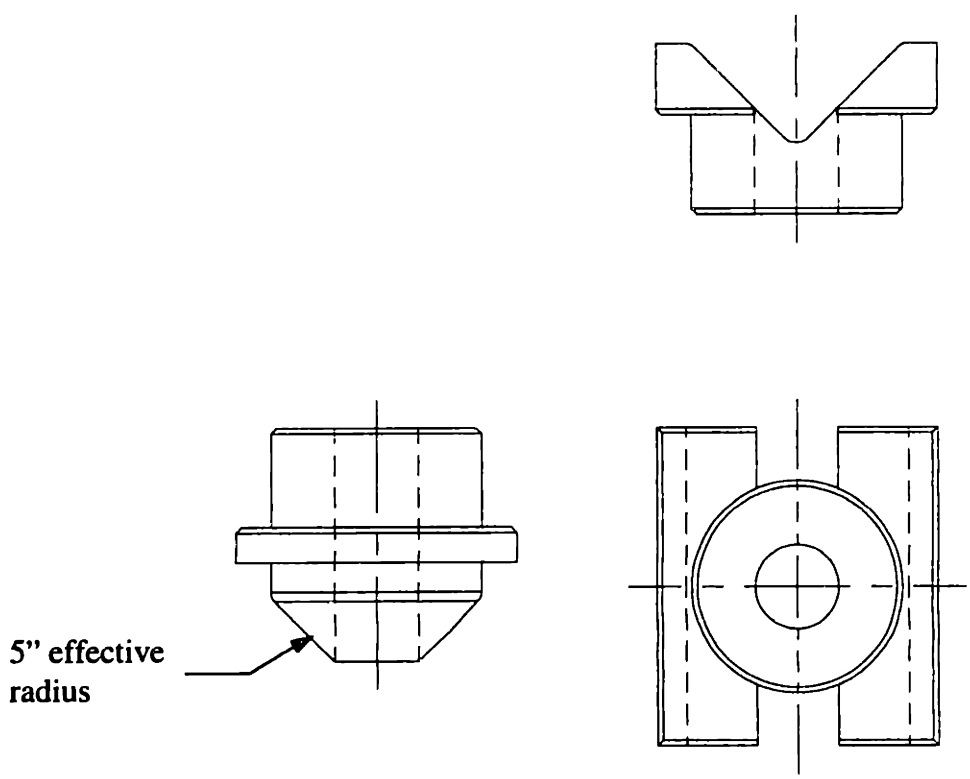


**Figure 4.5** Kinematic coupling ball shown at left and groove at right[41].

[41] Courtesy of Silicon Valley Group.

### 4.2.2 Case Study: Use of a Kinematic Coupling in a Wafer Handling Robot

Occasionally the wafer handling robot in this new photoresist processing system will require service. Because of the layout of the machine, the robot is not easily accessible to service personnel. For these reasons, the robot must be removed so service can be performed external to the machine. Also, the horizontal carriage rides on linear bearings and uses a linear motor and linear encoder; all of which are attached directly to the machine frame. It is, therefore, not feasible to remove the entire handler. The solution to this problem was to incorporate a kinematic coupling between the body of the robot and the horizontal carriage. Figure 4.6 shows how the robot lifts out of the carriage.

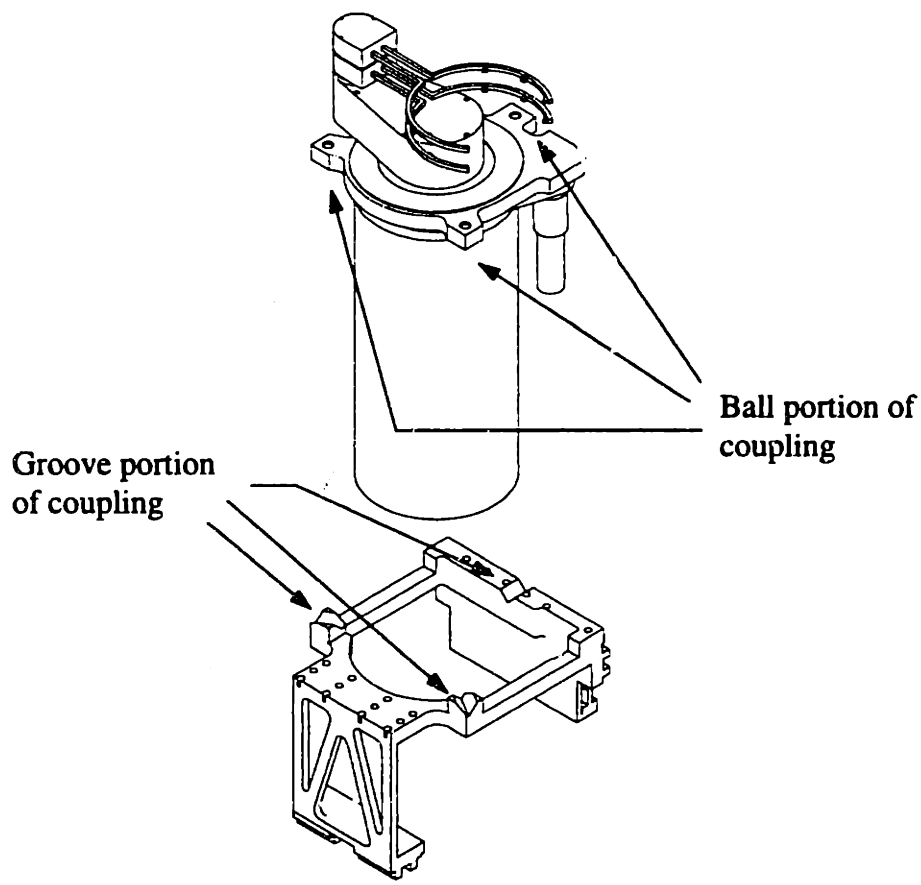


**Figure 4.6** Wafer handling robot body detached from carriage at kinematic coupling.

The body of the handler is removed simply by unbolting the three coupling preload bolts and disconnecting the wiring harness and then lifting the robot body out of the carriage. The process is reversed for installation. Because of the accuracy and

repeatability of the coupling, removal and reinstallation of the robot will not necessitate a recalibration of the robot.

The robot kinematic coupling uses the same balls and grooves as the process modules. For the robot, spring washers provide a 75 lbs. preload force between each ball/groove interface. This configuration results in a coupling with a stiffness of $3.7 \times 10^6$ lbs/in. Again, like the couplings between the process modules and frame, the error motions of this coupling are negligible for the levels of precision required in this application.

## 4.3 Elastic Averaging

Elastic averaging is another useful principle that is commonly employed in precision machine design. In contrast to deterministically designed couplings, elastic averaging relies on extensive over-constraint or forced geometric congruence between mechanical parts. Elastic averaging uses the inherent elasticity of engineering materials to average errors and achieve the desired performance. This over-constraint can sometimes be useful in spreading large forces over many contact points. Structural couplings are an area where elastic averaging is often used when kinematic couplings do not have the required stiffness or load capacity. Another common example of elastic averaging is the wide variety of rolling element bearings that are used almost universally. The large number of rolling elements distribute the loading and average the errors present in each of the rolling elements and the race ways. This arrangement results in a stiff, high load capacity, accurate bearing. Furthermore, when locally applied (as in the case of a rolling element bearing) the resulting unit can still be modeled with the techniques described in Chapter 3. For more information, the interested reader is referred to any one of the many machine design texts available that discuss rolling element bearings.

### 4.3.1 Elastic Averaging vs. Deterministic Design

The key to applying deterministic design and elastic averaging design principles successfully lies in understanding the circumstances in which each technique is

appropriate. The deterministic nature of a correctly designed kinematic coupling allows positioning errors to be accurately evaluated and therefore accounted for in the operation of a machine. However, deterministic designs cannot always be used because of their limited load capacity and stiffness. For example, it is often desirable to mount a machine on a floor with a three point, deterministic mount that does not create any over-constraint in the structure of the machine. However, some machines might be so large that they cannot support their own weight; in this case, many contact points have to be used to support the machine.

It would be quite possible (and often desirable) to use both principles side-by-side in one machine. For example, a material transfer robot might use rolling element bearings in both linear and revolute axes which rely on elastic averaging and extensive over-constraint for their load capacity, stiffness, and repeatability. This robot might, in turn, be used to transfer wafer cassettes with the groove portion of a three-groove kinematic coupling built-in into a load/unload station of a process tool with an integral three-ball mating portion of the coupling.

### 4.3.2 Case Study: Use of Rolling Element Bearings in a Wafer Handling Robot

For the design of SVG's new processing system, the use of rolling element bearings in the wafer handling robot is perhaps the most pervasive example of the application of the principles of elastic averaging in the design. Figure 4.7 shows the wafer handling robot with the locations of the various axes' support bearings shown. It should also be noted that all of the actuators, except the linear motor in the horizontal axis, use ball bearings to support the motor shafts and gear reducers. For this case study, though, the discussion will be limited to the bearings that support each axis.

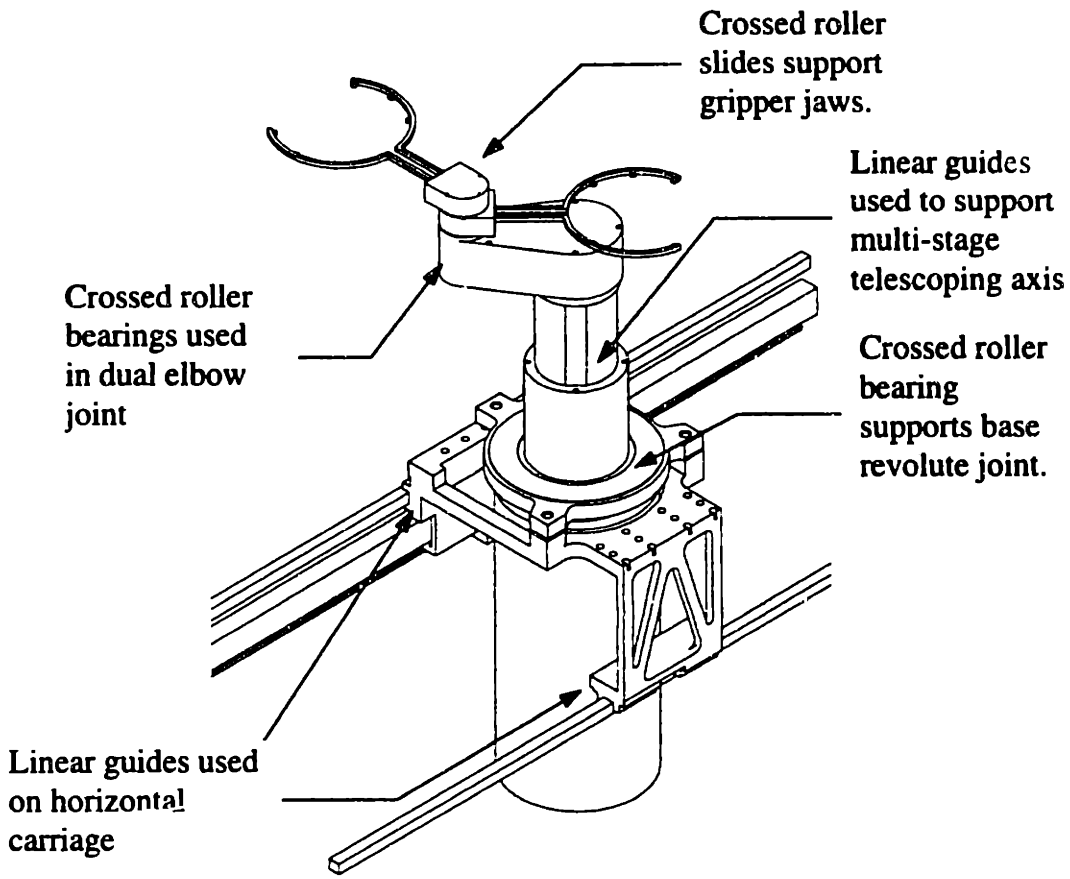


**Figure 4.7** Locations in the wafer handling robot where rolling element bearings are used.

Figure 4.8 shows a cutaway view of a crossed roller bearing. This type of bearing is used in all three rotary axes of the wafer handling robot. The rollers in this bearing are literally crossed so that the axes of rotation of the "even" rollers are at a 45° angle to the plane of rotation and the "odd" rollers are at a -45° angle.

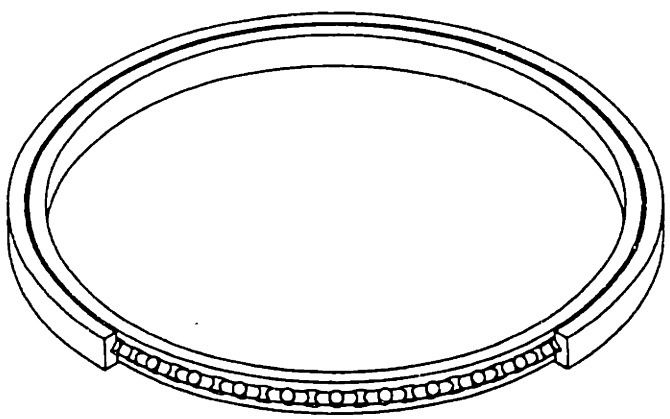

**Figure 4.8** Cutaway view of a crossed roller bearing.

Figure 4.9 shows the action of the crossed rollers within the bearing. The key element of this bearing is the retainer that holds the rollers in this configuration. The inner and outer races of the bearing are ground to form races for each roller orientation. Because of the crossed rollers, this bearing is able to support radial, axial, and moment loads. With typical ball bearings, usually at least two bearings on a single shaft separated by some distance are required to support a full set of loads. With these ball bearings, the moment capacity of the shaft and bearing arrangement is a function of the separation between the two bearings. In a crossed roller bearing, the moment capacity is a function of the diameter of the bearing. In effect, length is being traded for width.

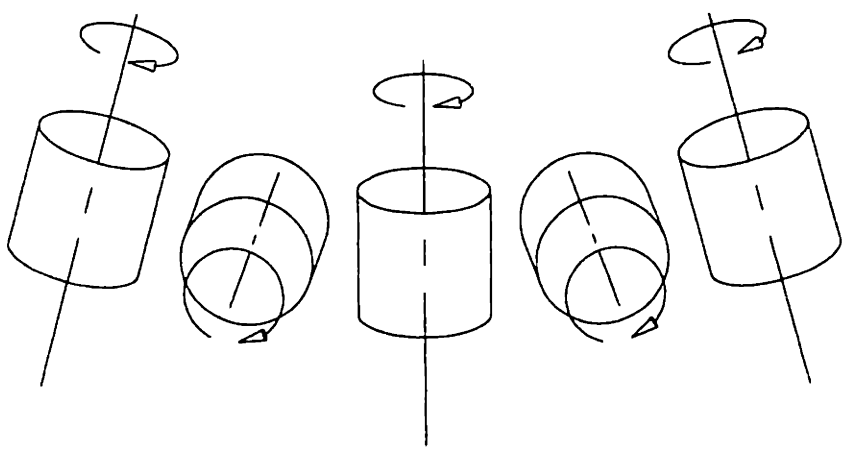

**Figure 4.9** Motion of crossed rollers.

The result is that crossed roller bearings are very attractive for supporting rotary joints in robots and rotary tables. A single, low profile bearing can be used in a joint. Additionally, because power transmission elements and electrical wires often need to be passed through these rotary joints, the increased diameter is also beneficial. In the case of the elbow joint of the wafer handling robot, the crossed roller bearing is especially effective. Figure 4.10 shows a section view of this joint.

Because the elbow joint is actually two independent rotary joints, the low profile crossed roller bearing makes space efficient packaging of the joint possible. In the figure, the lower crossed roller bearing supports the upper gripper using the narrow shaft that concentricly passes through the lower gripper shaft and bearing. Maintaining a small

footprint for the robot was important while it was still necessary to create a stiff, accurate system. The crossed roller bearing is extremely effective for this purpose.

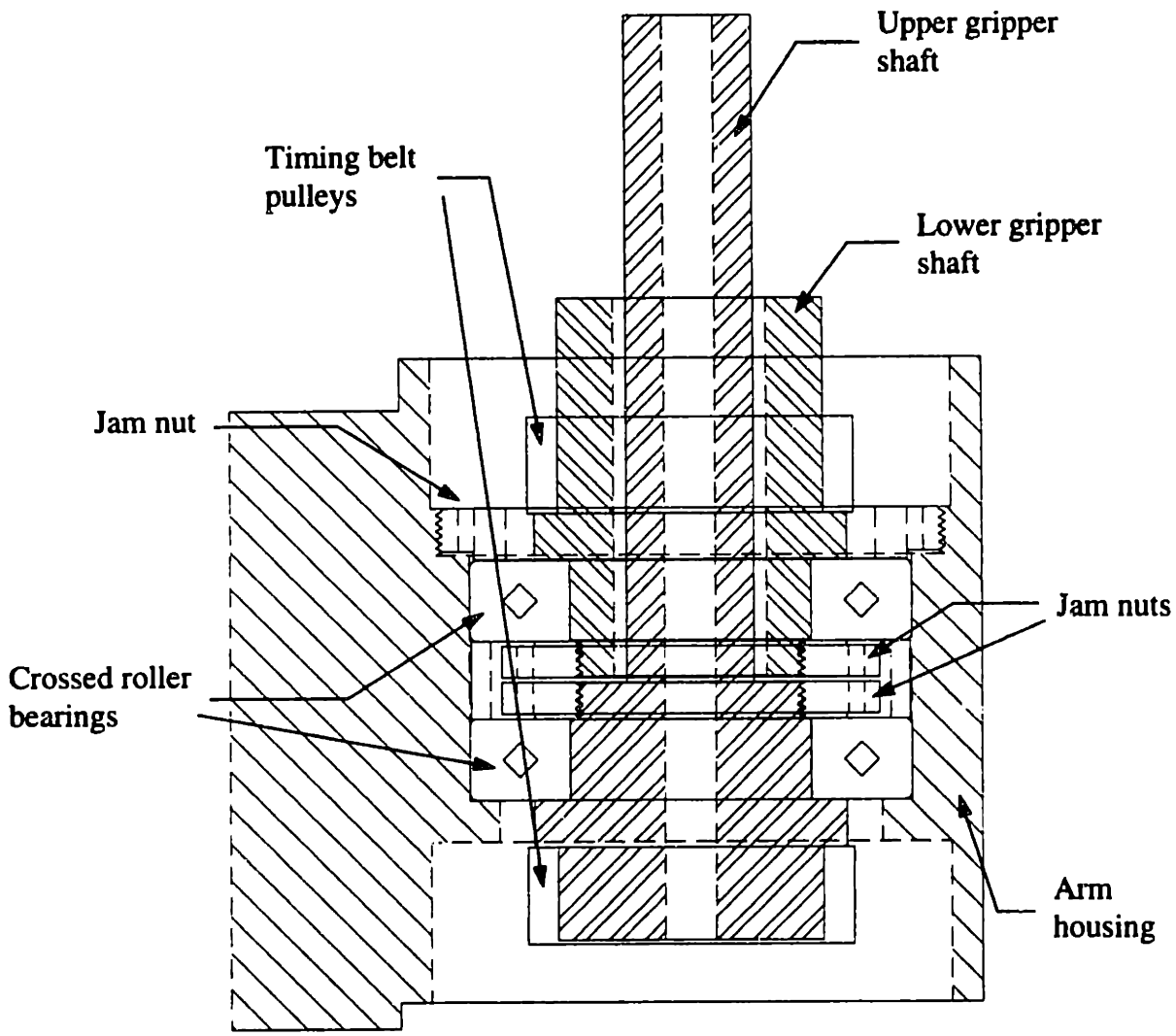


**Figure 4.10** Elbow joint using crossed roller bearings.

The two linear axes in the system, the horizontal and the vertical axes, both make use of linear recirculating ball bearings. These bearings are typically called linear guides and consist of a rail with bearing races ground in and individual bearing blocks with recirculating balls. These types of bearings are available with both gothic arch and circular arch races. The circular arch races are attractive because the balls in the bearing make a single point of contact unlike the gothic arches where differential slip occurs. The circular arch guides are available in both face-to-face and back-to-back configurations.

Figure 4.11 shows a circular arch guide with a face-to-face configuration. The back-to-back configuration actually has a larger moment stiffness about the axis of motion. Thus, these types of bearings are attractive for single rail applications. Conversely, the face-to-face configuration is good for multiple rail applications because the lower moment stiffness makes alignment less critical and the total system moment stiffness comes from the separation of the two (or more) bearing rails. Much detailed information on these types of bearings can be found in manufacturers' catalogues.

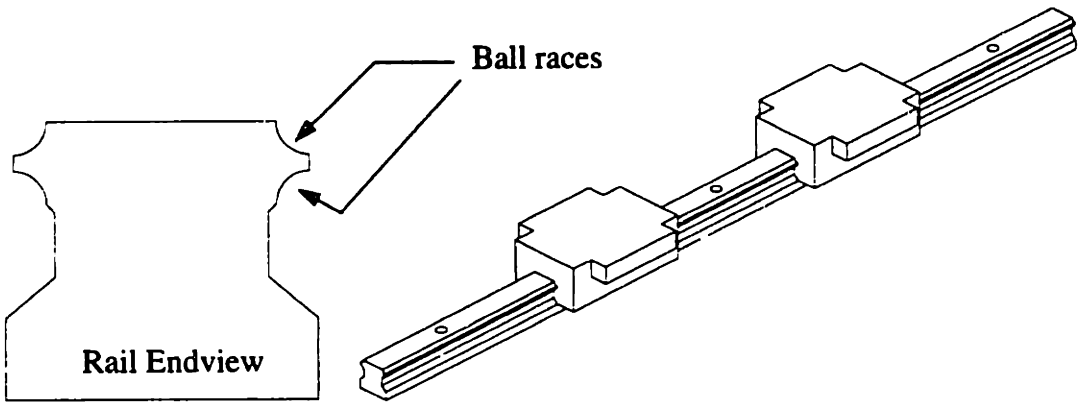


**Figure 4.11** Circular arch linear guide with recirculating ball bearing blocks.

The vertical axis in the wafer handling robot is a multi-stage telescoping joint. It uses two sets of two rails of the face-to-face circular arch variety. Each rail, in turn has two bearing blocks. Figure 4.12 shows top and side views of the bearing arrangement in this telescoping axis. Each stage has the same amount of travel. The telescoping ballscrew that drives the axis couples their motion so that each stage moves the same amount relative to its ground reference. Thus, the upper stage moves twice as far and twice as fast as the lower stage. The telescoping axis is used to reduce the vertical footprint of the wafer handling robot when it is fully collapsed. The use of these linear guides allows the system to maintain stiffness while still being very compact.

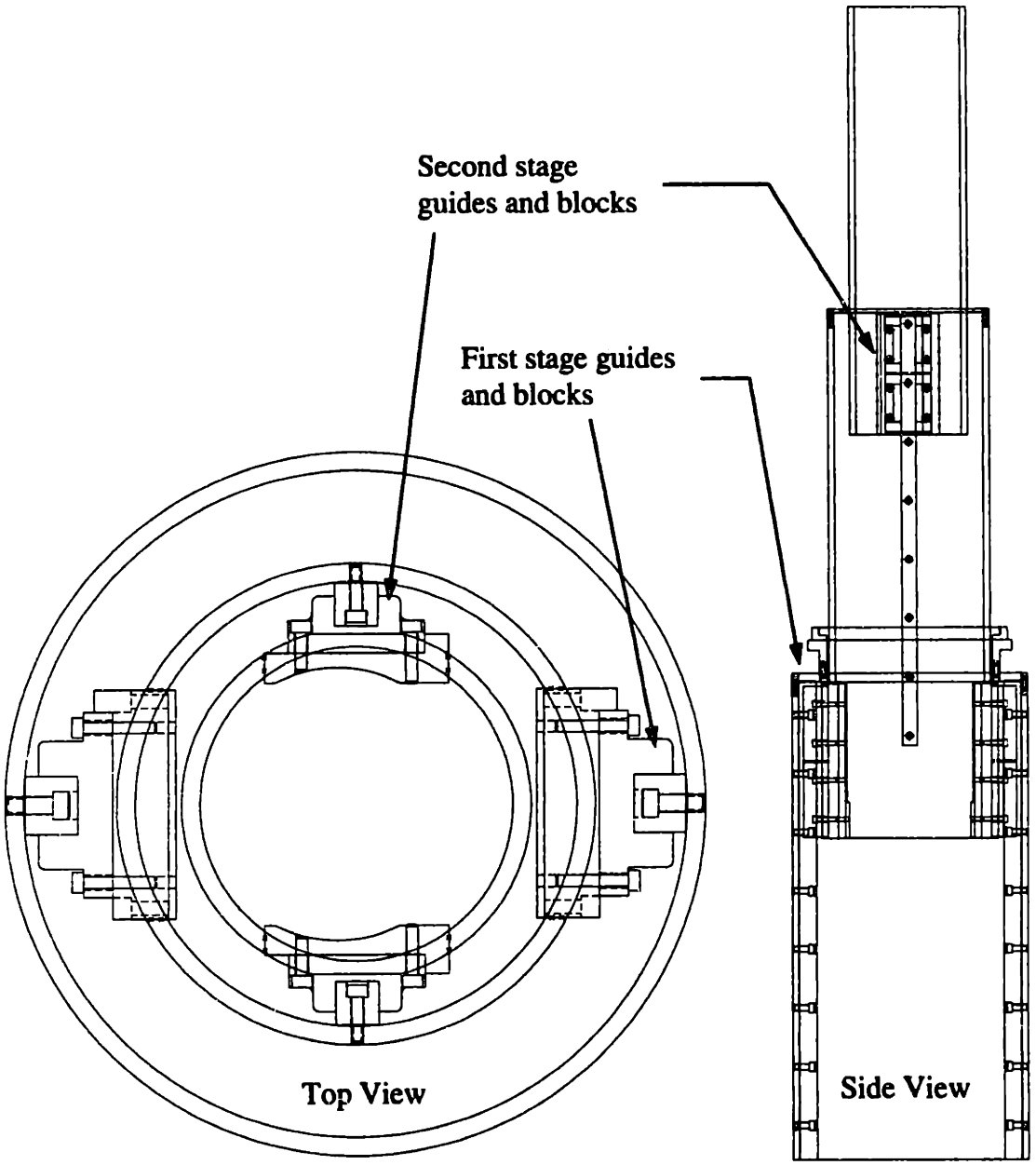


**Figure 4.12** Linear guides used in telescoping vertical axis.

## 4.4 Reduction of the Effects of Rotational Errors

One of the most insidious problems that can creep into the design of a machine is the amplification of rotational errors by a moment arm. In the design of any precision machine regardless of the level of precision, the designer must be aware of the large

errors that can occur at the end point of a system as the result of rotational errors farther back in the system.

### 4.4.1 Abbe Errors

These effects are called Abbe errors and were discussed initially in Chapter 2 and have been examined in some depth by other researchers [Bryan '79] [Slocum '92A]. Abbe errors cannot always be avoided, as shown in the following case study; but at the very least, the designer must be aware of their presence. If the designer makes uses of some geometry in his or her design that does amplify an angular by a moment arm, then he or she must carefully model the resulting errors to insure that they do not exceed the level acceptable for the design.

### 4.4.2 Case Study: A Wafer Gripping and Centering Mechanism

In the photoresist application process, high-acceleration, high-speed spindles are used to distribute a drop of photoresist uniformly across the surface of a wafer by centrifugal effects. Because the wafer must be dynamically balanced on the spindle and because the bead of resist that forms on the edge of the wafer must be carefully removed following the application process, it is important that a wafer is precisely centered on the spindle. Formerly, Silicon Valley Group has used a bulky iris mechanism housed within each spin station to perform that centering operation. Because of the desire to minimize the total footprint of the machine, the centering process was moved from the process module to the end effector of the wafer handling robot. In Appendix A, the design of the centering wafer gripper is discussed in greater detail. However, two of the most viable gripper candidate designs are discussed here briefly to illustrate the Abbe error principle.

Figure 4.13 shows the "fork type" gripper that is designed for accessing process modules from the central wafer handling robot. The two jaws of the gripper are each mounted on a separate crossed roller slide. Each jaw has a rack attached to it and a pinion mounted on the shaft of a stepper motor is sandwiched between the racks. The pinion couples the motion of the jaws so that both either open or close an equal amount. A spring is connected to one of the jaws and to the housing of the gripper. This spring

provides the return force that closes the gripper and holds the wafer in place once in has been gripped and centered. The stepper motor is used to provide a bias force that controls the closing motion and opens the jaws of the gripper. The coupled motion of the jaws is required because the gripper must center the wafer to better than ±0.002 inches. Furthermore, the wafer has a diameter tolerance of ±0.008 inches. However, the wafers tend to be very round because of the manner in which they are manufactured. The coupled jaws are, therefore, able to bring a round wafer repeatably to the same center position despite a fairly wide variation in the diameter of the wafers.

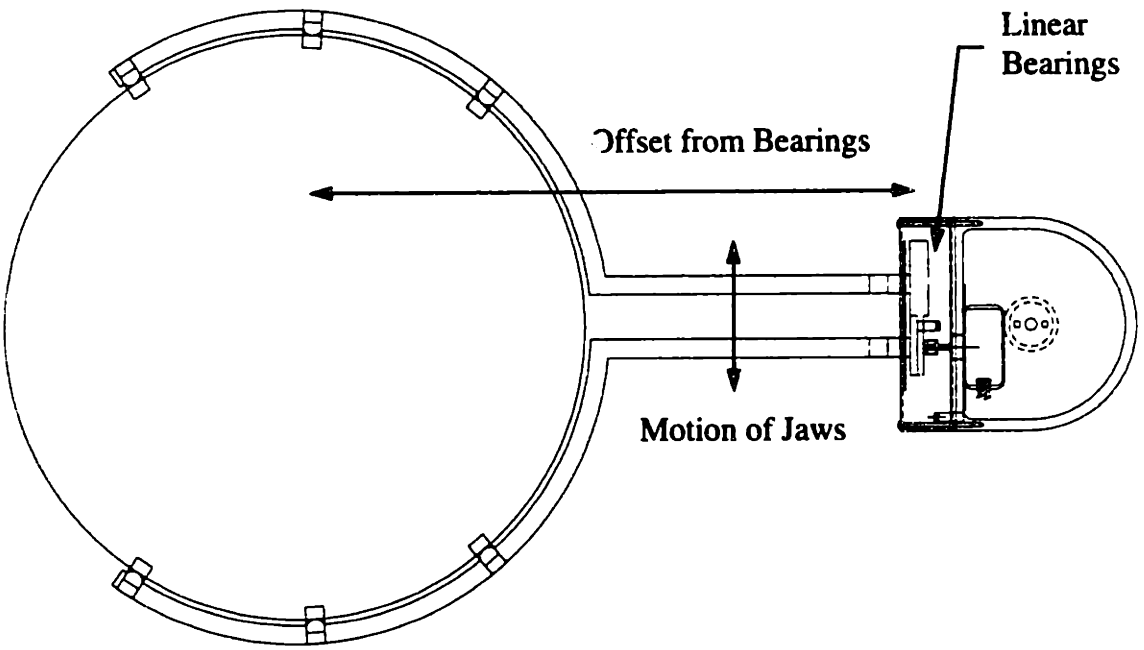


**Figure 4.13** Fork-type gripper showing Abbe error caused by bearing offset[42].

Because of the geometry of the vacuum chuck on the spindle that holds the wafer, the gripper jaws must move perpendicular to the direction in which the wafer is inserted into the process module. This arrangement causes the center point of the wafer to be offset from the axis of motion of the jaw bearings by 8.6 inches. So, any angular errors in the crossed roller slides will be magnified by this offset. The manufacturer specifies that the crossed roller slide has a straightness of travel of 0.0001 inch per inch of travel. The

[42] Six points of contact are used in the gripper because 200 mm wafers have either a flat or a notch. Because the orientation of the wafer is not important in a photoresist application process, the wafer handling robot moves wafers with random orientation and the gripper must be tolerant of this.

range of bearing travel in the gripper is 0.5 inches. The maximum deviation of the center point for one jaw is therefore 0.00043 inches. It should be noted that the six contact points tend to average the errors that may occur in the positioning of the jaws. An error model analysis of this gripper shows that at worst case the gripper centers the wafer to ±0.0015 inches. The presence of the Abbe error essentially establishes a requirement for the straightness of the jaw bearing travel. Because the crossed roller slides are within this limit, the design is able to perform as required despite the geometric constraints imposed by the spin station chuck and the resulting Abbe error.

The same centering operation could be performed without an Abbe error by placing the linear bearings in line with the center of the wafer if the vacuum chuck constraints did not exist. In the end stations of the photoresist processing system, the geometric requirements lead to just such a gripper. Figure 4.14 shows the "tongue type" gripper that is used in the end station and stepper interface where the robot must access wafer holding cassettes.

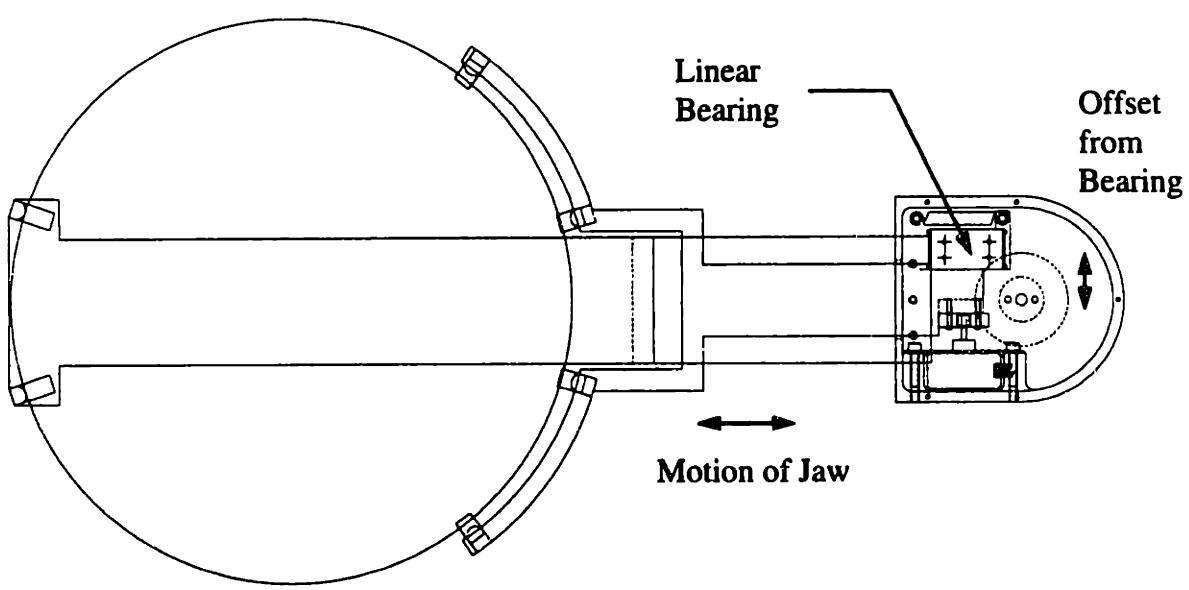


**Figure 4.14** Tongue-type gripper with very small Abbe error.

The geometry of the cassette requires that the gripper have a "tongue" that can reach through the cassette to grab the rear edge of the wafer. Because this gripper does not access spin stations, the centering requirements are not as demanding. For this reason

only the short jaw moves in this design. So, this gripper will be able to center wafers to ±0.004 inches, where the uncertainty is due primarily to the variation in wafer diameter. Also, because of packaging constraints in the housing of the gripper, the crossed roller slide is offset by 0.7 inches. This small offset does create a small Abbe error, but its magnitude is negligible relative to the variations in wafer diameter.

## 4.5 Static and Dynamic Structural Deformations

In Section 4.2 the importance of deterministic design was discussed. As a continuation of this discussion, it is also necessary to provide a stable, robust structure on which a machine is based. This section discusses the importance of static and dynamic stiffness in the machine structures of semiconductor processing equipment.

### 4.5.1 Static Effects

As has been discussed previously, one of the goals in using deterministic design techniques in the design of semiconductor processing equipment is the elimination of positioning adjustments in the mounting of process modules to the machine frame. The case study in 4.2.1 showed how kinematic couplings can be used to eliminate these adjustments. However, in the past these adjustments were included to compensate for an overly compliant machine frame. It is therefore also necessary to optimize the stiffness of the support structure in a machine where deterministic design principles are being applied. The goal is simply to create a rigid body that will not deflect significantly under normal operating conditions. In cleanrooms, this rigidity is especially important because floors are often used as return air vents. These floors are typically made of die cast aluminum tiles with many perforations and are supported at the corners with under-floor pedestals. These floors tend to be very compliant and deflect significantly under the weight of fab personnel. The process tool must therefore be rigid enough that it does not deflect as the floor deflects.

Many analytical and numerical tools are available to designers for structural design purposes. A designer's first reference should be a good strength of materials text

such as the one by Gere and Timoshenko [Gere '84]. Also, structural design handbooks are commonly available. Furthermore, finite element analysis may also be useful in analyzing design alternatives. Because the methods of structural design are discussed at great length elsewhere they will not be addressed further here.

### 4.5.2 Dynamic Effects

In addition to providing a statically stiff machine frame, the design engineer must also insure that the structure is dynamically stiff enough. Mechanical structures are usually characterized by very low damping. So, if some source of excitation is present in the machine, large vibration amplitudes may exist at the resonant modes of the structure. Although finite element methods can also be used to perform dynamic analysis of a structure, they can be numerically intensive and mechanical systems are often difficult to model. However, the designer can also employ a useful first order estimate to guide the design of the system.

Equation 4.1 shows the classical form of a second order system with velocity proportional damping and a linear spring.

$$m\ddot{x}(t)+c\dot{x}(t)+kx(t)=F(t) \tag{4.1}$$

where $m$ is the lumped mass, $c$ is the damping coefficient, $k$ is the spring constant, and $F(t)$ is the forcing function. This second order system can also be represented in the familiar form shown by Equation 4.2

$$\ddot{x}(t)+2\zeta\omega_n\dot{x}(t)+\omega_n^2x(t)=\omega_n^2f(t) \tag{4.2}$$

where $\zeta$ is the damping factor and $\omega_n$ is the natural frequency.

In most real systems, however, damping is not proportional to velocity. It has been shown that for many materials including most metals, the energy dissipated in a single cycle of stress is proportional to the displacement amplitude squared [Meirovitch '67]. This fact can be used to define an equivalent viscous damping coefficient that is

proportional to the system stiffness. This type of damping is generally called structural damping. Equation 4.3 shows the second order system with structural damping.

$$m\ddot{x}(t)+\frac{\gamma}{\omega_n}k\dot{x}(t)+kx(t)=F(t) \tag{4.3}$$

where $\gamma$ is the structural damping factor and the damping coefficient has been replaced by $\frac{\gamma}{\omega_n}k$. Equation 4.4 shows the Laplace transform of this system.

$$[ms^2+\frac{\gamma}{\omega_n}ks+k]X(s)=F(s) \tag{4.4}$$

Equation 4.5 shows the system evaluated at a frequency, $\omega$, in the complex plane.

$$\frac{X(j\omega)}{F(j\omega)}=\frac{1}{[-\omega^2 m+(1+\frac{\gamma}{\omega_n}\omega)k]} \tag{4.5}$$

It can be seen that the magnitude of the transfer function evaluated at the natural frequency of the system simplifies to the expression shown in Equation 4.6.

$$\left|\frac{X}{F}\right|=\frac{1}{\gamma k} \tag{4.6}$$

Often a loss factor, $Q$, is defined in terms of the structural damping factor as shown in Equation 4.7.

$$Q=\frac{1}{\gamma} \tag{4.7}$$

For most mechanical systems, $Q$ values range from 10 to 50. Equation 4.6 gives a very simple result in that the displacement magnitude at resonance is equal to the loss factor times the magnitude of the forcing function at that frequency divided by the system stiffness.

This analysis can also be easily extended to multibody discrete systems. Equation 4.8 gives the general form for linear discrete systems.

$$[m]\ddot{\underline{x}}(t)+[c]\dot{\underline{x}}(t)+[k]\underline{x}(t)=\underline{F}(t) \tag{4.8}$$

The structural damping idea can be used to create a diagonal damping matrix, $[c]$. If the system is lightly coupled, the result in Equation 4.6 can be used directly to estimate the system response of each rigid body in the system at its natural frequency. Furthermore, because the damping is a linear function of the system stiffness, the eigenvectors of the eigenvalue problem shown in Equation 4.9 for the equivalent undamped system can be used to uncouple the system of equations in Equation 4.8 [Meirovitch '67].

$$[k]\underline{u}=\omega^2[m]\underline{u} \tag{4.9}$$

The resulting uncoupled system of equations will be in the form of Equation 4.10.

$$\ddot{q}_i(t)+2\zeta_i\omega_i\dot{q}_i(t)+\omega_i^2 q(t)=Q(t) \tag{4.10}$$

Of course, real systems are continuous and have an infinite number of modes. However, it is possible to use modal analysis to evaluate these systems. For example, de Nijis et al. created a lumped parameter model of a coordinate measuring machine with the assistance of an experimental modal analysis of an existing system [de Nijis '88]. Similarly, Tlusty and Stern created a discrete model of an industrial robot, again using experimental modal analysis techniques [Tlusty '85]. The structural joints and bearings in systems are also commonly of interest. Lee used a discrete model, finite element analysis, and modal testing to model joints and bearings [Lee '88].

However useful, experimental modal testing can only be performed after a system has been constructed. During the design process, the designer must use either finite element techniques or first order analysis to assist in creating systems. It is suggested here that a designer use estimates of mass and stiffness properties in the system of interest to estimate the dynamic response with Equation 4.6. The lowest modes in the system will generally come from the most compliant parts of a structure or the bearings in a

mechanism. So by using a simple model, the designer will have some means to predict the dynamic performance of his or her system.

The designer can also apply simple design rules that are deduced from examining a linear second order system. Reducing the mass of a system will tend to increase the natural frequency and decrease the amplitude of the displacement response at resonance. This effect can be inferred from Equation 4.11.

$$2\zeta\omega_n = \frac{c}{m} \text{ and } \omega_n^2 = \frac{k}{m} \tag{4.11}$$

However, higher mass causes a system to look more like a low pass filter. Therefore, a reduction in mass will also be accompanied by a decrease in higher frequency noise attenuation. An increase in stiffness will also tend to increase the natural frequency and decrease the amplitude of the displacement response at resonance without the loss of high frequency attenuation. The final option is to add damping to the system. This addition will result in a smaller amplitude of vibration around the resonant frequency.

### 4.5.3 Case Study: The Structural Frame of a Process Tool

This case study describes the structural design of the machine frame for the Accipiter project. It also compares this new frame with the structure that is used in SVG's previous photoresist processing system. Appendix A describes in greater detail the functional requirements of the frame and some features of the design.

Figure 4.15 shows SVG's previous frame design. The structure is made primarily from square steel tube stock. The three H-shaped cross pieces are welded together. The rest of the frame structure is formed with bolted joints. Each joint interface requires finish machining. The U-shaped pieces protruding vertically provide the mounting locations for the process modules. The wafer handling mechanism for the machine rides on linear bearings mounted on an angle in the central portion of the machine.

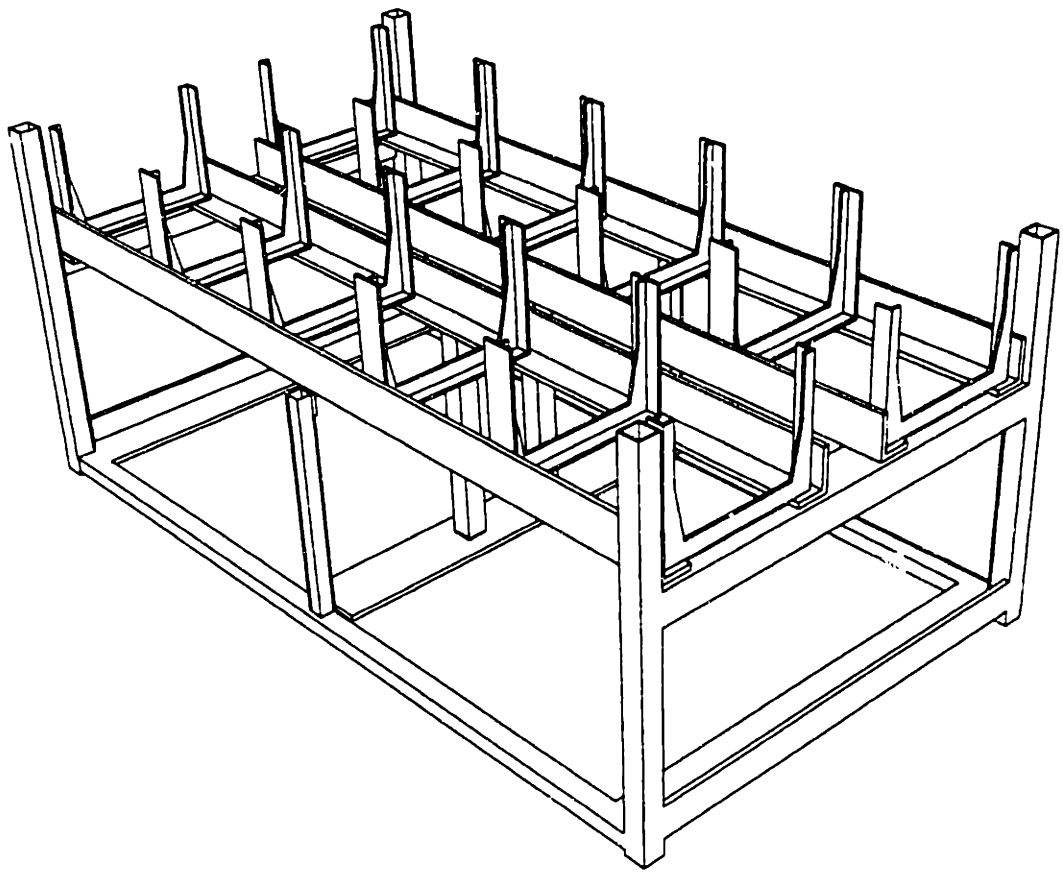

**Figure 4.15** Frame design for SVG 90 Series photoresist processing system[43].

Figure 4.16 shows the new frame design. In contrast to the 90 Series frame, this structure is a steel weldment with no bolted joints. Because the wafer handling robot in the new design has a much larger vertical stroke, a central alley exists in the machine to accommodate the body of the robot. Below this alley is a structural spine that gives the frame great torsional and bending stiffness. Because many elements of the photoresist processing system must be stored within the frame of the machine, the layout of the weldment was defined for accessibility. Compartments exist below both rows of process module locations and are open to the sides of the machine.

[43] Courtesy of Silicon Valley Group.

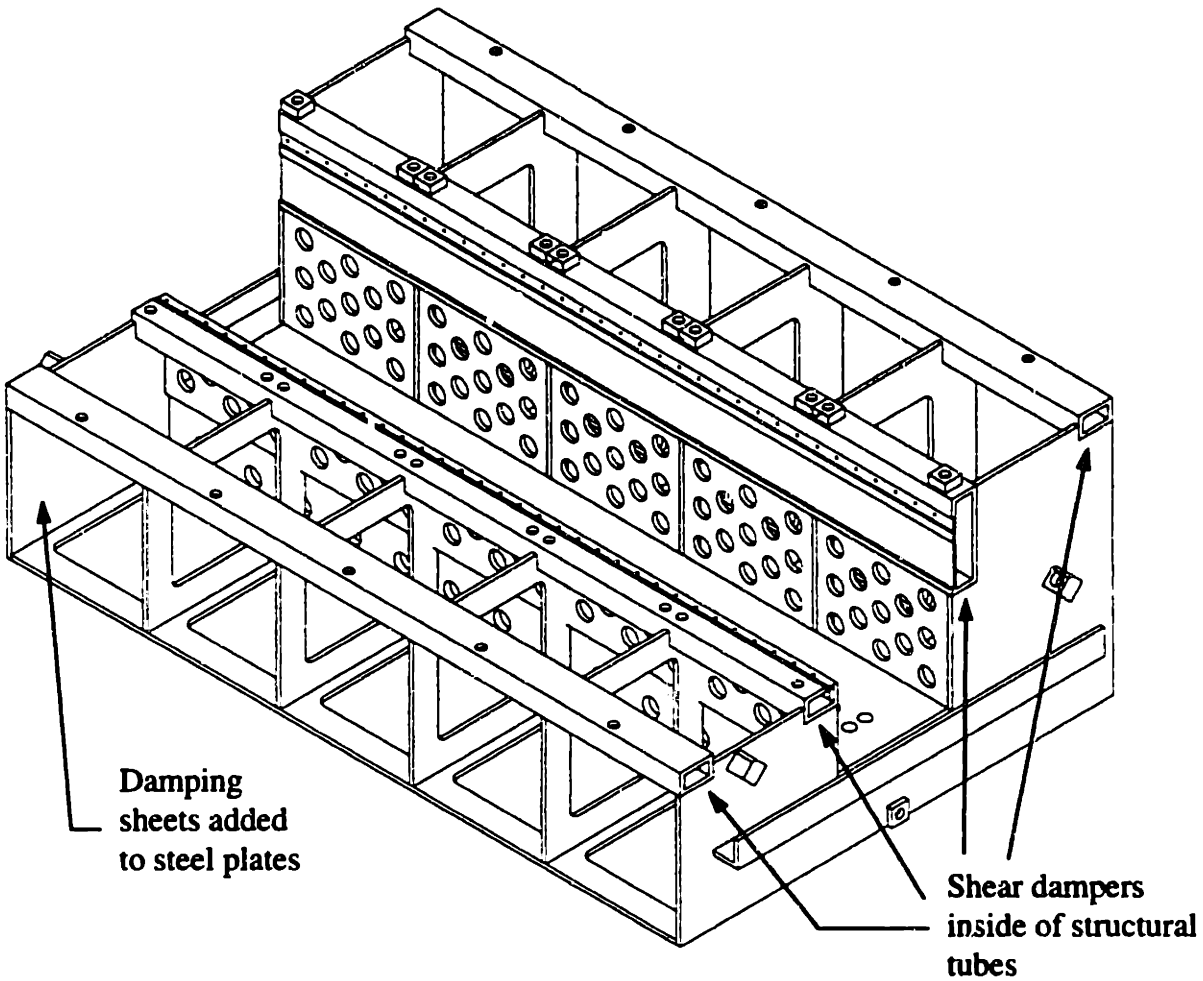


**Figure 4.16** Machine frame with structural damping added.

Finite element analysis indicates that the Accipiter frame design is more than 50 times stiffer than the 90 Series frame. Appendix C contains representative results from this analysis. As shown in the appendix, the 90 Series frame is especially compliant under torsion. This frame is also mounted on the floor with many feet. The result of this compliance and mounting method is that the 90 Series frame tends to conform to floor as it deflects. These instabilities in the frame have caused problems in the set up of the wafer handling mechanism, in turn. The Accipiter frame, by contrast, is mounted on a three point whiffle tree mount and is very rigid. The new frame will, therefore, act as a rigid body even when environmental disturbance occur.

The Accipiter frame also makes use of a new method for adding internal damping to a machine structure recently developed at MIT [Marsh '94]. Special shear dampers are

placed within four structural tubes at the top of the Accipiter frame as shown in Figure 4.16. This damping location is especially effective because these four tubes support the groove portions of the process module kinematic mounts. This configuration also helps to vibration isolate the modules. Additional damping is added to the Accipiter frame using thin metal sheets backed with a viscous adhesive attached to plates in the structure[44].

Figure 4.17 shows the details of a shear damped beam. The small insert beams are coated with a viscous layer and held in place within the structural beam with an epoxy filler. The inserts are not axially held within the beam. When the beam vibrates in bending, relative motion occurs between the inserts and the primary beam. This relative motion tends to create shearing stresses within the viscous layer; thus dissipating energy.

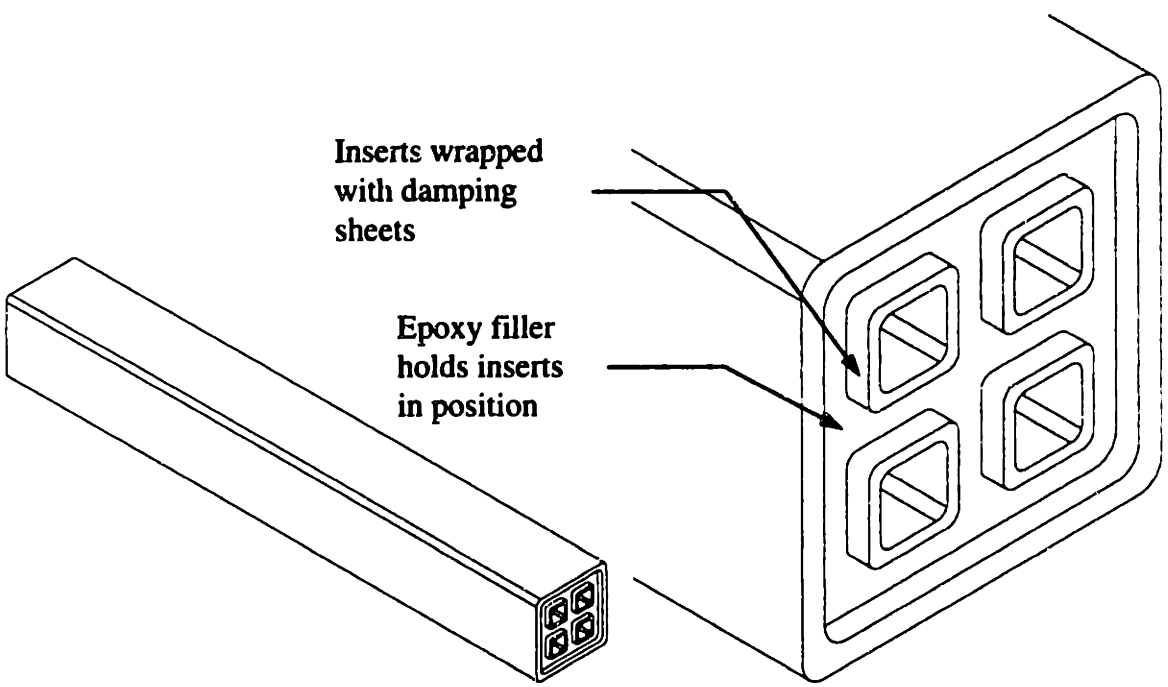


**Figure 4.17** Shear damped beam.

### 4.5.4 Case Study: The Design of a Ballscrew Support Structure

The dynamic performance of the wafer handling robot used for the Accipiter project is also improved with the addition of damping material.

[44] These sheets are called Soundcoat and are commercially available.

Figure 4.18 shows the fully collapsed multi-stage telescoping axis that is used to give the handler its large vertical stroke with a short collapsed height. The outer nut of the multi-stage ballscrew is fixed to the outer structure of the axis with a stand-off.

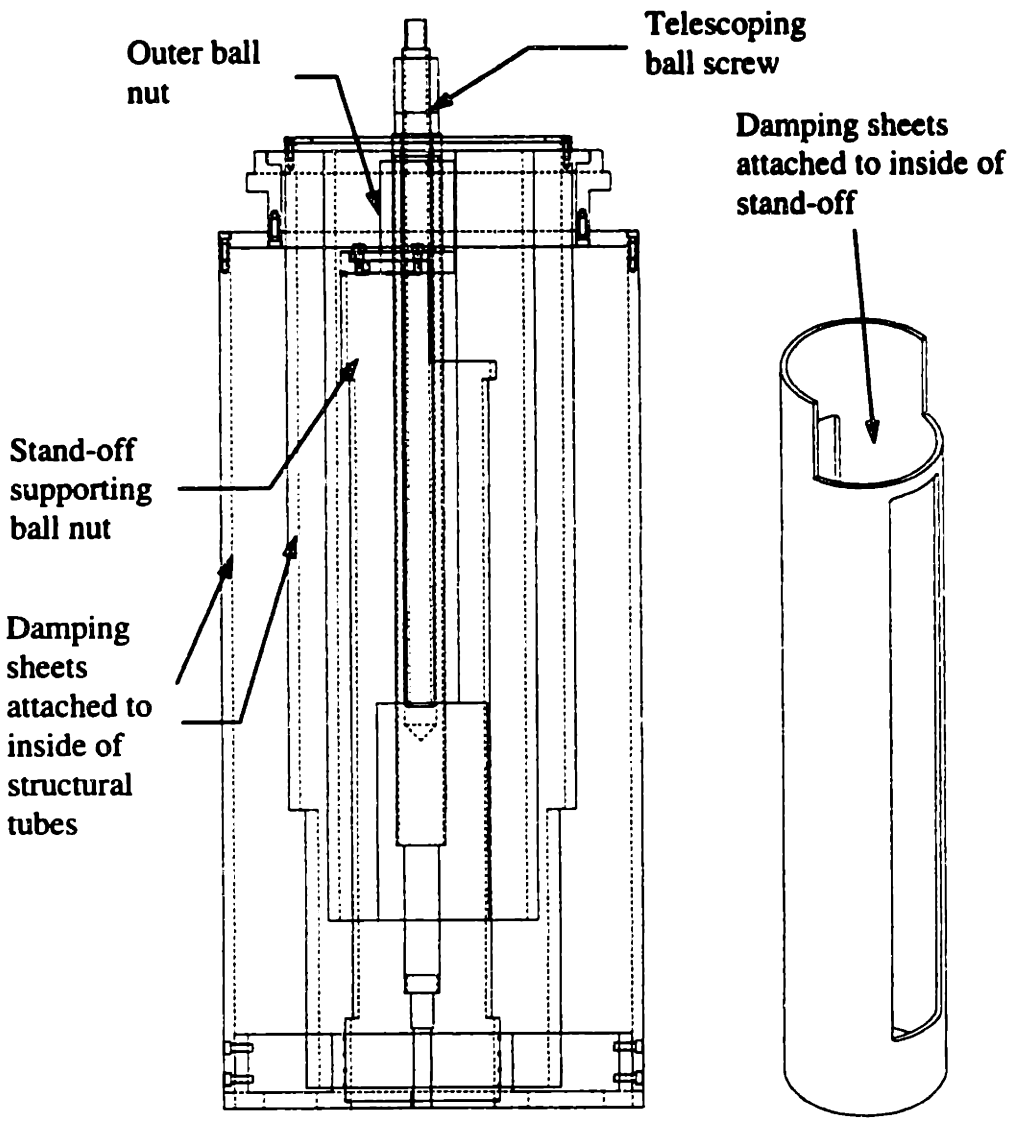


**Figure 4.18** Fully collapsed telescoping vertical axis shown at left with ball nut structural support at right.

Because of the cascaded structure of the telescoping axis, it was desirable to have some compliance in the stand-off so that small misalignments in the ballscrew assembly will not create large radial loads in the outer ball nut. The stand-off was therefore designed with a wall thickness of only 0.1 inch. A first order estimate of the bending

stiffness of this tube is $1.0 \times 10^4$ lbs/in. So a 0.005 inch deflection would only create a 50 lbs. radial load on the ball nut, which has a radial load capacity of about 200 lbs.

Although some static compliance in the stand-off is desirable, the dynamic stiffness of the tube could not be compromised. The first order estimate of the fundamental mode of vibration of this tube is 390 Hz. At the maximum travel rate of the axis, the ballscrew turns at 1500 rpm, which is 25 Hz. The primary excitation frequency is well below the fundamental mode of the stand-off as it should be. However, it is still necessary to make the stand-off as dynamically stiff as possible since the balls recirculating in the ballscrew create higher frequency noise. For this purpose, damping material similar to that used for the frame is added to the inside walls of the structural tubes and the stand-off. Damping the vibrations in the ballscrew will also help to reduce the levels of background vibration in the wafer handling robot.

Figure 4.19 to Figure 4.22 demonstrate the effects of damping the vibrations induced by the ballscrew. For these measurements, damping sheets were added as described above and the ballscrew was lubricated with a cleanroom acceptable grease.

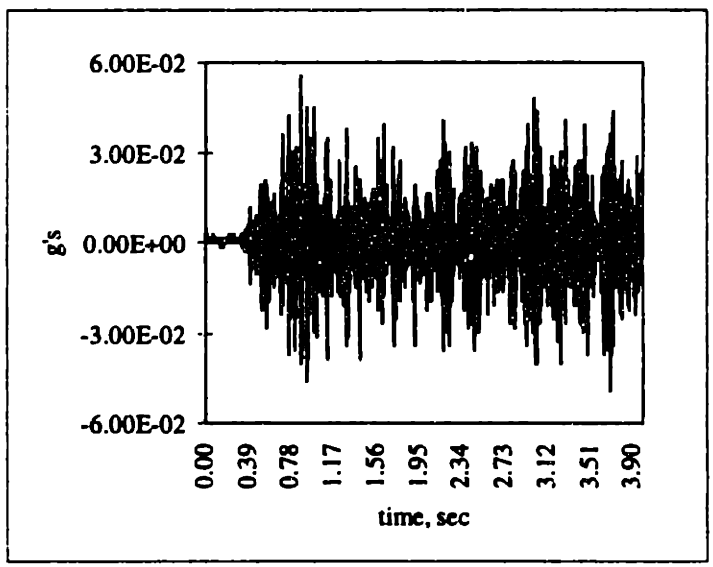


**Figure 4.19** Time history of acceleration amplitude from vibration of ballscrew before addition of damping material.

Both of these measures contributed to the vibration reduction shown here. Figure 4.19 and Figure 4.20 show the reduction in vibration amplitude for the time history.

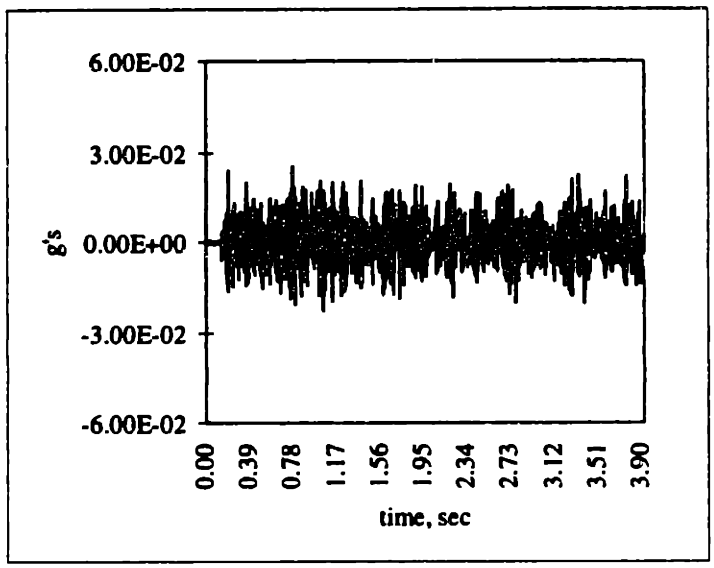


**Figure 4.20** Time history of acceleration amplitude from vibration of ballscrew after addition of damping material.

Fast fourier transforms of these data are presented in Figure 4.21 and Figure 4.22.

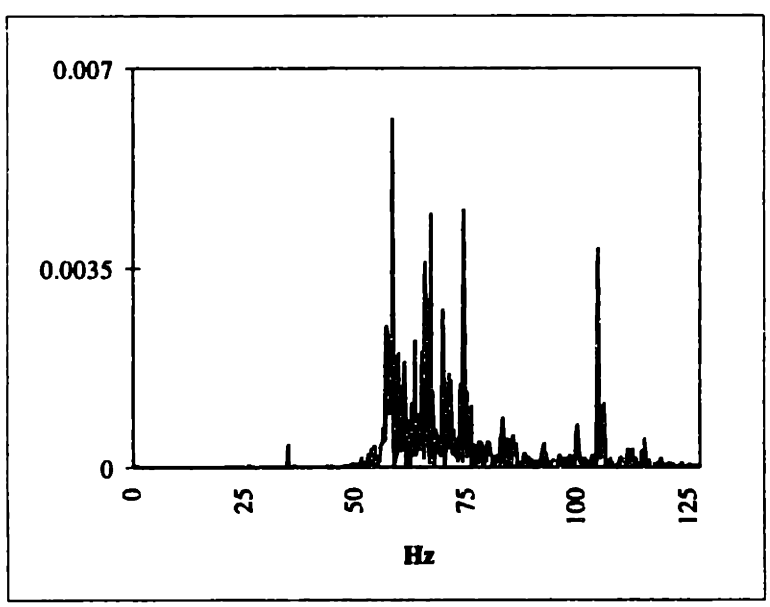


**Figure 4.21** Power spectral density of ballscrew vibration before addition of damping material (130 Hz bandwidth measurement).

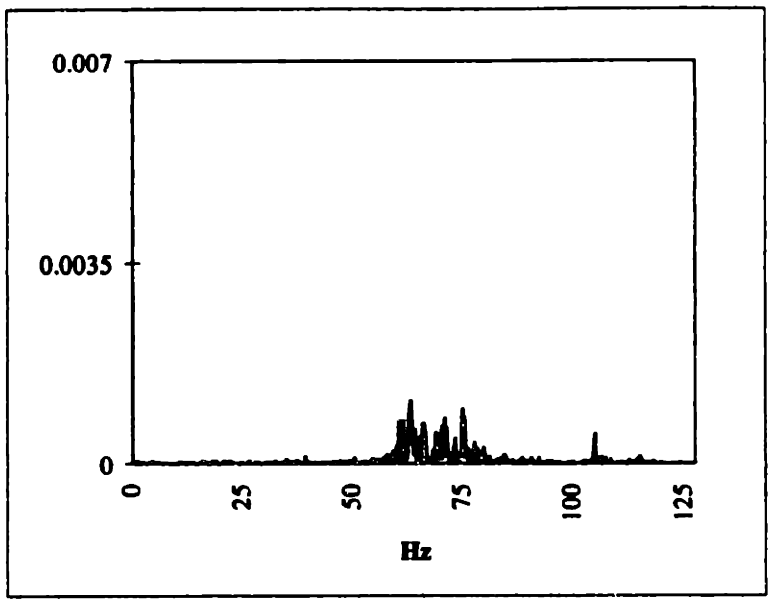


**Figure 4.22** Power spectral density of ballscrew vibration after addition of damping material (130 Hz bandwidth measurement).

## 4.6 Control and Mechanical System Integration

Control system development should proceed in parallel with the mechanical design of a system. A model of the system can be created based on the design and simulations can be performed to determine the effects of various types of controllers. The simulation results will provide feedback for mechanical designers and may provide information that can be used to optimize the design. Also, modeling and simulation can be useful tools in the selection of sensors, actuators, amplifiers, and power transmissions. Often nonlinear effects such as backlash, amplifier saturation, and quantization errors from digital position sensors such as optical encoders can be included in a simulation to determine system performance and potential problems before an actual prototype is built and tested. This type of approach can potentially reduce the time required to develop a successful system and increase the level of performance.

### 4.6.1 Control Systems in Cleanroom Robots

Many of the design reviews mentioned in Chapter 1 identified control system implementation issues that may improve the performance of a system. For example,

superior performance of a cassette handling robot has been achieved using advanced control algorithms [Van Doren '94]. In other cases, the vibration levels and settling times of servo-controlled mechanisms may be reduced simply by using trajectories that are free from the higher order trajectory discontinuities commonly present in the simplest controller implementations.

Other researchers have also explored the difficulties that can arise in control system development because of detrimental effects in the mechanical system. For example de Smet, Rivin, and Lou examined the effects of inertia, mechanical compliance, damping, and actuator overload in a robot control system [de Smet '90]. Additionally, several researchers have developed methods for preshaping trajectories commanded to a controller to account for the compliance in a mechanical system [Singer '90] [Tzes '93]. These methods are meant to reduce the end point residual vibration in systems such as robots. These examples further illustrate the need to integrate the control system development with the design of a mechanism.

The first step in developing a control system is the physical modeling of the mechanical system. Many techniques are available and the designer is referred to one of these common texts, such as the one written by Karnopp, Margolis, and Rosenberg [Karnopp '90]. Next, the control system algorithm must be developed. Depending on the system, different approaches may be appropriate. Classical methods for linear systems are described by Ogata [Ogata '70]. More advanced control systems, such as nonlinear or adaptive control may also be appropriate [Slotine '91] [Narendra '89].

Because robots are common in semiconductor manufacturing environments, their control deserves some special mention. Traditionally, PID control has been applied in the control systems of most manipulators. This practice is common not because PID is necessarily the most appropriate form of control, but because it is the most easily implemented. When PID control is used on a manipulator, each joint is assumed to be independent of the other joints. A separate control loop is then implemented for each joint.

This type of linear control algorithm can provide adequate performance under certain conditions. First, to understand the effects of using PID control in a manipulator made up primarily of revolute joints, one must understand the effects of the nonlinear and coupled dynamics characteristic of these manipulators[45]. The PID control algorithm is based on the assumption of a linear time invariant plant. As a manipulator changes configurations, the moment of inertia seen by the actuator at each joint varies. Therefore, a PID algorithm must be formulated based on an average or typical inertia value. As the manipulator changes configuration the system's poles will change and a controller tuned for a certain configuration may no longer exhibit the desired performance. For example, critically damped performance may become under damped as the manipulator moves. An additional effect that may upset the use of PID control on a manipulator is the coupling that exists between each joint. Accelerating a single joint causes a reaction to be felt at the other joints. Velocity-related centripetal and coriolis accelerations also cause coupling between joints. This coupling looks like a disturbance to a linear controller. So, the PID controller must reject these disturbances to accurately track the trajectory of interest.

Although limitations on the performance of a manipulator are introduced by using a linear control algorithm, the desired level of performance can still be achieved in many cases. For example, if a manipulator is being used primarily for pick and place tasks where the initial and final positions in a trajectory are of primary importance, the nonlinearities and coupling may not significantly degrade the performance. At these pick and place locations the manipulator is typically moving much more slowly (and not at all at the location of interest) so that it can closely track a trajectory. Also, the gear reducers which are typically present in the actuators of a manipulator tend to mitigate the effects of the nonlinear dynamics and coupling. The actuator sees the manipulator inertia divided by the square of the gear ratio. So, if the gear ratio is sufficiently large, the manipulator inertia will appear small relative to the inertia of the actuator itself. Thus, the nonlinear and coupling effects will have little impact on the performance of the manipulator. Many

[45] Manipulators made from linear or prismatic joints typically have linear, uncoupled dynamics. So, the difficulties discussed here are not encountered.

robots of this type use harmonic drives or similar reducers with high reduction ratios. The large reductions in the harmonic drives and the relatively slow speeds of many semiconductor manufacturing robots often allow a simple PID controller to work well.

Because the nonlinear, coupled dynamics that cause difficulties in controlling manipulators can be modeled, control algorithms can be formulated to compensate for these effects. Intuitively, one can understand how making use of dynamic equations that calculate torques required for the given manipulator geometry, inertia, and trajectory terms (velocities and accelerations) may be useful in controlling the robot. One drawback in implementing a controller with these feed forward terms is the complexity of the dynamic model required and the computational resources needed to calculate this model at the servo rate of the controller.

Terms for frictional and gravitational effects can also be included in the feed forward terms to provide for additional compensation. Many researchers have shown how the inclusion of these feed forward terms will cause the manipulator dynamics to reduce to a simple set of N linear and decoupled equations Paul, Luh [Paul '81], [Luh '85]. Proportional, integral, and derivative gains can easily be selected for desired performance for such a linear and decoupled set of dynamic equations. Basically, the only difference between this nonlinear controller and a linear PID controller is the insertion of terms for the dynamics of the robot in the feed forward path. If a perfect model of the manipulator were used and no disturbances were present, simply commanding the desired positions, velocities, and accelerations for each joint would result in perfect tracking and no feedback would be required. Obviously, in practice closed loop control is still needed for adequate performance but the feed forward terms may significantly improve the performance of the manipulator.

### 4.6.2 Case Study: Control System Development for a Wafer Handling Robot

This case study describes the kinematics and dynamics of the three planar joints of the wafer handling robot that was designed for SVG's Accipiter project. Both digital simulations and actual trajectory tracking results from the prototype wafer handling robot are presented below to further explain the development of the control system.

The discussion of the kinematics and dynamics forms the ground work for the development of the control system for this robot. The vertical axis of the manipulator is not discussed because this axis can accurately be modeled as a linear, second order system. These types of problems are discussed extensively in many introductory control texts [Ogata '70]. Furthermore, the dual concentric elbow joints are treated as a simple one degree of freedom elbow joint. This simplification is justified because only one of the two elbows will be moving while the other is stationary for a typical move into a process module. Consequently, the system is modeled as three planar axes, the first linear, and the next two revolute, as shown in Figure 4.23.

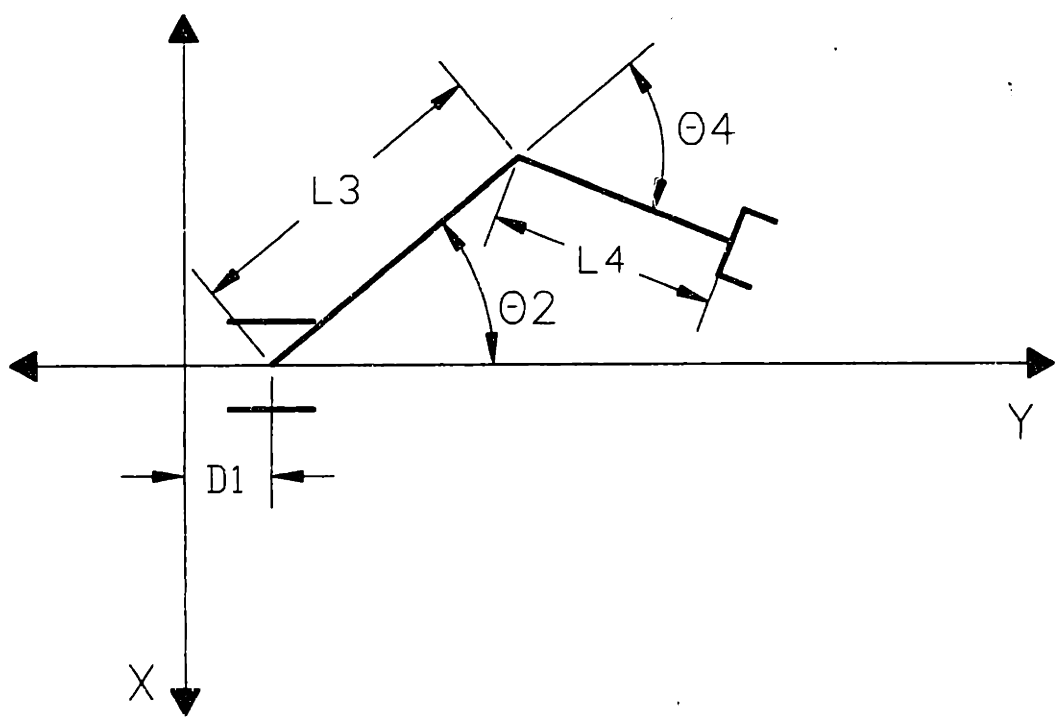


**Figure 4.23** Schematic representation of wafer handling robot.

In general, trajectories for a serial manipulator such as the wafer handling robot are defined in terms of the motion of the end effector of the arm. However, most control algorithms operate by controlling each of the joints of the manipulator, which requires trajectory information in the joint space of the arm. Therefore, it is convenient to define

the motion of the robot in end effector space and then transform that motion into joint space before or at execution time of the trajectory.

The kinematics of this robot were modeled in the case study in Chapter 3. For the control system development, these kinematics are simplified as explained above. Equation 4.12 shows how the Cartesian end effector positions, $X$ and $Y$, and the orientation, $\theta_H$, in the plane of motion can be written in terms of the link lengths and joint angles.

$$X = l_3 Sin\theta_2 - l_4 Sin(\theta_2 + \theta_4)$$

$$Y = d_1 - l_3 Cos\theta_2 + l_4 Cos(\theta_2 + \theta_4) \tag{4.12}$$

$$\theta_H = \theta_2 + \theta_4$$

where $l_3$ and $l_4$ are the link lengths and $d_1$ , $\theta_3$, and $\theta_4$ are the joint positions. Given end effector positions, the expressions in Equation 4.12 can be solved simultaneously for the corresponding joint angles. In fact a closed form solution is obtained easily for this system and has been shown to exist for six degree of freedom manipulators in general [Duffy '80]. Equation 4.13 gives the inverse kinematic solution for the wafer handling robot.

$$\theta_2 = Sin^{-1}\left(\frac{-X - l_4 Sin\theta_H}{l_3}\right)$$

$$\theta_4 = \theta_H - \theta_2 \tag{4.13}$$

$$d_1 = Y - l_3 Cos\theta_2 - l_4 Cos(\theta_2 + \theta_4)$$

For trajectory generation purposes, it is also necessary to solve the inverse kinematics problem at the velocity and acceleration level[46]. As was discussed previously, the end effector velocities can be written in terms of the Jacobian matrix and the joint velocities. To solve the inverse kinematics problem, the Jacobian must be inverted as shown in Equation 4.14.

[46] Depending on the control algorithm used, joint acceleration data may not be needed.

$$\underline{\dot{\theta}} = [J]^{-1}\underline{\dot{u}} \tag{4.14}$$

where $\underline{\dot{u}}$ is the vector of end effector velocities, $[J]$ is the Jacobian matrix, and $\underline{\dot{\theta}}$ is the vector of joint velocities. The Jacobian matrix for the simplified system being discussed here is given in Equation 4.15.

$$J = \begin{bmatrix} 0 & -l_3 Cos\theta_2 - l_4 Cos(\theta_2 + \theta_4) & -l_4 Cos(\theta_2 + \theta_4) \\ 1 & -l_3 Sin\theta_2 - l_4 Sin(\theta_2 + \theta_4) & -l_4 Sin(\theta_2 + \theta_4) \\ 0 & 1 & 1 \end{bmatrix} \tag{4.15}$$

In general, the inverse of the Jacobian matrix does exist. However, there are manipulator configurations that are characterized by a loss of one or more end effector degrees of freedom where the inverse of the Jacobian matrix does not exist. These configurations are called singularities and present a myriad of control problems which will not be discussed here, but are well documented in the research literature. For the robot in question, singularities occur only at workspace boundaries where the arm is fully outstretched. For normal operation, the robot does not come close to this singularity.

The end effector accelerations of a manipulator can be related to the joint accelerations and joint velocities as shown in Equation 4.16.

$$\underline{\ddot{u}} = [J]\underline{\ddot{\theta}} + \underline{\dot{\theta}}^T[H]\underline{\dot{\theta}} \tag{4.16}$$

where $[H]$ is the Hessian array and is defined in Equation 4.17. Also, the quadratic term is a plane-by-plane operation and is defined in the literature [Freeman '88].

$$[H] = \frac{\partial^2 \underline{u}}{\partial \underline{\theta}_i \partial \underline{\theta}_j} \tag{4.17}$$

The three planes of the Hessian array for this example are shown in Equation 4.18.

$$[H_1]=\begin{bmatrix}0 & 0 & 0\\ 0 & -l_3Sin\theta_2-l_4Sin(\theta_2+\theta_4) & -l_4Sin(\theta_2+\theta_4)\\ 0 & -l_4Sin(\theta_2+\theta_4) & -l_4Sin(\theta_2+\theta_4)\end{bmatrix}$$

$$[H_2]=\begin{bmatrix}0 & 0 & 0\\ 0 & l_3Cos\theta_2+l_4Cos(\theta_2+\theta_4) & l_4Cos(\theta_2+\theta_4)\\ 0 & l_4Cos(\theta_2+\theta_4) & l_4Cos(\theta_2+\theta_4)\end{bmatrix} \tag{4.18}$$

$$[H_3]=\begin{bmatrix}0 & 0 & 0\\ 0 & 0 & 0\\ 0 & 0 & 0\end{bmatrix}$$

To calculate the joint accelerations, Equations 4.14 and 4.16 must be solved to give the result shown in Equation 4.19.

$$\underline{\ddot{\theta}}=[J]^{-1}\underline{\ddot{u}}-[J]^{-1}(\underline{\dot{u}}^T[J]^{-T}[H][J]^{-1}\underline{\dot{u}}) \tag{4.19}$$

Articulated manipulators such as the example discussed here have nonlinear and coupled dynamics. Fortunately, these dynamics can be calculated in a relatively straight forward manor and frequently do not effect the operation of the manipulator. As will be shown below, these nonlinearities and coupling have no effect on the robot's ability to satisfy its cycle time and repeatability goals. Many techniques have been developed by various researchers to model robot dynamics and have been well documented in the literature [Book '84][ Hollerbach '83][ Kane '83][ Renaud '83][ Thomas '85].

For this example, the rigid body dynamic equations were calculated using the Lagrangian dynamics formulation method. The dynamic equations calculated by this method end up with the form shown in Equation 4.20.

$$\underline{T}=[I]\underline{\ddot{\theta}}+\left[V(\underline{\theta},\underline{\dot{\theta}})\right] \tag{4.20}$$

where $[I]$ is defined as the robot's inertia matrix and the quadratic terms, $\left[V(\underline{\theta},\underline{\dot{\theta}})\right]$, are torques produced by coriolis and centripetal acceleration effects. This method is easily implemented once the velocities of each link's center of mass have been determined. It is interesting to note that using other methods, the time dependencies in the dynamic

equations can be entirely separated from the geometric dependencies. For especially complicated manipulators this separation can give a designer special insight into the inertial properties of a manipulator and how they vary throughout the workspace of that manipulator [Van Doren '92].

Figure 4.24 shows the geometric and inertial properties that are required to derive the rigid body dynamic equations for the three degrees of freedom of interest in this manipulator

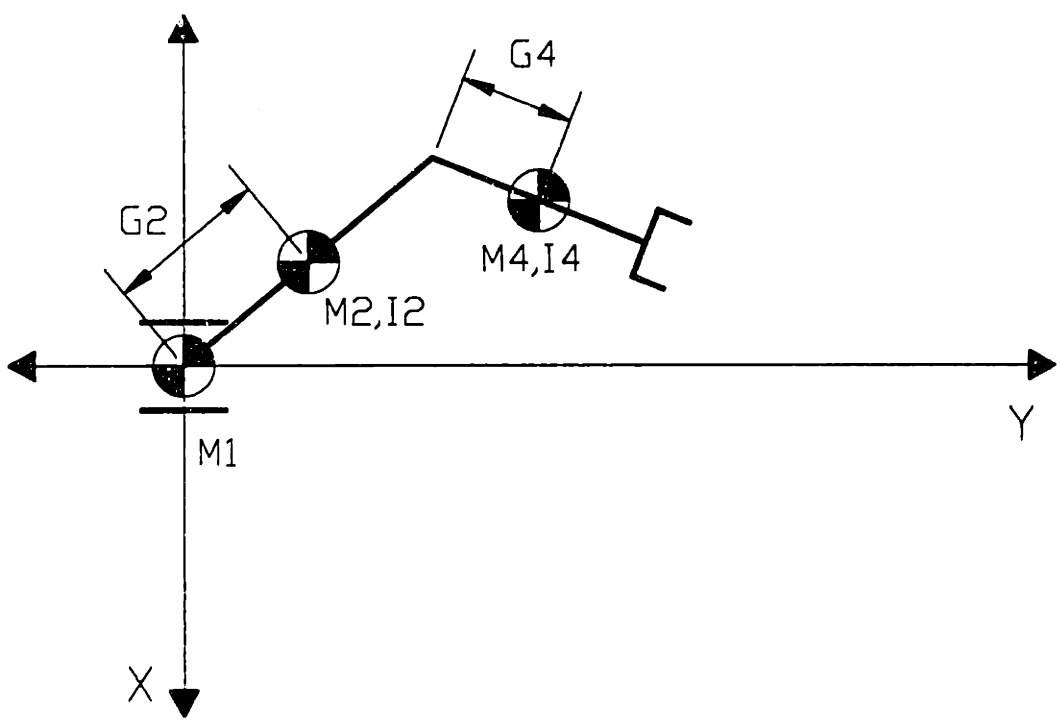


**Figure 4.24** Inertial properties for 3 DOF, planar manipulator.

Because the example manipulator operates in a plane, only moments of inertia for each link in that plane are required. For a general six degree of freedom manipulator, the complete inertia tensor for each link would be required. Also, note that because the example robot operates in a plane perpendicular to the gravity vector, it is not necessary to include any gravitational terms in the dynamic equations. For a manipulator of this type operating in plane not perpendicular to the gravity vector, the dynamic equations

would contain additional terms to account for the weight of each link as a function of the manipulator's joint positions.

For a planar manipulator with only three degrees of freedom, it is practical to derive the dynamic equations in closed form. However, these equations are still not compact even with simplifications using trigonometric identities where possible. The elements of the inertia matrix are shown below in Equation 4.21. The velocity terms are given in Equation 4.22.

$$I = \begin{bmatrix} I_{11} & I_{12} & I_{13} \\ I_{21} & I_{22} & I_{23} \\ I_{31} & I_{32} & I_{33} \end{bmatrix} \tag{4.21}$$

$$I_{11} = m_1 + m_2 + m_4$$

$$I_{12} = -m_2 g_2 Sin\theta_2 - m_4 l_2 Sin\theta_2$$

$$I_{13} = -m_4 g_4 Sin(\theta_2 + \theta_4)$$

$$I_{21} = I_{12}$$

$$I_{22} = I_2 + I_4 + m_2 g_2^2 + m_4 l_2^2 + m_4 g_4^2 + 2m_4 l_2 g_4 Cos\theta_4$$

$$I_{23} = I_4 + m_4 g_4^2 + m_4 l_2 g_4 Cos\theta_4$$

$$I_{31} = I_{13}$$

$$I_{32} = I_{23}$$

$$I_{33} = I_4 + m_4 g_4^2$$

$$[V] = \begin{bmatrix} V_1 \\ V_2 \\ V_3 \end{bmatrix} \tag{4.22}$$

$$V_1 = -(m_2 g_2 Cos\theta_2 + m_4 l_2 Cos\theta_2)\dot{\theta}_2^2 - m_4 g_4 Cos(\theta_2 + \theta_4)(\dot{\theta}_4^2 + \dot{\theta}_2\dot{\theta}_4)$$

$$V_2 = -m_4 l_2 g_4 Sin\theta_4(\dot{\theta}_4^2 + 2\dot{\theta}_2\dot{\theta}_4) - m_4 g_4 Cos(\theta_2 + \theta_4)\dot{d}_1\dot{\theta}_4$$

$$V_3 = m_4 g_4 Cos(\theta_2 + \theta_4)\dot{d}_1\dot{\theta}_4 + m_4 l_2 g_4 Sin\theta_4(\dot{\theta}_2\dot{\theta}_4 + \dot{\theta}_2^2)$$

Table 4.1 gives the geometric and inertial parameters for this set of dynamic equations. In this case, the dynamic equations are written in the joint space of the robot. It would also be possible to write the equations in motor space.

**Table 4.1** Control system parameters for wafer handling robot.

| joint number | moment of inertia | mass | link length | distance to center of mass | Peak actuator output |
|---|---|---|---|---|---|
| 1 | N/A | 11.8 kg | N/A | N/A | 270 N |
| 2 | 0.21 kg $m^2$ | 22.5 kg | 0.163 m | 0.025 m | 14 Nm |
| 4 | 0.044 kg $m^2$ | 0.7 kg | 0.254 m | 0.04 m | 2.6 Nm |

It should be noted that for this application, the use of a rigid body form of the dynamic equations is justified. The bandwidth of operation of this wafer handling robot is far below the fundamental mechanical mode of the arm. That is to say that the compliances of the transmissions, joints, and links of the arm are sufficiently small that they are negligible for normal operation of a manipulator of this type.

A simple, linear control algorithm was selected to control this robot. This type of control is capable of more than adequately achieving the position, velocity, and accelerations required of the wafer handling robot. Equation 4.23 gives the single axis form of the control law.

$$T = K_p E_{pos} + K_d E_{vel} + K_{accel}\ddot{\theta}_{command} + K_{vel}\dot{\theta}_{command} \tag{4.23}$$

where $K_p$ is the proportional gain, $E_{pos}$ is the difference between the commanded position and the actual position, $K_d$ is the derivative gain, $E_{vel}$ is the difference between the commanded velocity and the actual velocity, $K_{accel}$ is the acceleration feedforward gain, $\ddot{\theta}_{command}$ is the commanded acceleration, $K_{vel}$ is the velocity feedforward gain, and $\dot{\theta}_{command}$ is the commanded velocity. Integral control action is used only when the joint is stationary. By using integral control in this manner, disturbances or drift can be nullified when no motion is occurring. The acceleration and velocity feedforward gains are used to reduce following errors while a trajectory is being tracked. The acceleration feedforward

tends to reduce the effects of system inertia in causing following errors and the velocity feedforward reduces the effects of velocity proportional damping. The use of the acceleration feedforward also do not cause overshoot at the end of the trajectory that the integral control action would cause.

This type of linear control law is generally implemented for linear systems. By examining the dynamic equations in Equation 4.21, it can clearly be seen that this system is not linear. Furthermore, the system also contains acceleration and velocity coupling between each of the joints. The diagonal elements of the inertia matrix represent the inertia seen by each joint. That is, $I_{11}$ gives joint 1 inertia, $I_{22}$ joint 2, and $I_{33}$ joint 3. It can be seen that the inertia seen by joint one is just the total mass of the system. Joint 2 is the only joint in the system that has a nonlinearity in its inertia. The nonlinearity is related to the position of the final joint and is a function of the mass of the final link and the system geometry. However, because of the relatively small mass of the final link, this term causes only very small changes in joint 2's inertia as the robot's configuration changes. (The nonlinear terms causes the inertia to change by a maximum of 2.8% for this system.)

#### 4.6.2.1 Wafer Handling Robot Control System Simulations

A number of simulations were performed to test the functionality of the selected controller with this wafer handling robot. Appendix D contains the kinematics and dynamic simulation programs that were written to perform these simulations. First, it was necessary to generate joint trajectories that would actually be tracked by this robot. The inverse kinematics discussed previously were implemented in software to perform this trajectory generation function. The end effector trajectories used were straight lines with trapezoidal acceleration profiles based on the actual trajectories that would be used to move into a process module. Next, the rigid body dynamic model of the system was simulated using a 4th order Runga Kutta method. The control law described above was also implemented in this program. The gains used in the simulations were based on limitations imposed by the actuators used in the actual system and analytical determination of optimal gains using a linearized system as the basis for calculation.

More specifically, the proportional gains were set at a level that required the actuators to output less than 25% of their peak torque to track typical trajectories. Derivative gains were calculated to give critical damping ratios. The acceleration feedforward gains were selected based on the inertia being accelerated by each joint. Finally, velocity feedforward was not used in the simulation because no velocity proportional dissipation was modeled.

Three different sets of simulations are discussed below. The first set deals with the step response of both the nonlinear and linearized system. In the second set, typical trajectories are used and the resulting performance is examined. Finally, the third set of simulations uses trajectories that have accelerations and velocities that are several times larger than the maximum design values. The purpose of this final set of simulations is to show how the nonlinearities and dynamic coupling have no significance in this system even for conditions far exceeding the functional requirements of the design.

Figure 4.25 illustrates the small significance of the nonlinearities graphically. This figure shows the system response to simultaneous steps in each of the joint positions. The left column in the figure gives the responses for the nonlinear system and the right column, the linearized system. The only indication of nonlinearities and coupling in the left hand column are small differences in the peak magnitude of the velocities. Both system's exhibit excellent response.

Figure 4.26 shows the end effector and joint trajectories for a typical move by the wafer handling robot into a process module. Use of a trapezoidal acceleration profile is preferred over the more common trapezoidal velocity profile because the trapezoidal acceleration profile does not exhibit discontinuities in the accelerations that are commanded to each of the manipulator's joints. Smoother trajectories result in smoother performance.

Figure 4.27 gives the actual joint trajectories as produced by the controller simulation. These trajectories correspond very well to the set point trajectories given in Figure 4.26. The difference between the position set points and the simulated positions are given in Figure 4.28. It should be noted that no acceleration feedforward was used for

the simulation that resulted in these following errors. By using the acceleration feedforward, the following errors can be reduced greatly as shown in Figure 4.29.

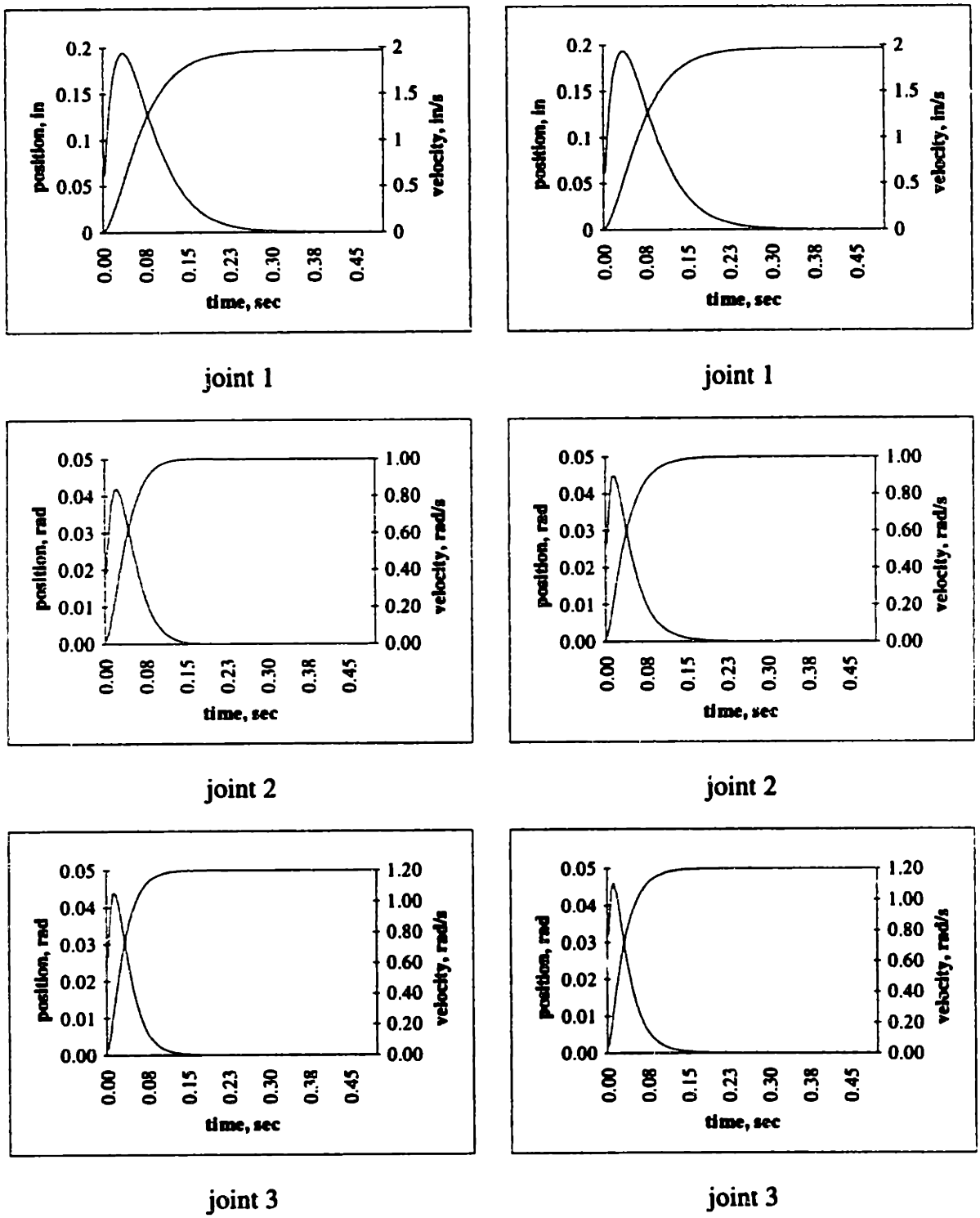


**Figure 4.25** Individual joint responses to simultaneous steps inputs to each joint for (i) fully nonlinear system in the left column and (ii) a linearized system in the right column.

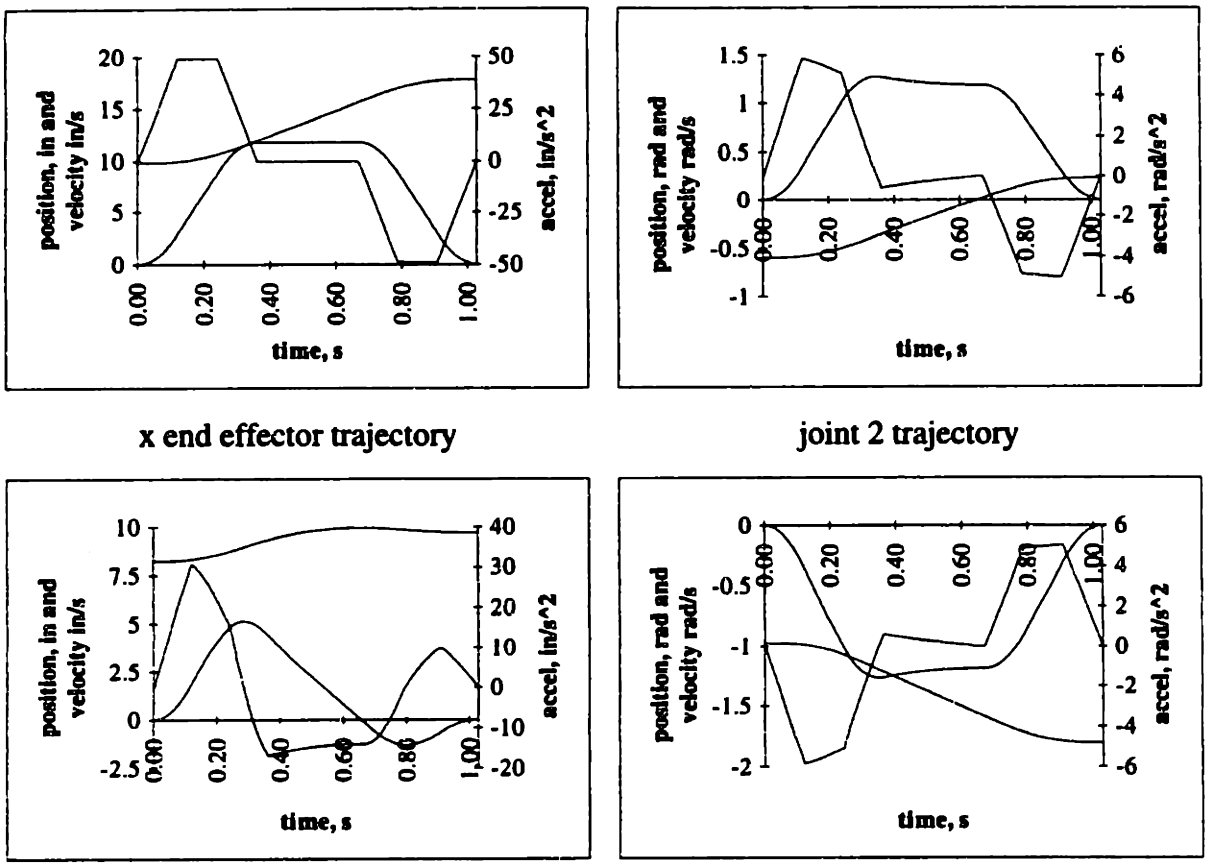


x end effector trajectory

joint 2 trajectory

joint 1 trajectory

joint 3 trajectory

**Figure 4.26** End effector and joint trajectories for typical straight line move into a process module.

Finally, it is interesting to examine the disturbance torques imposed on each joint that result from the accelerations and velocities of all of the joints in this three degree of freedom system. The total disturbance imposed on each joint over the trajectory is shown in Figure 4.30. For those concerned about coupling between the links, it can be seen that at worst, the magnitude of the coupling is less than 0.5% of the peak actuator output.

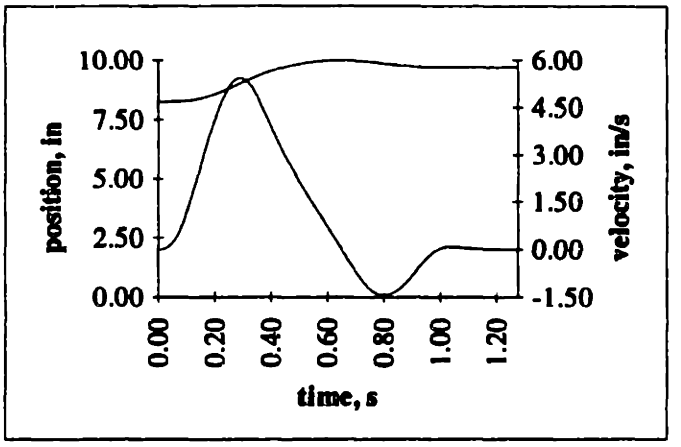


joint 1

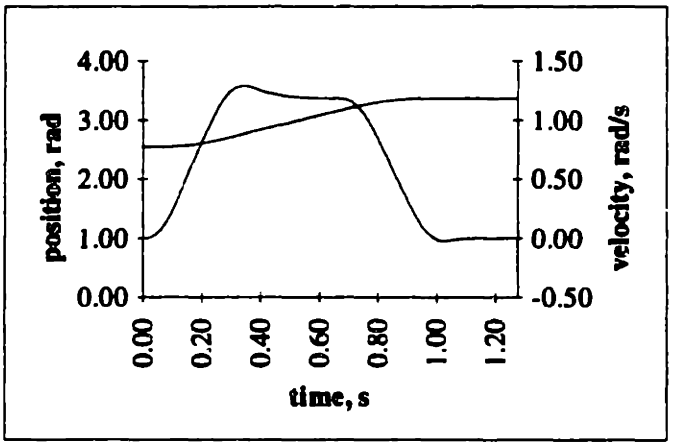


joint 2

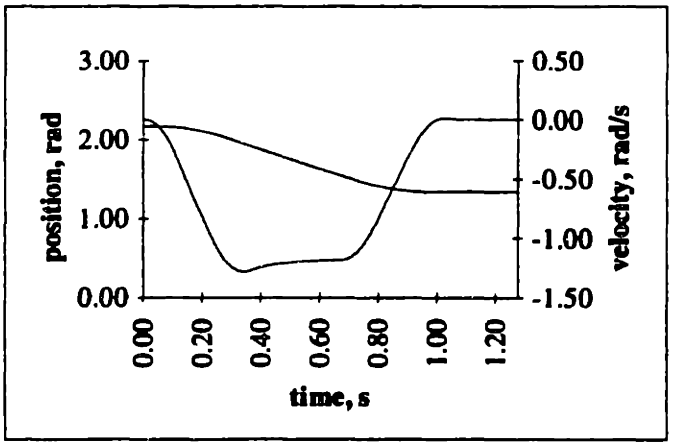


joint 3

**Figure 4.27** Actual joint trajectories for typical trajectory.

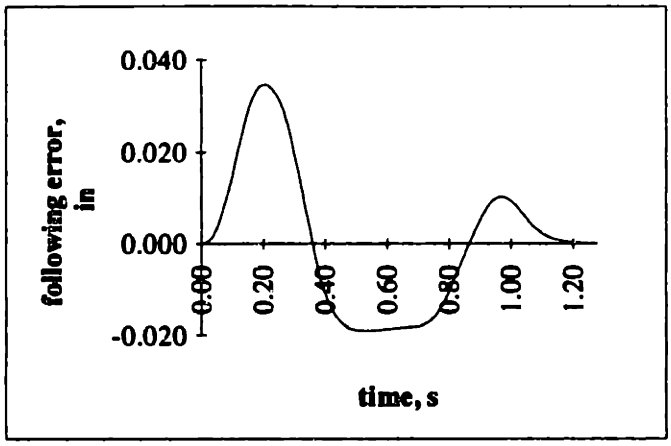


joint 1

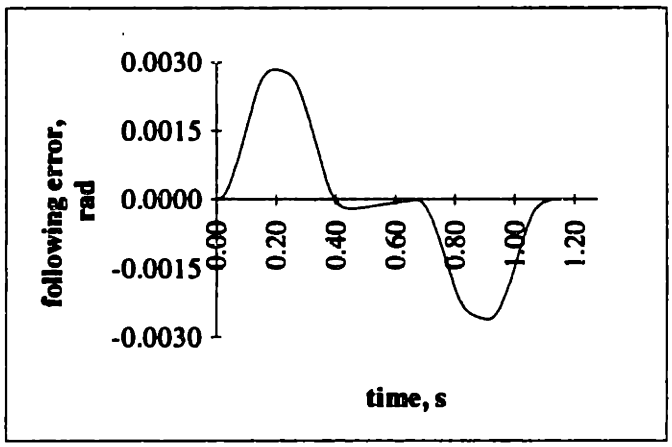


joint 2

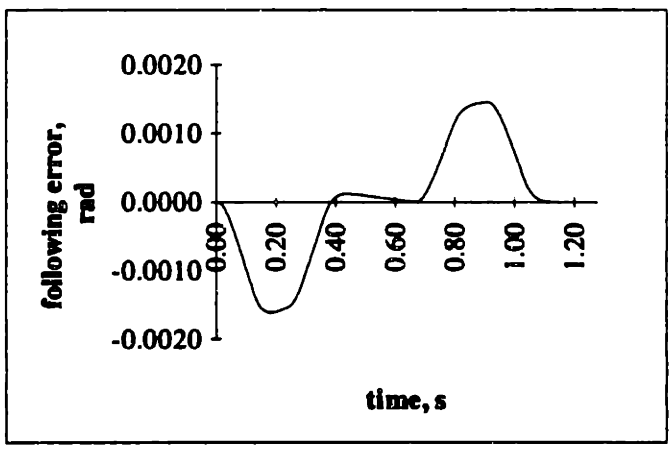


joint 3

**Figure 4.28** Following errors for typical trajectory.

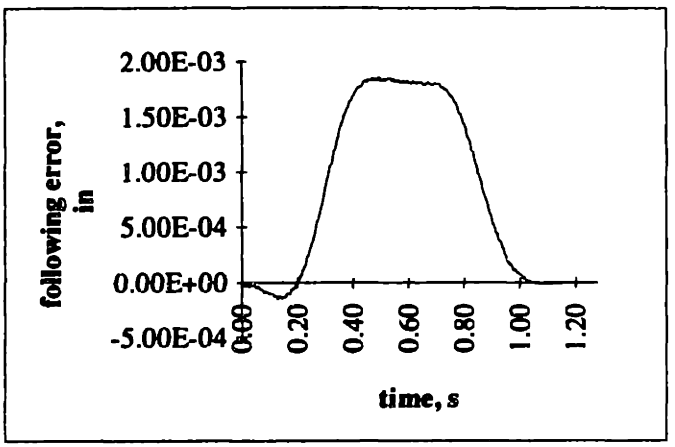


joint 1

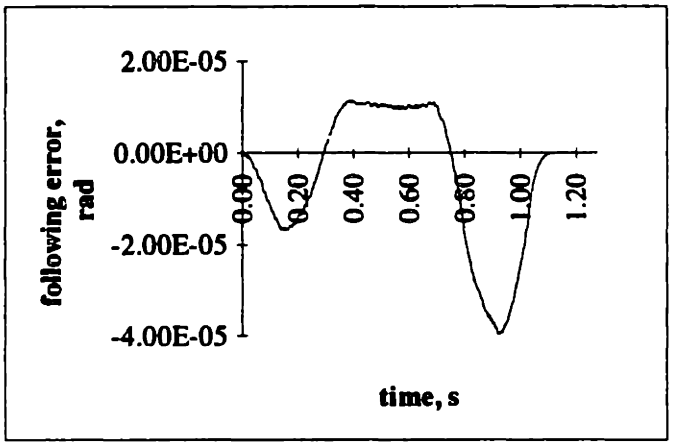


joint 2

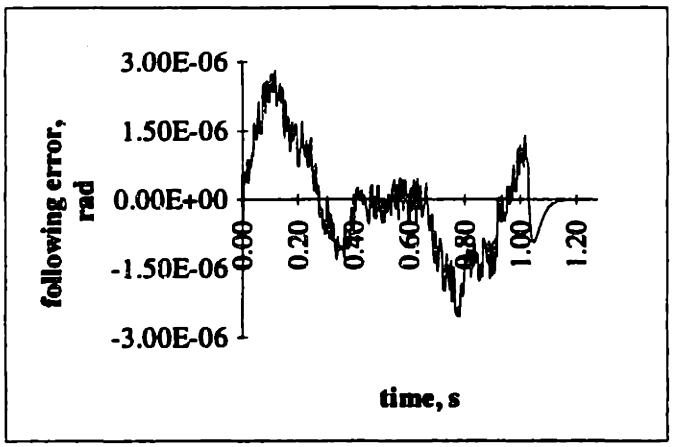


joint 3

**Figure 4.29** Following errors when feedforward acceleration is used for typical trajectory.

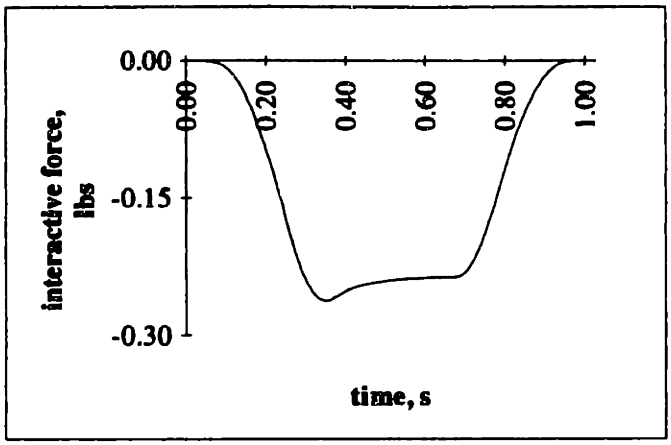


joint 1

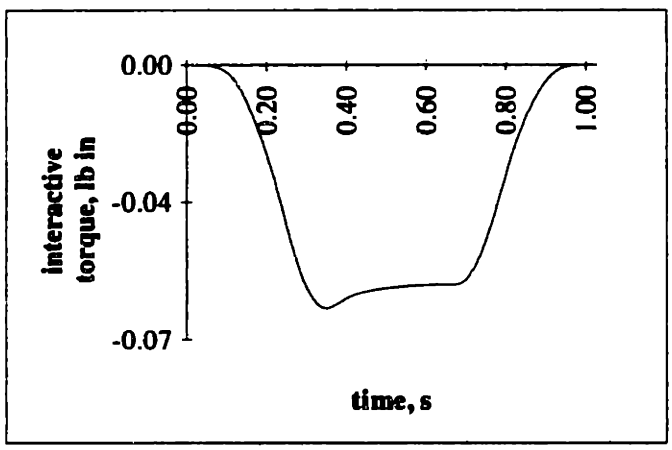


joint 2

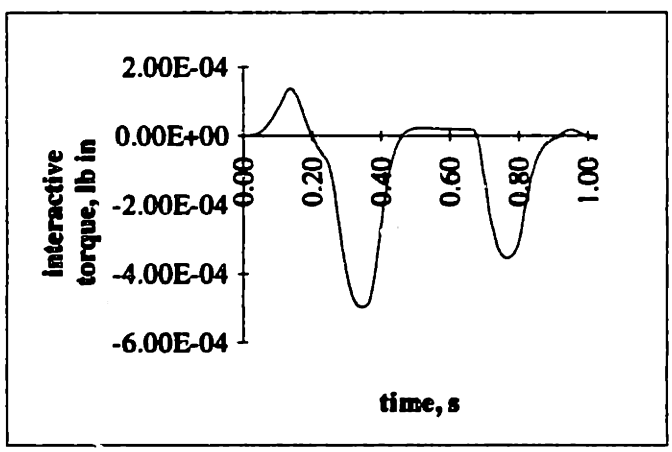


joint 3

**Figure 4.30** Interactive (disturbance) torques for each joint for typical trajectory.

The final set of simulations was performed using trajectories with much higher accelerations and velocities as can be seen in Figure 4.31. The end effector accelerations here are more than six times larger than the previous example and the velocities are more than three times larger. Consequently, these trajectories are a much more stringent test of the controller and far exceed the functional requirements of the robot.

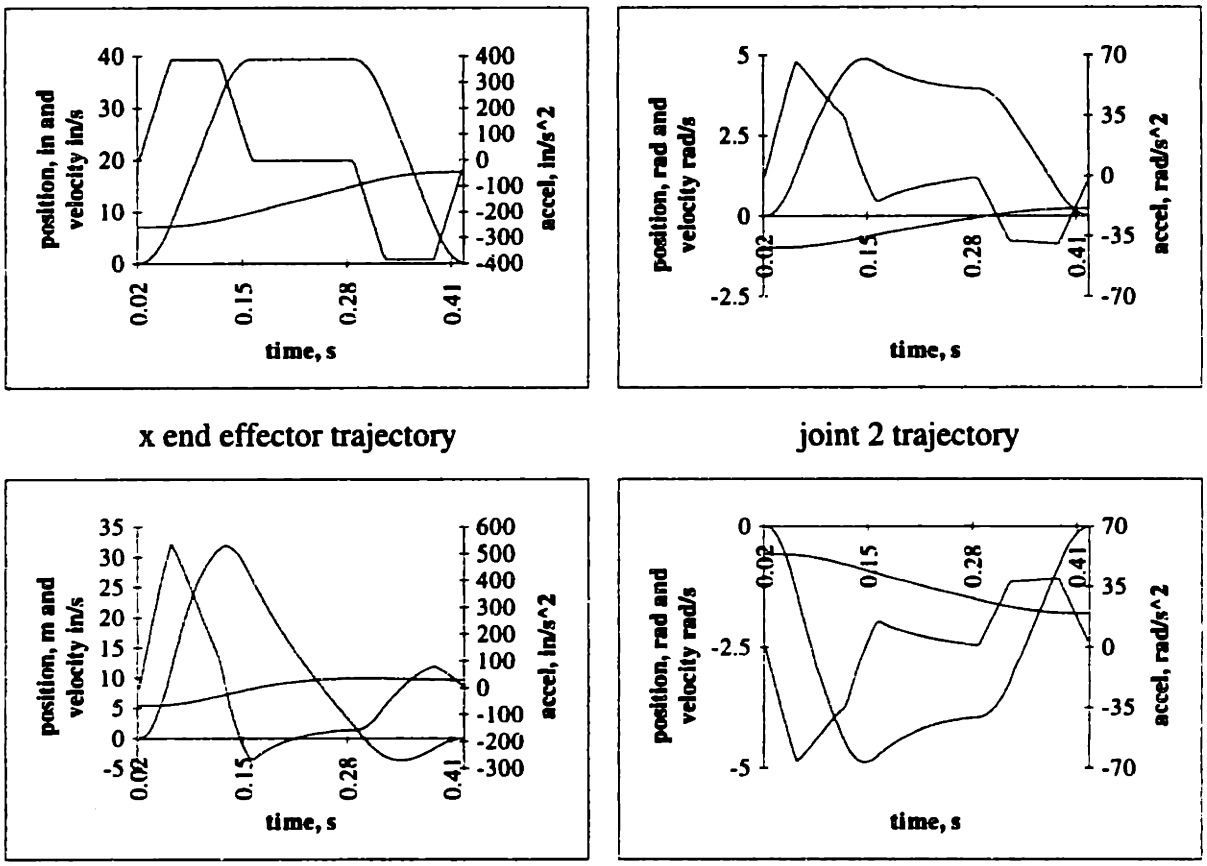


x end effector trajectory joint 2 trajectory

joint 1 trajectory joint 3 trajectory

**Figure 4.31** End effector and joint trajectories for high speed straight line move.

Figure 4.32, Figure 4.33, and Figure 4.34 give the actual joint trajectories, following errors without acceleration feedforward, and following errors with acceleration feedforward. Despite the large accelerations and velocities, performance is still good because the controller is still able to accurately track the trajectories even in the presence of the inertial disturbances. The final plots of simulation data given in Figure 4.35 show the interactive torques for this case. It is interesting to note that the largest disturbances

are still less than 7% of the possible actuator output indicating that the coupling is still not significant.

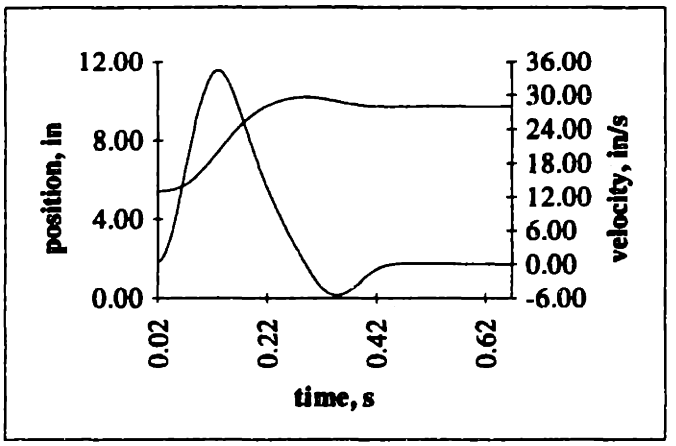


joint 1

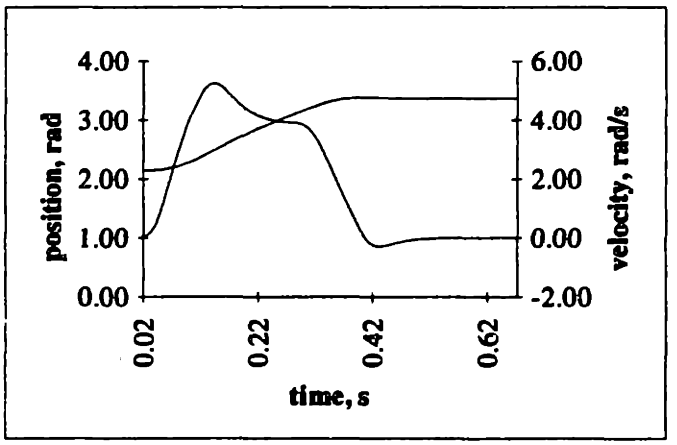


joint 2

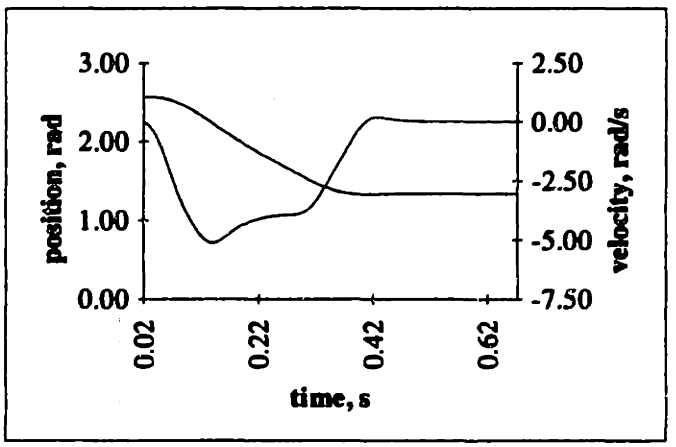


joint 3

**Figure 4.32** Actual joint trajectories for high speed trajectory.

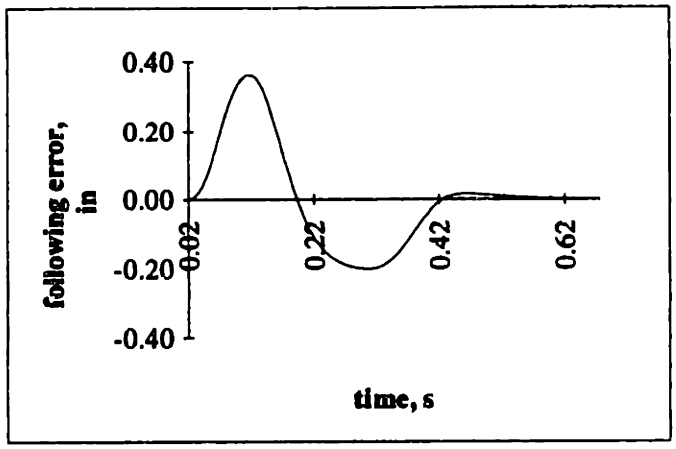


joint 1

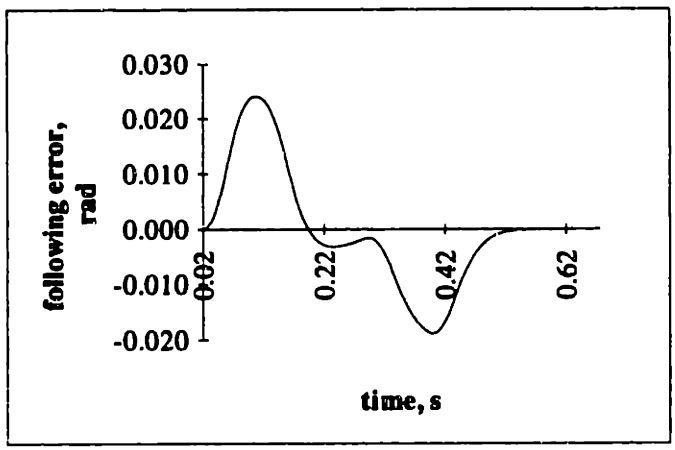


joint 2

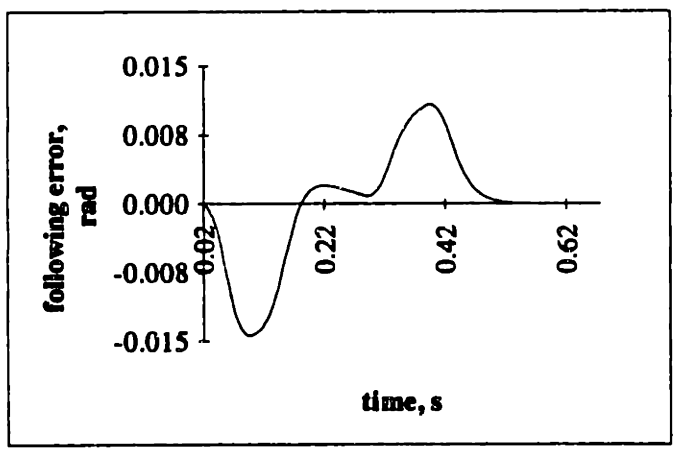


joint 3

**Figure 4.33** Following errors for high speed trajectory.

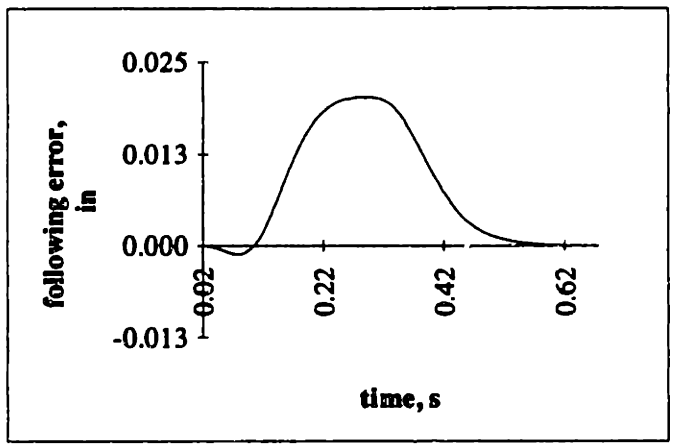


joint 1

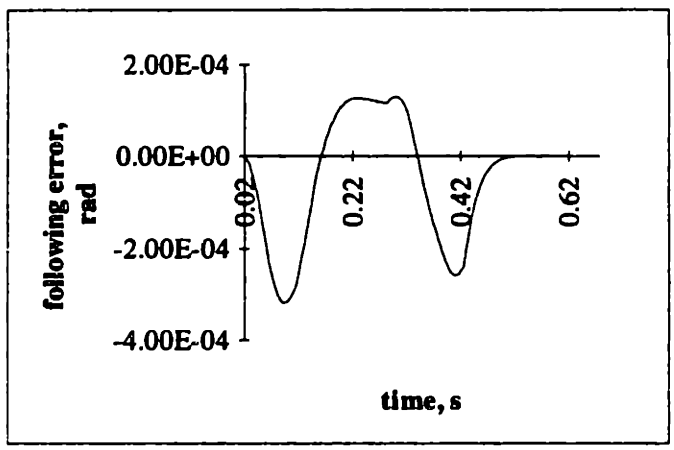


joint 2

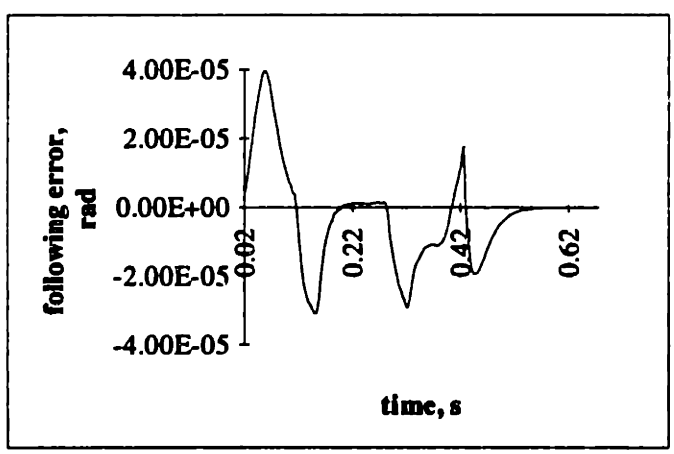


joint 3

**Figure 4.34** Following errors when feedforward acceleration is used for high speed trajectory.

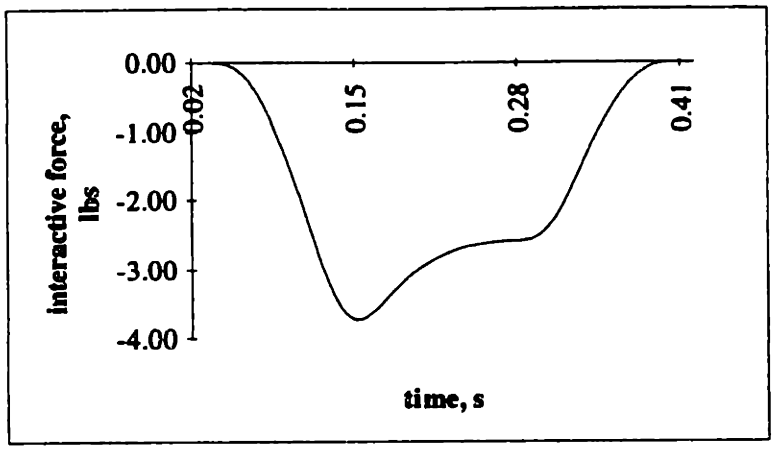


joint 1

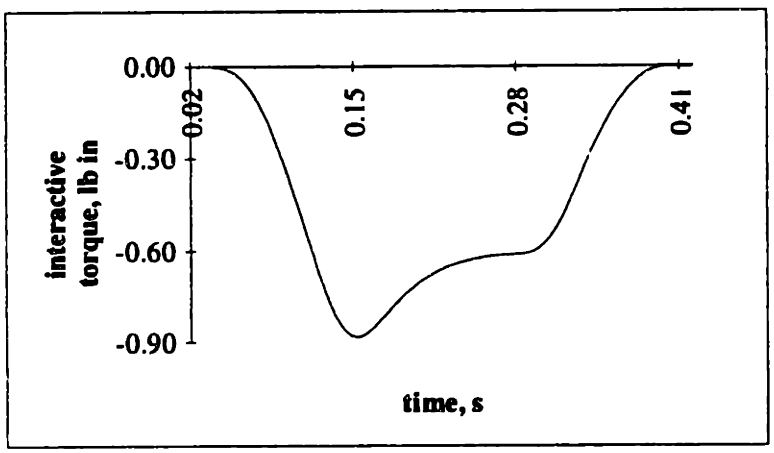


joint 2

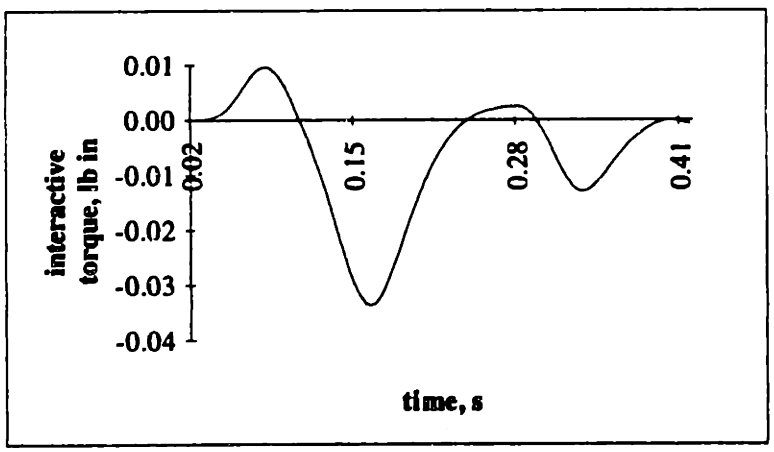


joint 3

**Figure 4.35** Interactive (disturbance) torques for each joint for high speed trajectory.

These simulations show that the simple linear controller is quite appropriate for this design given the level of complexity and the trajectory requirements. This is not meant to imply that coupling is not a problem in general. It simply is not in this case. Other multi-degree of freedom systems with revolute joints may require a different approach depending on their complexity and trajectory requirements [Suh '90].

#### 4.6.2.2 Wafer Handling Robot Prototype Control System Experimental Results

The control algorithm actually implemented in the wafer handling robot prototype is essentially identical to the one described above. Proportional and derivative terms along with velocity and acceleration feedforward are used in the control law. Integral control is used only to eliminate set point errors when the robot is holding position. The kinematics described above are also very similar to those used in the actual controller. Because of details of the operation of the particular control board used[47], a slightly different scheme was employed for the straight-line portions of the trajectories. The inverse kinematics solution was used to calculate a number of via points in the trajectory that were subsequently splined together to give a continuous motion profile. The resulting acceleration trajectories are slightly different than the trapezoidal profiles used in the simulations discussed above.

Figure 4.36 to Figure 4.47 below are for a single commanded move. In this trajectory, the robot moves from its home position in the center of the machine to the front of a process module. Next, the robot executes straight-line motion into the module. After a brief pause in the process module, the robot retracts out of the module and returns to its home position. As can be seen in the figures below, the initial move from the home position occurs between 0 seconds and approximately 2 seconds. The insertion into the process module then occurs between 2 and 4 seconds.

The position, velocity, and acceleration components of the commanded trajectory for the horizontal carriage are shown in Figure 4.36. Figure 4.37 shows the actual

[47] A PMAC™ control board from Delta Tau Data Systems was used. The board can operate stand alone and is based on a Motorola digital signal processor (DSP).

position and velocity executed by the robot carriage[48]. The corresponding following errors are shown in Figure 4.38. For each of the joints in the robot, the actual position settles to within one encoder count of the commanded position. Therefore, control system related errors in positioning of the robot are limited only by the resolution of the encoders used. The robot was designed so that the controller only needed to settle within five encoder counts for each axis.

Figure 4.39, Figure 4.40, and Figure 4.41 show the commanded and actual trajectories along with the following errors for the telescoping axis. Similarly, the trajectories and following errors for the proximal revolute joint are shown in Figure 4.42, Figure 4.43, and Figure 4.44. Finally, Figure 4.45, Figure 4.46, and Figure 4.47 present the corresponding trajectories and following errors for the distal revolute joint.

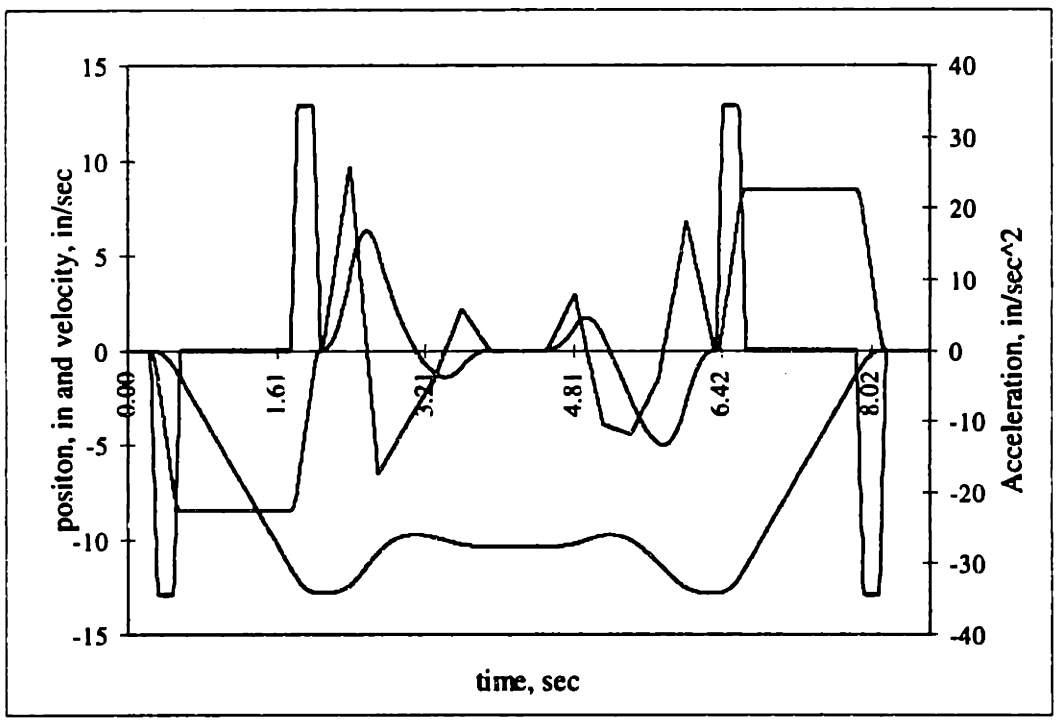


**Figure 4.36** Commanded trajectory for the robot's linear carriage.

[48] The actual position, velocity, and following errors are based on feedback data from each joint's optical encoder.

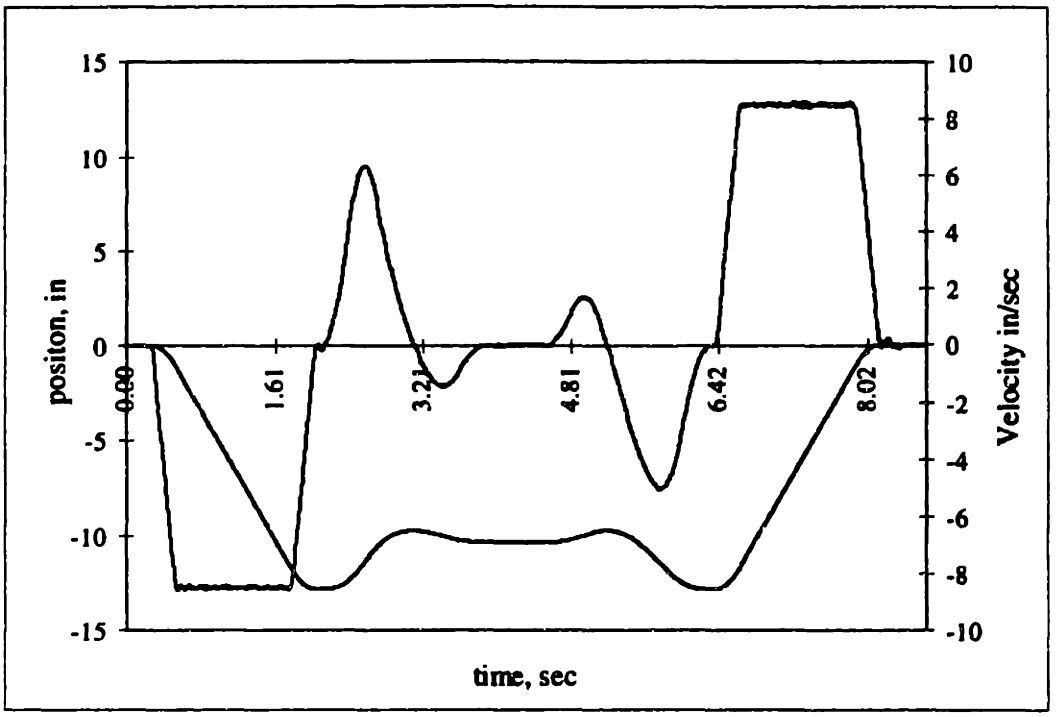


**Figure 4.37** Actual trajectory for the robot's linear carriage.

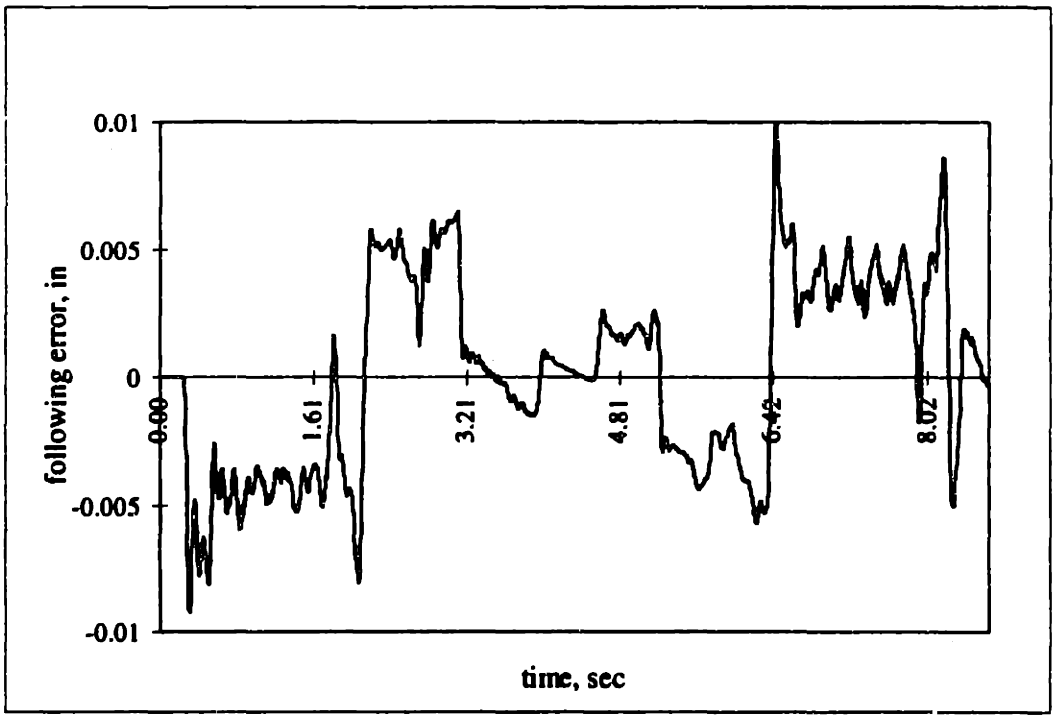


**Figure 4.38** Following errors for the robot's linear carriage.

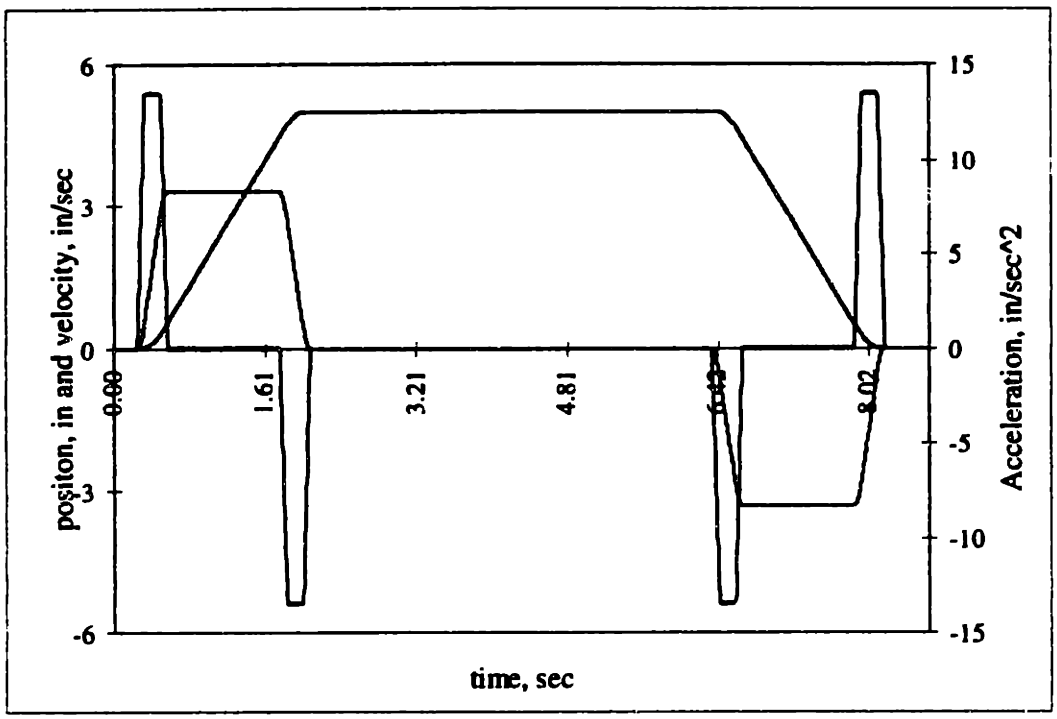


**Figure 4.39** Commanded trajectory for the robot's telescoping axis.

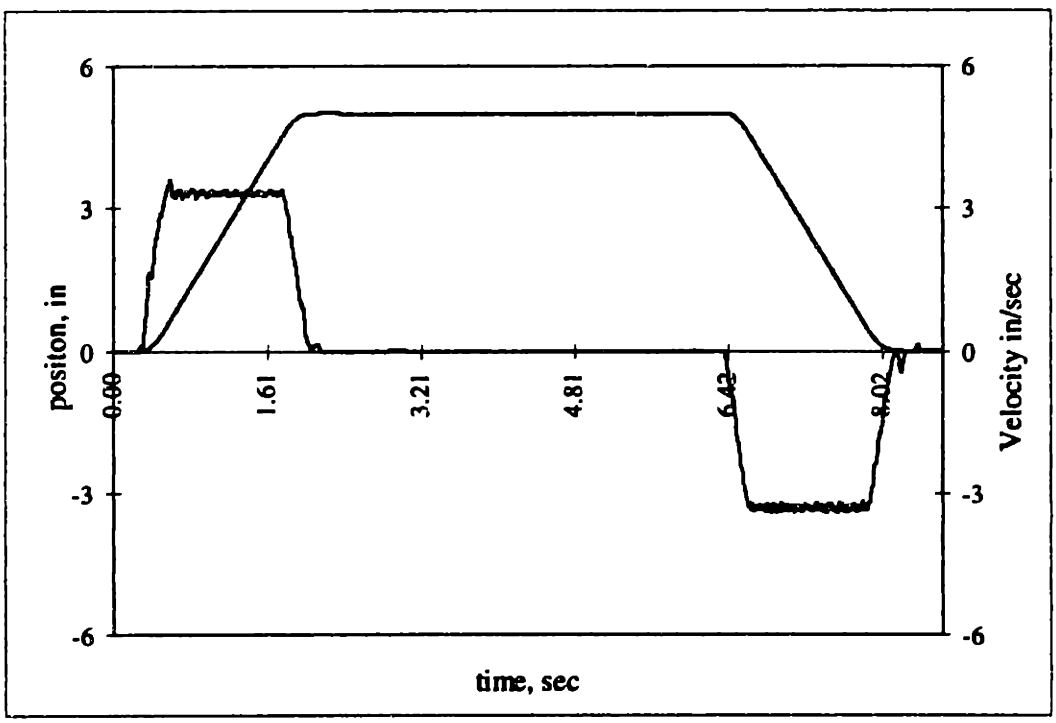


**Figure 4.40** Actual trajectory for the robot's telescoping axis.

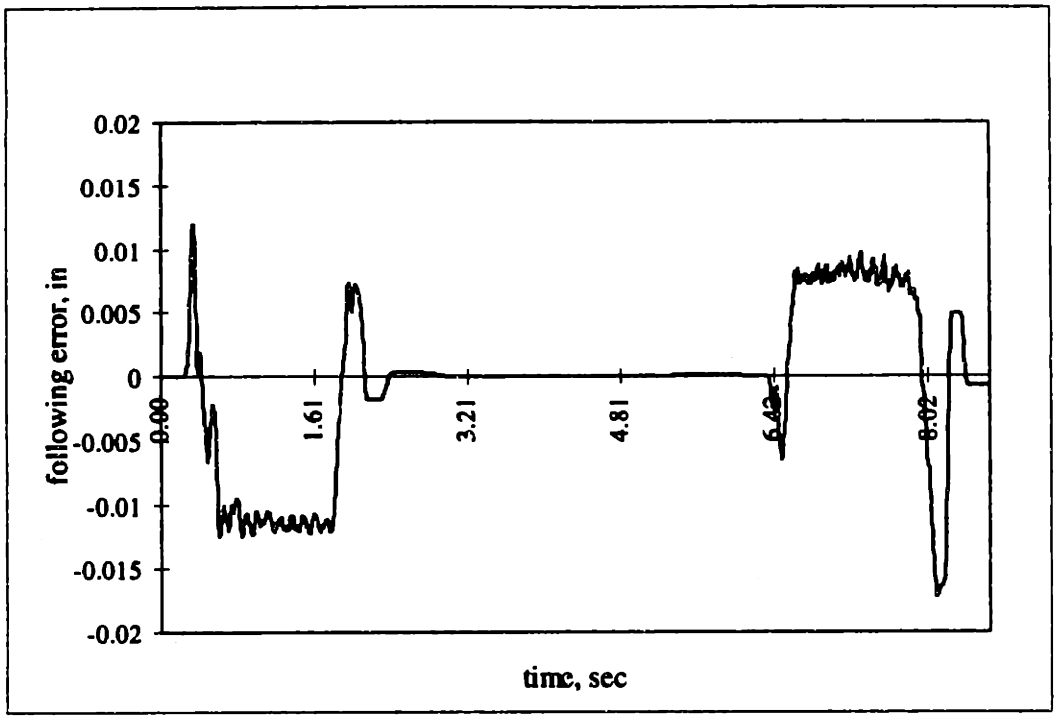


**Figure 4.41** Following errors for the robot's telescoping axis.

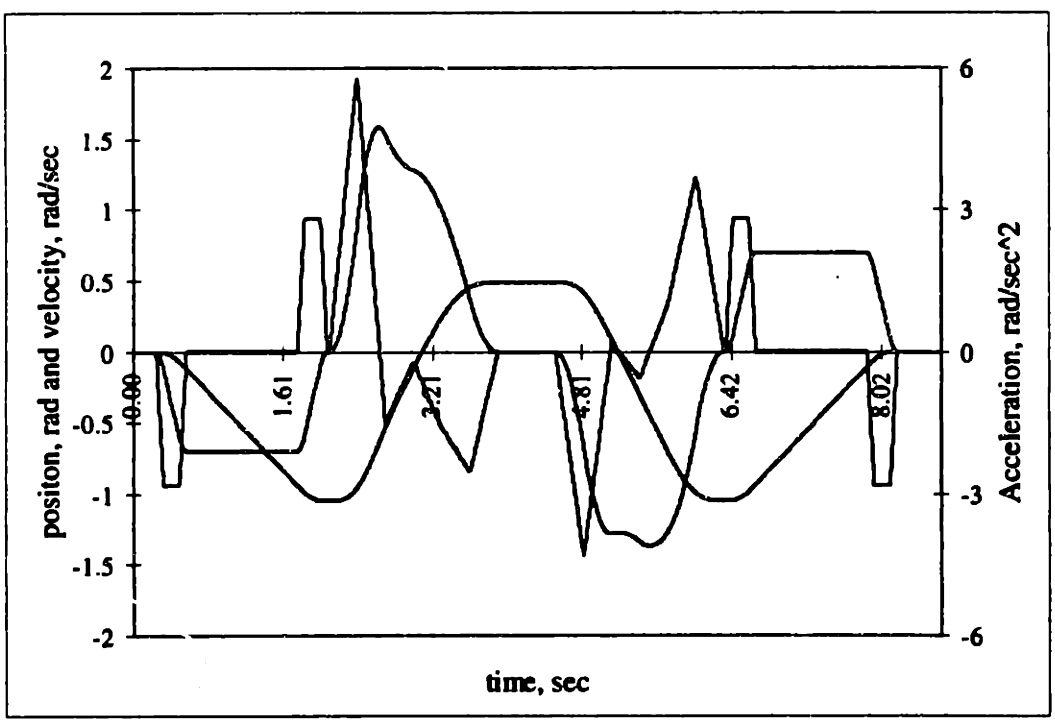


**Figure 4.42** Commanded trajectory for the robot's proximal revolute joint.

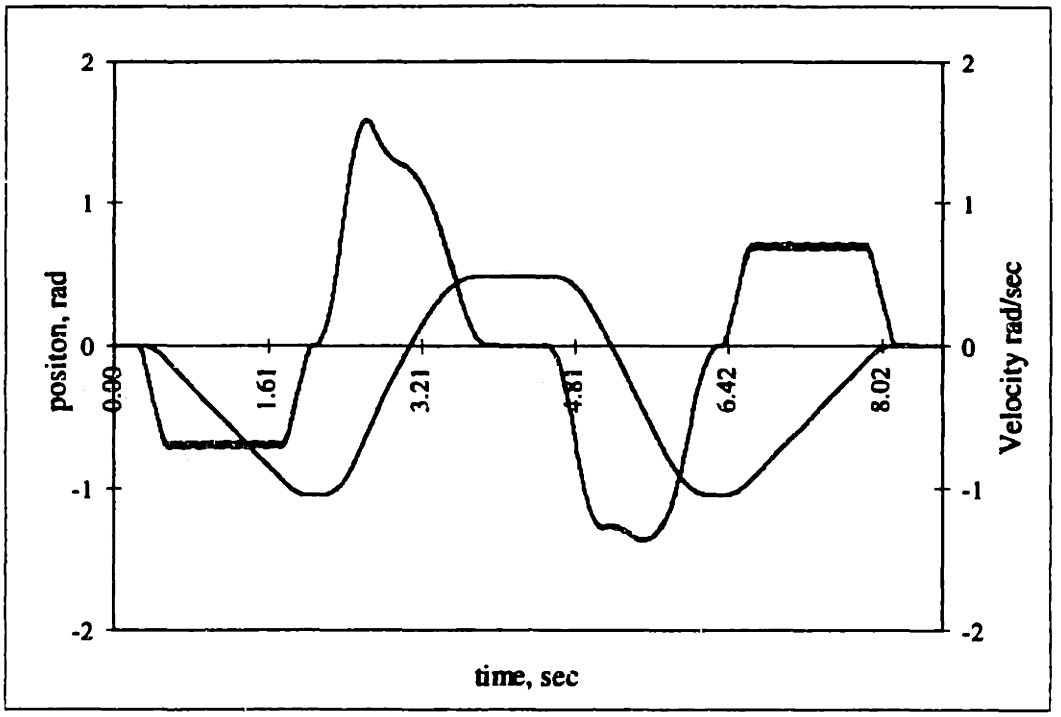


**Figure 4.43** Actual trajectory for the robot's proximal revolute joint.

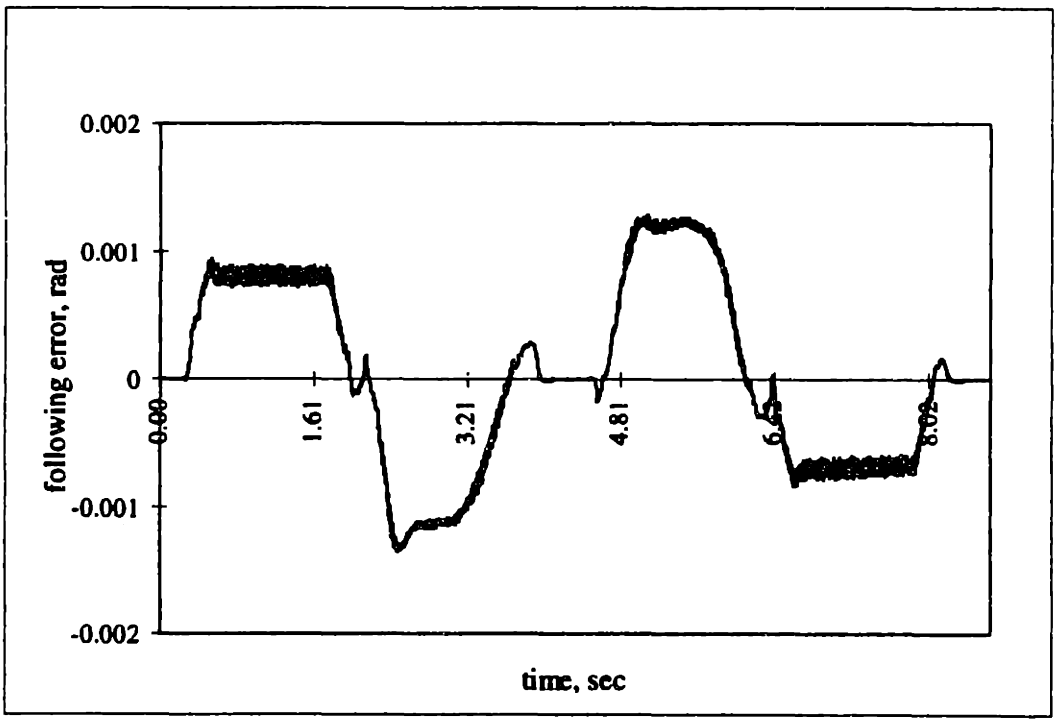


**Figure 4.44** Following errors for the robot's proximal revolute joint.

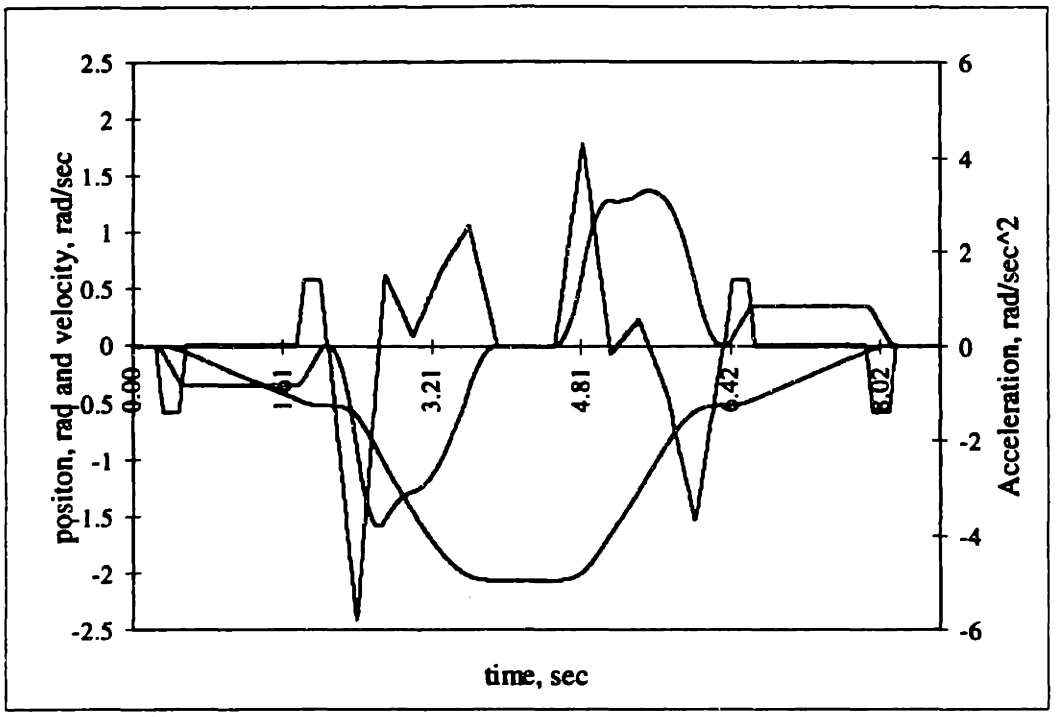


**Figure 4.45** Commanded trajectory for the robot's distal revolute joint.

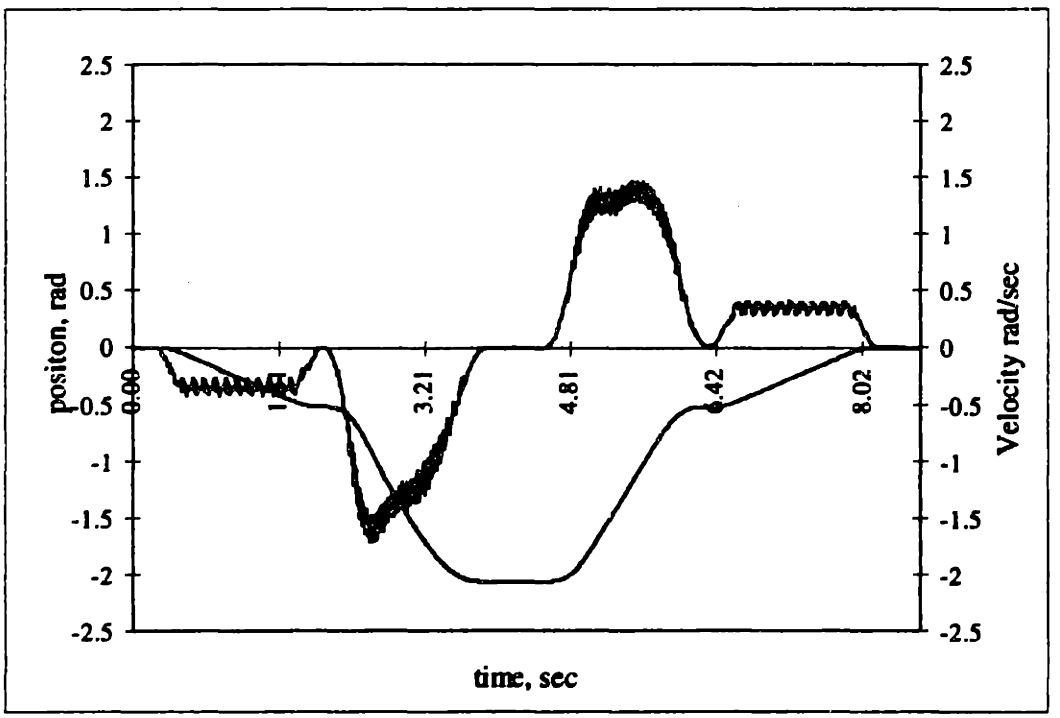


**Figure 4.46** Actual trajectory for the robot's distal revolute joint.

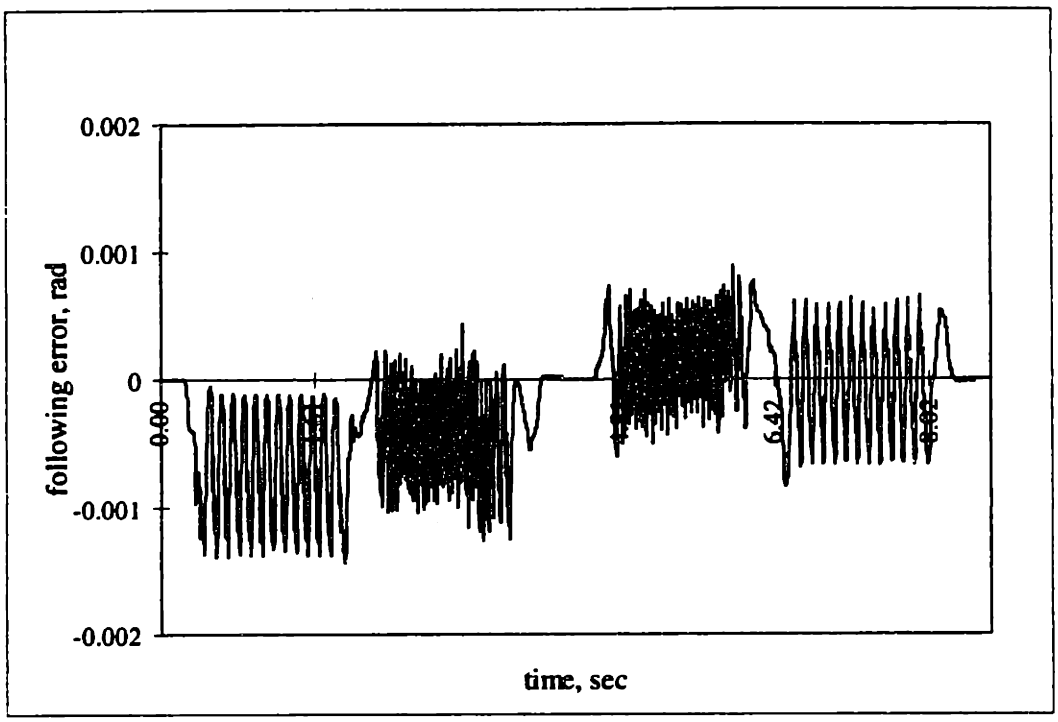


**Figure 4.47** Following errors for the robot's distal revolute joint.

Plots of the actual velocities and the following errors for both revolute joints show a residual vibration. This disturbance is especially noticeable in the distal revolute joint trajectory data. Figure 4.48 shows the frequency content of the vibration taken on the gripper housing during a constant velocity move of the distal revolute joint. This plot shows clearly that the primary harmonic occurs at exactly twice the motor shaft rotation rate. The disturbance is created by the elliptical wave generator which rotates within the flex spline of the harmonic drive reducer used in the revolute joints. However, the vibration does not affect the positioning repeatability of the revolute joints.

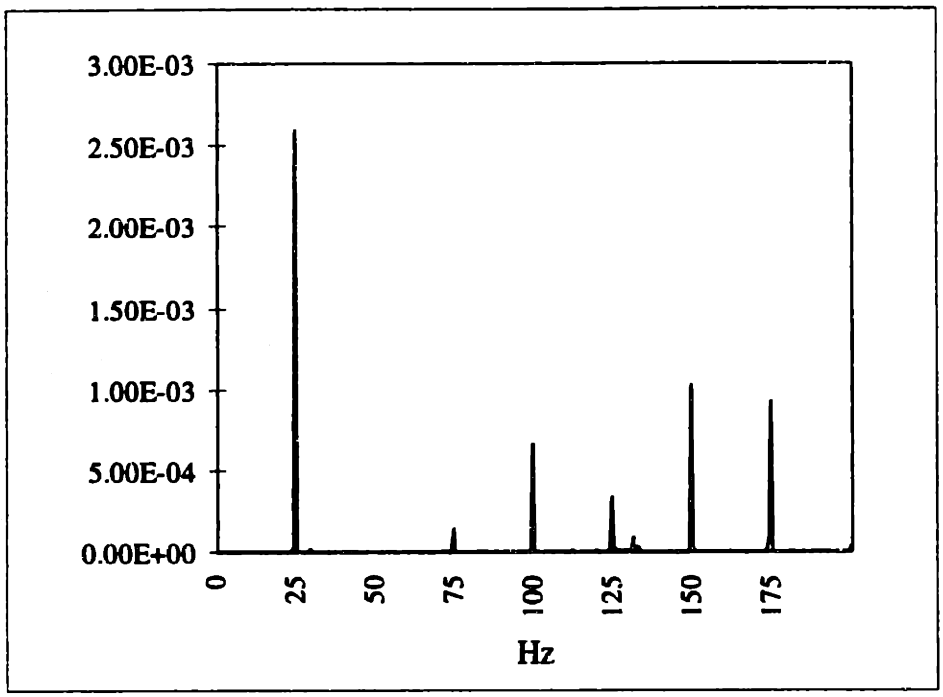


**Figure 4.48** Power spectral density for accelerometer placed on gripper housing for constant speed distal revolute move.

## 4.7 Cleanroom Equipment Design Considerations

The final area discussed in this chapter deals with the design considerations necessitated by the contamination free environmental needed for semiconductor manufacture. Although unwanted particles[49] are the primary form of contamination, other sources such as heat, humidity, static electricity, vibration, and electromagnetic radiation might also be considered as sources of contamination. This short discussion will deal primarily with particulate contamination, however.

In addition to limits in process technology, defects created in integrated circuits by particle contamination are one of the primary gates on the advance toward smaller device geometries. It is, therefore, not surprising that the functional requirement for cleanliness in semiconductor manufacturing equipment plays a dominate roll in the design of these types of machines. Also, because sources of contamination can be difficult to identify

[49] Generally, particles are considered to be either liquid or solid matter with a minimum characteristic dimension of at least 0.05 μm.

and rectify in an operating process tool, the designer must incorporate cleanliness requirements into the core of the design effort.

Although the cleanliness requirements have obvious direct impacts on the mechanical design of a system, there are also indirect effects. These effects were mentioned previously in Chapter 1, but it is important to keep them in perspective. The cleanroom environment helps to create the need for high throughput, ultra-reliability, and small footprint equipment. The remainder of this section deals with the direct effects of cleanliness requirements on mechanical design.

### 4.7.1 Cleanrooms

Most cleanrooms use laminar air flow to help maintain the cleanliness levels. Generally, the air flow is vertical and has a velocity of about 65 feet per minute. Air is "pushed" through filters in the ceiling of the cleanroom. In turn, the air is "pulled" through the perforated floor. The cleanroom usually also has a slight overpressure relative to the surrounding environment to prevent leakage of dirty air into the manufacturing areas.

This laminar air flow has several effects. First, particles generated in the manufacturing operation are continuously flushed out of the cleanroom. The continuous processing required to maintain the air flow also helps control the temperature and humidity levels in the cleanroom. Additionally, the vertical air flow tends to inhibit the migration of particles horizontally through the cleanroom. As a result cross contamination between different tools can be minimized. However, the air flow can promote the build up of static electricity, especially on plastic surfaces, which can damage the integrated circuits in wafers and may also cause problems with delicate control systems. Static electricity may also attract particles and loosely bind them to a surface. Air ionizers are sometimes used to create charged molecules that will dissipate static charges. The floors are also usually conductive and grounded to help prevent large static charge build ups.

Individual process tools can also be outfitted with minienvironments to create a cleaner environment within the machine. These machines are fitted with an environmental hood, similar to the one on the machine in Figure 4.3. This hood contains a set of filters for only that machine. As a result, the cleanroom used with process tools possessing minienvironments does not have to be as clean.

### 4.7.2 Mechanical Guidelines for Minimizing Wafer Contamination

Materials and finishes can be major sources of particles if they are not carefully selected. Many common engineering materials will generate particles when used in a cleanroom. Oxidation, sloughing, and outgassing are three common sources of material contamination. Also, the surface finish can result in particle generation. Most paints oxidize as they age. Additionally, machined metal surfaces have asperities that can create particles from mechanical wear of the surface. Materials such as unfinished aluminum should be avoided. Furthermore, brushed or textured surface finishes should not be used. Elastomeric foams and unstable plastics cannot be used in cleanrooms either.

Materials that are desirable generally are hard, smooth, and resistant to oxidation and chemical effects. Hard coated or heavily anodized aluminum can be used. Stainless steel is also commonly used. Construction plastics like PVC and polypropylene can be employed in certain applications. Although slightly less desirable, tightly bonded plastic coatings and two part epoxy paints can be used in some areas.

It is usually not possible to economically eliminate all sources of particle generation. Another strategy is to contain and remove particles that are generated. For example, the moving mechanical components of wafer handling robots can be housed inside a closed structure. This structure can be sealed and/or exhausted to remove particles and prevent their migration to unwanted areas.

Particle contamination is usually associated with airborne migration of particles. However, the vertical laminar flow in the cleanroom is very effective at containing this contamination route. Migration of particles through surface contact can still be a problem. For example, the back side of a wafer might pick up a particle from an abraded

surface in a wafer cassette. When the wafer is unloaded by a wafer handling robot, the particle might be transferred to the robot's gripper. Subsequently, that particle could find its way from the gripper on to the surface of another wafer. The designer must also be aware of this mechanism of contaminating wafers.

Although the laminar air flow is effective, it is often necessary to create aerodynamic surfaces so air flow is not disrupted. Abrupt changes in machine geometry, especially horizontal surfaces, may cause a transition to turbulent airflow. Particles adhering to surfaces may become airborne because of the turbulent disturbance. Also, it is desirable to use the slowest transfer speeds for wafer handling robots allowed by cycle time requirements to minimize turbulent wakes. The wafer handling robot should be designed so that the wafers are transported such that the robot does not interrupt the laminar air flow above the wafer. The robot also should not carry the wafer in the wake created by the robot's motion.

### 4.7.3 Case Study: The Clean Design of a Wafer Handling Robot

The requirements for cleanliness played a major role in defining both the layout of the Accipiter project's wafer handling robot and details of the design. The configuration of the robot, which is shown in Figure 4.7, was affected greatly by the need to position the wafers above the body of the robot at all times. This requirement combined with the large vertical stroke needed and the desire to limit the footprint led to the development of the multi-stage telescoping axis. In Appendix A, alternate designs for the wafer handler are discussed. One of these designs uses a fixed mast with a shuttle that moves up and down the mast. This design is much simpler then the telescoping design and is also very space efficient. However, the fixed mast is unacceptable because it disrupts the laminar airflow above the robot. Also for cleanliness reasons, the upper portions of the mechanisms of the robot had to be fully enclosed. As a result, the grippers, the dual elbow joints, and the telescoping vertical axis were carefully designed so that none of the moving parts were exposed to the cleanroom.

To help maintain the cleanliness of the robot, two fans located at the bottom of the main column of the telescoping axis evacuate the inside of the robot. These fans create

low pressure inside the robot, which tends to pull dirty air out of the body of the robot. It would be possible to use seals in each of the joints to prevent air from leaking out of the arm. However, because the seals themselves will generate particles as they wear and because the inside of the robot is evacuated no seals are used. As a result, there will actually be a slight air flow into the upper portions of the arm. When the telescoping axis is retracting, it acts as a piston moving into a cylinder and could potentially pump air out the upper portions of the telescoping axis. However, the fans in the body are sized so that they can maintain sufficient air flow to prevent leakage even when the vertical axis is moving downward at top speed.

The robot also uses best known industrial practices for materials and finishes. Conductive, abrasion resistant plastic is used in the contact points in the gripper. Electro-polished stainless steel is used as a structural material near the wafer, also. The remainder of the arm is made from aluminum with a heavy nickel plating. This plating gives the arm a clean surface that is resistant to the chemicals used in the photoresist application process. Furthermore, the use of aluminum as a structural material is desirable to keep the total robot weight down.

Many aspects of the Accipiter project design were driven by the cleanliness requirements. Because of the large importance of these effects, they are discussed later in the thesis. Appendix A discusses the complete Accipiter design project and the impact of the functional requirement to reduce particle contamination at length.

## 4.8 Summary

This chapter contained discussions of six areas that support the precision machine design methodology for semiconductor manufacturing equipment. The error modeling techniques described in Chapter 3 are supported by the use of these design principles. The six areas are deterministic design, elastic averaging, the reduction of the effects of rotational errors, static and dynamic structural design, control system and mechanical design integration, and cleanroom design considerations. The significance of each of these areas was explained in the chapter and case studies from the design of a

semiconductor process tool were employed extensively to illustrate the use of each of the principles.

# Chapter 5: Summary and Conclusions

## 5.1 Introduction

This chapter briefly reviews the precision machine design methodology for semiconductor manufacturing equipment as presented in this thesis. Additionally, the chapter discusses several areas of research that are important to the design of clean wafer handling systems. Finally, the thesis concludes with a discussion of future areas of research in precision machine design for semiconductor manufacture.

## 5.2 Summary of the Precision Machine Design Methodology for Semiconductor Manufacturing Equipment

A number of observations made of various semiconductor manufacturing systems prompted the development of a precision machine design methodology for semiconductor equipment, as was discussed in Chapter 1. The thesis established a general set of functional requirements for the types of manufacturing systems found in cleanrooms, especially the wafer handling automation systems. These functional requirements are stated again here:

- High reliability
- Clean mechanical design to minimize contamination
- Short cycle times (fast transfers)
- Repeatable positioning of wafers
- Small footprint.

These requirements are a direct consequence of the special manufacturing conditions found in cleanrooms. For example, the high cost to build and maintain ultra-clean manufacturing facilities translates into a need to run production lines nearly continuously

with little machine downtime. For these reasons, high reliability, small footprint, and short cycles times are especially important. Also, the increasingly stringent cleanliness requirements necessitated by the decreasing size of device geometries necessitate clean mechanical design and repeatable wafer positioning.

In the course of developing this new design methodology, the thesis made two primary contributions. First, a set of numerical error modeling technique were developed to guild the design of wafer handling systems in semiconductor processing tools. These error modeling tools are useful in efficiently developing designs that meet performance and positioning repeatability requirements. Both displacement level and velocity/force transmission level modeling tools were developed. The models are based on geometric descriptions of structures and mechanisms. Coordinate frames are placed at key points in the system and errors from various sources are lumped at these reference frames. This arrangement allows a designer to calculate error gains that quantify how a system's geometry magnifies errors present in the design. Second, a set of mechanical design rules targeted specifically at cleanroom equipment was developed to supplement the error modeling techniques. The following areas were targeted for design rule development:

- Deterministic design
- Elastic averaging
- Reduction of the effects of rotational errors
- Static and dynamic structural deformations
- Control and mechanical system integration
- Considerations for cleanroom equipment design.

The application of the methodology developed by this research will guarantee equipment designs that economically and reliably meet their performance goals. Because of improvements in structure, mechanism, and control system design, machines will not exhibit the failures caused by overly compliant, under damped components, and mechanical drift that are currently observed. Semiconductor processing equipment manufacturers stand to gain substantial increases in reliability and performance of

processing systems by applying this precision machine design methodology to correct many of the previously observed problems in the development of their systems.

There are additional benefits that will come from the application of a precision machine design methodology. A few of these include the following:

- A streamlined design process resulting in decreased time from concept to shipping of final product
- Reduced assembly and service labor costs
- Decreased need for downstream design changes.

The first point above can be understood by considering that the precision machine design methodology developed in this thesis replaces the current undisciplined and chaotic design process. Furthermore, the use of deterministic design principles will eliminate unnecessary adjustments in process tools thereby easing assembly and service requirements. The new design methodology will also result in production machines that do not require downstream "tweaking" and design revisions to improve performance and reliability.

This thesis not only developed a new design methodology, but also demonstrated it in detail through the design of a new photoresist processing system. Silicon Valley Group, Inc. of San Jose, California sponsored the involvement of MIT in their Accipiter project. As described in this thesis, the primary contributions of the design methodology were to the development of a new structural frame and an innovative wafer handling robot. SVG's previous frame was a very compliant structure made from bolted square steel tube stock. Because of the frame flexibility, process modules were mounted to the frame with many positioning adjustments. The new frame, in contrast, is a rigid weldment with integral passive damping inserts. Accurate, deterministic mounting of process modules was achieved using kinematic couplings without any position adjustments. Deterministic design principles were also applied to the wafer handling robot. The new design incorporated several desirable and unique features. First, wafer centering was integrated into a new gripper that contacts the wafer only in its exclusion

zones. Next, the robot features two independent grippers mounted on a dual, concentric elbow joint. Another innovative feature of this robot is the multi-stage telescoping vertical axis that keeps all of the mechanism below the wafer surfaces and is packaged space efficiently. Finally, a kinematic coupling is integrated into the robot between the body of the robot and its horizontal carriage. This coupling allows the robot to be easily removed for service.

## 5.3 Other Technologies for Ultra-Clean Wafer Handling

Because of the importance of cleanliness in semiconductor manufacturing, new technologies for transferring wafers are of interest. Although, mechanical systems with rolling element bearings are currently the only economically feasible way to perform some of the material movements tasks required, several promising new technologies exist. For example, any type of system that does not require actual contact with the wafer or mechanical contact in the moving joints of a transfer system would be attractive from a cleanliness standpoint. Air bearings and magnetic bearings are two such systems that come to mind.

Air bearings have been used for various tasks in cleanrooms previously. However, their use is actually discouraged because the air blowing out of the bearing tends to create turbulence and therefore disturb particles settled on adjacent surfaces. Ohmi proposed a similar concept where wafers are transferred within a semiconductor fab in special tunnels using ultra-pure nitrogen as the operating fluid in an air bearing/drive system [Ohmi '92].

Magnetic bearings might be a more attractive noncontact bearing because no atmospheric disturbances are created in the cleanroom. A number of researchers have investigated magnetic bearings and actuators for use both in and out of cleanrooms. For example, Busch-Vishniac et al. have described the early development efforts toward magnetic levitation systems for transporting wafers in cleanrooms [Busch-Vishniac '90] [Wang '91] [Wang '93]. In a similar effort, Higuchi discusses the development of noncontact actuators for use in cleanrooms by combining magnetic bearings and stepper

motor technology [Higuchi '93]. Williams, Trumper, and Hocken have developed a magnetic bearing stage for use in photolithography [Williams '93]. Wafer steppers are a good example where these technologies can be applied beneficially now. The use of magnetic bearings in systems with fairly complex kinematic requirements and large workspaces, such as the wafer handling robot described in this thesis, may not be good candidates for the application of these technologies, at least with current levels of development. The material, power, and control requirements for such a system would make it prohibitively complex and expensive.

Another area that is worthy of mention, but was not addressed directly by the design methodology presented in this thesis, is the design of wiring harnesses for robots. Many industrial robots have special harnesses housed outside of the mechanical structure for design convenience. In cleanrooms, the wiring harnesses must be located inside the robot for the distal axes near the wafer surface. Although, methods for routing cables through a robot are well-known, these cables are often a source of packaging and reliability problems. It is suggested here that the number of wires used in these harness (and therefore the complexity of the harness) can be reduced using a distributed control system. By using such a system, the robot need only be supplied with a single DC power line and a serial communication line[50]. Amplifiers and individual axis controllers can be housed at or near each joint. Multiplexed communications can deliver digital commands to the individual joints and provide feedback to a high level controller located outside the robot.

## 5.4 Future Areas of Research in Precision Machine Design for Semiconductor Manufacture

A number of areas remain in the design of semiconductor manufacturing systems that could benefit from the application of a precision machine design methodology. For example, this thesis explored in depth the application of the methodology to a single process tool. Many other systems could be studied and redesigned to achieve

[50] In some cases it may even be possible to use optical communications and a sliding commutator for power distribution thereby further reducing the required number of wires.

performance benefits. One process tool design in particular deserves special mention. The silo concept for a new photoresist processing system mentioned in Chapter 5 was discarded from consideration in the Accipiter project. However, this type of system still has a potentially advantageous layout and may be developed into a successor for the rectangular layouts of photoresist processing systems.

Additionally, there are a number of supporting automation systems in semiconductor manufacturing facilities that are not integrated directly into process tools. These forms of automation, sometimes called interbay and intrabay automation, were mentioned briefly in Chapter 1. Examples of these systems, such as wafer stockers that store work-in-progress wafers and AGV mounted robots, might also benefit from the application of the tools and principles described in this thesis.

Because humans are best suited to perform tasks that are challenging and require creativity, further integration of automation systems into wafer fabs seems desirable. The routine transfers of wafers between and within process tools are best executed by automatic systems that perform the tasks both repeatably and reliably. Also, because the cleanroom manufacturing environment is an ultra-clean one, using automatic systems to remove particle producing humans is another large benefit.

The final, and potentially most rewarding, area of research is a system-level approach to the design of the entire semiconductor manufacturing operation. Because of the extreme demands found in cleanroom manufacturing environments and because of the complex processes required to fabricate increasingly intricate semiconductor devices, an integrated design philosophy that is reflected in the design of the manufacturing facility, the process tools, and supporting automation should help to drive these manufacturing endeavors forward. Future designs of semiconductor manufacturing facilities would benefit strongly from the integration of precision machine design techniques at all levels. An ideal that may be achievable in a semiconductor fab is a lights out manufacturing operation where no humans are required on a regular basis in the cleanest portions of the manufacturing area.

# Appendix A: Precision Machine Design Applied to a Photoresist Processing System

## A.1 Introduction

The first four chapters of this thesis explained the need for and the elements of a precision machine design methodology for the semiconductor manufacturing industry. This appendix continues the discussion by focusing on Silicon Valley Group's Accipiter project, which involves the development of a new photoresist processing system. The methodology developed in this thesis has been applied rigorously to this new design project. This appendix describes the application of the methodology from the project inception to the prototyping stage.

This appendix begins with a brief discussion of the rudiments of the photoresist application process and some historical details on the development of the process. Next, the appendix describes some of the characteristics of SVG's 90 Series Track, which is the immediate predecessor of the Accipiter project. Then the appendix describes the initial formulation of the Accipiter project requirements. The appendix continues with a discussion of the development of conceptual designs for the new machine that incorporate the new requirements and are deterministically designed. Various machine configurations are explained and evaluated. The conceptual design process continues with the development of a structural frame for the selected machine layout. The conceptual design of a wafer handling robot for the new machine is also discussed. Next, the appendix describes various concepts for gripping and centering wafers in the new photoresist processing system. The embodiment and detailed design stages for the frame and wafer handling robot are discussed following the conceptual design section. Finally, the appendix presents the prototype wafer handling robot and a test frame.

## A.2 The Photoresist Application Process

One of the primary steps in semiconductor manufacture is photolithography, a process in which patterns are transferred to silicon wafers. Many variations of the photolithography process exist. In general though, a complex circuit pattern is produced on a mask which is then used to expose wafers coated with resist. Photoresists are light sensitive and undergo chemical or physical changes when exposed to the proper wavelength of light. Resists may be either positive or negative in nature. Positive resist becomes soluble when exposed and negative resist, insoluble. In the photolithography process, the wafer is first coated with a thin layer of resist[51]. Next, the pattern is transferred to the coated wafer often in a wafer stepper. Finally, the patterned wafer is developed with a solvent to remove the appropriate parts of the resist coating. Following the photolithography step the wafer will proceed to other process steps such as etching. Also, because integrated circuits contain multiple layers wafers will require several lithography steps before the circuit is complete.

A photoresist processing system is typically operated in a linked configuration with a wafer stepper to form a complete photolithography system. The photoresist processing tool applies a uniform coating of resist to a silicon wafer and then passes the wafer to the stepper. After being exposed in the stepper, the wafer is developed in the photoresist processing tool and is then ready for further processing. Application of the photoresist before exposure in a wafer stepper and developer after exposure is performed in one of several spin stations that use a spindle with a vacuum chuck to hold the wafer. The resist is applied by placing a drop in the center of a wafer and then spinning it rapidly so that the resist spreads because of centrifugal effects. A series of hot plates and chill plates are also used to perform processing before and after the wafers are processed in spin stations.

Insight in the manufacture of photoresist processing systems can be gained by considering the history of this process technology. According to von Hippel, one of the

[51] The resist layer thickness is generally on the order of 1 μm with required uniformity in the tens of Angstroms.

earliest uses of a wafer spinner to apply photoresist was found at Fairchild in 1962 [von Hippel '88]. The first commercial spinners were on the market by 1964. The next major innovation in the application process was the use of high acceleration spinners in late 1964 [von Hippel '88]. A high rate of acceleration is advantageous because most of the resist spreads across the wafer during the first several rotations and better uniformity is achieved with higher rotational speeds.

Today the same basic process is used to apply the resist. However, the supporting machine has changed dramatically. The early spinners were stand alone modules that required manual loading. The first automated photoresist application systems used o-ring belts to move the wafers automatically through a series of processing modules[52]. The o-rings were replaced with simple automatic shuttles that held the wafer on a vacuum equipped spatula. This improvement eliminated the belts that added particles to the backs of wafers and introduced the ability to move wafers "randomly". This random movement meant that the user could reprogram the machine to move wafers through process modules in a different order, thus allowing more process flexibility. The photoresist processing systems currently being produced are fully automated. Cassettes of wafers may be loaded into the system manually or by a robot equipped AGV. The wafers are automatically moved throughout the many process steps in the photolithography process. Wafers are automatically passed between the photoresist system and the wafer stepper. These machines also contain sophisticated high level control systems to allow the user to adjust the process recipes used and otherwise control the operation of the machine. SVG's 90 Series is a representative example of these systems.

## A.3 The 90 Series Photoresist Processing System

Before considering the design of a new photoresist processing system, it is worthwhile to briefly consider the design of the system to be replaced. A top view of Silicon Valley Group's 90 Series photoresist processing system is shown in Figure A.1.

[52] These machine were called "tracks" because of the o-ring belts on which the wafers rode. This appellation is still commonly used for photoresist system although they no longer contain the original tracks.

This system contains the necessary photoresist application, developing, and support modules to perform the process. These modules are arranged in a rectangular machine with two lines of modules on either side of a shuttle car for transferring wafers between modules. The shuttle has two degrees of freedom; both are linear. The first is the long horizontal travel. The second degree of freedom uses two mechanically coupled links with revolute joints to generate straight line motion perpendicular to the horizontal travel. Dedicated serial transfer arms are also used between certain modules to speed the transfer of wafers.

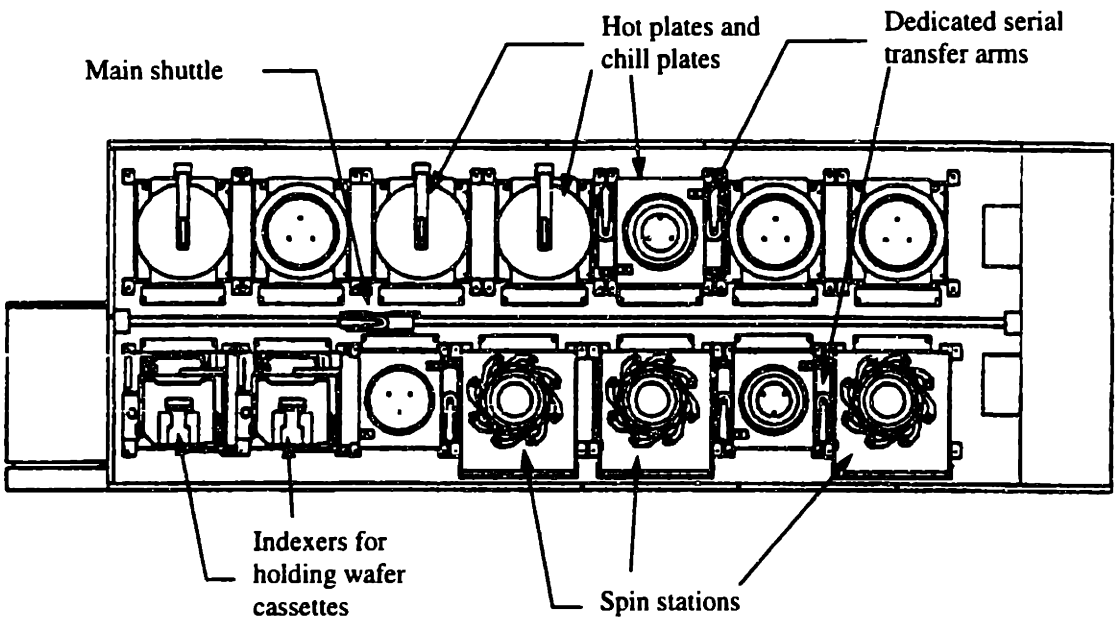


**Figure A.1** Top view of the 90 Series photoresist processing system.

The machine is constructed of light steel tubing with minimal cross bracing which results in a compliant, non-deterministic structure as was discussed in Chapter 4. As a result, the alignment of process modules requires extensive adjustments. Additionally, the adjustments cause part count, complexity, and assembly time to be unnecessarily high. Also, reliability is reduced because the adjustments in the compliant frame are not always dimensionally stable. Furthermore, the myriad of adjustments required in the 90 Series system are representative of design practices that reduce reliability and increase

manufacturing and set-up time in addition to increasing the need for recalibration of the material handling system at frequent intervals.

This photoresist processing system may also use a universal interface mounted on one end of the machine. This interface is used to automatically transfer wafers to a wafer stepper and receive wafers from the stepper. The 90 Series also typically contains indexer modules that hold wafer cassettes. The indexer contains a vertical degree of freedom that moves the cassette to allow the shuttle to remove and deposit wafers.

Figure A.2 shows several typical process modules in the 90 Series photoresist processing system. Special note should be made of the iris mechanism on the left most module, which is used to center wafers on the spin station chuck.

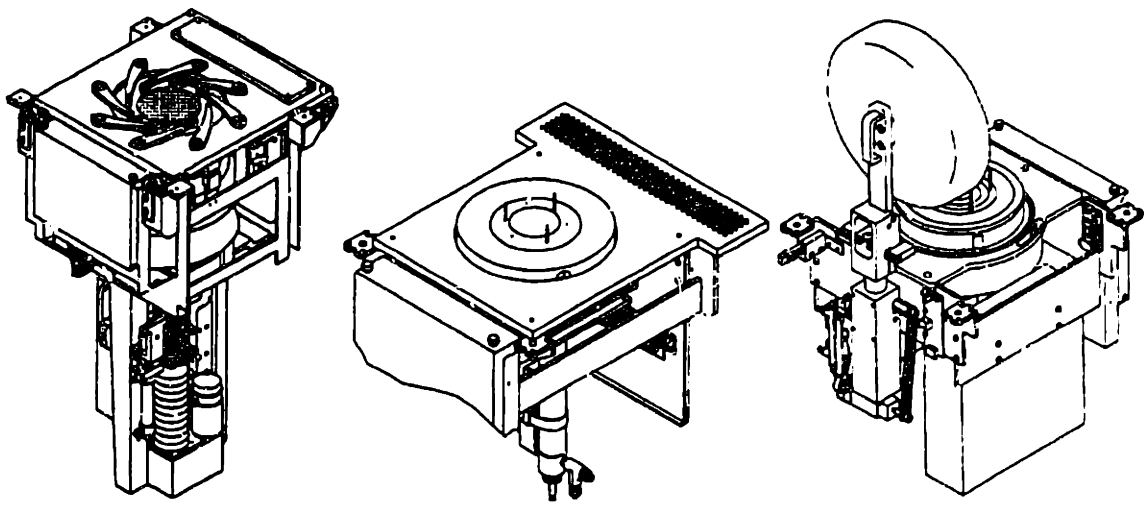

**Figure A.2** Process modules from 90 Series Track. Spin module at left, chill plate center, and vapor prime (hot plate) at right[53].

Several views of the wafer transfer mechanism are shown in Figure A.3. This mechanism uses a narrow vacuum equipped spatula to hold a wafer.

[53] Courtesy of Silicon Valley Group.

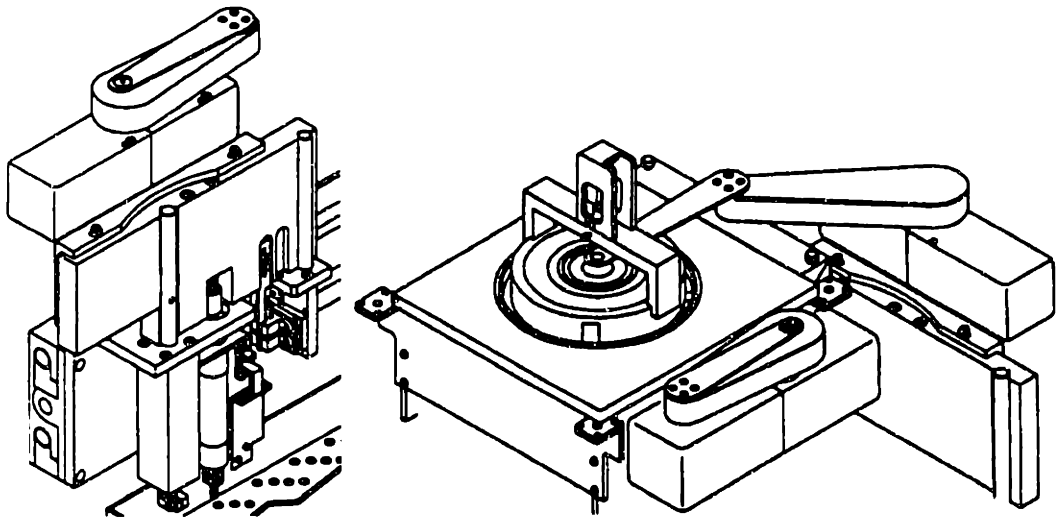

**Figure A.3** Shuttle arm for wafer handling in 90 Series. Fully retracted arm shown at left and arm insertion calibration shown at right[54].

SVG's products have been noted for their world class performance with respect to the semiconductor wafer processing steps. However, their products have experienced reliability problems in the material handling systems. These systems are a crucial component necessary for clean, repeatable, and reliable operation. The automated wafer handling systems can potentially provide reduced cycle times, fewer requirements for human intervention, and reduced particle contamination in critical processing steps if they are implemented properly. The following several paragraphs detail some of the difficulties in the machine as pointed out by field service personnel[55].

In the course of installing a photoresist processing systems in a working wafer fab, field service personnel must "set-up" the machine. This procedure involves first leveling the entire machine. Next, the shuttle mechanism is leveled. Note that the level of the shuttle changes with position along the track. Informal measurements indicated as much as ±0.3° of variation along the shuttle track. Because of this variation, the shuttle is often leveled relative to the most critical module, such as the indexer. Finally, the individual modules must be leveled relative to the shuttle.

[54] Courtesy of Silicon Valley Group.
[55] The people who fix machines with problems can give invaluable feedback to the design engineer.

This set-up procedure must be performed in both the final test/assembly area at SVG and then again at the delivery location. This labor intensive procedure requires several days to perform. Furthermore, the numerous position adjustments that must be performed are indicative of the indeterminacies in the design of the 90 Series.

Additionally, field service personnel felt that the large number of adjustments and the associated indeterminacies in the wafer handling systems seem to be related to the need to frequently recalibrate the random arm second link position relative to various process modules. Simply restarting and homing the shuttle arm often does not correct the second link positioning inaccuracies which show up on the machine controller as a drift error that requires physical recalibration of the system. This type of failure indicates the problem is probably mechanical in nature. The loss of calibration may be due to backlash in the arm drive train, wobble in the shuttle car bushings, and/or slippage of various mechanical drive components. Informal measurements showed a variation in shuttle car position of ±0.004 inches occurring approximately 5 inches away from the shuttle linear bearing due to inadequate bearing preload.

Many serial arms in various installed track systems exhibit nonplanar motion of the gripping portion of the second link. Again, informal analysis indicated that the problem is more complex than a simple orthogonality misalignment of the base drive axis. Rather a parallelism error between the two joints of the serial arm probably causes an Abbe error and the resultant end effector misalignment. SVG engineers have noted as much as ±2° of droop at the second link in various 90 Series systems.

The parallelism problem in the joint axes of the serial arm may be caused by manufacturing inaccuracies or may be the result of fluctuating tensions in the drive belts of both the base and tip joints. Errors of as much as ±0.005 inches in the concentricity of the joint axes and sprocket alignments could cause significant variations in the belt tensions. These alternating tensions along with overly compliant bearing mount geometries may result in the observed variations of the second link height.

In addition to the nonplanar motion of the serial arm, a large amount of backlash exists in the arm drive unit. As much as 0.125 inches of equivalent backlash was

observed at the tip of the arm. An attempt by SVG design engineers was made to eliminate this backlash using a torsional spring. However, apparent fatigue failures in this spring have prevented it from functioning reliably in the field.

As will be seen in the following sections, one of the goals of the new design project was to eliminate problems similar to the ones discussed here by using a deterministic approach to the design of both the machine's structure and its wafer handling systems.

## A.4 The Design of a New Photoresist Processing System: The Accipiter Project

Silicon Valley Group, Inc. initiated the Accipiter project as a natural evolutionary step to replace the aging 90 Series photoresist processing system. The new machine is positioned to improve many aspects of the 90 Series performance. The machine must offer a more competitive footprint based on the number of process modules. Additionally, the new system should offer higher throughput. Furthermore, the deficiencies in previous system's reliability need to be overcome. Because of decreasing characteristic line widths, cleanliness requirements for the new machine are more stringent and process performance must be improved.

The need for a new photoresist processing system is determined largely from market requirements. In this case, the design of a new machine does not contain a radical shift in process technology. The same basic techniques for applying photoresist are employed. Evolutionary improvements in the process modules are being made, however. Additionally, the project does involve a large shift in the paradigm used to design the machine's structure and wafer handling mechanisms. The methods discussed in the first four chapters of this thesis are used to improve the design of these systems.

This shift to a deterministic strategy is helping to reduce some of the 90 Series' reliability problems. Additionally, this new approach to the design of the structure and wafer handling system is expected to have several benefits. First, by creating a stiff structure on which the machine is built, a robust, deterministic system can be created.

The stiff structure allows reference surfaces to be machined directly into the frame. Process modules are kinematically coupled directly to the frame thereby eliminating many position adjustments. This elimination helps to reduce the manufacturing and set-up time. Furthermore, system complexity and cost are reduced. The same deterministic approach is applied to the automatic wafer handling systems. Error modeling is used to guide the development and selection of conceptual designs and the detailed design is also guided in this manner. Design practices that guarantee repeatability are used in the wafer handling robot. The lost motion and mechanical drift observed in the 90 Series is dramatically reduced.

The most general level of functional requirements can be stated as they were in Chapter 1 as follows:

- High reliability
- Small footprint
- Clean mechanical design to minimize contamination
- Short cycle times
- Repeatable positioning of wafers.

These functional requirements are used in the design process to determine characteristics or parameters of the design that are needed to give the desired performance. Constraints are also imposed on the design solution by the environment in which the machine will operate and by market requirements. The design process is both hierarchical and iterative in nature. Once higher level aspects of the design solution have been determined, new sets of more specific functional requirements must be stated at the lower levels. The design characteristics or parameters of the previous level may become constraints in the design at lower levels. If the design contains an inadequacy of some type it may be necessary to move back to a higher level and redesign all or part of the system. These inadequacies are often caused by new information about the problem to be solved or other changes in the design functional requirements. Iteration is generally required. However,

unnecessary delays may result from too many iterations especially if the design problem is not acceptably stated at the inception of the project.

Silicon Valley Group is an ISO 9001 certified company. As such, they follow a well-defined design process. This process is consistent with the one described in Chapter 2. The process begins with a product request, which is essentially the initial problem definition stage. Following that, a feasibility stage is completed that further refines the problem definition. Next, conceptual designs are generated. At this point, the project enters the design stage. The ISO 9001 design stage includes both the embodiment and detailed design phase. Next, a prototype stage is entered. This phase is followed by a preproduction stage. Finally, the design enters the production stage.

The definition of this new design project was strongly influenced by requirements from SVG's marketing department. The actual design project also benefited from interaction between design engineers, marketing, field service, and manufacturing engineering. In fact, manufacturing personnel were included in the design team at the detailed design stage to insure the manufacturability of the finished design.

Many detailed aspects of the functional requirements, especially those dealing principally with the process technology, are beyond the scope of this thesis and will not be discussed here. The marketing department at SVG created a detailed document that quantified many of the functional requirements and constraints for the Accipiter project. These goals and constraints guided engineers in the design process. Again, only those details required to explain the elements of the design presented here are discussed. The primary focus of the precision machine design methodology is the structural frame of the machine and the wafer handling systems. The discussion here reflects this emphasis. However, a fairly complete picture of the design requirements is still necessary to proceed with the development of these machine concepts.

In addition to the primary functional requirements discussed above, the design of the new photoresist processing system is subject to many constraints. For example, the machine must interface with existing and future wafer stepper designs. Also, the new system's end station must comply with ergonomic and AGV requirements for loading

cassettes into the machine. Furthermore, numerous safety and facility specifications must be complied with. The machine must also be designed to be used in both bay and chase and ballroom style cleanrooms.

Another constraint that the Accipiter project must comply with relates to the size of the wafers to be processed. The economics of semiconductor production is continually driving manufacturers to larger wafers [Bullis '93]. Consequently, in the new design considerations for larger wafers must be accounted for. Current leading edge manufacturers use 200 mm wafers; although, by volume 150 mm wafers are the most popular in the world. Advanced manufacturers are already considering the jump to the next wafer size, which will probably be 300 mm. These larger wafers, as compared to 200 mm wafers, have 2.25 times as much surface area. However, because of the spacing of the usually square die around the periphery of the wafer, an average 300 mm wafer will have about 2.4 times as many chips compared to a 200 mm wafer [Bullis '93].

Although, photoresist processing systems capable of processing 300 mm wafer may be needed before the end of the century, they are not needed now. Because of the penalties associated with larger machine size, incorporating 300 mm capability into a system too soon would not be beneficial. The current design project, therefore, is targeted at 200 mm wafers. However, it is desirable to create a design that can be scaled directly to 300 mm wafers simply by adjusting wafer handling mechanisms for the larger wafers and increasing machine size and process module size as necessary to accommodate the larger wafers. Therefore, the design produced by the Accipiter project can be directly scaled to process 300 mm wafers when market conditions require.

## A.5 The Conceptual Design Stage of the Accipiter Project

This section of the thesis describes the conceptual design of the Accipiter project. First, the development of machine layouts for the new system are discussed. Next, this section presents the development of a deterministically designed machine frame. The description of the conceptual design stage concludes with the development of wafer handling robot concepts and wafer gripper concepts.

### A.5.1 Conceptual Design of the Machine Configuration

The first requirement in the conceptual design of a new photoresist processing system is the consideration and selection of a machine configuration. The configuration is the layout of the entire machine; how process modules fit into the machine, how the machine interfaces with wafer steppers, what the requirements of the wafer handling mechanisms are, etc. Because the conceptual design of the machine configuration is the highest level of the hierarchical design process, the functional requirements are the same as mentioned in Section A.4. This section describes an effort to consider a wide variety of possible layouts.

A worthwhile first step in this conceptual design process is the study of competitors' designs and available patent literature. The successful designer will benefit from being aware of other design solutions to similar problems. Most competitors' systems have a similar rectangular configuration as compared to the 90 Series[56].

One of the most valuable resources for the engineer in the study of other designs is the patent literature. This documentation is a public record so access is unrestricted. Of course patented ideas cannot be used without a license, but these ideas can spur the designer's creativity. Existing patents may even help a designer to develop an innovative way to solve an existing problem. There are a variety of patents for various types of process tools. Most of these patents, however, describe facets of the process technology used in the machine. A few do pertain to the construction of the process tool. For example, Wu's patent describes a wafer manufacturing systems where wafers are transferred individually rather than in cassettes [Wu '93]. Rubin's patent describes a modular process tool [Rubin '89]. However, none of these are similar to the deterministic design approach being used here.

It has been mentioned several times prior to this point in the thesis, that the desired method to improve the reliability and robustness of the machine is to employ the precision machine design methodology as described in this thesis. Virtually, any machine configuration could be designed deterministically. So, the examination of machine

[56] A detailed discussion of these systems is beyond the scope of this document.

configurations is driven by the high level functional requirements. As will be seen in Sections A.6 and A.7, the precision machine design methodology is applied specifically to the design of the machine frame and the wafer handling robot.

The requirement for small footprint is one of the primary considerations in the development of conceptual machine layouts. The layout also must accommodate the process modules and wafer handling robots in such a way that the design is clean, the throughput goals can be achieved, and repeatability and reliability are not compromised. Additionally, the machine configuration must satisfy many constraints. For example, some process modules require visual access to allow operators to set up manually process operation. Furthermore, the system must be designed for service access so that preventative and emergency maintenance can be easily and efficiently performed. The machine must also satisfy the requirements of various customers. The machine must be suitable for different styles of productions fabs. Also, because many aspects of the process tool must be tailored to a particular customers requirements, the design should be modular and easily customized.

Another requirement of the Accipiter project, is increased throughput. However, process times for individual modules are relatively fixed using the current technology. Therefore, throughput improvements can be achieved only by increasing the number of modules available to process wafers. As a result, a novel solution is required to accommodate both an increased number of modules and a decreased machine footprint. Currently, the 90 Series has a purely horizontal layout[57]. An analogous situation has occurred in nearly every large city in the world. Architecture is initially confined to low rise buildings. However, as real-estate becomes less available and more expensive, building become taller. Vertical expansion of the machine is clearly the way to satisfy the system's requirements. The situation is still rather complicated, however, because of the other requirements and constraints that are negatively affected by vertical stacking of modules.

[57] There a variant of the product, the 90S, with a small number of modules stacked two high.

### A.5.1.1 Machine Concepts

Figure A.4 shows two variants of a modular, vertically stacked silo concept. The silo is formed from a number of layers, each of which is kinematically coupled to the lower layer. Process modules are arranged around a circular inner core. The layers also have removable sections to allow service access. The "square" silo show on the left side of the figure would allow electric, chemical, and exhaust plumbing to be routed up the corners of the machine.

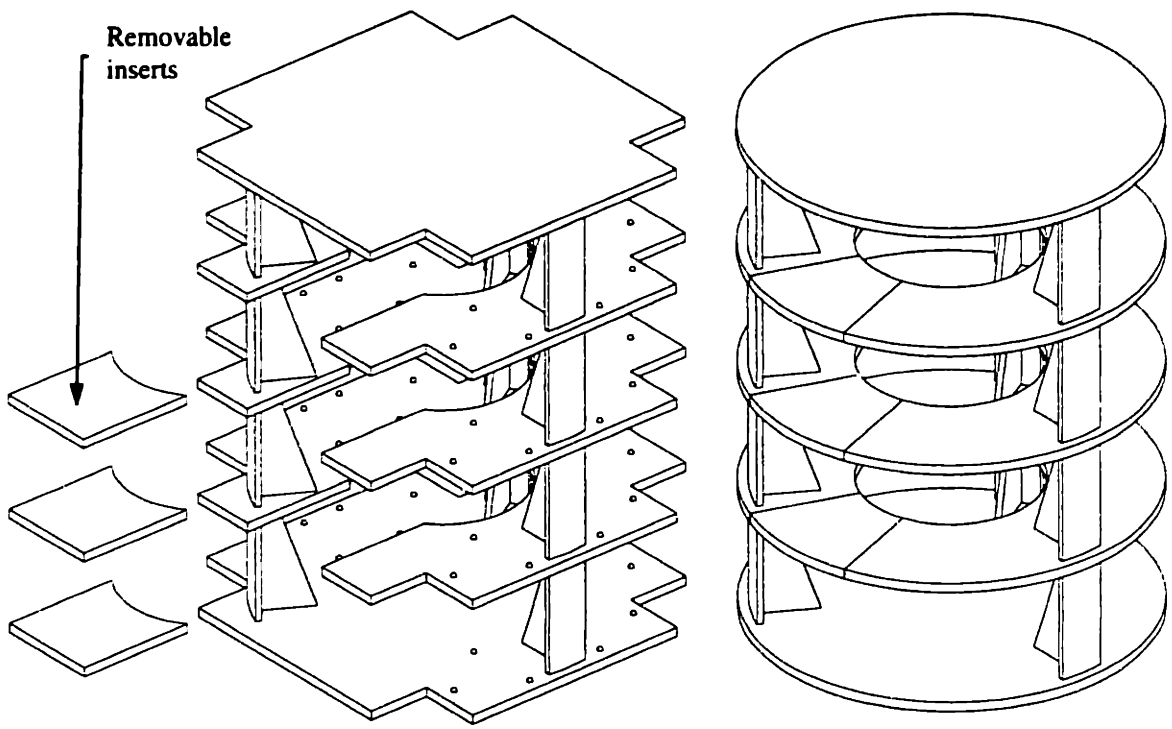


Modified Silo Original Silo

**Figure A.4** Silo machine concept with kinematically coupled layers.

A vertical cross section of the silo concept is shown in Figure A.5. One of the primary concerns in a vertically stacked machine is the flow of air through the machine that prevents airborne particles from lingering above wafer surfaces. This figure shows how air could be routed from the top of the machine through each of the layers. The vertical column supporting the robot used for wafer transfers also serves as an exhaust return that helps to direct air flow from the outside of the machine to the inner core.

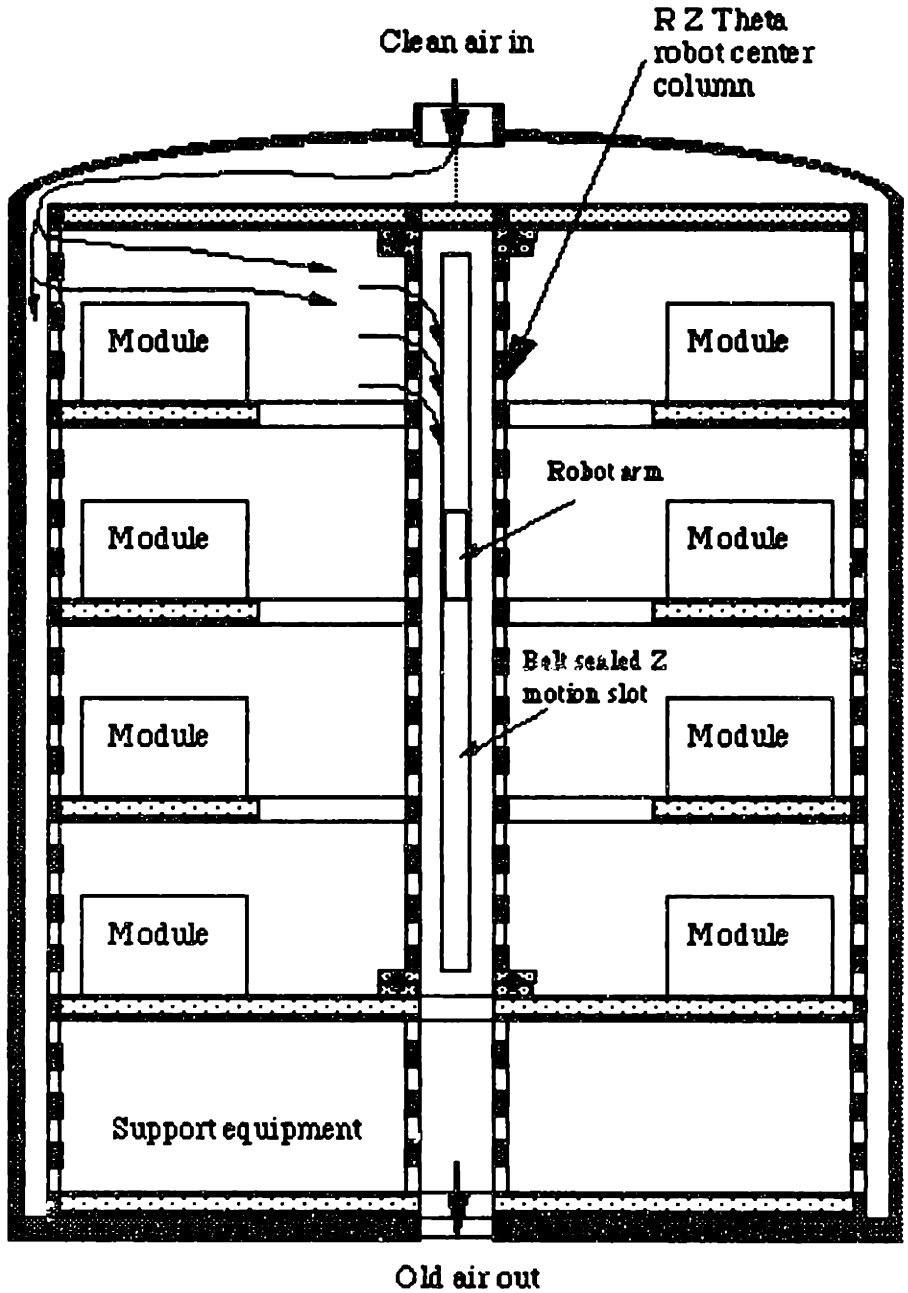


**Figure A.5** Vertical section of the silo concept showing air flow and modules.

Figure A.6 shows a top view of a single module layer in the silo concept. In this case, the figure is scaled for 400 mm wafers, but the concept is essentially the same for any size of wafer. The primary means to transfer wafers in this concept is the central robot. However, higher throughput might be obtained by positioning dedicated transfer arms between critical process modules.

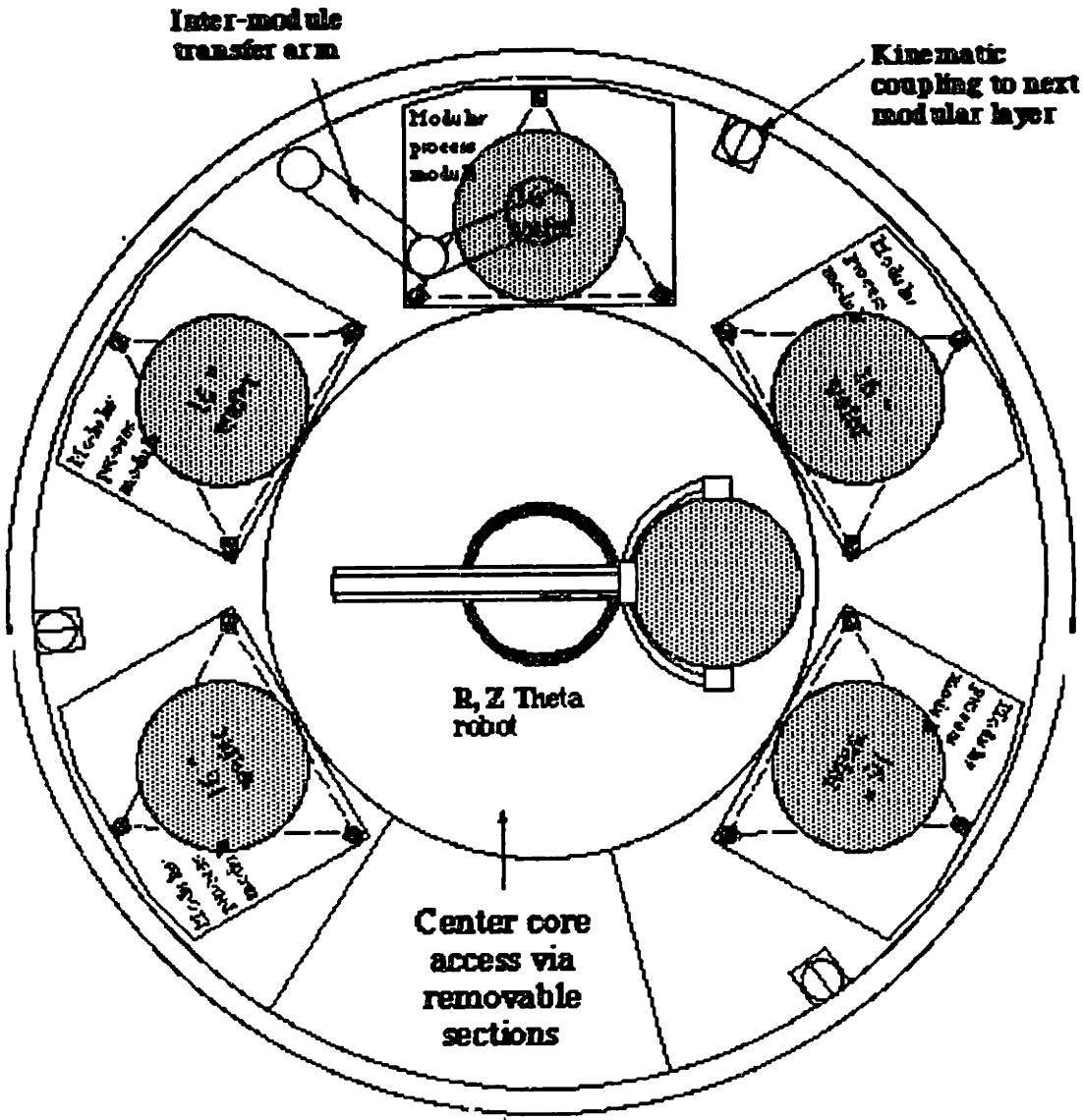


**Figure A.6** Top view of single layer in the silo concept.

To visualize the modular stacked nature of this concept, a two thirds scale wooden mock-up was constructed as shown in Figure A.7. This type of model is often useful in the conceptual design stage for visualization purposes. It can be especially useful for presenting an idea to non-technical members of a design team such as marketing and management.

**Figure A.7** Two thirds scale wooden model of the silo concept (with an extra layer)[58].

A number of other vertically stacked configurations were considered. These are shown in Figure A.8, Figure A.9, and Figure A.10. Because these concepts did not show as much promise, they were not developed as fully as the silo concept.

The final machine configuration considered was a rectangular arrangement similar to the existing 90 Series. Figure A.11 shows one possible rectangular configuration. For this type of machine, only the hot and chill plates are stacked. The spin stations are still housed in only a single level. A number of variants of this configuration were developed as candidate designs.

[58] This model was constructed by a group of MIT freshman under the supervision of the author.

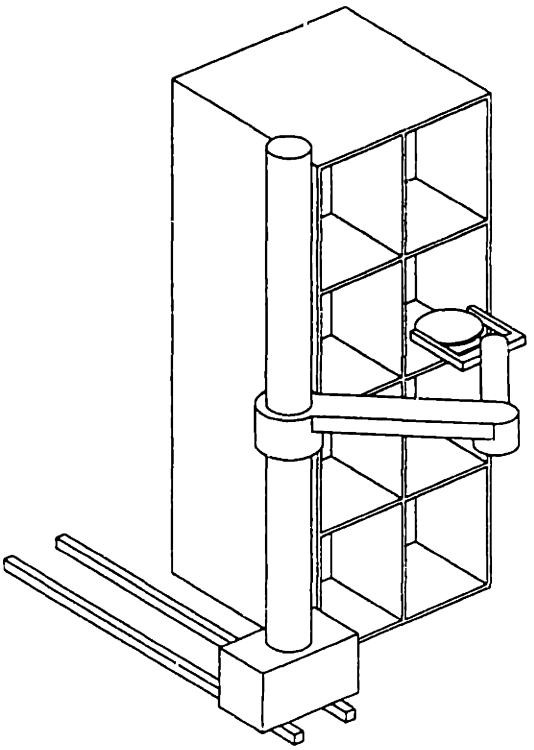

**Figure A.8** Vertical box machine concept.

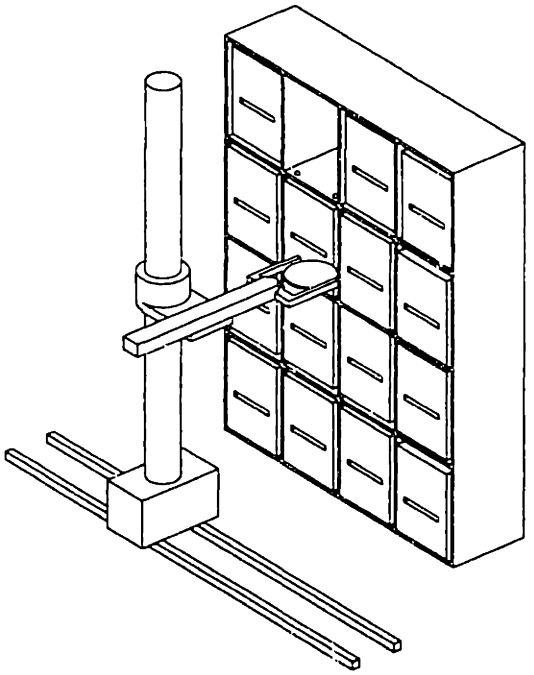

**Figure A.9** Wall-mounted machine concept.

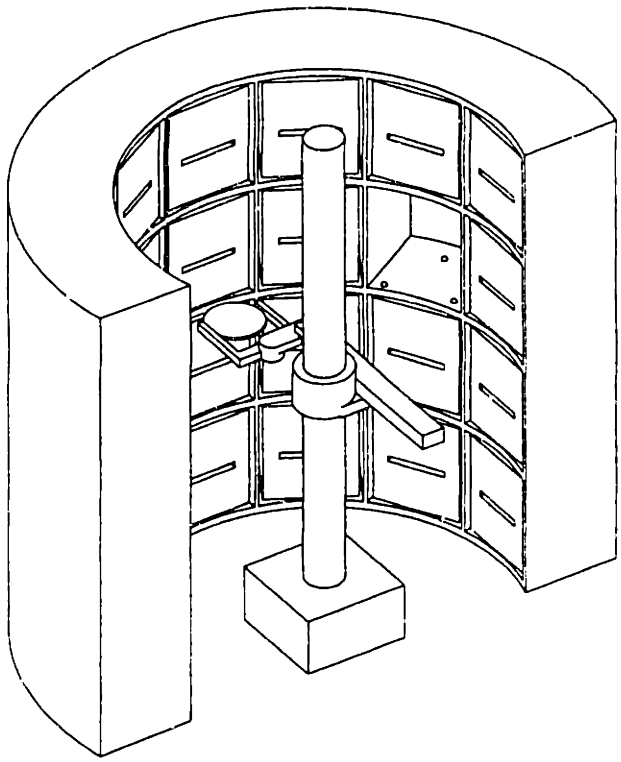

**Figure A.10** Semicircular machine concept.

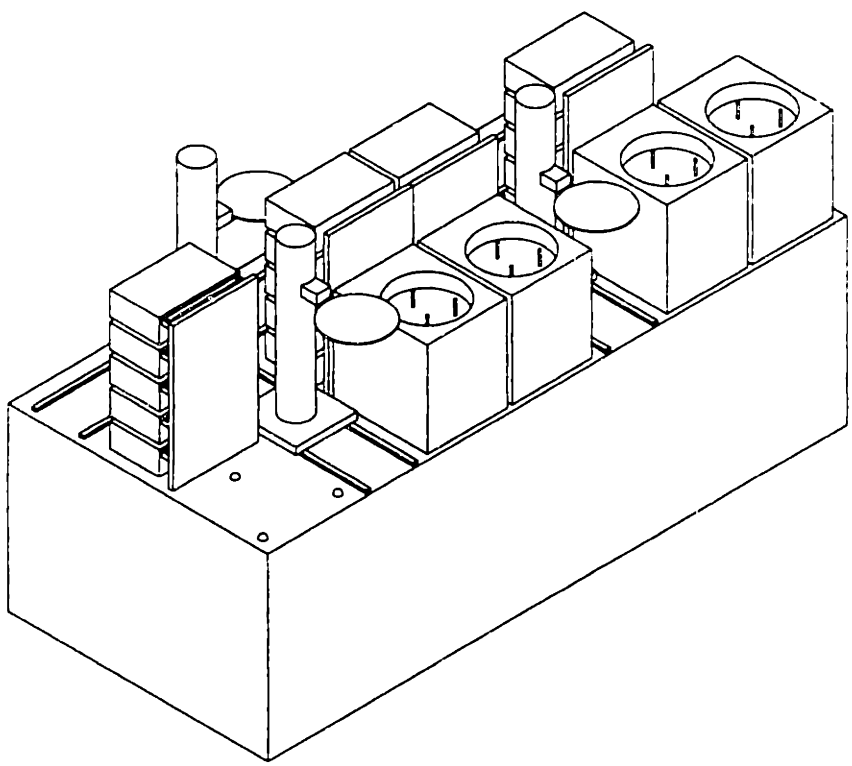

**Figure A.11** Traditional horizontal machine concept.

### A.5.1.2Selection of the Machine Concept Layout

Appendix E contains the numerical results of the application of the analytical hierarchy process to the selection of the machine layout. The traditional rectangular configuration was selected for a variety of reasons. First, the vertically stacked concepts potentially obstructed operator access to modules for process set up. Second, service access to these stacked modules might also be difficult. Finally, having all process modules stacked might create a dirty atmosphere above modules lower in the machine. The traditional concept offers a compromise in that critical spin modules can be housed with nothing above them. In turn, the more numerous and less voluminous support modules can be stacked to gain the required footprint benefits.

In excess of twenty five specific configurations for the traditional rectangular machine layout were considered. These configurations included details on exact placement of process modules and wafer handling mechanisms. Primary concerns in choosing a layout involved machine footprint and service access to modules and robots. Two of the leading candidates are shown in Figure A.12 and Figure A.13. The first of these concepts uses a modular frame that is repeated to obtain different machine sizes. The machine shown in Figure A.12 has two of these modules with end station and stepper interfaces attached to the ends of the machine.

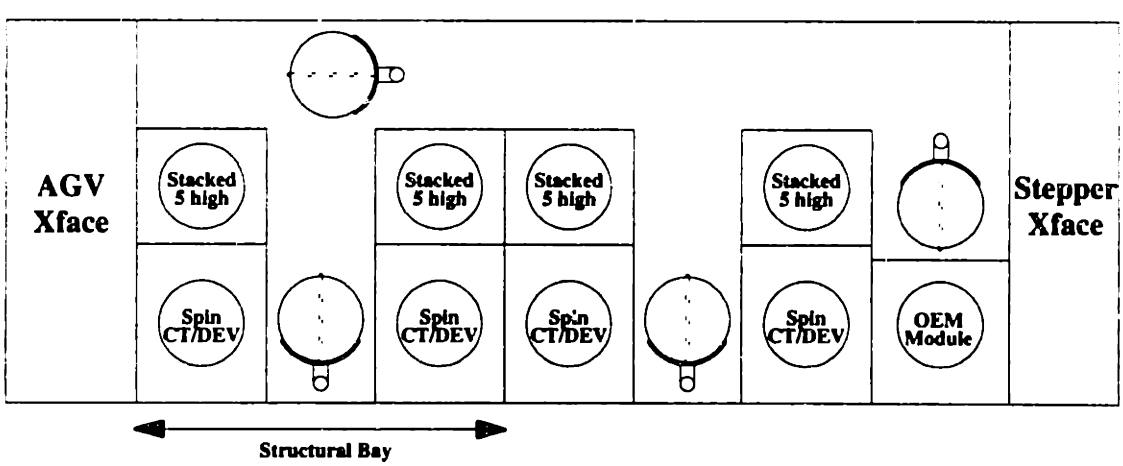


**Figure A.12** Rectangular configuration with modular frame concept.

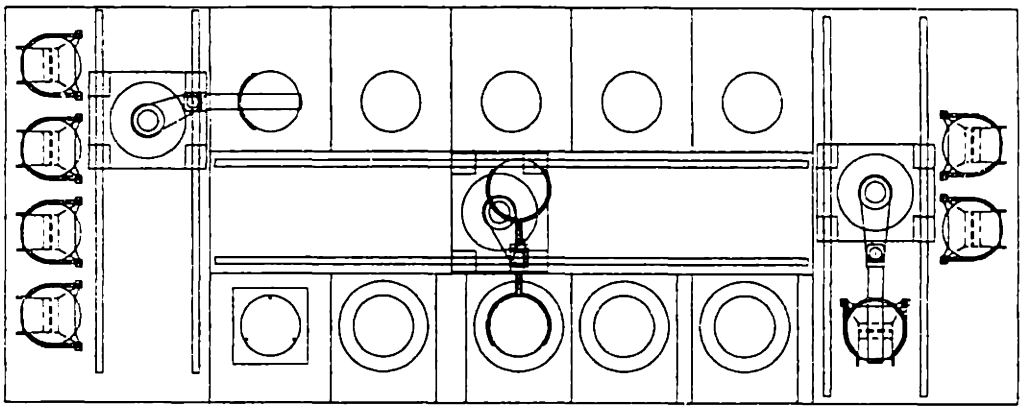

**Figure A.13** Traditional rectangular machine configuration[59].

One concern in a machine with stacked modules housed directly next to unstacked modules, such as is the case in Figure A.12, is the potential disruption in the laminar air flow above the process modules. Any structure next to the unstacked module might promote the generation of a dirty boundary layer that could detrimentally affect wafers being processed nearby. Figure A.14 shows a concept for preventing this boundary layer from developing by applying suction to a perforated wall.

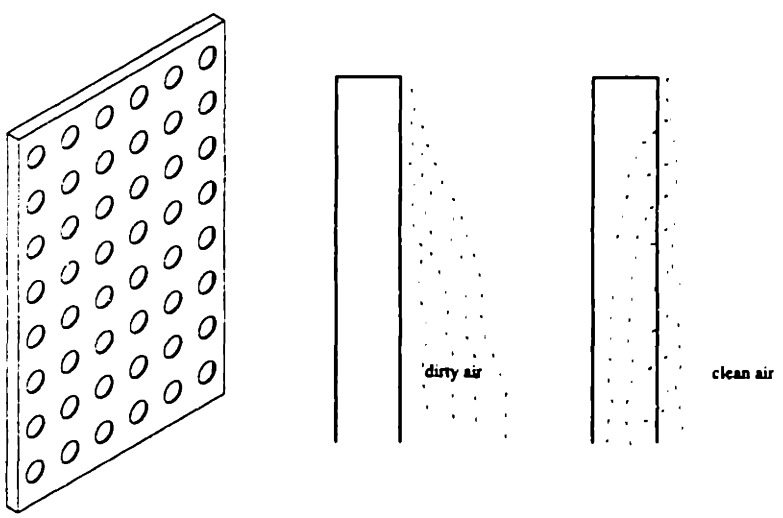


**Figure A.14** Concept for perforated vertical wall with suction to prevent dirty boundary later development.

The rectangular machine configuration shown in Figure A.13 was ultimately selected for the Accipiter project. The layout is among the most conservative considered.

[59] Courtesy of Silicon Valley Group.

However, the machine offers several benefits. The machine size is easily customized simply be shortening or lengthening the central frame. The end station and stepper interface can be attached to either end of the machine so left and right hand versions can be produced. All of the stacked modules are on one side of the machine and the spin modules on the other. In installations where the machine is mounted against a wall, the spin stations can be positioned in the front of the machine where they are easily accessible. Also, this machine concept offers under cabinet packaging space below both the front and rear modules. This space can be fitted with pull out drawers to allow easy service access. Additionally, this machine concept can use three virtually identical wafer handling robots. Furthermore, the end station, stepper interface, and central portion of the machine all have similar kinematic requirements so the wafer handler design is simplified.

### A.5.2 Conceptual Design of the Machine Frame

After the Accipiter design team had selected the rectangular machine configuration, conceptual development of machine frame concepts began. One of the primary goals of the frame design was to provide a stiff structure that would allow process modules and wafer handling mechanisms to be deterministically attached to the frame. This frame needed to give the necessary support without increasing the machine footprint or compromising packaging space within the machine. The frame also had to provide some means to route the extensive electrical, exhaust, and chemical lines that are used in the photoresist processing system. Also, it was desired to use a welded frame design rather than the previous bolted structural to give a stiffer, more robust structure[60]. Figure A.15 shows an early model of a concept for a rigid machine with kinematically coupled process modules that contains many of the desired structural characteristics.

The frame designs considered had to give high torsional, lateral bending, and transverse bending stiffness. First order estimates were used to approximate the stiffness of each frame concept. Also, scaled wooden models of the first two concepts discussed

[60] Final analysis also showed the weldment to be considerably less expensive than the previous bolted structure.

below were constructed for further evaluation. As was discussed in Section 4.5.3 and shown in Appendix C, finite element analysis was used to further refine the final frame design after the conceptual design had been selected.

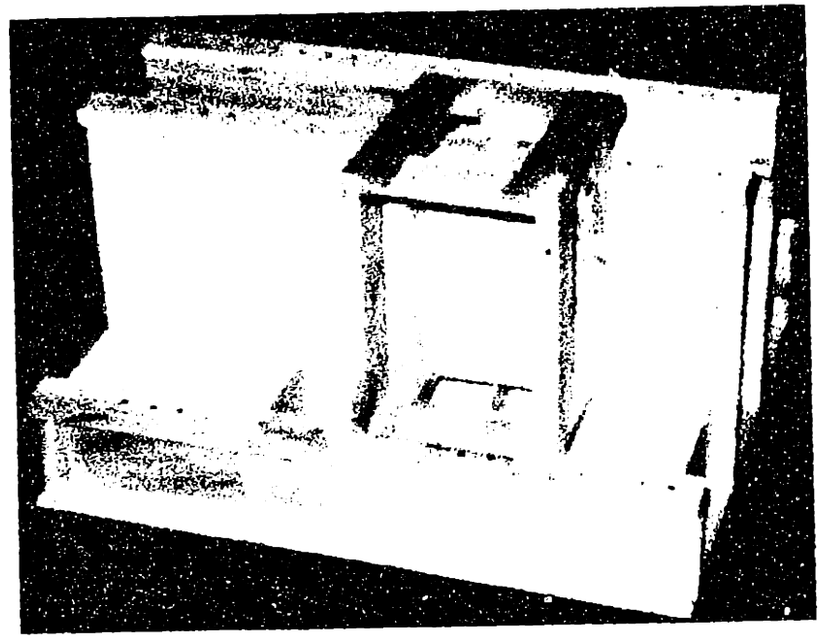

**Figure A.15** Wooden model of a machine tool type track base with integral kinematic couplings[61].

Figure A.16 shows a simple box structure with a central I-beam and cross panels.

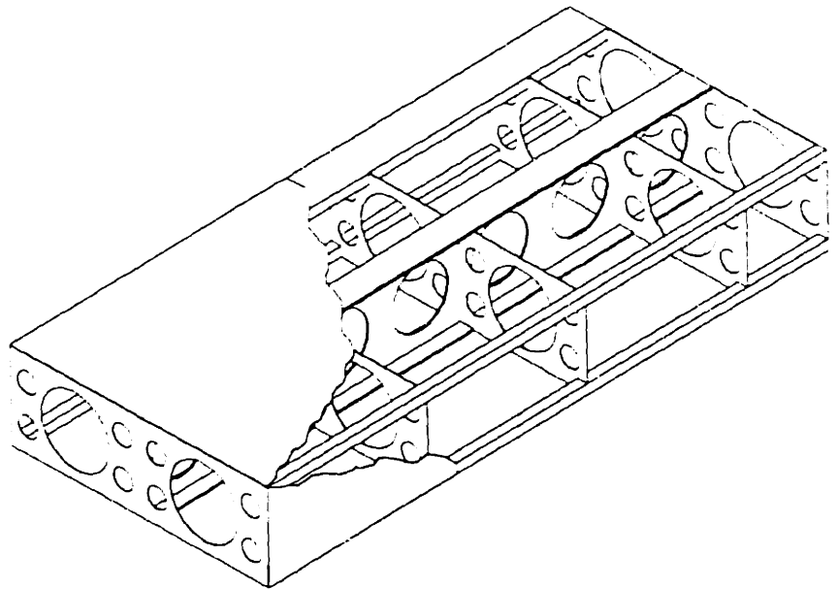

**Figure A.16** Box-type substructure concept with central I-beam for bending stiffness.

[61] This model was constructed by Prof. Alex Slocum.

This concept uses an outer skin to give additional stiffness. Tube sections span the length of the machine along the corners to provide a solid structure for the mounting of process modules. Also, numerous lightening holes are used to increase the structural efficiency of the frame concept.

Figure A.17 shows a similar frame. The structure makes use of a central tube with channel sections welded to the top and bottom of the tube.

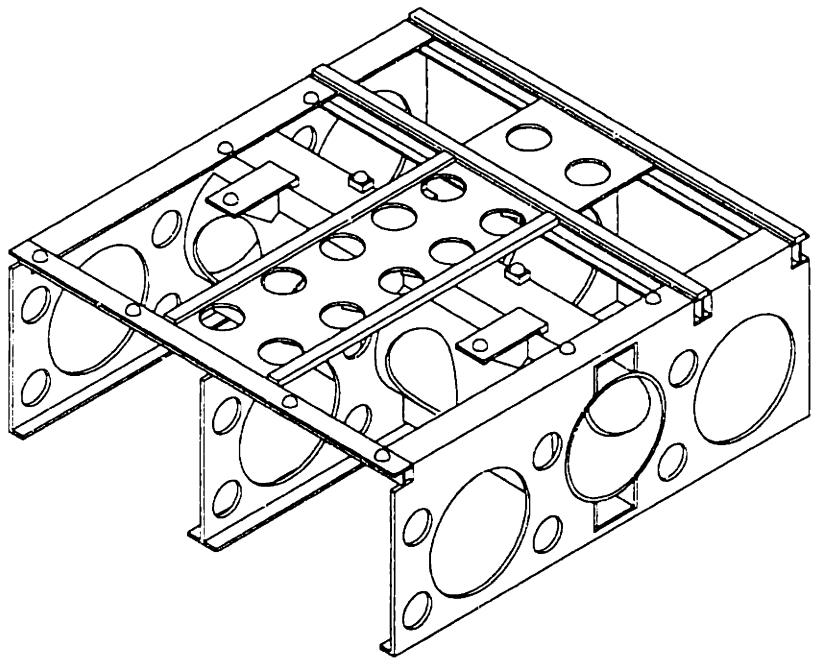

**Figure A.17** Modular machine substructure concept with central tube for bending and torsional stiffness.

This arrangement gives additional torsional rigidity to the frame. The tube also provides a conduit through which electrical and other plumbing can be routed. Like the previous frame, numerous lightening holes are used to increase structural efficiency. Ball locations for integral kinematic couplings are shown in the figure also. This particular frame was designed to be used with the modular machine concept shown in Figure A.12. Several frame modules would make up a complete machine. However, a longer version of the same frame concept could easily be used for a non modular machine frame.

A three view drawing of an early version of the final machine frame concept is shown in Figure A.18. This frame was designed for use with the machine configuration

shown in Figure A.13. Figure A.19 shows a more developed version of this structural concept. Spin stations mount to the lower, front part of the frame and other stacked modules to the back portion of the frame. To give additional clearance for the body of the wafer handling robot, this frame concept has an alley way down the center of the machine. The open space in the frame is accessible from both sides of the machine.

Because the torsional and bending stiffnesses of the frame are important, a specially designed central spine, shown in Figure A.20, is used to give the frame additional stiffness. The spine is formed from four smaller tubes placed at the inside corners of a large tube which is made up of steel plate. Finite element analysis was used to select the spine shown from four candidate designs. In addition to stiffening the structure of the machine, the spine serves as a conduit for electrical plumbing. The spine also has clearance to pass utilities from the front of the machine to the rear. Finally, the spine contains vertical passage ways to collect and route through the machine, the vertical air flow.

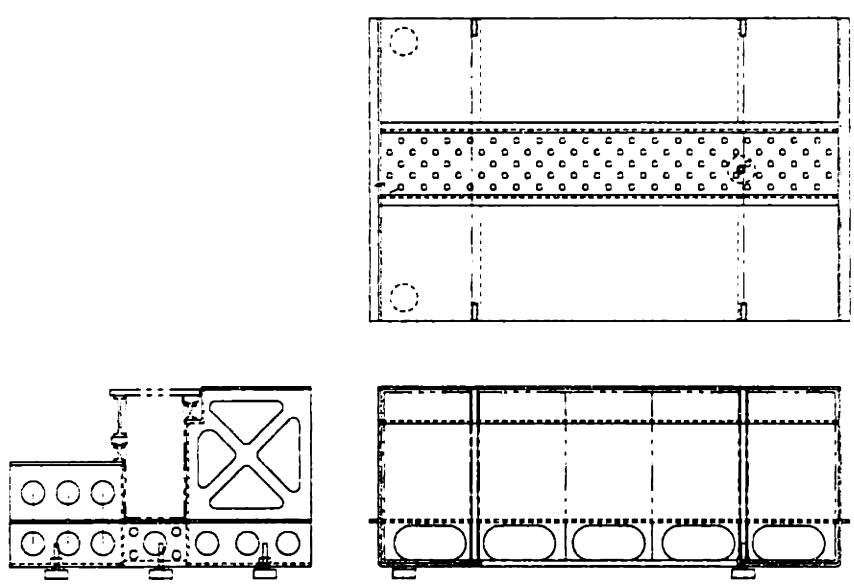

**Figure A.18** Early version of final machine frame design[62].

[62] Courtesy of Silicon Valley Group.

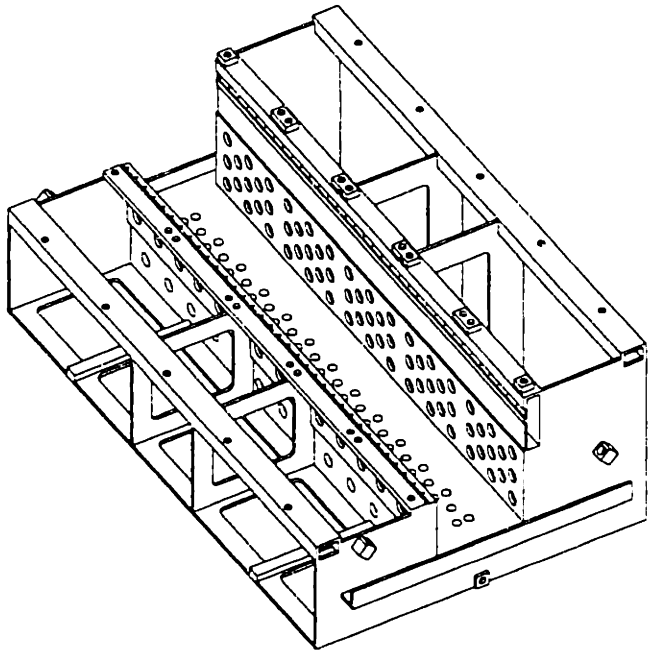

**Figure A.19** Refined concept for final machine frame design with central spine for torsional and bending stiffness.

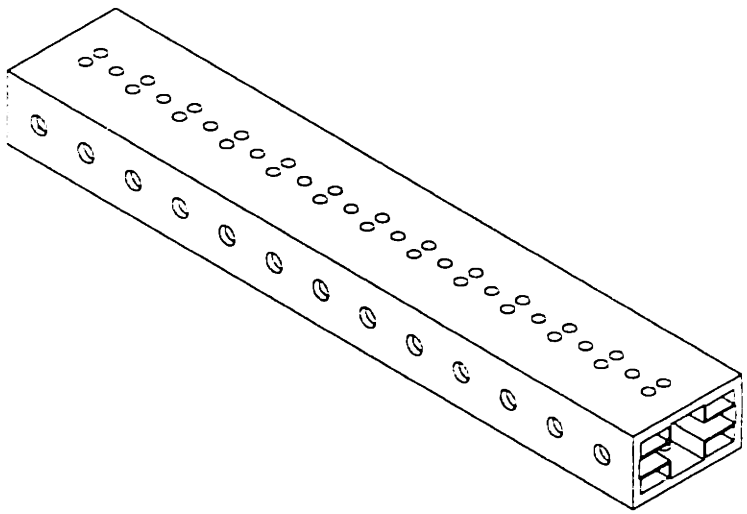

**Figure A.20** Central spine for final machine frame design.

This final frame concept was selected to be used for the Accipiter project. An evaluation similar to the one performed for the machine layout was used for this selection. The numerical results of the comparison of these three frame concepts are contained in Section E.2.2 of Appendix E.

In addition to the layout of the frame, the conceptual design stage involved the selection of appropriate materials for the frame. Only common, inexpensive materials such as structural steel and aluminum were considered because the necessary stiffness could be achieved within weight restrictions. More exotic, higher performance materials were not need. Steel and aluminum both have approximately the same ratio of the elastic modules to density. Therefore, by weight there is no advantage to using aluminum. However, by volume of material used steel is more attractive. Special alloys of aluminum can provide high yield strengths, but not higher stiffness moduli. Also, aluminum is easily corroded by some chemicals used in developing exposed wafers. Furthermore, steel is more easily welded than aluminum. Therefore, structural steel was selected for most of the structure. Parts of the frame with exposed machined surfaces are made from stainless steel because the added corrosion resistance gives added cleanliness. Additionally, the structure can be coated with a special epoxy to make it more suitable for use in cleanrooms.

### A.5.3 Conceptual Design of the Wafer Handling Robot

The next step in the conceptual design of this new photoresist processing system is the development of design candidates for the wafer handling mechanisms. The functional requirements for the wafer handler are essentially the same as for the complete machine except that they are specifically applied to the robot. These requirements are listed here again:

- High reliability
- Small footprint
- Clean mechanical design to minimize contamination
- Short cycle times
- Repeatable positioning of wafers.

Because each wafer processed by the system is handled many times, successful operation of the machine is very much dependent on a good robot design. In the 90 Series many

reliability problems were attributed directly to the wafer handling mechanism. Therefore, it is necessary to significantly increase the wafer handling automation reliability in the Accipiter project. Because total machine footprint is significantly affected by the space taken by the robot, it is important to minimize the robot footprint. Again, because the handler contacts the wafers frequently, a clean design is paramount. Furthermore, the robot must be designed to transfer wafers fast enough that machine throughput is not limited by the transfer time. Ideally, the throughput is determined primarily by processing time in each module. Finally, repeatable positioning of wafers on the spin stations chucks is a key to the quality of the resist coating. An off-center wafer will create dynamic imbalance in the rotation. Additionally, the removal of the bead of resist that forms on the edge of the wafer requires the wafer to be centered accurately on the spindle.

In addition to the functional requirements that must be satisfied by the design of the wafer handling robot, a number of constraints are imposed by the selected machine configuration. First, the kinematic requirements of the robot are largely determined by the layout of the machine[63]. For example, so that the robot can move along the length of the machine, it must have a long horizontal travel axis. Also, the stacked modules require a fairly large vertical axis travel. Finally, the wafer drop-off locations within the process modules establish a minimum reach distance for the robot.

Again, before embarking on the conceptual design of this wafer handling robot, a review of existing designs is worthwhile. Market forces in the semiconductor process tool manufacturing industry have created a demand for wafer handling robots designed and built by companies not directly affiliated with either the process tool manufacturers or the consumers of the process tools. Therefore, a wide variety of product literature contains descriptions of these existing designs. This resource was examined in detail for the Accipiter project[64].

---

[63] The requirements in the end station, stepper interface, and central machine are very similar. Therefore, these requirements are not distinguished for the different robot mounting positions.

[64] In addition to the design of the wafer handling robot by MIT presented in this thesis, SVG also explored the possibility of purchasing the robot from a third party. However, no designs existed that satisfied the functional requirements and constraints for the Accipiter design project. The only way to use an existing design would have been to design the machine "around" the robot, which was unacceptable.

In addition to the product documentation, patent literature also provides a useful resource. For example, Genov and Cameron's patent describes a dual end effector wafer handling robot [Genov '91A]. In this case however, both wafer grippers are fixed to a single link. Another patent by Genov et al. and one by Abbe and Baker describe belt systems used to create straight-line motion from a serial arm with three revolute joints [Genov '91B], [Abbe '90]. These patents are representative of a number of semiconductor handling robots that rely on mechanical coupling of joints with belts to give the desired end effector motion. Also, requirements for vertical travel axes in this industry are not common only to this design; Iwasawa's patent describes a cassette handling robot with a single stage telescoping axis [Iwasawa '90].

#### A.5.3.1 Development of Design Concepts

Although literally an infinite number of variations of the wafer handling design could satisfy the kinematic requirements of this wafer handling robot, an effort was made to use the functional requirements of the system to narrow the focus to the most attractive candidate designs. These alternate designs were then evaluated using the analytical hierarchy procedure as was done for the machine layout and frame. The development of the wafer handling robot occurred in parallel with the development of a centering wafer gripper. The discussion of the gripper conceptual design is contained in Section A.8. However, some of the requirements related to the gripper are presented here to further clarify the requirements of the wafer handling robot design.

Unlike previous designs, one requirement for the Accipiter project was that the wafer handler have two independent wafer grippers. These two grippers allow faster effective move times because two wafers can be transferred simultaneously. Also, because some of the process steps are performed in ovens, wafers are heated to temperatures in excess of 250° C. The hot wafer is then cooled back to ambient temperature with a chill plate. Furthermore, any temperature variations across a wafer can effect the quality of the resist coating. It is, therefore, desired to use one gripper for handling hot wafers and the other for cool wafers. In this manner, no thermal

contamination is introduced to a wafer before it is moved into a process module[65]. Figure A.21 shows several ways to incorporate dual grippers into the wafer handling mechanism. The middle configuration is similar to that described in Genov's patent [Genov '91A]. While this arrangement is simple and does not involve placing one wafer above another and thereby interfering with the laminar airflow, it is very space inefficient. Therefore, only the leftmost and rightmost configurations were considered for the wafer handler development.

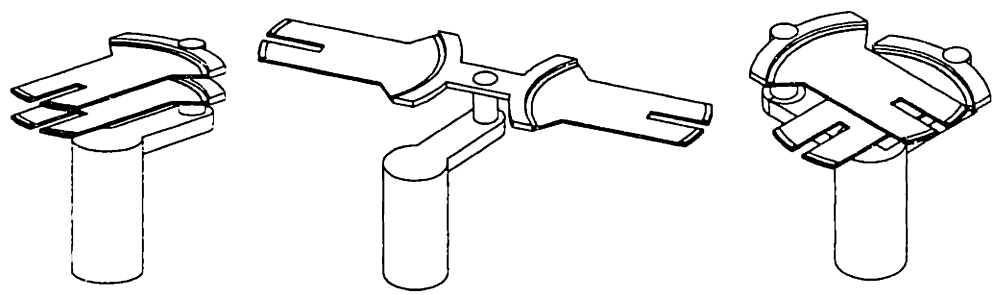

**Figure A.21** Early concepts for dual grippers mounted on a wafer handling robot.

The first step in developing conceptual designs for the wafer handling robot, is the exact determination of its kinematic requirements. As stated previously, the robot needs both horizontal and vertical linear travel axes. Theoretically, it would be possible to use revolute joints to satisfy these motion requirements. However, because of the layout of the machine, linear axes are much more practical. Therefore, only linear joints were considered for these travel axes. The robot also must be able to access process modules and/or cassettes over a 270° range of motion in the horizontal plane[66]. Additionally, because the robot gripper contacts the wafer only close to its edge, straight line motion into process modules and cassettes is needed to avoided interfering with process module chucks and cassette walls[67]. Consequently, the robot needs a full range of planar motion. The result of these requirements is that the robot must have five controlled degrees of

[65] It might also be possible to use thermal electric coolers or similar devices to control the temperature of the gripper to prevent thermal contamination, thus not requiring two grippers. This idea was discarded because of its complexity and because two grippers were needed for throughput reasons anyway.
[66] The range is only 180° in the central portion of the machine.
[67] The 90 Series used a spatula contacting the back of the wafer, which was inserted in a straight line. However, the nature of the coupling in the mechanism caused the wafer orientation to change as the wafer was inserted. The Accipiter project requires that the orientation not change when the wafer is inserted.

freedom. One degree of freedom is the vertical axis. Three of the degrees of freedom provide the planar motion. Finally, the most distal degree of freedom is duplicated so that the second gripper can move independently. Therefore, kinematically, the robot has four degrees of freedom, although it physically has five.

Using these kinematic requirements, a systematic approach was used to formulate design alternatives. First, combinations of lower pair joints were synthesized to fulfill the motion requirements. Next, design concepts were developed based on the possible combinations of joints from the kinematic analysis. Following that, simple geometric models of each concept were formulated to facilitate initial error modeling for comparison purposes. Also, the geometric models helped to determine the necessary volume required for the motions given the reach requirements imposed by the machine layout. Finally, for the most promising candidates the initial stages of embodiment design were addressed. This additional layer of details helped determine the functional feasibility of the designs. For example, initial concepts for mechanical transmission types and placement were developed. Also, preliminary analysis was performed to determine actuator types and feedback sensor requirements. Other considerations such as bearing types, joint ranges of motion, and routing of control system cables were addressed. These details helped to access the complexity, performance, and reliability of several of the most promising concepts, so that the best could be selected.

For this discussion, the letter P will be used to represent a linear or prismatic joint and the letter R, a revolute joint. Furthermore, a serial kinematic chain will be described by a string of these letters where the leftmost letter represents the most proximal joint in the system and each preceding letter represents the next distal joint in the chain. For example, PRPR refers to a four degree of freedom mechanism where the first or base joint is linear, the next revolute, the third linear, and the final joint revolute. Assuming that lower pair joints are used (revolute and linear) and further assuming that the first joint must be prismatic (the long horizontal travel) there are only eight possible combinations of joints for the four degrees of freedom required by the kinematics of the system. These eight combinations are: PPPP, PPPR, PPRP, PRPP, PPRR, PRPR, PRRP,

PRRR. However, several of these combinations cannot satisfy the motion requirements here. First, at least one joint must be revolute to allow the two independent grippers to access with straight line motion modules over 270°. Thus, the combination PPPP cannot be used. Next, at least one joint must give the required vertical travel. Therefore, the combination PRRR cannot be used. Of the remaining six combinations, two more would be highly impractical - PRRP and PPPR. The remaining four kinematic combinations were the basis for developing eight individual wafer handling concepts. A ninth concept was considered that employs a common semiconductor robot configuration with one vertical, linear degree of freedom and three horizontal, planar degrees of freedom. To give the required horizontal travel, this concept was placed on a long linear axis.

Because each of the design concepts involves a linear horizontal axis, a linear vertical axis, and at least one revolute axis, several individual joint concepts are considered first. These concepts can be used as building blocks from which the handler concept is assembled. Figure A.22 shows three possible drive concepts for a simple linear axis.

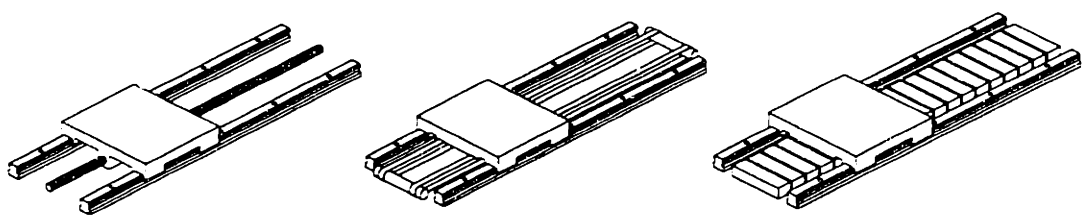

**Figure A.22** Horizontal linear drive concepts - ballscrew, belt drive, and linear motor.

The first is a ballscrew, which is a common drive mechanism in machine tool axes. The ballscrew can be effective, but long travel lengths and relatively high speeds often require the use of prohibitively large screw diameters. The middle concept shown is a belt drive. These systems are simple and common. However, performance and reliability are limited in axes where these drives are employed. The third concept shown is a linear motor[68]. The linear motor is a high performance, high reliability actuator. Unfortunately, these motors tend to be expensive especially for long travel distances. Other linear drive

[68] Like rotary motors, there are a number of different linear motor types. For cleanroom operation, brushless DC servo motors are the most attractive.

methods such as rack and pinion drives and friction or capstan drives may be effective for certain types of systems.

Other linear axes concepts, which might be useful in vertical or distal linear joints, are shown in Figure A.23. The first concept shown is a simple shuttle similar to the ones shown in Figure A.22. For vertical axes and distal axes the size of the joint's packaging is often of concern and so a telescoping axis such as the intermediate one below can be useful. The third concept shown is a piston-like arrangement that can be especially useful in cleanroom designs.

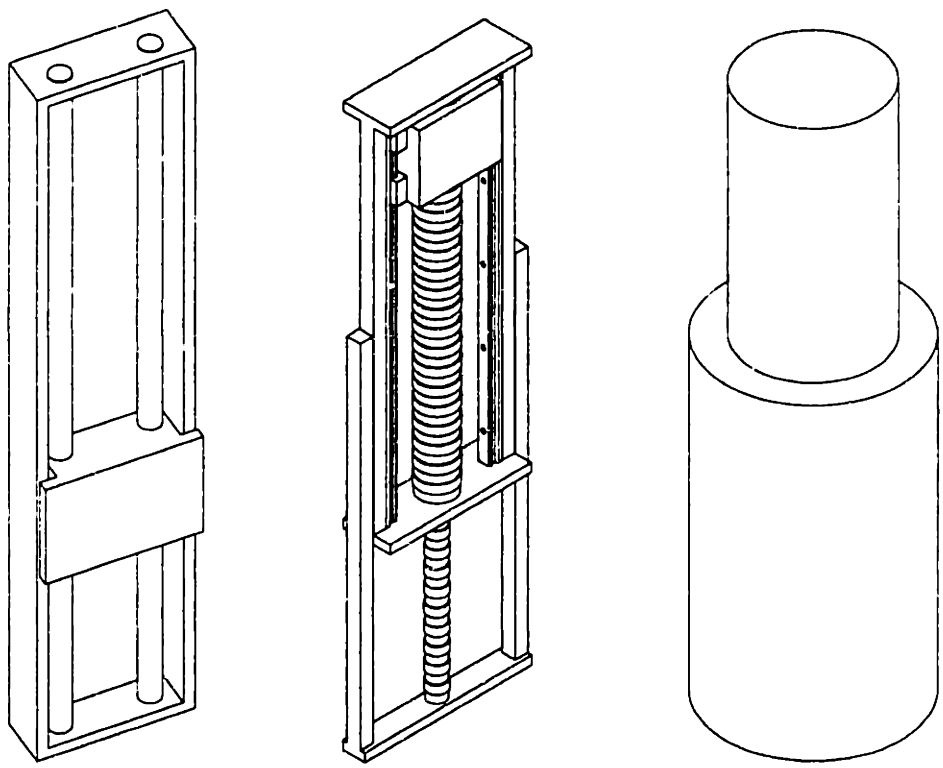

**Figure A.23** Vertical (or distal) linear drive concepts - telescoping shuttle, simple shuttle, and piston.

Revolute joints are especially common in the design of robots where dexterity is usually important. Rather than identify various configurations for revolute joints independent of the robots in which they are housed, a few options for actuating these joints are mentioned. Because the wafer handling robot for the Accipiter project must be very repeatable, it is desirable to reduce or eliminate any backlash in the joint transmission.

One method is to use direct drive where the rotor of an electromagnetic actuator is coupled directly to the output link of the revolute joint. This type of arrangement can eliminate the backlash, mechanical compliance, and friction that are common problems in joints. However, for large output torques direct drive joints rapidly become large because of the relatively poor torque to weight ratio of motors without mechanical reductions. The requirement for large actuators can be especially troublesome when a serial chain of directly driven actuators is used because the more proximal motors have to move the mass of the robot and the more distal actuators.

A second alternative is to use an anti-backlash gear train. Simple versions of these gear trains are not suitable for use in high performance applications because of their limited torque ratings. However, Hale designed a novel gear train with spring loaded dual pinions which engaged an output spur gear to give an effective reduction that could be used in a robot joint [Hale '94]. Additionally, friction and wear can be problems in these types of gear trains if they are not designed properly.

Another type of an anti-backlash reducer is a harmonic drive. Originally used in military applications, these reducers often are used in robot designs. Figure A.24 shows an example of a harmonic drive.

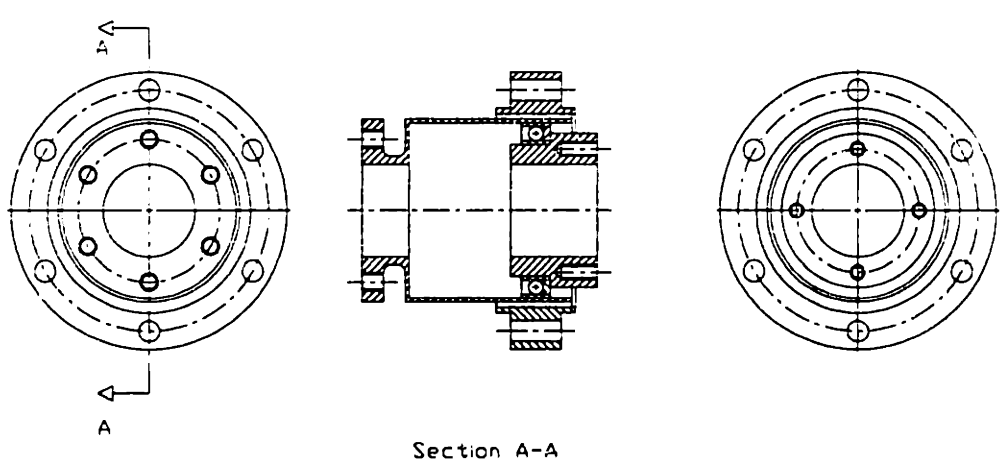


**Figure A.24** Harmonic drive gear reducer.

The high speed input to the reducer is connected to an elliptically shaped wave generator. The outer surface of the wave generator forms the inner race of a ball bearing. The outer

race of this ball bearing is a flexible spine with teeth on its outside surface. This flexible spine engages (at the major axis of the ellipse) a toothed stator which is normally fixed to ground. The stator typically has two more teeth than the flexible spine. As the high speed input rotates the wave generator, the flexible spine, which is attached to the output, is forced to slowly counter rotate. The exact reduction is a function of the number of teeth on the flexible spine and the stator. However, very large reductions with virtually zero backlash can be obtained in a compact, light weight package. Properly designed harmonic drives have long life because the flexible spine has been optimized for fatigue resistant performance. Though the harmonic drive does not exhibit backlash, there is a small amount of lost motion and compliance in the transmission because of the flexible nature of the spine. For applications such as wafer handling, where loads are light, these reducers can be applied effectively.

The first wafer handling robot concept, which is kinematically a PRPP mechanism, is shown in Figure A.25. This concept is perhaps kinematically the simplest. It makes use of a revolute joint mounted on the first horizontal carriage. Next a fixed vertical tower carries two telescoping linear axes (each with its own gripper). The primary drawback is the presence of a linear axis directly above the top surface of a wafer. Because a perfect seal cannot be created on the linear axis, the concept is flawed from a particle contamination stand point. It would be possible to house both drive mechanisms below both wafers by using left and right hand versions of the grippers attached to the drive with a vertical offset. Because of the additional clearance needed, this arrangement tends to dramatically increase the required width of the robot, however.

Another difficulty, in this design is the presence of the vertical mast that the distal axes move up and down. The mast makes the robot vertically very space efficient because the only dead space required is for the horizontal carriage. However, the mast protrudes above the wafer surfaces and will therefore interrupt the laminar flow of air and degrade the cleanliness of the design. As will be seen below, the mast can be eliminated in favor of a vertical axis design that is less space efficient, but does rise above the wafer surface.

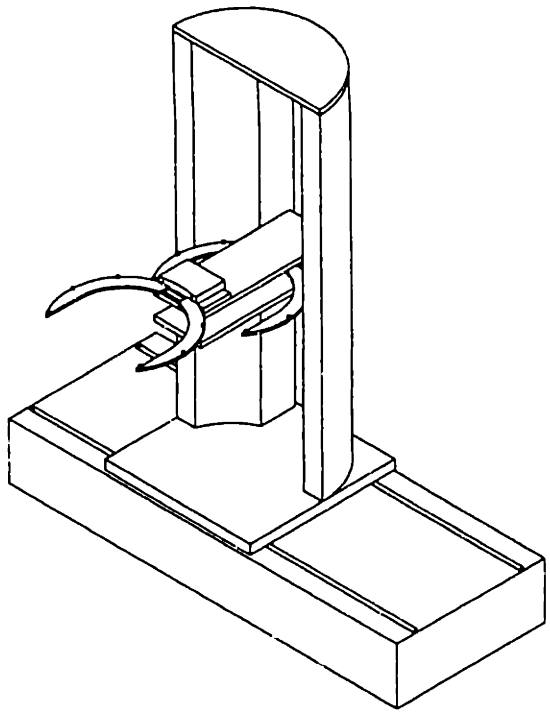

**Figure A.25** Wafer handler concept with linear final joint and a fixed tower.

The second robot concept, which is shown in Figure A.26, is similar to the first except the final joint is revolute rather than prismatic making the robot kinematically a PRPR mechanism. The gripper arrangement used is similar to the rightmost concept in Figure A.21. These two revolute joints can be coordinated with the horizontal linear axis for straight line motion. The use of revolute joints eliminates the concern about the cleanliness of a distal linear axis. However, the design still uses the problematic fixed mast.

Figure A.27 shows the third robot concept, which is a PPRR mechanism. Unlike the two concepts already described, both revolute axes are positioned on the vertical shuttle. Also, the final revolute joint is a dual, concentric design. One problem with the design, however, is the limitation of the range of motion of the first revolute joint created by the presence of the fixed mast. Again, the fixed mast is undesirable for clean performance of the robot.

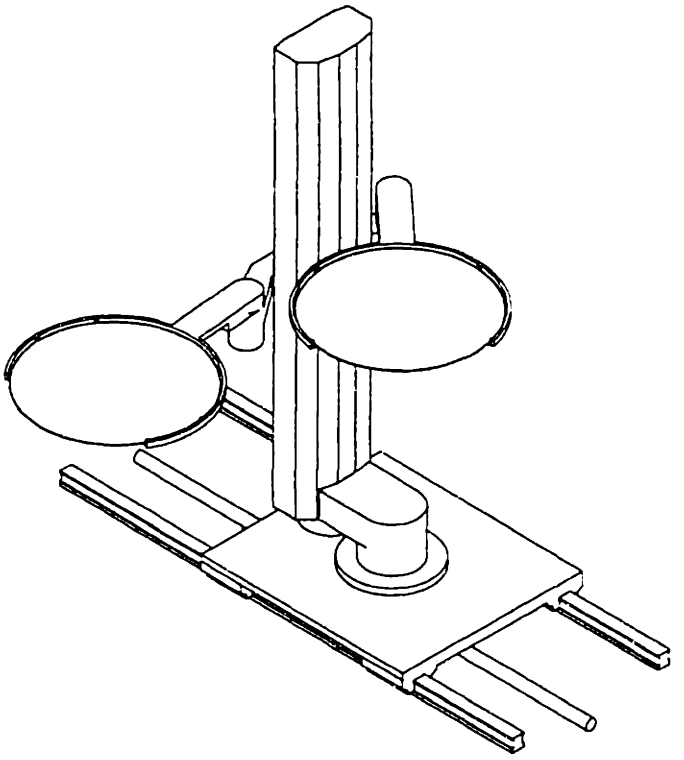

**Figure A.26** Wafer handler concept with dual output revolute joints and a fixed mast.

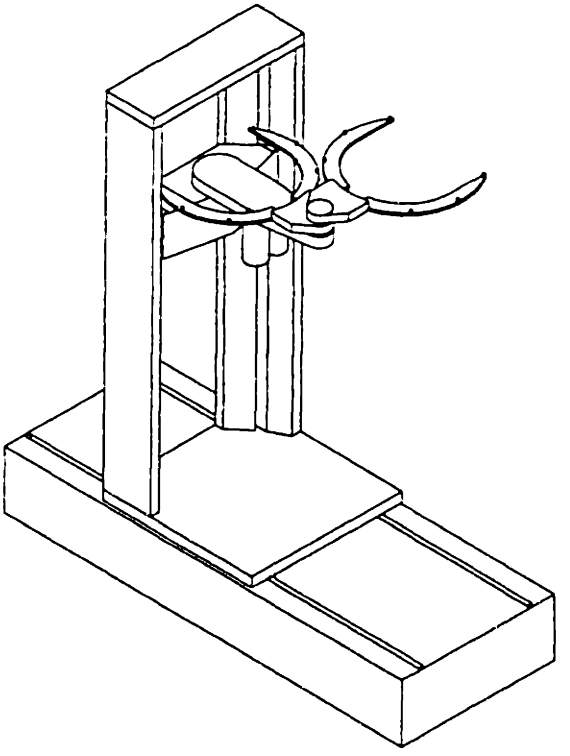

**Figure A.27** Handler concept with two concentric revolute final joints and a fixed mast.

The fourth concept, which is shown in Figure A.28, is dissimilar from the other design alternatives in that it is kinematically a five degree of freedom mechanism (PPRRR). The use of two independent grippers would, therefore, add a sixth degree of freedom. This wafer handler has a prismatic axis (the horizontal motion axis), another prismatic axis (the linear motion axis on a fixed mast), and a serial chain of three planar revolute axes. For the two grippers, the last revolute axis is duplicated. The addition of a revolute axis in this design adds considerable complexity to the design, an additional actuator, additional link parts, additional wires, additional weight, an additional servo amp, and additional complexity in the controller to coordinate the additional joint. All of these additions add up to a more complex, more expensive, less reliable mechanism. The primary advantage of this robot concept is the additional dexterity afforded by the kinematic redundancy present in the system. The additional dexterity allows the robot a greater range of motion since it can more easily reach behind its fixed mast.

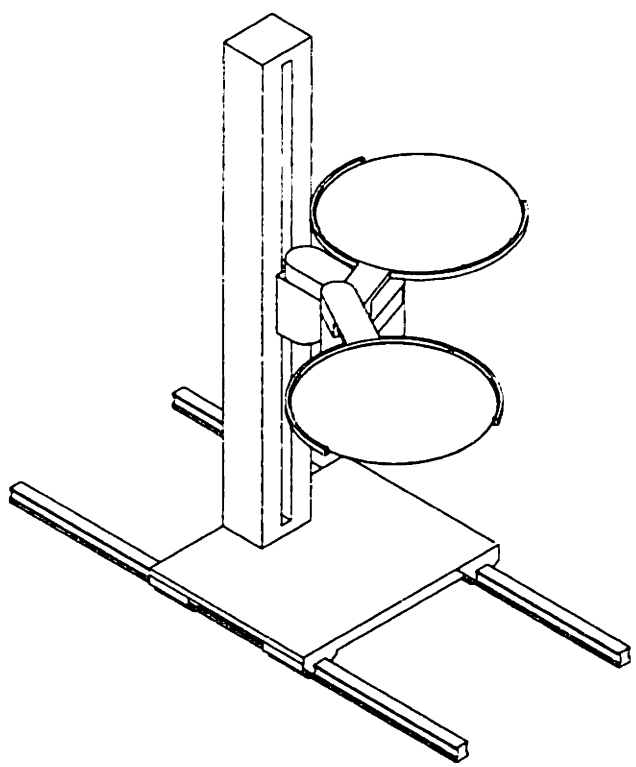

**Figure A.28** Kinematically redundant wafer handler concept.

This robot was considered because of its similarities to many robots used in handling wafer cassettes. However, the presence of the fixed mast and the unnecessary complexity precluded it from serious consideration for use in the Accipiter project.

The remaining five robot concepts do not use the fixed mast that was present in the preceding four alternatives. As will be seen below, these robot concepts all use some variation of the piston concept shown in Figure A.23. This arrangement gives the robot a larger vertical footprint, but is much cleaner because airflow above the wafer plane is not interrupted.

The fifth robot concept is shown in Figure A.29. For this concept, three distal revolute joints are used, but these are mechanically coupled to form a one degree of freedom revolute joint. Therefore, kinematically this concept is a PPRP mechanism. This coupling is similar to that described in several patents discussed earlier [Abbe '90], [Genov '91B].

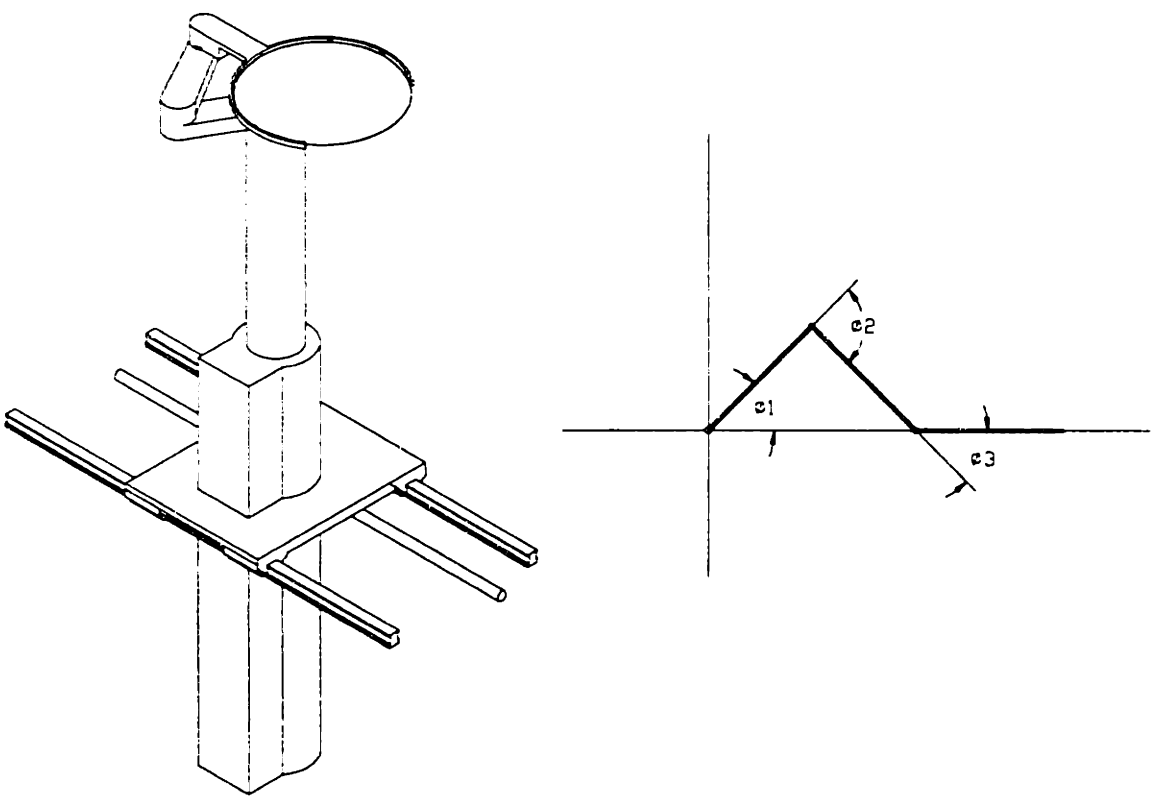


**Figure A.29** Handler concept with linear motion produced by three coupled revolute joints.

The figure also gives a kinematic definition of the three joint angles that make up the coupled linear axis. By examining the geometric model of this mechanism the constraints required for coupling can be easily derived and are shown in Equation A.1.

$$\phi_2 = 180^\circ - 2\phi_1 \qquad \text{(A.1)}$$
$$\phi_3 = \phi_1$$

where $\phi_1$ is considered the input. This type of arm could be used in a single gripper configuration. However, a major concern would be insuring that the coupling between the three joints does not degrade the repeatability and tracking capability of the handler. The primary difficulty with this concept is implementing two grippers. Because the mechanism must swing back over its first revolute joint, mounting a second mechanism concentricly with the first at the base revolute joint would be difficult.

The sixth robot concept, shown in Figure A.30, also uses mechanical coupling to create a one degree of freedom linear joint from revolute joints. This wafer handler concept uses a prismatic axis (horizontal linear motion axis), a revolute axis (revolution of the column about the center of the carriage), another prismatic axis (vertical axis), and two coupled revolute axes for the final degree of freedom. The final coupled joints rotate about horizontal axes. Kinematically, this mechanism is a PRPP mechanism. Figure A.30 also shows the definition of the joint angles for the two coupled revolute joints. When coordinated with the motion of the vertical axis, these two coupled joints can produce straight line motion. This concept can be implemented simply by coupling the most distal revolute joint directly to the vertical axis so that their relative orientation does not change. Equation A.2 shows how the second joint angle must be related to the first.

$$\phi_2 = 180^\circ - \phi_1 \qquad \text{(A.2)}$$

For a wafer handler of this type with only one gripper, the mechanism has four degrees of freedom much like the concepts discussed previously. However, the addition of a second gripper actually requires two additional degrees of freedom rather than just one. This extra degree of freedom, which is a small vertical stroke linear axis, is required because the two grippers must be housed one above the next to fit in the narrow alley. When the

lower gripper moves outward with straight line motion, the second vertical axis is used to coordinate the motion and to prevent the lower gripper from physically interfering with the upper gripper. An additional side effect of this extra vertical degree of freedom is that an increase in the range of motion of the primary vertical axis is required to accommodate the secondary axis at all levels of a stacked station.

Several additional complicating factors associated with the orientation of the coupled revolute axes exist for this concept. First, because the distal joints rotate about horizontal axes, fail-safe brakes would be required to prevent the mechanism from "wilting" if motor power fails. Second, the weight of the links in the coupled portion of the mechanism will cause disturbance forces on the joint actuator which vary with the orientation of the joint. However, this effect could be modeled and appropriate compensation added to the controller if necessary[69].

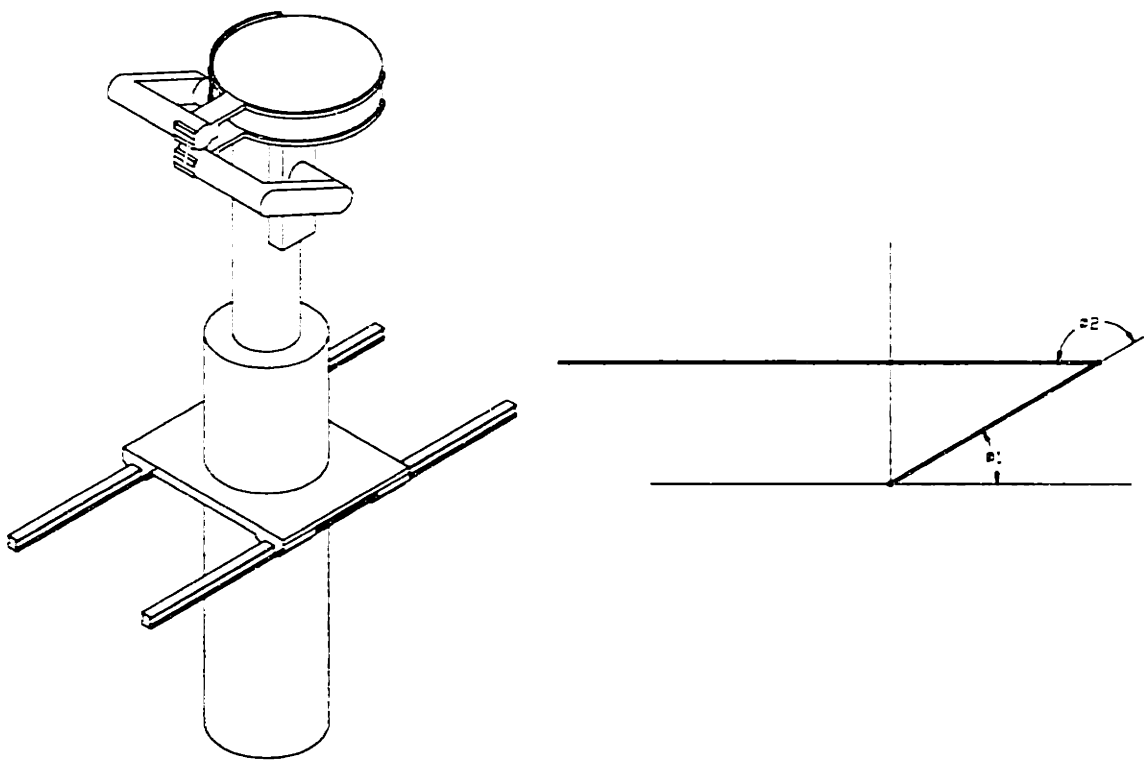

**Figure A.30** Out-of-plane coupled straight line motion handler concept.

Although, the piston-type vertical axis is more desirable from a cleanliness stand point than the fixed mast concept, the piston takes up more vertical space. Figure A.31

[69] If the closed loop system is stiff enough compensation would not be required.

shows the seventh robot concept, which reduces the vertical space penalty associated with the piston-type vertical axis using a multi-stage telescoping vertical axis. This alternative is a PPRR mechanism and is kinematically identical to the concept shown in Figure A.27. The only difference is that the fixed mast has been replaced by a multi-stage telescoping axis. Eliminating the fixed vertical axis also increases the possible range of motion of the first joint and eliminates the interference problem with the fixed mast. One difficulty associated with this multi-stage telescoping axis is the actuation method. Hydraulic actuators are not acceptable for cleanroom use. Furthermore, a pneumatic cylinder might be able to actuate the drive, but controllability would be questionable. For this design, several alternatives were developed using cascaded belt drives and multi-stage, nested ballscrews. Because the compliance and reliability for a complex belt drive are suspect, a multi-stage ballscrew drive is the most promising for this telescoping axis.

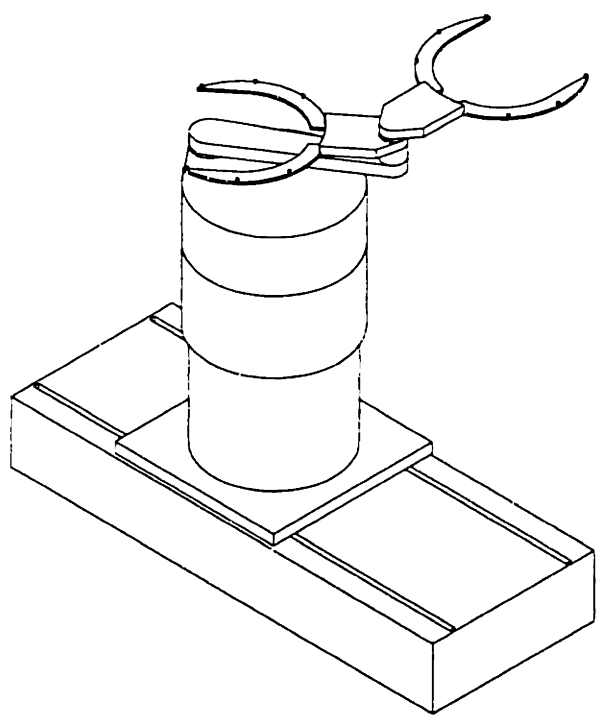

**Figure A.31** Initial telescoping handler concept.

Figure A.32 shows another PPRR robot concept. The first axis is the horizontal linear axis; the second, is the linear vertical axis. The final two axes are revolute and are mounted on top of the rising column of the vertical axis. This concept is kinematically identical to the telescoping tower concept discussed above. The only difference is the

replacement of the three-stage telescoping vertical axis with a simple ballscrew driven single stage axis. The column on which the distal axes are mounted is essentially the carriage of the lead screw which is mounted offset in the rectangular portion of the enclosure covering the lower portion of the vertical axis. Packaging of the fixed vertical axis is the primary drawback of this concept. The relatively long vertical stroke required to access all levels of a stacked station means that in this concept the column must reach all the way to the floor of the machine. However, the portion of the column that reaches below the surface of the structure will not occupy the entire alley width.

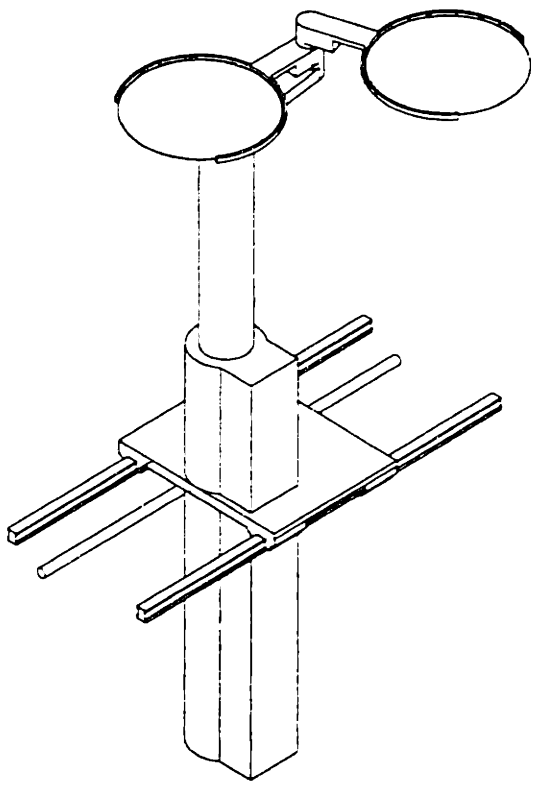

**Figure A.32** Diving tower handler concept with two revolute joints.

The ninth and final robot concept is shown in Figure A.33. This concept is derived from the ideas in the seventh and eighth concepts shown in Figure A.31 and Figure A.32, respectively. This robot uses a two stage telescoping axis driven by a nested ballscrew. To allow easier packaging of the telescoping axis, the position of the first revolute joint and the vertical joint are swapped in the kinematic chain. This robot is, therefore, a PRPR mechanism. It uses the clean, dual revolute elbow design.

Additionally, the concept benefits from the piston-type vertical drive without a too large vertical space penalty.

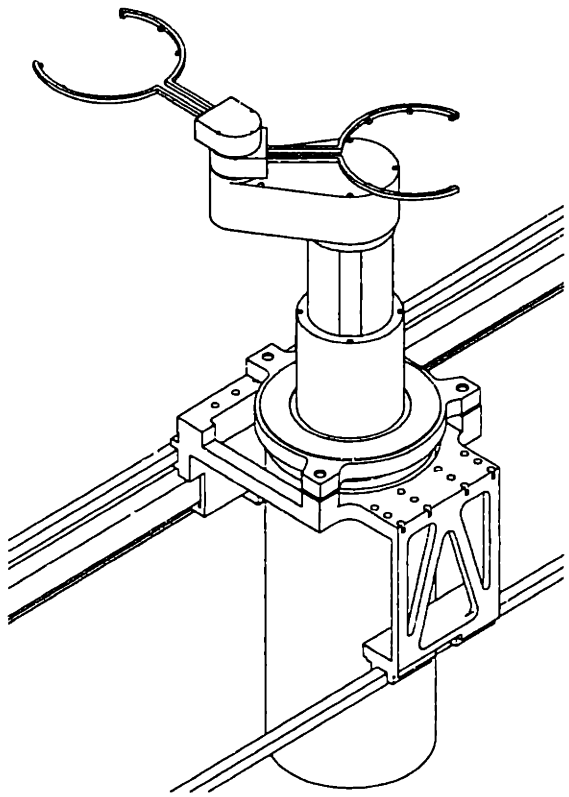

**Figure A.33** Telescoping handler concept derived from concepts shown in Figure A.31 and Figure A.32.

### A.5.3.2Selection of the Design Concept

As the reader is already aware from the discussion in Chapter 3 and Chapter 4, the final concept described above was selected from the nine candidates. Section A.2.3 in Appendix A gives the numerical results of the AHP selection process. Although, all of the functional requirements played a role in developing and selecting alternate designs, the requirements for cleanliness and small footprint were especially dominant. To some degree, the requirements for reliability, positioning repeatability, and short cycle time are determined by the embodiment and detailed design of the robot, which are described later in this Appendix. At the conceptual level, selecting the simplest, most straight forward design is also contributive in allowing these performance related goals to be achieved.

The mechanical layout of the robot is driven by cleanliness requirements. A wafer handler that meets all other requirements in an outstanding manner is still a failure if it contributes an unacceptably large number of particles to the manufacturing process. The use of a piston-type vertical drive allows all of the mechanical portions of the robot to be housed below the wafer surfaces at all times. Also, the use of revolute joints in the most distal axes is advantageous because these joints can be made much more cleanly than linear joints. Furthermore, concerns about kinematic and dynamic complexity created by the use of revolute joints is unwarranted. As described at length in the case study in Section 4.6.1, the use of these revolute joints in no way impairs the performance of the robot as related to its functional requirements.

Additionally, the careful selection of the wafer handling robot concept is useful in minimizing the total footprint of the new photoresist processing system. The benefits of using a multi-stage telescoping axis have already been mentioned above. The total dimensions of the horizontal layout of the machine is also strongly affected by the width of the alley in which the robot moves. Figure A.34 shows some of the geometric definitions used in selecting the appropriate alley width and link lengths to achieve the reach requirements, minimum footprint, and required positioning repeatability.

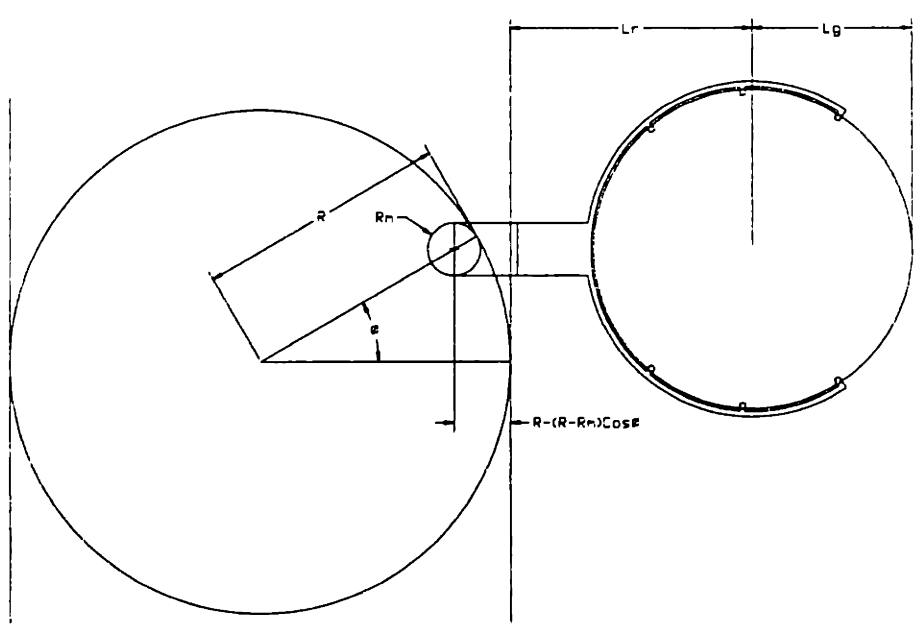


**Figure A.34** Geometric parameters required to determine alley width and handler reach into process modules.

These parameter were used in a displacement error model to guide the design process. For example, as the arm links become shorter, the alley width can be reduced[70]. However, if the links are made too short, the positioning repeatability is impaired because the robot losses resolution as the arm nears a configuration perpendicular to the alley in which the robot travels.

### A.5.4 Conceptual Design of the Wafer Gripping and Centering Mechanism

The final segment of the conceptual design phase is the development of gripper concepts for the wafer handling robot discussed above. In the 90 Series system and many other process tools a spatula is used to pick up the wafer on its backside. The spatula contains vacuum lines and small ports on its surface to allow a positive hold on the wafer. This spatula is visible on the 90 Series shuttle mechanism shown in Figure A.3. The vacuum can also be useful as a wafer presence sensor. For the Accipiter project, the increasingly stringent cleanliness requirements dictate that backside contact with the wafer is no longer acceptable for the wafer handling robot[71]. Rather, the wafer must be held in an exclusion zone on the back side of the wafer around its periphery. Furthermore, because one of the goals of the Accipiter project is a reduction in machine footprint, the space consuming iris mechanism in spin stations for wafer centering, shown in Figure A.1 and Figure A.2, must be eliminated. The logical way to do this is to move the centering operation to the wafer gripper.

In developing conceptual designs for the wafer gripper several functional requirements and constraints must be satisfied. First, the gripper must hold the wafer cleanly in the acceptable area as described above. Next, the gripper must center the wafer to better than ±0.002 inches[72]. This centering accuracy is needed so that a wafer is

---

[70] The alley width is also constrained by the room necessary to house the body of the telescoping axis and the horizontal carriage.

[71] A particle on the back of a wafer can be harmful for several reasons. First, it might migrate to the top side of another wafer in a wafer cassette. Second, a particle as small as 1 μm on the back of wafer where a stepper chuck is holding the wafer can cause a displacement large enough to interfere with the depth of focus of the stepper optics.

[72] The difficulty of this centering operation can be better understood when one considers that the specifications SEMI M1.9-91 and SEMI M1.10-91 give a tolerance of ±0.20 mm (or about ±0.008 inches) for a flatted or notched 200 mm polished monocrystalline silicon wafer.

dynamically balanced on a spindle and so that the edge bead of photoresist can be accurately removed. Next, the gripper must be able to reach into process modules and cassettes. In fact, because the cassette geometry is considerably different than the process modules, two gripper configurations are required. Figure A.35 shows the constraints on the contact locations imposed by the chuck used in a spin station.

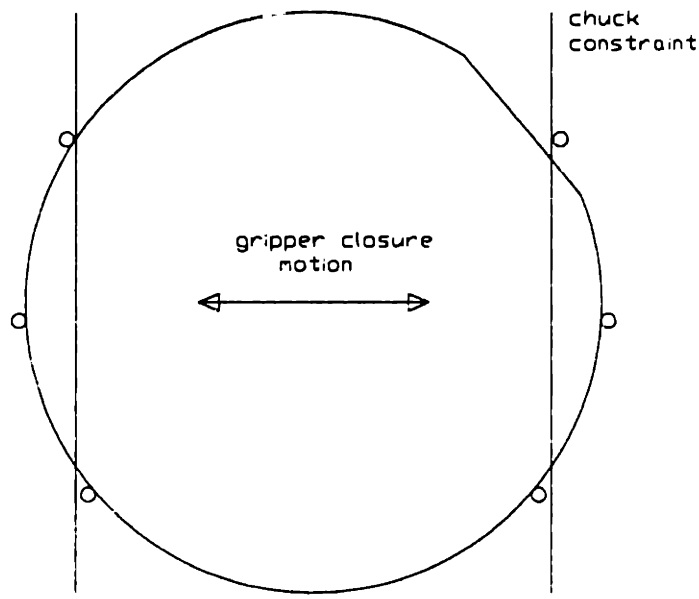


**Figure A.35** Process geometric module constraints.

The geometric constraints imposed by a standard cassette are shown in Figure A.36. In addition to the geometric constraints imposed by the process modules and cassettes, it is also important to minimize the vertical height of the gripper, so that the total high of the wafer handling robot is not increased unnecessarily. Figure A.37 depicts this concern. An additional constraint placed on the design of wafer grippers is the presence of flats or notches in wafers[73]. Both Figure A.35 and Figure A.36 show flatted wafers. These features are used to align the crystal structure of the monocrystaline wafers in other processing operations. These features are not used in photoresist processing systems, but they do affect the design of the wafer grippers.

[73] Leading U.S. manufacturers use notched wafers. However, some foreign manufacturers use flatted wafers, so the wafer grippers must be compatible with both types.

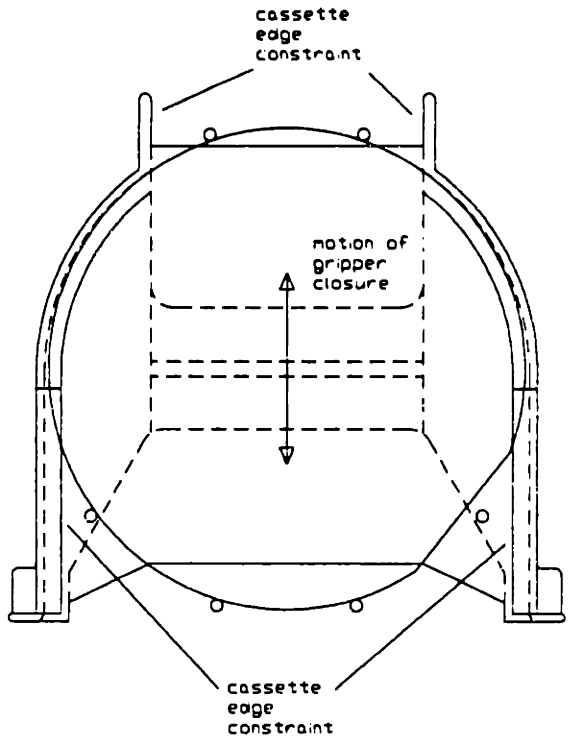


**Figure A.36** Cassette geometric constraints.

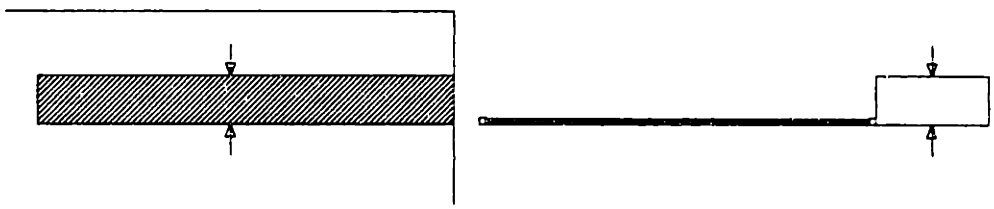

**Figure A.37** Vertical process module constraints.

Additionally, as discussed previously the gripper must not introduce any thermal contamination into the wafer. However, the use of two grippers will satisfy this requirement.

Because of the importance of the centering operation more discussion is warranted. The operation must be performed quickly so that transfer times are not affected. Ideally, the centering would be transparent to the transfer process. If this centering requires some special movement by the robot, it must be extremely fast. For example, an average transfer might take a total of six seconds, so very little time would be available to center the wafer. Also, the centering operation should disturb the wafer as

little as possible. It is undesirable to slide the wafer across surfaces or to apply large forces to the edge of the wafer. The most desirable method of centering would involve no contact with the wafer whatsoever.

A noncontact sensor or simple machine vision system might be an ideal choice for centering a wafer. In fact, a number of patents exists for various types of noncontacting centering and aligning systems. Most of these systems use either linear charge coupled devices (CCD's) or arrays of simple through beam optical sensors to detect the edge of a wafer being spun on a spindle [Cheng '89], [Poduje '92], [Spencer '89], [Volovich '92]. For the Accipiter project, the complexity, cost, space taken up by a special centering module, and time consumed in centering the wafer make all of these alternatives unattractive. Alternatively, it might be possible to use a machine vision system to acquire a wafer during a normal transfer. The system could calculate the wafer's center and pass an offset value to the robot controller, so that the wafer could be placed accurately. Unfortunately, such a system is cost prohibitive with the current level of technology.

Another alternative is to center the wafer mechanically as was done with the iris mechanism in the 90 Series system. Again, a number of patents exist for this type of wafer centering. For example, Nishiyama describes a centering mechanism with six contact points that move radially to center wafers with a variety of diameters [Nishiyama '92]. Matsumoto describes another mechanical centering scheme [Matsumoto '90]. The previous two patents do not involve mechanisms integrated into a robot gripper. However, several interesting gripper concepts were turned up by the patent search. Ben's patent is for a tongue-like gripper that is driven pneumatically [Ben '90]. Also, the patent by Lee describes a similar tongue-like gripper that is capable of gripping wafers from two to eight inches in diameter [Lee '90].

Several conceptual gripper designs were developed. The first is shown in Figure A.38. This gripper is a vacuum type like the one used in the 90 Series. However, the contact points have been moved from the center of the wafer to the exclusion zone near the edge of the wafer. This concept does not have integrated centering capability, so it

would be feasible only with one of the noncontact sensor schemes briefly described above.

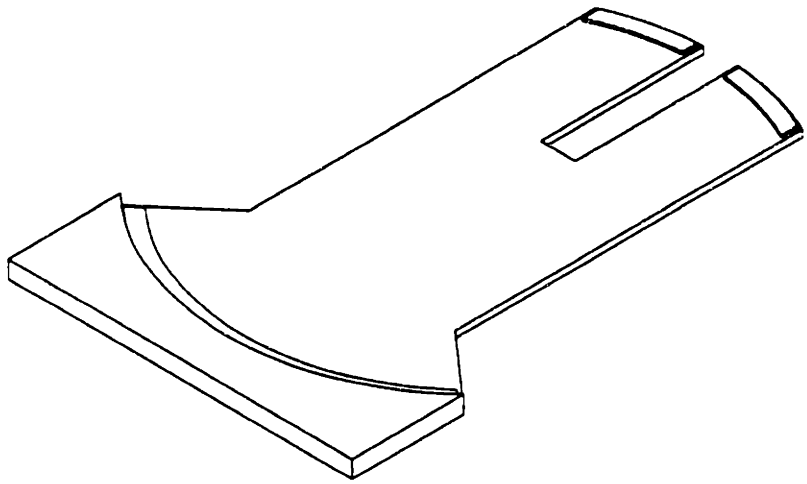

**Figure A.38** Early vacuum gripper concept.

Figure A.39 shows a totally passive self-centering gripper. For this concept, the contact occurs along the edge of the wafer. The gripper contact area forms a funnel. The contact areas could be adjusted so that they do not form a complete circle to satisfy the constraints imposed by the process modules and the cassettes. If a low friction contact material were used, the wafer would, in theory settle into a centered position. A major concern with this design is the nondeterministic nature. The wafer is not actively held in a centered position. Some anomaly or disturbance could easily cause the gripper to lose its centering.

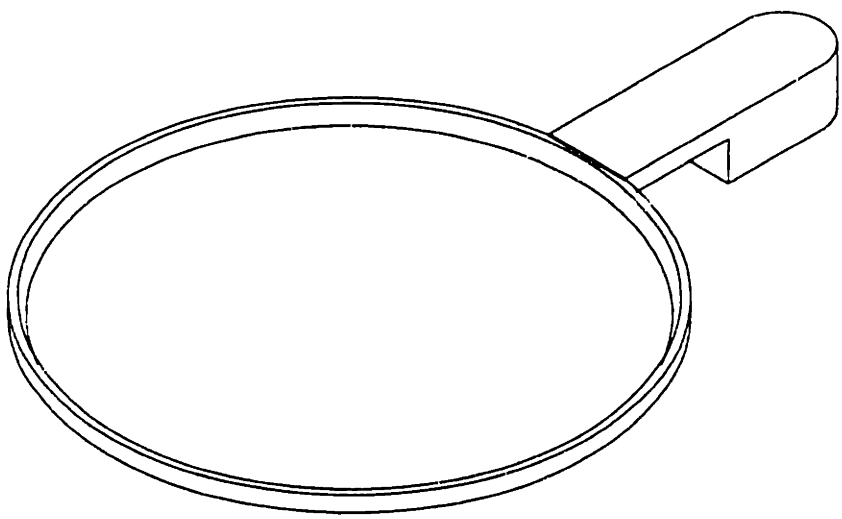

**Figure A.39** Passive gripper concept.

The final concept was previously discussed in the case study in Section 4.4.2. This gripper concept was selected form the alternatives described here. Section E.2.4 of Appendix E contains the numerical results of the selection process. A detailed discussion of the centering mechanism used in this concept will not be repeated here. However, the mechanically coupled parallel motion of the jaws seems to be a desirable and compact way to reliably center the wafer. An early variant of this concept is shown in Figure A.40. This fork gripper is designed for use in accessing the process modules in the center of the machine. Figure A.41 shows a more developed version of this fork gripper. The tongue gripper concept for use in accessing cassettes in the end stations and stepper interface in the system is shown in Figure A.42

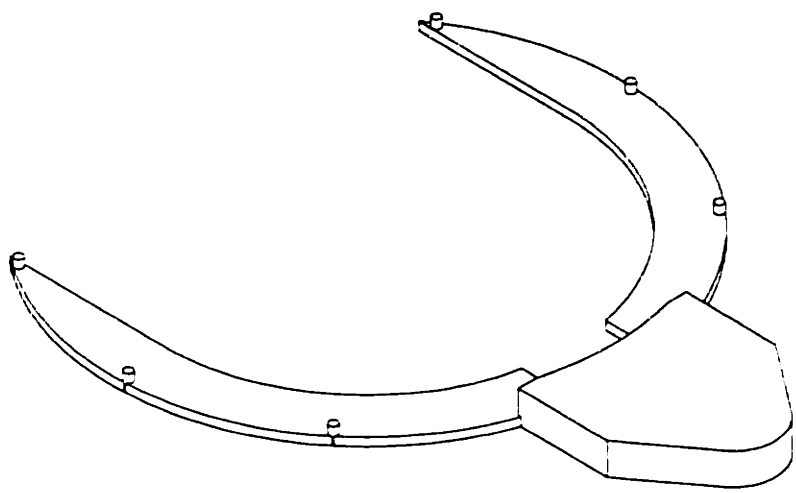

**Figure A.40** Early fork gripper concept with edge contact on wafer.

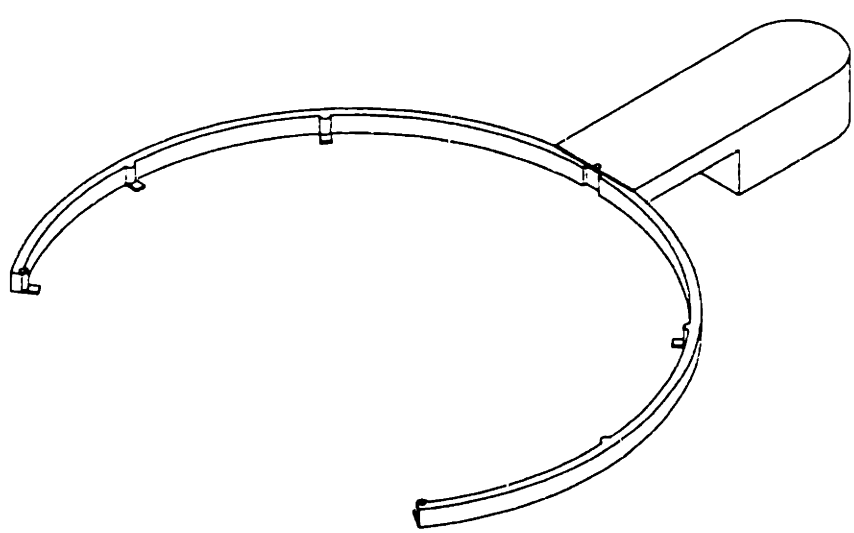

**Figure A.41** Fork gripper concept.

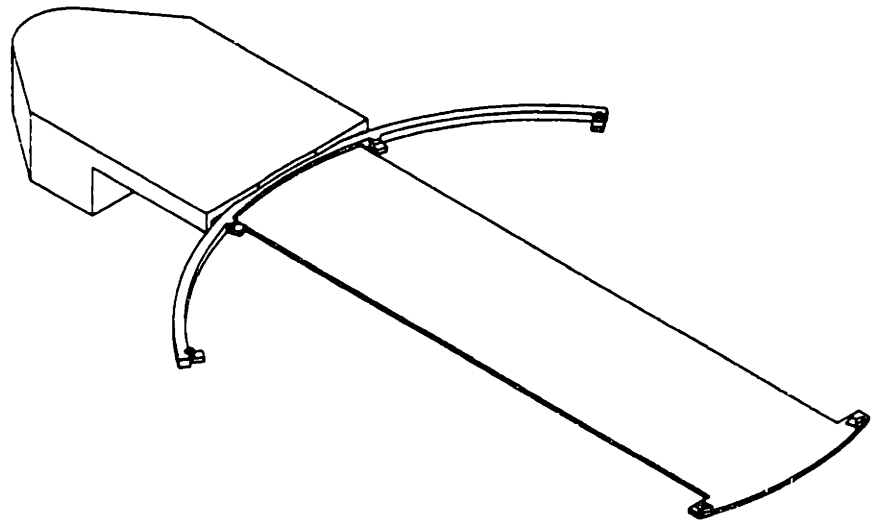

**Figure A.42** Tongue gripper concept.

One additional concern in using the two moving jaws to center a wafer is the force with which the wafer is squeezed. To avoid creating particles at the interface of the gripper contact point and the wafer, a minimum contact force should be used. For the fork and tongue gripper concepts described here, the force used should be just large enough to overcome frictional forces and to prevent the wafer jaws from opening during robot motion because of inertial forces.

## A.6 Embodiment and Detailed Design of the Accipiter Project

This section briefly presents the embodiment and detailed design of the machine frame and the wafer handling robot developed for the Silicon Valley Group's Accipiter project. To remain concise, only high level details of this stage of the design process needed to illustrate the design methodology discussed in this thesis are presented here. Details of the selection of commercial parts and design of fabricated components are beyond the scope of this thesis[74].

[74] The wafer handling robot design alone contains in excess of 60 unique purchased assemblies and 70 unique fabricated components. The detail design of each of these components along within interactions of the components had to be carefully considered.

### A.6.1 The Machine Frame Embodiment Design

Figure A.43 shows a perspective drawing of the finished frame design for the new photoresist processing system. As was discussed previously, this weldment is dramatically stiffer compared to the 90 Series frame due to its manner of construction. After the steel plates and tubes have been cut to shape for the frame, they are welded together to form the basic structure. Next, the frame is heat treated to remove any residual stresses before the finish machining operation. Following the stress relief, the frame is shot blasted to remove scale and other debris.

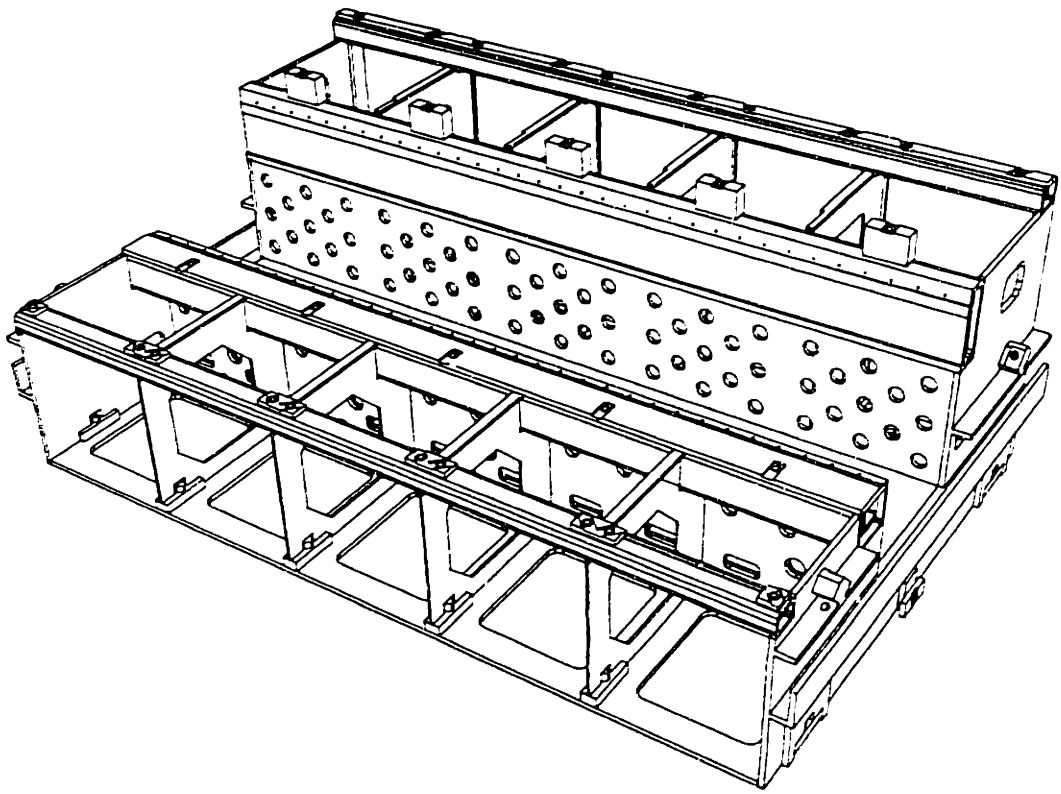

**Figure A.43** Machine frame[75].

To prepare the frame for the cleanroom environment, it is coated with an epoxy finish. Prior to the final machining, the shear dampers discussed in Chapter 4 are added to the four structural tubes along the top of the machine. Finally, all necessary reference surfaces for the kinematic couplings and linear bearings of the wafer handling robot are machined into the frame using a single fixturing operation on a large machining center.

[75] Courtesy of Silicon Valley Group. Detailed design of the machine frame was carried out at SVG.

The frame is primarily a structural support for the entire photoresist processing system. However, the frame was also designed to accommodate packaging drawers along both the front and rear portions of the machine beneath the process modules. Additionally, provisions were made in the design to facilitate the routing of electrical conduits and chemical and exhaust plumbing.

### A.6.2 The Wafer Handling Robot Embodiment Design

A rendered solid model of the wafer handling robot design is shown in Figure A.44.

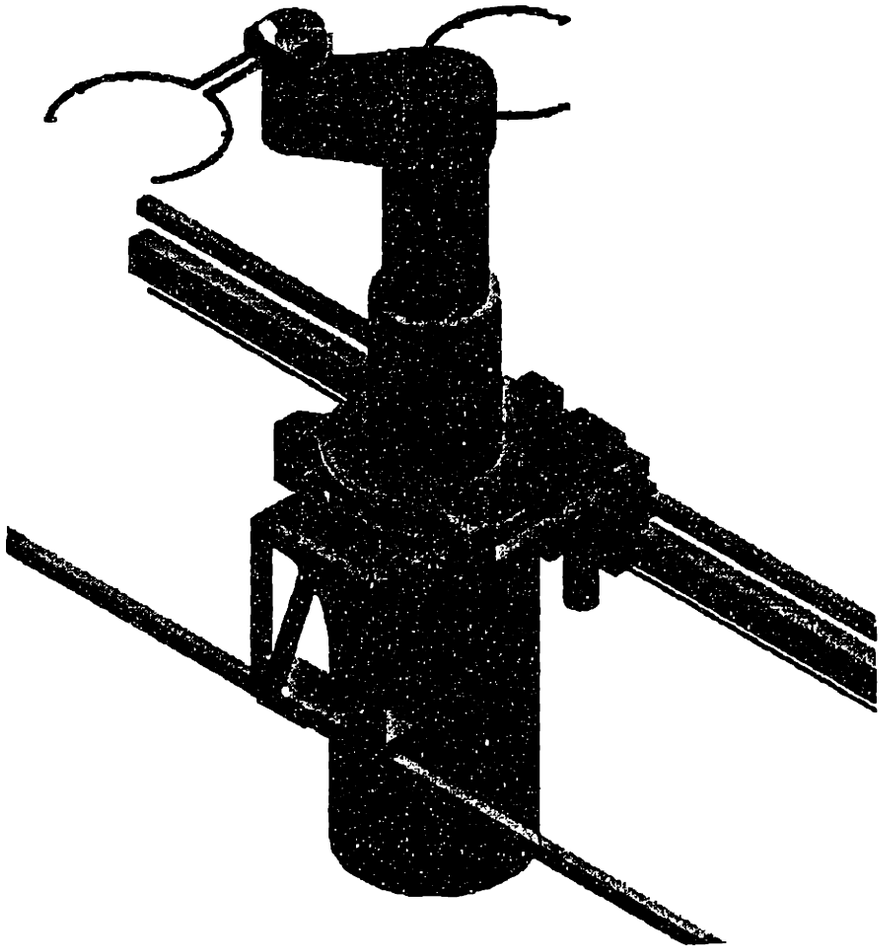

**Figure A.44** Wafer handling robot[76].

[76] Detailed design of the wafer handling robot was performed at MIT

The robot possesses seven degrees of freedom. Five of these control the joints of the robot and the other two control the wafer grippers. The first degree of freedom is the long horizontal travel. This axis is driven by a linear motor. Other actuation concepts, such as a belt drive or a rack and pinion drive, were considered for this axis, but the linear motor was selected for its combination of high performance and reliability[77]. One of the novel features of this robot is the vertical axis which is a multi-stage telescoping linear joint shown in Figure A.45. This axis keeps the robot mechanism below the wafer surfaces at all times and gives a large vertical stroke in a compact collapsed package. The other three axes are all revolute joints.

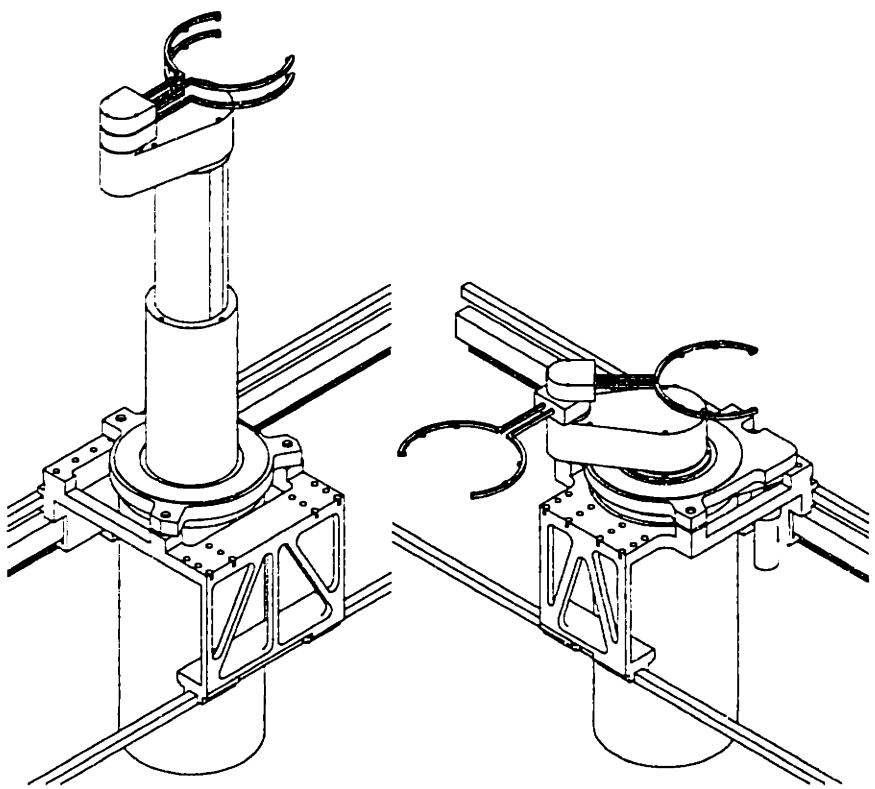

**Figure A.45** Wafer handling robot with fully extended and fully retracted telescoping axis.

The first of the revolute joints drives the rotation of the robot body about the center of the column. The other two revolute joints drive the two independent grippers.

[77] The linear motor is a brushless type without any mechanical contact which results in higher reliability.

Figure A.46 shows the detailed layout of the upper portion of the robot. Both grippers are shown attached to concentric drive shafts. These shafts allow the internal routing of sensor and motor power wires to the grippers. These two shafts are supported by crossed roller bearings, as was discussed in Chapter 4. Timing belts link the DC brushless servo motors with attached harmonic drives to the gripper shafts. The servo motors are housed within the column of the robot to save vertical space in the arm.

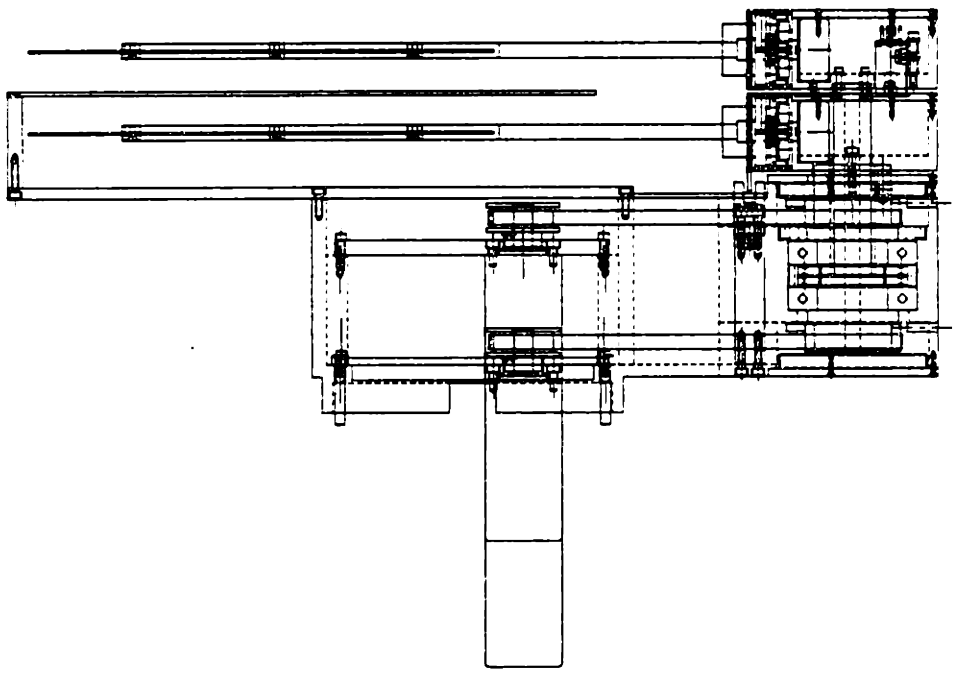

**Figure A.46** Side view of fork grippers and upper arm assembly.

A top view of the grippers and upper arm assembly is shown in Figure A.47. The side view above and the top view below also show a barrier plate, which is rigidly connected to the arm cover, between the two wafer grippers. This plate will help to minimize the effects of disturbances in airflow above the lower wafer.

Figure A.48 shows a redesigned version of the fork gripper concept. The operational principles of this gripper are identical to those previously discussed. The gripper housing was widened to accommodate a much larger and stiffer bearing. The jaws were also widened. These changes were made to increase the gripper's robustness to possible rough handling when the photoresist system is not operational.

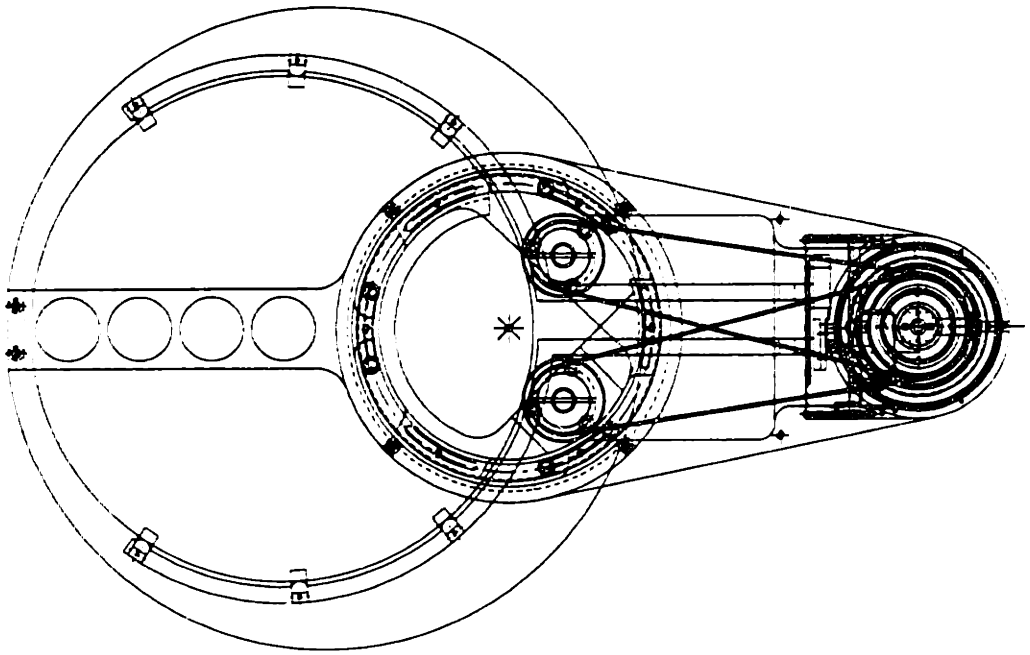

**Figure A.47** Top view of fork grippers and arm assembly.

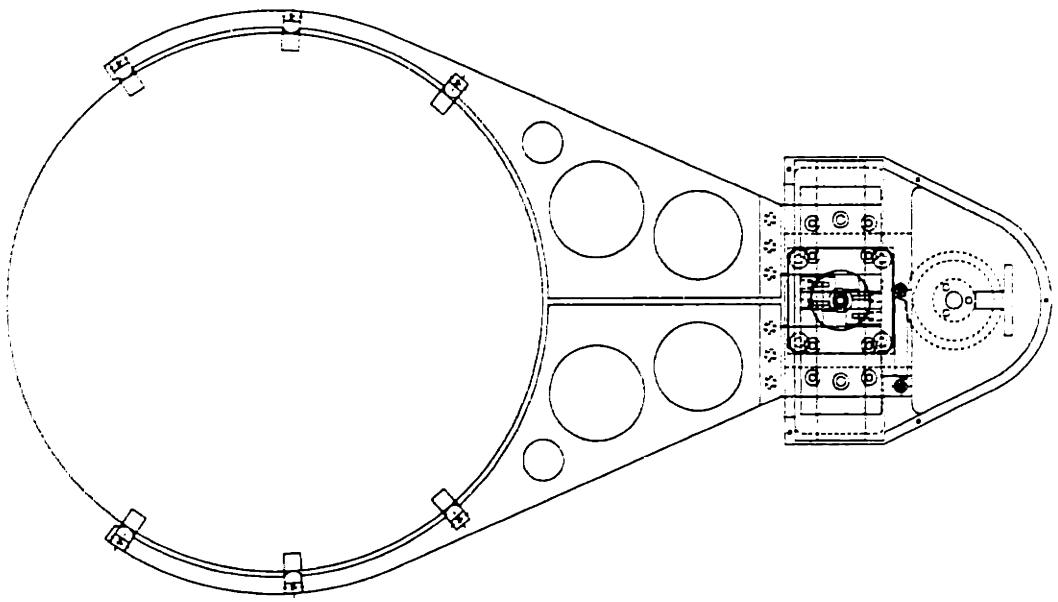

**Figure A.48** Finished fork gripper design.

Similarly, Figure A.49 shows an updated version of the tongue gripper. The primary change in this design was the inclusion of a larger set of crossed roller bearings to support the tongue. The bearings were moved out to the gripper housing. The back stop section of the gripper with four contact points is now fixed to the gripper housing.

The tongue portion moves and is supported by crossed roller bearings on both sides of the tongue immediately behind the back stop portion of the gripper. The gripper is still actuated by a stepper motor inside the gripper housing.

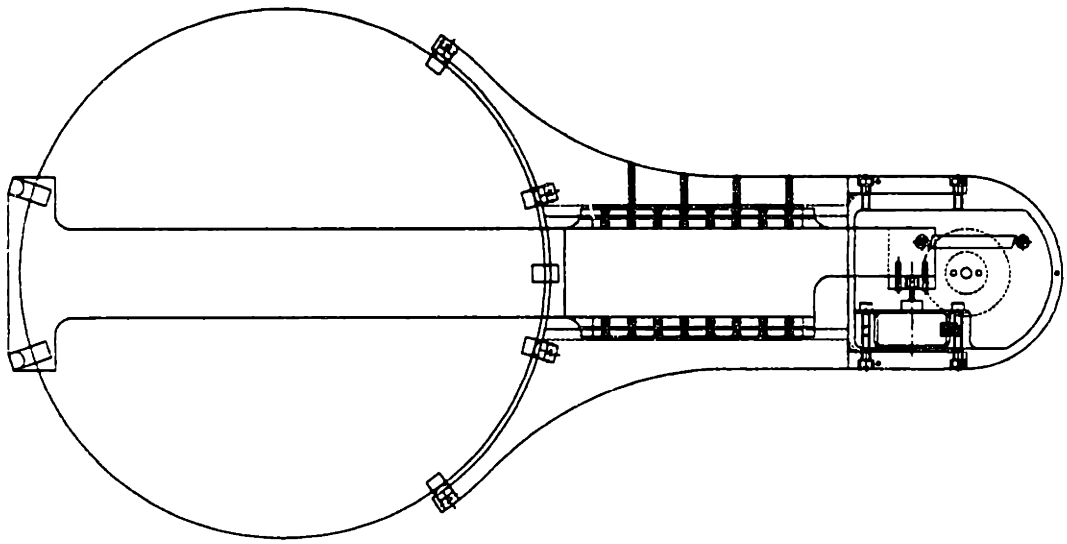

**Figure A.49** Finished tongue gripper design[78].

Additionally, potentiometer feedback and a simple dash pot were added to both grippers to enhance the controllability of the closing motion. The potentiometer will add simple position feedback so that the stepper motor can be operated in a closed loop manner. The potentiometer also serves as an over travel sensor to indicate when the gripper jaws have closed beyond the minimum diameter of a wafer. This over travel condition would indicate that a wafer was not properly gripped by the closing motion. Both grippers use a high resolution hybrid stepper motor with a microstepping driver for smooth, high resolution motion. However, the dashpot is added to reduce the magnitude of any slight vibration induced in the gripper jaws by the discrete steps produced by the stepper motor.

In regard to the gripper design, one final point about the six contact points used in each gripper is worthy of discussion. Only three points of contact would ideally be required to perform the centering operation on a round wafer. However, because wafers may be flatted or notched, the gripper jaws possess six points of contact. With this

[78] Courtesy of Silicon Valley Group.

number of contact points, the centering operation is insensitive to the location of flats or notches on the wafer. The positioning of the contact points has been optimized for maximum centering accuracy given the geometric constraints imposed by wafer holding cassettes and process module wafer chucks. Although, six points of contact (each contact point is formed from a cylinder) are used to center the wafer, the weight of the wafer is supported by small tabs that contact the wafer back surface near the wafer's edge.

Details of the multi-stage telescoping axis are shown in Figure A.50 and Figure A.51.

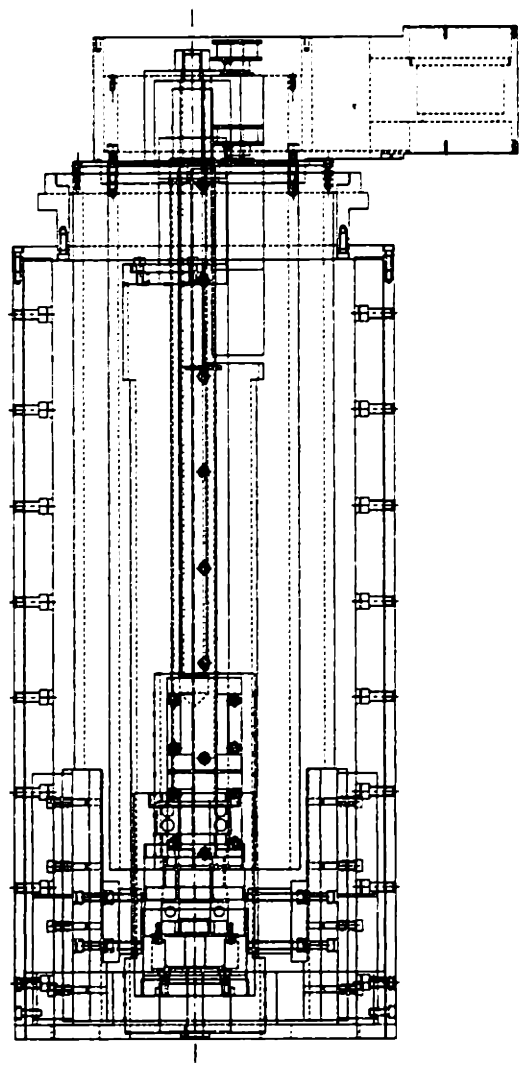

**Figure A.50** Side view of the fully collapsed telescoping axis.

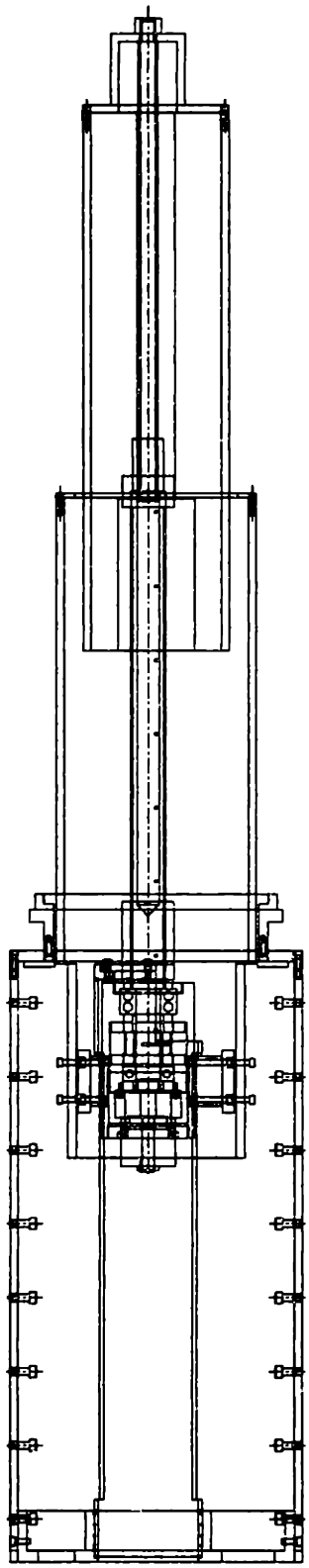

**Figure A.51** Fully extended telescoping axis. (Shown without linear bearings.)

In addition to providing a long vertical stroke in a compact package, the telescoping axis is suitable for use in the clean manufacturing environment required for semiconductor production because the bearings and drive actuator are fully enclosed by the outer tubes making up the structural portions of telescoping axis. The collapsed view of the axis in Figure A.50 shows the placement of the ballscrew, linear bearings, and structural tubes that make up this unique vertical motion axis. Figure A.51 shows the axis fully extended and does not include the linear bearings for clarity.

The multi-stage telescoping axis consists of two linear stages, each with equal travel, mounted within three concentric tubes. These two stages are referred to as the intermediate stage and the top stage. The intermediate stage, which consists of the intermediate tube, rides on bearings mounted on the inside wall of the outer tube. The top stage, in turn, which consists of the top tube, rides on bearings mounted on the inside wall of the intermediate tube. The two linear stages are actuated such that their motion is coupled. The top stage moves twice as far and twice as fast as the intermediate stage, while the relative motion between the intermediate tube and the outer tube is the same as the relative motion between the top tube and the intermediate tube. This coupled motion is accomplished using a one degree of freedom multi-stage ballscrew assembly, which is really two ballscrews driven by only one servo motor. This multi-stage ballscrew is also shown in Figure A.57. The ballscrew assembly consists of an outer screw and an inner screw. The outer screw ball nut is fixed to the outer most tube with a stand-off so that it does not rotate or translate. This outer ballscrew is driven by a motor (with position sensor and fail-safe brake) which is attached to the intermediate tube via a yoke that fits through slots on either side of the stand-off tube. Because the outer ball nut is fixed, the ballscrew motor moves with the intermediate tube as the motor turns. The inner screw fits inside the hollow outer screw when the telescoping axis is fully collapsed. The inner screw ball nut is rigidly attached to the top of the outer screw so that the inner ball nut rotates with the outer ballscrew. The outer ballscrew has left-handed threads and the inner screw right-handed threads. With this thread configuration, the inner screw moves up relative to the outer screw as the outer screw rotates within its ball nut also causing

upward motion. The result of this actuation scheme is a top stage that displaces twice as quickly as the lower stage.

An end view of the horizontal carriage of the wafer handling robot is shown in Figure A.52. The carriage can also be seen clearly in Figure A.44. The carriage rides on linear bearings with recirculating balls. Furthermore, the carriage is driven by a linear motor and receives feedback from an optical encoder. The robot also incorporates a kinematic couplings between the proximal revolute joint and the carriage structure.

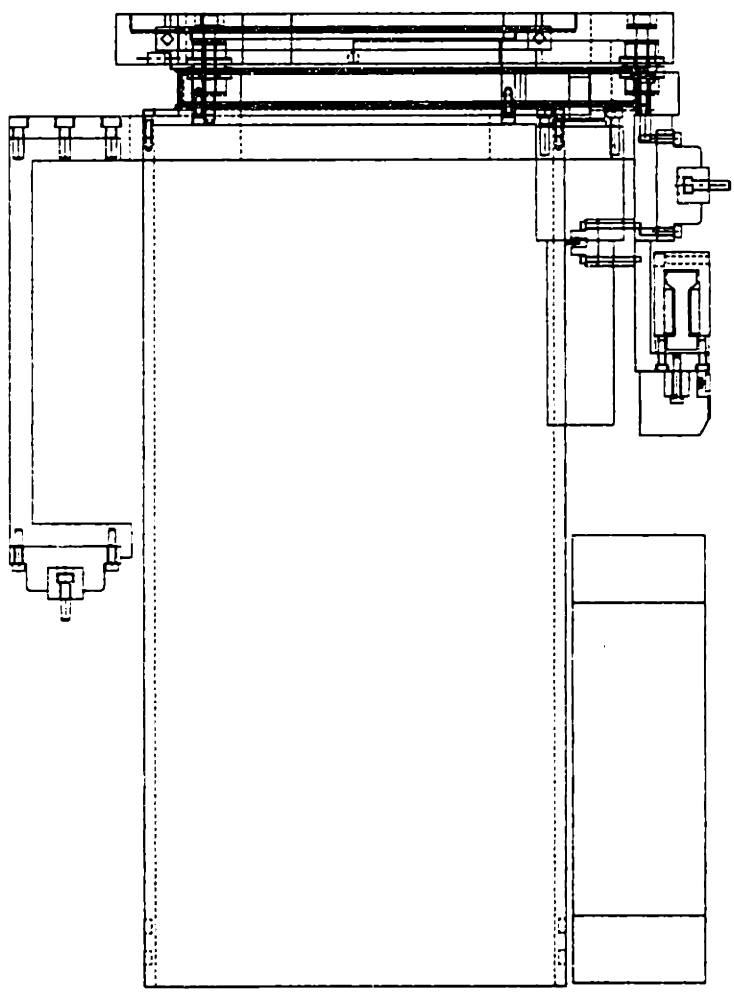

**Figure A.52** End view of the horizontal carriage.

The concept of kinematically coupling the robot body to its horizontal carriage was previously described in the case study in Section 4.2.2 of Chapter 4. The idea of using a kinematic coupling within the structure of the robot seems to be a novel one. A

patent search did reveal one similar and interesting application of a kinematic coupling in a robot. Vranish describes an invention whereby a space robot attaches to an orbiting workpiece (e.g. a satellite) using a kinematic coupling [Vranish '92].

The kinematic coupling of the wafer handling robot body to the horizontal carriage in the system allows the handler to be easily removed and subsequently replaced for servicing in the field without any subsequent recalibration requirements. The kinematic coupling has three balls which are rigidly attached to the outside portion of the base revolute joint of the robot. Three grooves are, in turn, rigidly mounted to the system's horizontal carriage. Each ball/groove interface forms two distinct points of contact. So, the three ball/groove combinations result in six distinct points of contact between the robot body and the horizontal carriage. These six contact points fully constrain the six spatial degrees of freedom of the robot body. Therefore, the robot body is rigidly and deterministically coupled to the horizontal carriage. This coupling is designed with appropriate ball and groove dimensions, locations, and preload forces between each ball/groove joint to give a large amount of static and dynamic stiffness. The preload force is obtained by passing a threaded fastener with spring washers through the center of each ball/groove joint.

## A.7 The Finished Design

Figure A.53 shows a graphic of Silicon Valley Group's Accipiter photoresist processing system. The system includes three nearly identical versions of the wafer handling robot discussed previously. Also, the process modules are kinematically coupled to the frame pictured in Figure A.43. The end station, shown at left in the figure, and the stepper interface, shown at right, are also kinematically coupled to the machine frame and house the two additional wafer handling robots.

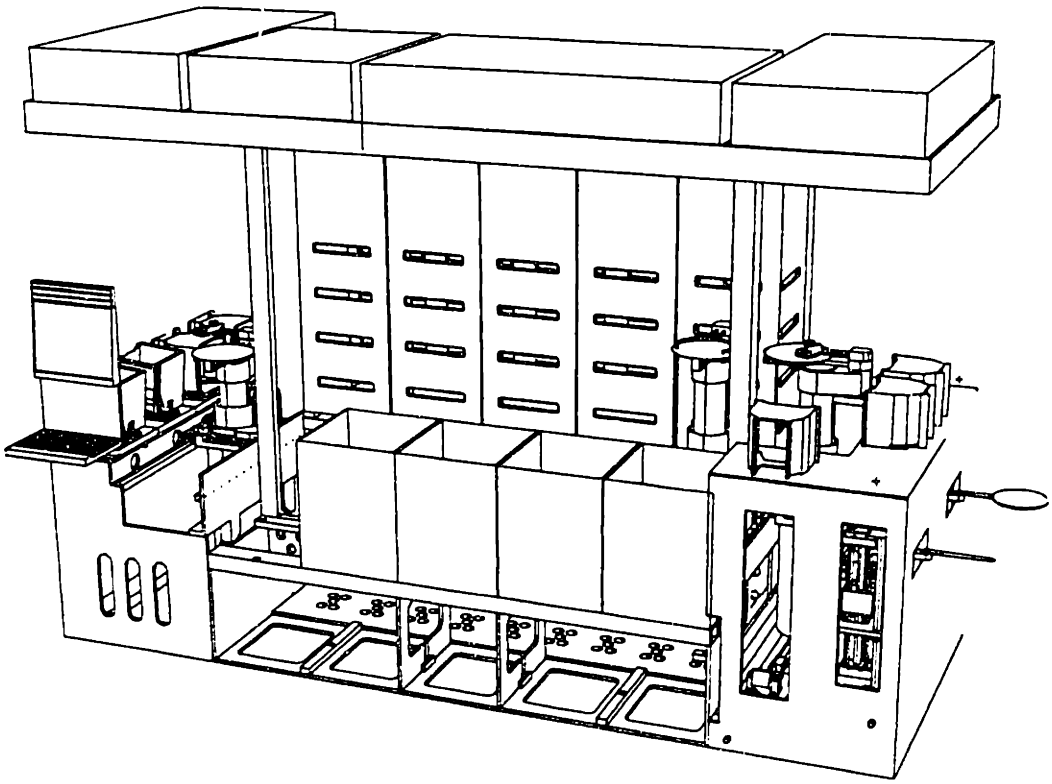

**Figure A.53** Finalized machine concept[79].

## A.8 The Prototype Wafer Handling Robot and Test Frame

This section briefly presents the first prototype of the wafer handling robot along with a simplified test frame on which the robot was mounted. This first robot was used to debug the operation of the individual joints and verify the detailed design of the robot. After each joint became operational, the robot was assembled into a complete unit and mounted in a test frame. Figure A.54 shows the body of the prototype robot next to the test frame with the horizontal carriage. The test frame, except for its shorter length, is dimensionally identical to the actual frame. However, the test frame design was simplified somewhat because this frame was intended to serve only as a platform for control system development and initial performance testing.

[79] Courtesy of Silicon Valley Group.

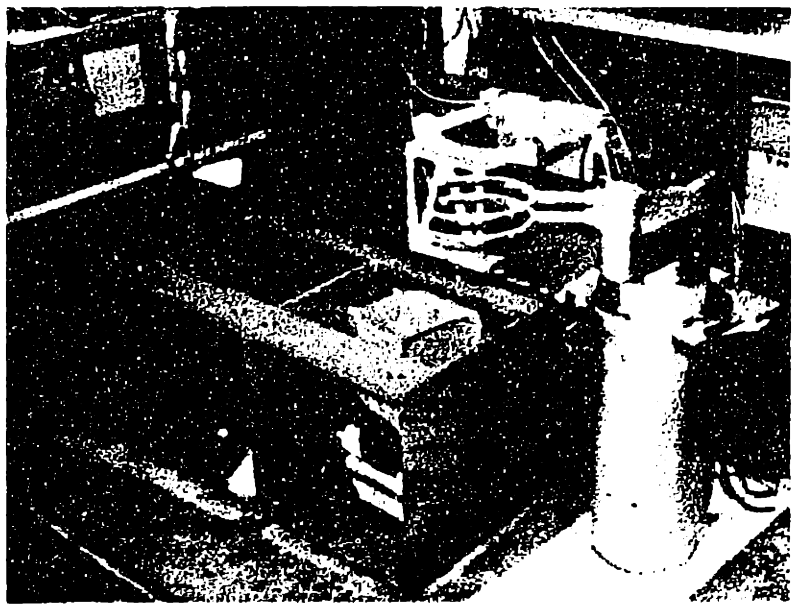

**Figure A.54** Prototype wafer handling robot next to test frame.

Figure A.55 shows the robot's upper arm assembly with the two fork-type grippers attached. This arm module was initially mounted on a small test stand so that both elbow joints could be operated after assembly.

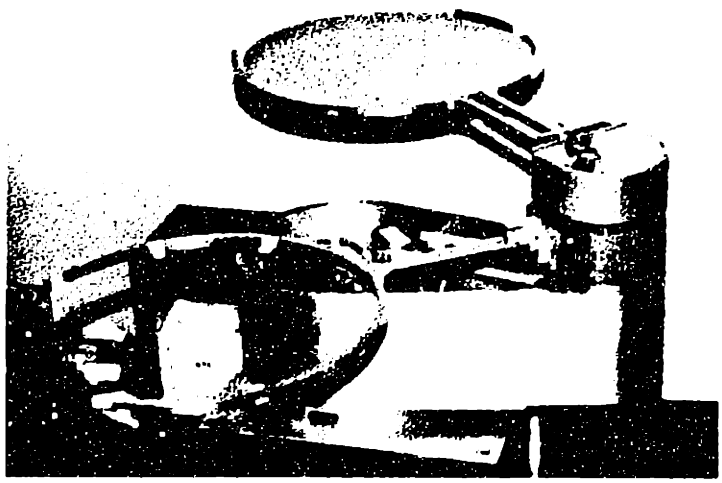

**Figure A.55** Prototype fork grippers and arm assembly in test fixture.

After the fork grippers and arm assembly prototype modules had been assembled, the telescoping vertical joint was constructed. Figure A.56 shows the dual ballscrew assembly that was designed to actuate this joint. Also, shown in the photograph are components of the drive motor that is mounted directly on the outer ballscrew shaft to allow a more compact design.

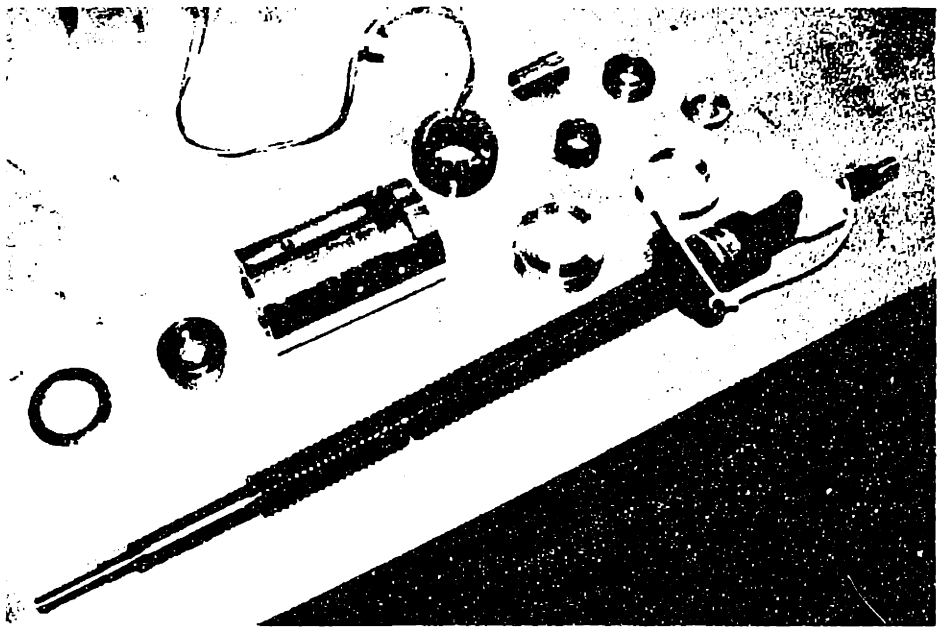

**Figure A.56** Telescoping ballscrew and motor parts.

Various stages in the assembly of the telescoping axis are shown in Figure A.57.

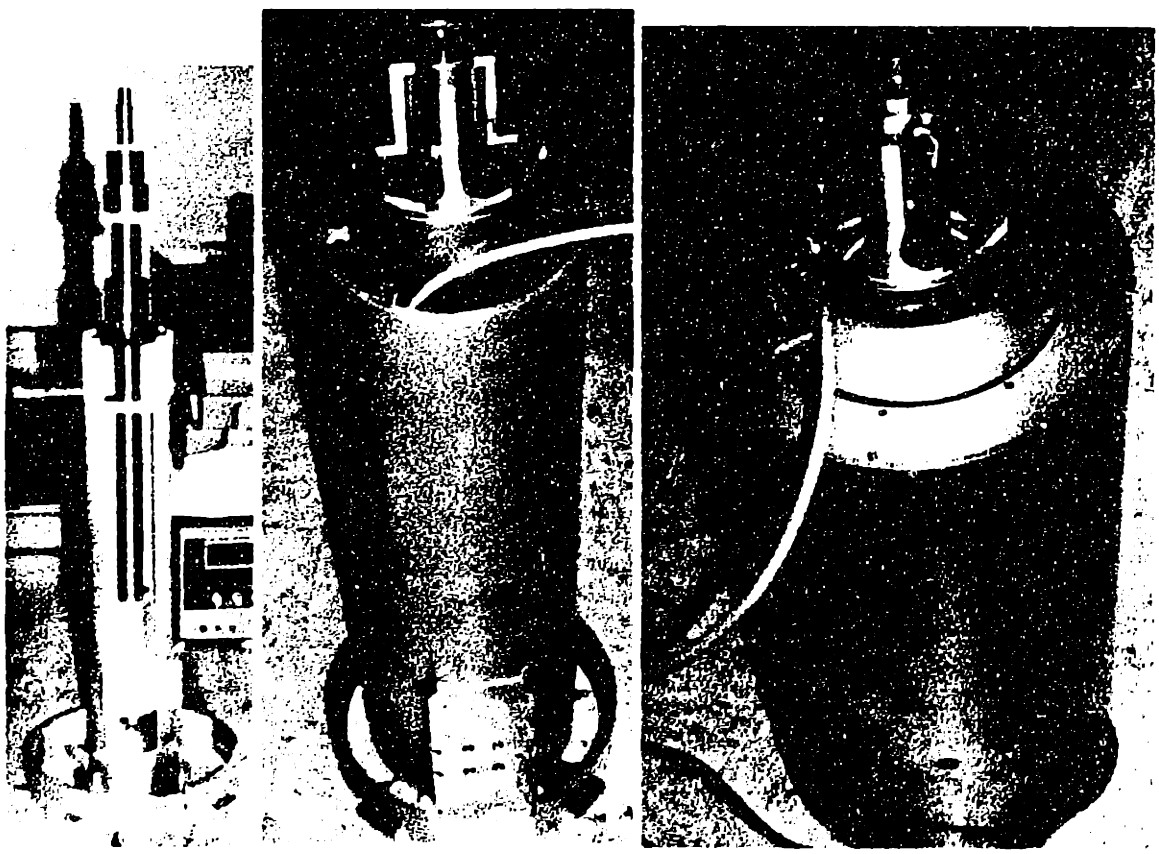

**Figure A.57** Stages in the assembly of the prototype telescoping axis.

The leftmost photograph in Figure A.57 shows the ballscrew assembly mounted inside the support stand-off. The middle photograph shows the ballscrew, inner tube, and intermediate tube assembly. Finally, the rightmost photograph shows the fully assembled telescoping axis. Figure A.58 gives another perspective of the telescoping ballscrew after the unit was assembled into the horizontal carriage. The inner screw, small ball nut, and the top of the outer screw can be seen in the figure.

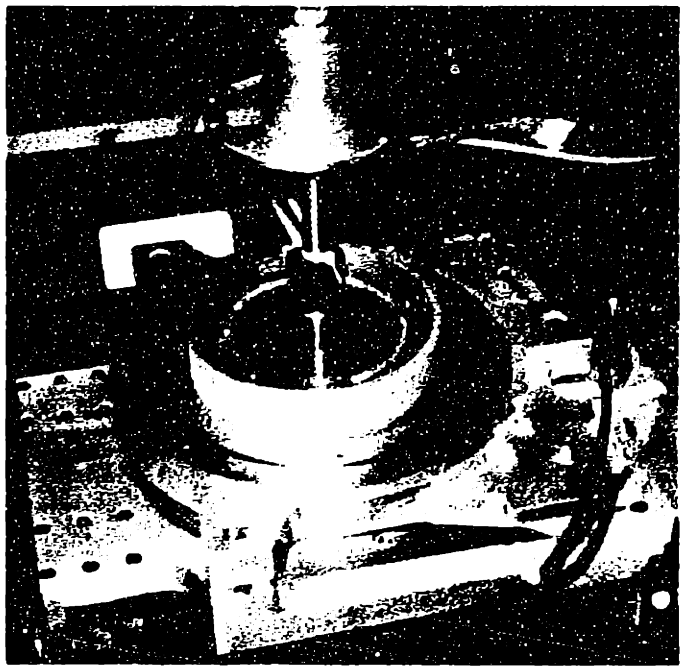

**Figure A.58** Prototype wafer handling robot partially disassembled in test frame.

Figure A.59 shows the fully assembled robot with the telescoping axis in fully retracted and fully extended configurations.

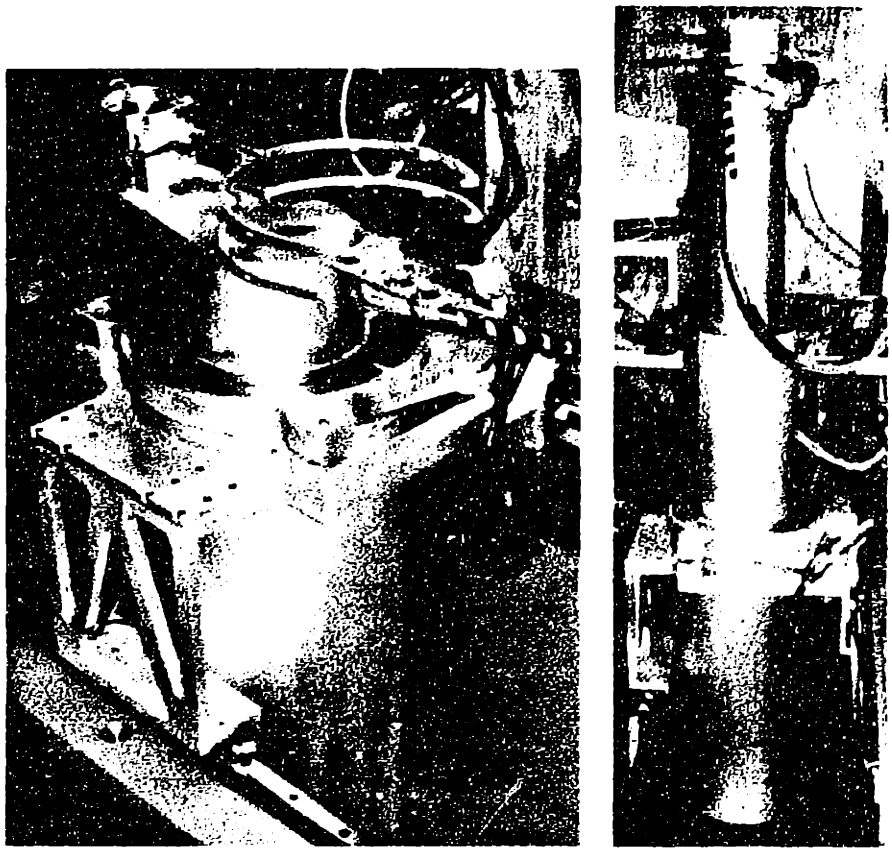

**Figure A.59** Prototype wafer handling robot with telescoping axis in fully retracted and fully extended configurations.

The value of the kinematic coupling integrated into the horizontal carriage is demonstrated in Figure A.60. In this photo, the robot body is being hoisted out of the carriage with a manual crane. For actual service in a cleanroom, a specially designed "clean" crane will be used to remove the robot.

Finally, Figure A.61 shows the fully assembled and operational robot executing a straight line move similar to the ones that will be used in the functioning photoresist processing system.

**Figure A.60** Robot body detached from horizontal carriage at kinematic coupling being lifted out of carriage with a manual crane.

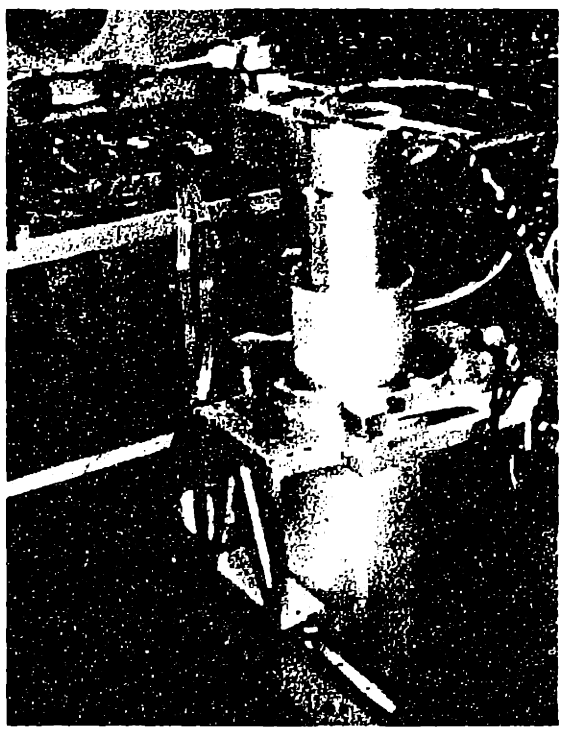

**Figure A.61** Prototype wafer handling robot executing straight-line motion.

## A.9 Summary

This appendix continued the discussion of the precision machine design methodology presented in this thesis by focusing on Silicon Valley Group's Accipiter project. This project deals with the development of a new machine for the application of photoresist to semiconductor wafers. The precision machine design techniques discussed in this thesis were applied throughout this design process. This appendix briefly described the photoresist application process and presented some of the characteristic of SVG's previous system, the 90 Series. The appendix continued with an explanation of the functional requirements for the new machine. Next, the appendix described the conceptual design stage of the Accipiter project. Machine configurations, structural frame designs, wafer handling robot concepts, and wafer gripping mechanisms were also discussed. Following the development of conceptual designs for the Accipiter project, the appendix continued by describing the embodiment and detailed design phases of the project. Specifically, the machine frame and wafer handling robot design were presented. Finally, the appendix discussed the prototype wafer handling robot and test frame, which were constructed and tested to verify the design methodology presented in this thesis.

# Appendix B: Error Modeling Case Study Data

## B.1 Introduction

This appendix contains the tables of data for the error model case studies described in Chapter 3. The last section in the appendix also contains position repeatability test data for the prototype wafer handling robot.

## B.2 Displacement Error Model

The displacement portions of the error model were generated in a spreadsheet program. Table B.1 shows the displacement errors gains for a representative configuration of the wafer handling robot. The resulting end effector errors for these error gains are shown in Table B.2. Similarly, the total end effector errors are shown in Table B.3. Table B.4 gives the error gains for the error model of the machine frame. The resulting errors at the wafer locations in the process modules are shown in Table B.5 and Table B.6.

**Table B.1** Wafer Handler Displacement Error Gains

| | | | | | | |
|---|---|---|---|---|---|---|
| horizontal axis | | | frame 1 | | | |
| Error gains at end effector | | | | | | |
| | dx | dy | dz | ex | ey | ez |
| dx | 1.00E+00 | 7.31E-17 | -2.28E-08 | 0.00E+00 | 0.00E+00 | 0.00E+00 |
| dy | -7.31E-17 | 1.00E+00 | 1.24E-24 | 0.00E+00 | 0.00E+00 | 0.00E+00 |
| dz | 2.28E-08 | 8.27E-25 | 1.00E+00 | 0.00E+00 | 0.00E+00 | 0.00E+00 |
| ex | 0.00E+00 | -2.64E+01 | -2.45E-07 | 1.00E+00 | 7.31E-17 | -2.28E-08 |
| ey | -3.29E-07 | -1.64E+01 | 5.26E-08 | -7.31E-17 | 1.00E+00 | 1.24E-24 |
| ez | 2.64E+01 | -5.26E-08 | -1.64E+01 | 2.28E-08 | 8.27E-25 | 1.00E+00 |
| | | | | | | |
| Base revolute | | | frame 2 | | | |
| Error gains at end effector | | | | | | |
| | dx | dy | dz | ex | ey | ez |

| | | | | | | |
|---|---|---|---|---|---|---|
| dx | 9.96E-08 | -3.21E-09 | 1.00E+00 | 0.00E+00 | 0.00E+00 | 0.00E+00 |
| dy | -1.00E+00 | -3.19E-16 | 9.96E-08 | 0.00E+00 | 0.00E+00 | 0.00E+00 |
| dz | 0.00E+00 | -1.00E+00 | -3.21E-09 | 0.00E+00 | 0.00E+00 | 0.00E+00 |
| ex | 2.64E+01 | -2.03E-06 | -1.64E+01 | 9.96E-08 | -3.21E-09 | 1.00E+00 |
| ey | 2.03E-06 | 2.64E+01 | -1.02E-06 | -1.00E+00 | -3.19E-16 | 9.96E-08 |
| ez | 2.45E-07 | 1.64E+01 | 0.00E+00 | 0.00E+00 | -1.00E+00 | -3.21E-09 |
| | | | | | | |
| Telescoping axis | | | frame 3 | | | |
| Error gains at end effector | | | | | | |
| | dx | dy | dz | ex | ey | ez |
| dx | -1.00E+00 | -3.09E-16 | 9.64E-08 | 0.00E+00 | 0.00E+00 | 0.00E+00 |
| dy | -9.64E-08 | 3.21E-09 | -1.00E+00 | 0.00E+00 | 0.00E+00 | 0.00E+00 |
| dz | 0.00E+00 | -1.00E+00 | -3.21E-09 | 0.00E+00 | 0.00E+00 | 0.00E+00 |
| ex | 1.01E-07 | 1.38E+00 | -9.63E-07 | -1.00E+00 | -3.09E-16 | 9.64E-08 |
| ey | -1.38E+00 | 1.01E-07 | 1.64E+01 | -9.64E-08 | 3.21E-09 | -1.00E+00 |
| ez | 2.45E-07 | 1.64E+01 | 0.00E+00 | 0.00E+00 | -1.00E+00 | -3.21E-09 |
| | | | | | | |
| Elbow axis | | | frame 4 | | | |
| Error gains at end effector | | | | | | |
| | dx | dy | dz | ex | ey | ez |
| dx | 1.00E+00 | 0.00E+00 | 0.00E+00 | 0.00E+00 | 0.00E+00 | 0.00E+00 |
| dy | 0.00E+00 | -3.21E-09 | 1.00E+00 | 0.00E+00 | 0.00E+00 | 0.00E+00 |
| dz | 0.00E+00 | -1.00E+00 | -3.21E-09 | 0.00E+00 | 0.00E+00 | 0.00E+00 |
| ex | 0.00E+00 | 0.00E+00 | 0.00E+00 | 1.00E+00 | 0.00E+00 | 0.00E+00 |
| ey | 0.00E+00 | 0.00E+00 | -9.99E+00 | 0.00E+00 | -3.21E-09 | 1.00E+00 |
| ez | -2.28E-07 | 9.99E+00 | 0.00E+00 | 0.00E+00 | -1.00E+00 | -3.21E-09 |
| | | | | | | |
| Gripper closure | | | frame 5 | | | |
| Error gains at end effector | | | | | | |
| | dx | dy | dz | ex | ey | ez |
| dx | 1.00E+00 | 0.00E+00 | 0.00E+00 | 0.00E+00 | 0.00E+00 | 0.00E+00 |
| dy | 0.00E+00 | 1.00E+00 | 0.00E+00 | 0.00E+00 | 0.00E+00 | 0.00E+00 |
| dz | 0.00E+00 | 0.00E+00 | 1.00E+00 | 0.00E+00 | 0.00E+00 | 0.00E+00 |
| ex | 0.00E+00 | 0.00E+00 | 0.00E+00 | 1.00E+00 | 0.00E+00 | 0.00E+00 |
| ey | 0.00E+00 | 0.00E+00 | 0.00E+00 | 0.00E+00 | 1.00E+00 | 0.00E+00 |
| ez | 0.00E+00 | 0.00E+00 | 0.00E+00 | 0.00E+00 | 0.00E+00 | 1.00E+00 |

**Table B.2** Individual Axis Errors and End Effector Equivalent Errors

| | | | | | |
|---|---|---|---|---|---|
| frame 1 | | | | | |
| Joint | Joint | Joint | Mech. | Sensor | Repeat |
| mech. | sensor | repeat | error | error | error |
| error | error | error | at end eff. | at end eff. | at end eff. |
| 2.00E-04 | 0.00E+00 | 0.00E+00 | 1.26E-03 | 4.56E-12 | 0.00E+00 |
| 2.00E-04 | 0.00E+00 | 0.00E+00 | -2.28E-04 | 1.65E-28 | 0.00E+00 |
| 1.00E-04 | 2.00E-04 | 0.00E+00 | -5.56E-04 | 2.00E-04 | 0.00E+00 |
| 1.00E-05 | 0.00E+00 | 0.00E+00 | 1.00E-05 | 0.00E+00 | 0.00E+00 |
| 1.00E-05 | 0.00E+00 | 0.00E+00 | 1.00E-05 | 0.00E+00 | 0.00E+00 |
| 4.00E-05 | 0.00E+00 | 0.00E+00 | 4.00E-05 | 0.00E+00 | 0.00E+00 |
| frame 2 | | | | | |
| Joint | Joint | Joint | Mech. | Sensor | Repeat |
| mech. | sensor | repeat | error | error | error |
| error | error | error | at end eff. | at end eff. | at end eff. |
| 2.00E-04 | 0.00E+00 | 0.00E+00 | 6.38E-05 | 2.45E-12 | 1.96E-11 |
| 2.00E-04 | 0.00E+00 | 0.00E+00 | 6.20E-04 | 1.64E-04 | 1.31E-03 |
| 3.00E-04 | 0.00E+00 | 0.00E+00 | 3.59E-05 | 0.00E+00 | 0.00E+00 |
| 1.00E-05 | 0.00E+00 | 0.00E+00 | -1.00E-05 | 0.00E+00 | 0.00E+00 |
| 1.00E-05 | 0.00E+00 | 0.00E+00 | -4.00E-05 | -1.00E-05 | -8.00E-05 |
| 4.00E-05 | 1.00E-05 | 8.00E-05 | 1.00E-05 | -3.21E-14 | -2.56E-13 |
| frame 3 | | | | | |
| Joint | Joint | Joint | Mech. | Sensor | Repeat |
| mech. | sensor | repeat | error | error | error |
| error | error | error | at end eff. | at end eff. | at end eff. |
| 5.00E-04 | 0.00E+00 | 0.00E+00 | -5.28E-04 | 0.00E+00 | 0.00E+00 |
| 5.00E-04 | 0.00E+00 | 0.00E+00 | 1.84E-04 | -1.00E-04 | -2.00E-04 |
| 5.00E-04 | 1.00E-04 | 2.00E-04 | -1.72E-04 | -3.21E-13 | -6.41E-13 |
| 2.00E-05 | 0.00E+00 | 0.00E+00 | -2.00E-05 | 0.00E+00 | 0.00E+00 |
| 2.00E-05 | 0.00E+00 | 0.00E+00 | -4.00E-05 | 0.00E+00 | 0.00E+00 |
| 4.00E-05 | 0.00E+00 | 0.00E+00 | -2.00E-05 | 0.00E+00 | 0.00E+00 |
| frame 4 | | | | | |
| Joint | Joint | Joint | Mech. | Sensor | Repeat |
| mech. | sensor | repeat | error | error | error |
| error | error | error | at end eff. | at end eff. | at end eff. |
| 2.00E-04 | 0.00E+00 | 0.00E+00 | 2.00E-04 | -4.79E-12 | -3.42E-11 |
| 2.00E-04 | 0.00E+00 | 0.00E+00 | 9.94E-05 | 2.10E-04 | 1.50E-03 |
| 3.00E-04 | 0.00E+00 | 0.00E+00 | 1.00E-04 | 0.00E+00 | 0.00E+00 |
| 1.00E-05 | 0.00E+00 | 0.00E+00 | 1.00E-05 | 0.00E+00 | 0.00E+00 |
| 1.00E-05 | 0.00E+00 | 0.00E+00 | -4.00E-05 | -2.10E-05 | -1.50E-04 |

| | | | | | |
|---|---|---|---|---|---|
| 4.00E-05 | 2.10E-05 | 1.50E-04 | 1.00E-05 | -6.73E-14 | -4.81E-13 |
| frame 5 | | | | | |
| Joint | Joint | Joint | Mech. | Sensor | Repeat |
| mech. | sensor | repeat | error | error | error |
| error | error | error | at end eff. | at end eff. | at end eff. |
| 5.00E-04 | 0.00E+00 | 0.00E+00 | 5.00E-04 | 0.00E+00 | 0.00E+00 |
| 5.00E-04 | 0.00E+00 | 0.00E+00 | 5.00E-04 | 0.00E+00 | 0.00E+00 |
| 2.50E-04 | 1.00E-03 | 2.00E-04 | 2.50E-04 | 1.00E-03 | 2.00E-04 |
| 2.00E-05 | 0.00E+00 | 0.00E+00 | 2.00E-05 | 0.00E+00 | 0.00E+00 |
| 2.00E-05 | 0.00E+00 | 0.00E+00 | 2.00E-05 | 0.00E+00 | 0.00E+00 |
| 4.00E-05 | 0.00E+00 | 0.00E+00 | 4.00E-05 | 0.00E+00 | 0.00E+00 |

**Table B.3** Total End Effector Errors

| Errors in inches and radians | | | |
|---|---|---|---|
| | | Mech. | Mech. |
| | Mech. | RMS | Expected |
| | total | total | value |
| | error | error | (avg. total and RMS) |
| dx | 1.49E-03 | 1.47E-03 | 1.48E-03 |
| dy | 1.18E-03 | 8.55E-04 | 1.02E-03 |
| dz | -3.42E-04 | 6.43E-04 | 4.92E-04 |
| ex | 1.00E-05 | 3.32E-05 | 2.16E-05 |
| ey | -9.00E-05 | 7.28E-05 | 8.14E-05 |
| ez | 8.00E-05 | 6.16E-05 | 7.08E-05 |
| | | | |
| | | Sensor | Sensor |
| | Sensor | RMS | Expected |
| | total | total | value |
| | error | error | (avg. total and RMS) |
| dx | 2.23E-12 | 7.05E-12 | 4.64E-12 |
| dy | 2.74E-04 | 2.84E-04 | 2.79E-04 |
| dz | 1.20E-03 | 1.02E-03 | 1.11E-03 |
| ex | 0.00E+00 | 0.00E+00 | 0.00E+00 |
| ey | -3.10E-05 | 2.33E-05 | 2.71E-05 |
| ez | -9.94E-14 | 7.45E-14 | 8.70E-14 |
| | | Repeat | Repeat |
| | Repeat | RMS | Expected |
| | total | total | value |

| | error | error | (avg. total and RMS) |
|---|---|---|---|
| dx | -1.46E-11 | 3.94E-11 | 2.70E-11 |
| dy | 2.61E-03 | 2.00E-03 | 2.31E-03 |
| dz | 2.00E-04 | 2.00E-04 | 2.00E-04 |
| ex | 0.00E+00 | 0.00E+00 | 0.00E+00 |
| ey | -2.30E-04 | 1.70E-04 | 2.00E-04 |
| ez | -7.37E-13 | 5.45E-13 | 6.41E-13 |
| | | Total | Total |
| | | RMS | Expected |
| | Total | total | value |
| | error | error | (avg. total and RMS) |
| dx | 1.49E-03 | 1.47E-03 | 1.48E-03 |
| dy | 4.06E-03 | 2.20E-03 | 3.13E-03 |
| dz | 1.06E-03 | 1.22E-03 | 1.14E-03 |
| ex | 1.00E-05 | 3.32E-05 | 2.16E-05 |
| ey | -3.51E-04 | 1.86E-04 | 2.69E-04 |
| ez | 8.00E-05 | 6.16E-05 | 7.08E-05 |

**Table B.4** Machine Frame Displacement Error Gains.

| | | | | | | |
|---|---|---|---|---|---|---|
| **spin stations** | | | | | | |
| frame 0 | | | | | | |
| Error gains at wafer position | | | | | | |
| | dx | dy | dz | ex | ey | ez |
| dx | 1.00E+00 | 0.00E+00 | 0.00E+00 | 0.00E+00 | 0.00E+00 | 0.00E+00 |
| dy | 0.00E+00 | 1.00E+00 | 0.00E+00 | 0.00E+00 | 0.00E+00 | 0.00E+00 |
| dz | 0.00E+00 | 0.00E+00 | 1.00E+00 | 0.00E+00 | 0.00E+00 | 0.00E+00 |
| ex | 0.00E+00 | -1.80E+01 | 2.40E+01 | 1.00E+00 | 0.00E+00 | 0.00E+00 |
| ey | 1.80E+01 | 0.00E+00 | -1.50E+01 | 0.00E+00 | 1.00E+00 | 0.00E+00 |
| ez | -2.40E+01 | 1.50E+01 | 0.00E+00 | 0.00E+00 | 0.00E+00 | 1.00E+00 |
| | | | | | | |
| Frame 1 | | | | | | |
| Error gains at wafer position | | | | | | |
| | dx | dy | dz | ex | ey | ez |
| dx | 1.00E+00 | 0.00E+00 | 0.00E+00 | 0.00E+00 | 0.00E+00 | 0.00E+00 |
| dy | 0.00E+00 | 1.00E+00 | 0.00E+00 | 0.00E+00 | 0.00E+00 | 0.00E+00 |
| dz | 0.00E+00 | 0.00E+00 | 1.00E+00 | 0.00E+00 | 0.00E+00 | 0.00E+00 |
| ex | 0.00E+00 | -1.80E+01 | 0.00E+00 | 1.00E+00 | 0.00E+00 | 0.00E+00 |
| ey | 1.80E+01 | 0.00E+00 | 1.50E+00 | 0.00E+00 | 1.00E+00 | 0.00E+00 |

| | | | | | | |
|---|---|---|---|---|---|---|
| ez | 0.00E+00 | -1.50E+00 | 0.00E+00 | 0.00E+00 | 0.00E+00 | 1.00E+00 |
| **stacked stations** | | | | | | |
| frame 0 | | | | | | |
| Error gains at wafer position | | | | | | |
| | dx | dy | dz | ex | ey | ez |
| dx | 1.00E+00 | 0.00E+00 | 0.00E+00 | 0.00E+00 | 0.00E+00 | 0.00E+00 |
| dy | 0.00E+00 | 1.00E+00 | 0.00E+00 | 0.00E+00 | 0.00E+00 | 0.00E+00 |
| dz | 0.00E+00 | 0.00E+00 | 1.00E+00 | 0.00E+00 | 0.00E+00 | 0.00E+00 |
| ex | 0.00E+00 | -1.50E+01 | 2.40E+01 | 1.00E+00 | 0.00E+00 | 0.00E+00 |
| ey | 1.50E+01 | 0.00E+00 | 1.45E+01 | 0.00E+00 | 1.00E+00 | 0.00E+00 |
| ez | -2.40E+01 | -1.45E+01 | 0.00E+00 | 0.00E+00 | 0.00E+00 | 1.00E+00 |
| | | | | | | |
| Frame 1 | | | | | | |
| Error gains at wafer position | | | | | | |
| | dx | dy | dz | ex | ey | ez |
| dx | 1.00E+00 | 0.00E+00 | 0.00E+00 | 0.00E+00 | 0.00E+00 | 0.00E+00 |
| dy | 0.00E+00 | 1.00E+00 | 0.00E+00 | 0.00E+00 | 0.00E+00 | 0.00E+00 |
| dz | 0.00E+00 | 0.00E+00 | 1.00E+00 | 0.00E+00 | 0.00E+00 | 0.00E+00 |
| ex | 0.00E+00 | -1.50E+01 | 0.00E+00 | 1.00E+00 | 0.00E+00 | 0.00E+00 |
| ey | 1.50E+01 | 0.00E+00 | -3.00E+00 | 0.00E+00 | 1.00E+00 | 0.00E+00 |
| ez | 0.00E+00 | 3.00E+00 | 0.00E+00 | 0.00E+00 | 0.00E+00 | 1.00E+00 |

**Table B.5** Individual Axis Errors and End Point Equivalent Errors.

| **spin stations** | |
|---|---|
| | Mech. |
| mech. | error |
| error | at wafer |
| 1.00E-04 | 4.00E-05 |
| 1.00E-04 | 7.00E-05 |
| 1.00E-04 | 1.90E-04 |
| 1.00E-05 | 1.00E-05 |
| 1.00E-05 | 1.00E-05 |
| 1.00E-05 | 1.00E-05 |
| | |
| Joint | Mech. |
| mech. | error |
| error | at wafer |
| 1.00E-04 | 2.80E-04 |
| 1.00E-04 | -9.50E-05 |

| | |
|---|---|
| 1.00E-04 | 1.15E-04 |
| 1.00E-05 | 1.00E-05 |
| 1.00E-05 | 1.00E-05 |
| 1.00E-05 | 1.00E-05 |
| **stacked stations** | |
| | Mech. |
| mech. | error |
| error | at wafer |
| 1.00E-04 | 1.00E-05 |
| 1.00E-04 | -1.95E-04 |
| 1.00E-04 | 4.85E-04 |
| 1.00E-05 | 1.00E-05 |
| 1.00E-05 | 1.00E-05 |
| 1.00E-05 | 1.00E-05 |
| | |
| Joint | Mech. |
| mech. | error |
| error | at wafer |
| 1.00E-04 | 2.50E-04 |
| 1.00E-04 | -2.00E-05 |
| 1.00E-04 | 7.00E-05 |
| 1.00E-05 | 1.00E-05 |
| 1.00E-05 | 1.00E-05 |
| 1.00E-05 | 1.00E-05 |

**Table B.6** Total End Effector Errors.

| **spin stations** | | | |
|---|---|---|---|
| Errors in inches and radians | | | |
| | | Mech. | Mech. |
| | Mech. | RMS | Expected |
| | total | total | value |
| | error | error | (avg. total and RMS) |
| dx | 3.20E-04 | 2.83E-04 | 3.01E-04 |
| dy | -2.50E-05 | 1.18E-04 | 7.15E-05 |
| dz | 3.05E-04 | 2.22E-04 | 2.64E-04 |
| ex | 2.00E-05 | 1.41E-05 | 1.71E-05 |
| ey | 2.00E-05 | 1.41E-05 | 1.71E-05 |
| ez | 2.00E-05 | 1.41E-05 | 1.71E-05 |

| stacked stations | | | |
|---|---|---|---|
| Errors in inches and radians | | | |
| | | Mech. | Mech. |
| | Mech. | RMS | Expected |
| | total | total | value |
| | error | error | (avg. total and RMS) |
| dx | 2.60E-04 | 2.50E-04 | 2.55E-04 |
| dy | -2.15E-04 | 1.96E-04 | 2.06E-04 |
| dz | 5.55E-04 | 4.90E-04 | 5.23E-04 |
| ex | 2.00E-05 | 1.41E-05 | 1.71E-05 |
| ey | 2.00E-05 | 1.41E-05 | 1.71E-05 |
| ez | 2.00E-05 | 1.41E-05 | 1.71E-05 |

## B.3 Velocity Error Model

The velocity error model was calculated in the program Mathematica™ using the Jacobian matrix of the wafer handling robot. Errors gains are shown for three configurations of the wafer handling robot. The results for the first configuration are shown in Table B.7. These gains were generated for revolute joints angles, $\theta_2 = 100°$ and $\theta_4 = 100°$. The condition number for this configuration is $\sigma = 836$.

Table B.8 shows a similar set of velocity error gains for $\theta_2 = 45°$ and $\theta_4 = 45°$. The condition number of the Jacobian in this configuration is $\sigma = 119$. A final set of velocity error gains are shown in Table B.9 for $\theta_2 = 0°$ and $\theta_4 = 0°$. The condition number in this configuration is $\sigma = 17.8$.

**Table B.7** Table of Velocity Error Gains

| | X | Y | $\theta_H$ | Z |
|---|---|---|---|---|
| $d_1$ | 0 | 1 | 0 | 0 |
| $\theta_2$ | 8.87 | 6.64 | 1 | 0 |
| $d_3$ | 0 | 0 | 0 | 1 |
| $\theta_4$ | 9.98 | 0.32 | 1 | 0 |

**Table B.8** Table of Velocity Error Gains

| | X | Y | $\theta_H$ | Z |
|---|---|---|---|---|
| $d_1$ | 0 | 1 | 0 | 0 |
| $\theta_2$ | 4.54 | 5.44 | 1 | 0 |
| $d_3$ | 0 | 0 | 0 | 1 |
| $\theta_4$ | 0 | 9.98 | 1 | 0 |

**Table B.9** Table of Velocity Error Gains

| | X | Y | $\theta_H$ | Z |
|---|---|---|---|---|
| $d_1$ | 0 | 1 | 0 | 0 |
| $\theta_2$ | 3.56 | 0 | 1 | 0 |
| $d_3$ | 0 | 0 | 0 | 1 |
| $\theta_4$ | -9.98 | 0 | 1 | 0 |

## B.4 Positioning Repeatability Test Data for the Prototype Wafer Handling Robot

This section of the appendix contains data from the repeatability testing of the wafer handling robot prototype. This data was measured with dial indicators with 0.0001 inch and 0.001 inch resolution. These tests were not meant to serve as exhaustive verification of the positioning performance of the robot. Rather, they were intended to give an initial indication of the robot's capabilities. An indicator was set-up on the prototype test frame at an appropriate location for each test. After initially moving the robot to the test point and setting a zero reference position with the indicator, actual testing commenced. Each measurement was taken after the robot had moved from its home location to the test point. Following each measurement the robot returned to its home location. Between tests the robot was commanded to perform various moves and other trajectories which varied in both velocity and range of motion. Following the "random" movements between measurements, the robot returned to its home position and then to the test point. These movements between tests were performed to give a better

indication of positioning repeatability especially as affected by mechanical imperfections in the robot's transmissions.

**Table B.10** Table of Horizontal Carriage Repeatability Data

| positive travel | | negative travel |
|---|---|---|
| out board side | | out board side |
| tenth gage | | tenth gage |
| 0.0001 | | -0.0002 |
| 0.0001 | | -0.0002 |
| 0.0002 | | -0.0002 |
| 0.0002 | | -0.0002 |
| 0.0001 | | -0.0001 |
| 0.0002 | | -0.0001 |
| 0.0002 | | -0.0002 |
| | | |
| positive travel | | positive travel |
| motor side | | motor side |
| tenth gage | | tenth gage |
| 0.0001 | | -0.0001 |
| 0.0001 | | 0.0000 |
| 0.0001 | | 0.0000 |
| 0.0001 | | 0.0000 |
| 0.0001 | | -0.0001 |
| 0.0001 | | 0.0000 |
| 0.0001 | | 0.0000 |

**Table B.11** Table of Telescoping Axis Repeatability Data

| negative travel |
|---|
| 0.0000 |
| -0.0001 |
| -0.0001 |
| -0.0001 |
| -0.0001 |
| -0.0001 |
| -0.0002 |
| -0.0002 |

**Table B.12** Table of Proximal Revolute Joint Repeatability Data

| negative travel | | same setup |
|---|---|---|
| w/6.425 moment arm | | small overtravel |
| tenth gage | | tenth gage |
| 0.0012 | | 0.0011 |
| 0.0019 | | 0.0024 |
| 0.0001 | | 0.0024 |
| 0.0017 | | 0.0024 |
| 0.0021 | | 0.0025 |
| 0.0015 | | |
| 0.0010 | | |
| 0.0006 | | |
| 0.0011 | | |

**Table B.13** Table of X-direction Robot Repeatability Data

| indicating off gripper housing | | |
|---|---|---|
| X direction | | X direction |
| | | with more cycling between tests |
| thousandth gage | | thousandth gage |
| 0.0000 | | 0.0000 |
| 0.0000 | | -0.0010 |
| 0.0000 | | -0.0010 |
| 0.0000 | | -0.0010 |
| 0.0000 | | 0.0000 |
| 0.0000 | | -0.0010 |
| 0.0010 | | 0.0000 |
| 0.0010 | | 0.0010 |
| 0.0010 | | 0.0010 |
| 0.0010 | | 0.0000 |
| 0.0010 | | 0.0000 |
| 0.0010 | | 0.0000 |
| 0.0010 | | 0.0000 |
| 0.0010 | | 0.0020 |
| 0.0010 | | 0.0000 |
| 0.0010 | | -0.0010 |
| 0.0010 | | 0.0000 |
| 0.0010 | | -0.0020 |
| 0.0010 | | 0.0020 |
| 0.0010 | | 0.0020 |

**Table B.14** Table of Y-direction Robot Repeatability Data

| Y direction |
|---|
| thousandth gage |
| 0.0000 |
| -0.0010 |
| -0.0010 |
| -0.0010 |
| -0.0010 |
| -0.0010 |
| -0.0020 |
| -0.0010 |
| -0.0020 |
| -0.0020 |
| -0.0020 |
| -0.0020 |
| -0.0020 |
| -0.0020 |
| -0.0020 |
| -0.0020 |
| -0.0020 |
| -0.0020 |
| -0.0020 |
| -0.0020 |

# Appendix C: Finite Element Analysis Results for Machine Frame

## C.1 Introduction

This appendix contains some representative plots of the finite element analysis results for the Accipiter frame and the 90 Series frame. The complete analysis is not detailed here. However, the analysis showed that the Accipiter frame is more than 50 times stiffer than the 90 Series frame.

## C.2 The 90 Series Frame

Figure C.1 shows the deformed shaped of the 90 Series frame loaded in torsion.

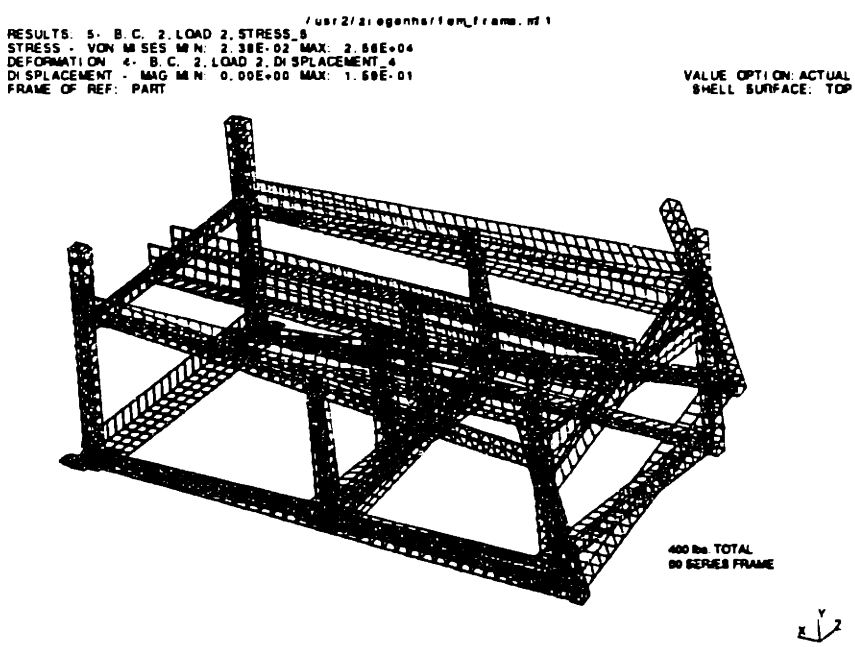


**Figure C.1** 90 Series frame loaded under torsion.[80]

[80] All finite element analysis was conducted by Scott Zeigenhagen at Silicon Valley Group using SDRC Ideas software.

## C.3 The Accipiter Frame

Figure C.2 shows the spine of the Accipiter frame loaded in torsion.

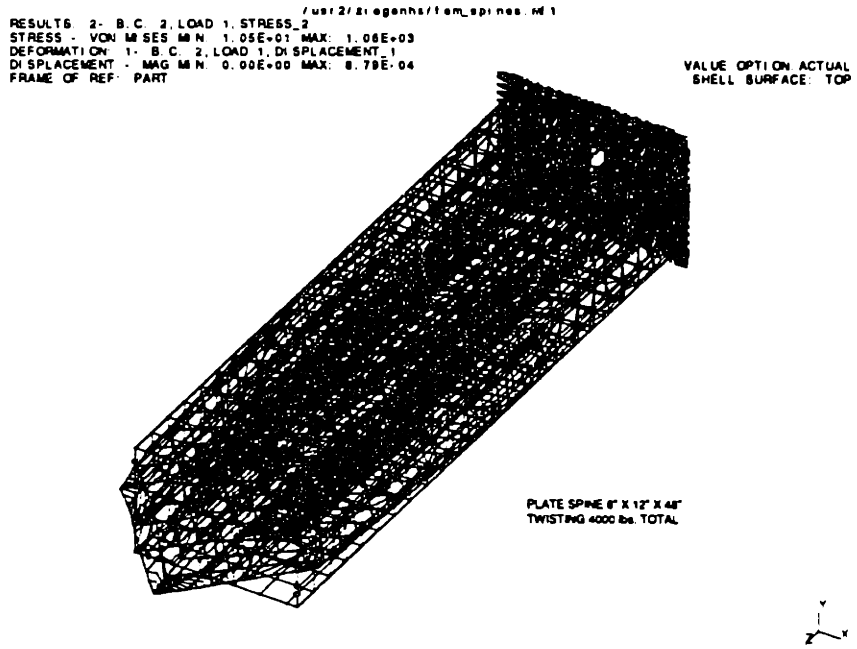


**Figure C.2** Spine of the Accipiter frame loaded under torsion.

Finally, the rear portions of the Accipiter frame are shown in Figure C.3.

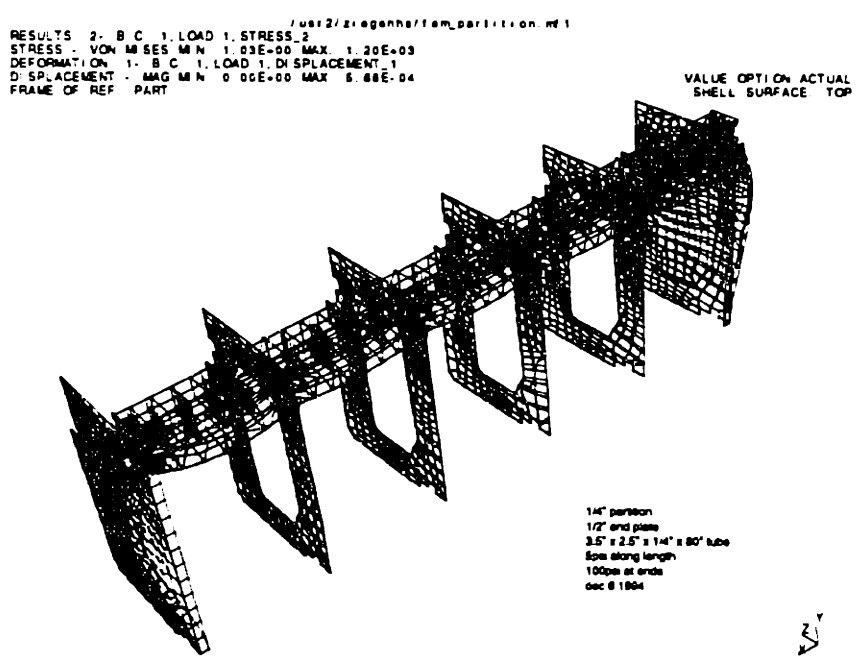


**Figure C.3** Rear portion of Accipiter frame with normal loads on top of structure.

# Appendix D: Trajectory Generation and Control System Simulation Software

## D.1 Introduction

This appendix contains the software written to generate trajectories and to simulate the control system operation for the wafer handling robot discussed in this thesis.

## D.2 Trajectory Generation Source Code

```
/*****************************************************************************
*       kin.h Matthew J. Van Doren 12/9/94
*****************************************************************************/
#define PI                      3.14159265359

#define L2                      0.2530          /* link lengths */
#define L3                      0.3921

#define LENGTH                          1000

#define SERVO                   1000            /* servo rate */

#define JT1POSLIMIT             40              /* joint limits */
#define JT1NEGLIMIT             -40
#define JT2POSLIMIT             3.054
#define JT2NEGLIMIT             -3.054
#define JT3POSLIMIT             3.054
#define JT3NEGLIMIT             -3.054


/*****************************************************************************
*               kin.c Matthew J. Van Doren 12/9/94
*               calculates trajectories for MIT/SVG handler
*****************************************************************************/
#include "kin.h"
#include <stdio.h>
#include <math.h>
#include <stdlib.h>

/* function prototypes */
void mat_mult33(double mat1[3][3],double mat2[3][3],double mat[3][3]);
void mat_mult31(double mat1[3][3],double mat2[3][1],double mat[3][1]);
```

```
void mat_mult13(double mat1[1][3],double mat2[3][3],double mat[1][3]);
void inv_pos_kin(void);
void inv_va_kin(void);
void ee_traj(double ee[],double eed[],double eedd[], double maxacc,
                double acctime, double velt, double ttime, double pstart);
void fill(int i);
void read_data(void);

/* trajectory definition stuff */
double xinit, xfinal, yinit, yfinal, theinit, thefin;
int itottime, ijerkt;
double tottime, atottimex, atottimey,atottimet,maxtime;
double jerkt, accelxt, velxt, accelyt, velyt, acceltt, veltt;
double maxxdd, maxydd, maxtdd;
double maxxd,maxyd,maxtd;
int intgain;

double J[3][3];          /* Jacobian matrix */
double invJ[3][3];                          /* inverse of the Jacobian */
double TinvJ[3][3];
double H1[3][3];          /* Hessian */
double H2[3][3];
double H3[3][3];
double ux[LENGTH],uy[LENGTH],utheta[LENGTH];        /* ee positions */
double udx[LENGTH],udy[LENGTH],udtheta[LENGTH];      /* ee velocities */
double uddx[LENGTH],uddy[LENGTH],uddtheta[LENGTH]; /* ee accelerations */
double t1[LENGTH], t2[LENGTH], t3[LENGTH];                        /* joint angles */
double te1[LENGTH],te2[LENGTH],te3[LENGTH];/* joint angles-integration*/
double te1d[LENGTH],te2d[LENGTH],te3d[LENGTH];/* joint velocities-integration*/
double t1d[LENGTH], t2d[LENGTH], t3d[LENGTH];      /* joint velocities */
double t1dd[LENGTH], t2dd[LENGTH], t3dd[LENGTH];   /* joint accelerations*/


void main() {
 FILE *eetrajx, *eetrajy, *eetrajt, *theta1, *theta2, *theta3,
  *poschck, *velchck;
 int i;
 double t;

 if((eetrajx = fopen("eetrajx.txt","w")) == NULL)
  printf("\nunable to open test data file for writing\n");
 if((eetrajy = fopen("eetrajy.txt","w")) == NULL)
  printf("\nunable to open test data file for writing\n");
 if((eetrajt = fopen("eetrajt.txt","w")) == NULL)
  printf("\nunable to open test data file for writing\n");
 if((theta1 = fopen("theta1.txt","w")) == NULL)
  printf("\nunable to open test data file for writing\n");
 if((theta2 = fopen("theta2.txt","w")) == NULL)
  printf("\nunable to open test data file for writing\n");
 if((theta3 = fopen("theta3.txt","w")) == NULL)
  printf("\nunable to open test data file for writing\n");
 if((poschck = fopen("poschck.txt","w")) == NULL)
  printf("\nunable to open test data file for writing\n");
 if((velchck = fopen("velchck.txt","w")) == NULL)
  printf("\nunable to open test data file for writing\n");
```

```
        read_data();

/* fill end effector data array */
        ee_traj(ux,udx,uddx, maxxdd, accelxt, velxt, atottimex,xinit);
        ee_traj(uy,udy,uddy, maxydd, accelyt, velyt, atottimey,yinit);
        ee_traj(utheta,udtheta,uddtheta,maxtdd,acceltt,veltt,atottimet,theinit);

  i = 0;
        for(t=0;t<=maxtime;t+=(((double) intgain))/((double) SERVO)){
         fprintf(eetrajx,"\n %lf\t%lf\t%lf",ux[i],udx[i],uddx[i]);
         i++;
        }
        i = 0;
        for(t=0;t<=maxtime;t+=(((double) intgain))/((double) SERVO)){
         fprintf(eetrajy,"\n %lf\t%lf\t%lf",uy[i],udy[i],uddy[i]);
         i++;
        }
        i = 0;
        for(t=0;t<=maxtime;t+=(((double) intgain))/((double) SERVO)){
         fprintf(eetrajt,"\n %lf\t%lf\t%lf",utheta[i],udtheta[i],uddtheta[i]);
         i++;
        }

/* calculate joint angles */
        inv_pos_kin();

/* calculate joint velocities and accelerations */
        inv_va_kin();

  i = 0;
        for(t=0;t<=maxtime;t+=(((double) intgain))/((double) SERVO)){
         fprintf(theta1,"\n %lf\t%lf\t%lf",t1[i],t1d[i],t1dd[i]);
         i++;
        }

  i = 0;
        for(t=0;t<=maxtime;t+=(((double) intgain))/((double) SERVO)){
         fprintf(theta2,"\n %lf\t%lf\t%lf",t2[i],t2d[i],t2dd[i]);
         i++;
        }

  i = 0;
        for(t=0;t<=maxtime;t+=(((double) intgain))/((double) SERVO)){
         fprintf(theta3,"\n %lf\t%lf\t%lf",t3[i],t3d[i],t3dd[i]);
         i++;
        }

        /* sanity check */
  i = 0;
        for(t=0;t<=maxtime;t+=(((double) intgain))/((double) SERVO)){
         fprintf(poschck,"\n %lf\t%lf\t%lf",te1[i],te2[i],te3[i]);
         i++;
        }
```

```
  i = 0;
        for(t=0;t<=maxtime;t+=(((double) intgain))/((double) SERVO)){
         fprintf(velchck,"\n %lf\t%lf\t%lf",te1d[i],te2d[i],te3d[i]);
         i++;
        }

}


/* creates the end effector positions, velocities, and accelerations */
/* uses trapezoidal acceleration profile */
/* used for staight lines, repeated once for each ee DOF */
void ee_traj(double ee[],double eed[],double eedd[], double maxacc,
        double acctime, double velt, double ttime, double pstart) {
        int i,ii;
        double time, sectime;
/*   printf("\n max accel %lf",maxacc); */

  i = 0;
        for( time = 0; time <= ttime; time+=(((double)intgain))/((double)SERVO)){
        /*      printf("\n time is %lf",time);*/
                if(time < jerkt) {
                        eedd[i] = (maxacc/jerkt)*time;
                        eed[i] = (maxacc/(2*jerkt))*time*time;
                        ee[i] = pstart + (maxacc/(6*jerkt))*pow(time,3);
                }
                if(time >= jerkt && time < (jerkt+acctime)) {
                        eedd[i] = (maxacc/jerkt)*(jerkt);
                        eed[i] = (maxacc/(2*jerkt))*(pow(time,2) - pow(time-jerkt,2));
                        ee[i] = pstart+(maxacc/(6*jerkt))*(pow(time,3)-pow(time-jerkt,3));
                }
                if(time >= (jerkt+acctime)&& time < (2*jerkt+acctime)) {
                        eedd[i] = (maxacc/jerkt)*(2*jerkt - time + acctime);
                        eed[i] = (maxacc/(2*jerkt))*(pow(time,2) - pow(time-jerkt,2) -
                                        pow(time-(jerkt+acctime),2));
                        ee[i] = pstart+(maxacc/(6*jerkt))*(pow(time,3)-pow(time-jerkt,3)-
                                        pow(time-(jerkt+acctime),3));
                }
                if(time >= (2*jerkt+acctime)&& time < (2*jerkt+acctime+velt)) {
                        eedd[i] = 0;
                        eed[i] = (maxacc/(2*jerkt))*(pow(time,2) - pow(time-jerkt,2) -
                                        pow(time-(jerkt+acctime),2) +
                                        pow(time - (2*jerkt+acctime),2));
                        ee[i] = pstart+(maxacc/(6*jerkt))*(pow(time,3)-pow(time-jerkt,3)-
                                        pow(time-(jerkt+acctime),3) +
                                        pow(time - (2*jerkt+acctime),3));
                }
                if(time >= (2*jerkt+acctime+velt)&& time < (3*jerkt+acctime+velt)) {
                        eedd[i] = -(maxacc/jerkt)*(time - (2*jerkt+acctime+velt));
                        eed[i] = (maxacc/(2*jerkt))*(pow(time,2) - pow(time-jerkt,2) -
                                        pow(time-(jerkt+acctime),2) +
                                        pow(time - (2*jerkt+acctime),2) -
                                        pow(time - (2*jerkt+acctime+velt),2));
                        ee[i] = pstart + (maxacc/(6*jerkt))*(pow(time,3)-pow(time-jerkt,3) -
```

```
                                        pow(time-(jerkt+acctime),3) +
                                        pow(time - (2*jerkt+acctime),3) -
                                        pow(time - (2*jerkt+acctime+velt),3));
                }
                if(time >= (3*jerkt+acctime+velt)&& time < (3*jerkt+2*acctime+velt)) {
                        eedd[i] = -(maxacc/jerkt)*(jerkt);
                        eed[i] = (maxacc/(2*jerkt))*(pow(time,2) - pow(time-jerkt,2) -
                                        pow(time-(jerkt+acctime),2) +
                                        pow(time - (2*jerkt+acctime),2) -
                                        pow(time - (2*jerkt+acctime+velt),2) +
                                        pow(time - (3*jerkt+acctime+velt),2));
                        ee[i] = pstart + (maxacc/(6*jerkt))*(pow(time,3)-pow(time-jerkt,3) -
                                        pow(time-(jerkt+acctime),3) +
                                        pow(time - (2*jerkt+acctime),3) -
                                        pow(time - (2*jerkt+acctime+velt),3) +
                                        pow(time - (3*jerkt+acctime+velt),3));
                }
                if(time >= (3*jerkt+2*acctime+velt)) {
                        eedd[i] = (maxacc/jerkt)*(-jerkt + time-(3*jerkt+2*acctime+velt));
                        eed[i] = (maxacc/(2*jerkt))*(pow(time,2) - pow(time-jerkt,2) -
                                        pow(time-(jerkt+acctime),2) +
                                        pow(time - (2*jerkt+acctime),2) -
                                        pow(time - (2*jerkt+acctime+velt),2) +
                                        pow(time - (3*jerkt+acctime+velt),2) +
                                        pow(time - (3*jerkt+2*acctime+velt),2));
                        ee[i] = pstart + (maxacc/(6*jerkt))*(pow(time,3)-pow(time-jerkt,3) -
                                        pow(time-(jerkt+acctime),3) +
                                        pow(time - (2*jerkt+acctime),3) -
                                        pow(time - (2*jerkt+acctime+velt),3) +
                                        pow(time - (3*jerkt+acctime+velt),3) +
                                        pow(time - (3*jerkt+2*acctime+velt),3));
                }
        i++;
        }

        if(maxtime > ttime) {
         ii = i;
         printf("\n mod called");
         for(sectime=ttime;sectime<=maxtime;
         sectime+=(((double)intgain))/((double)SERVO))
         {
          /*printf("\n sectime %lf maxtime %lf",sectime,maxtime);*/
          ee[ii] = ee[i-1];
          eed[ii] = 0;
          eedd[ii] = 0;
          ii++;
         }
        }

}

/* reads trajectory data file */
void read_data(void){
 char junk[80];
 FILE *datafile;
```

```
  double interm;

  if((datafile = fopen("traj.dat","r")) == NULL)
    printf("\nunable to open trajectory data file for reading\n");

  fgets(junk,80,datafile);
  fgets(junk,80,datafile);
  sscanf(junk,"%lf",&xinit);
 printf("\n initial x: %lf",xinit);

  fgets(junk,80,datafile);
  fgets(junk,80,datafile);
  sscanf(junk,"%lf",&xfinal);
 printf("\n final x: %lf",xfinal);

  fgets(junk,80,datafile);
  fgets(junk,80,datafile);
  sscanf(junk,"%lf",&yinit);
 printf("\n initial y: %lf",yinit);

  fgets(junk,80,datafile);
  fgets(junk,80,datafile);
  sscanf(junk,"%lf",&yfinal);
 printf("\n final y: %lf",yfinal);

  fgets(junk,80,datafile);
  fgets(junk,80,datafile);
  sscanf(junk,"%lf",&theinit);
 printf("\n initial theta: %lf",theinit);

  fgets(junk,80,datafile);
  fgets(junk,80,datafile);
  sscanf(junk,"%lf",&thefin);
 printf("\n final theta: %lf",thefin);

  fgets(junk,80,datafile);
  fgets(junk,80,datafile);
  sscanf(junk,"%d",&itottime);
 printf("\n total time %d",itottime);

  fgets(junk,80,datafile);
  fgets(junk,80,datafile);
  sscanf(junk,"%d",&ijerkt);
 printf("\n constant jerk time: %d",ijerkt);

  fgets(junk,80,datafile);
  fgets(junk,80,datafile);
  sscanf(junk,"%lf",&maxxd);
 printf("\n max velocity x: %lf",maxxd);

  fgets(junk,80,datafile);
  fgets(junk,80,datafile);
  sscanf(junk,"%lf",&maxyd);
 printf("\n max velocity y: %lf",maxyd);
```

```
  fgets(junk,80,datafile);
  fgets(junk,80,datafile);
  sscanf(junk,"%lf",&maxtd);
printf("\n max velocity theta: %lf",maxtd);


  fgets(junk,80,datafile);
  fgets(junk,80,datafile);
  sscanf(junk,"%lf",&maxxdd);
printf("\n maximum x acceleration: %lf",maxxdd);

  fgets(junk,80,datafile);
  fgets(junk,80,datafile);
  sscanf(junk,"%lf",&maxydd);
printf("\n maximum y acceleration: %lf",maxydd);

  fgets(junk,80,datafile);
  fgets(junk,80,datafile);
  sscanf(junk,"%lf",&maxtdd);
printf("\n maximum theta acceleration: %lf",maxtdd);

  fgets(junk,80,datafile);
  fgets(junk,80,datafile);
  sscanf(junk,"%d",&intgain);
printf("\n interpolation gain: %d",intgain);

  jerkt = ((double)ijerkt)*((double)intgain)/((double)SERVO);
  tottime =  ((double)itottime)*((double)intgain)/((double)SERVO);
  printf("\n jerk time: %lf",jerkt);
  printf("\n tottime time: %lf",tottime);

  if(xfinal-xinit<0) {
    maxxd = -maxxd;
    maxxdd = -maxxdd;
  }

  if(yfinal-yinit<0) {
    maxyd = -maxyd;
    maxydd = -maxydd;
  }

  if(thefin-theinit<0) {
    maxtd = -maxtd;
    maxtdd = -maxtdd;
  }

  if(maxxdd == 0) accelxt = 0;
  else accelxt = -jerkt + maxxd/maxxdd;
  if(maxydd == 0) accelyt = 0;
  else accelyt = -jerkt + maxyd/maxydd;
  if(maxtdd == 0) acceltt = 0;
  else acceltt = -jerkt + maxtd/maxtdd;

  interm = (maxxdd/(6*jerkt))*(pow(2*jerkt + accelxt,3) - pow(jerkt+accelxt,3)
                                - pow(jerkt,3));
```

```
 if(maxxd == 0) velxt = 0;
 else velxt = (xfinal - xinit - 2*interm)/maxxd;
 if(velxt < 0 ){
        printf("\n x constant velocity negative!");
        exit(0);
 }
 interm = (maxydd/(6*jerkt))*(pow(2*jerkt + accelyt,3) - pow(jerkt+accelyt,3)
                        - pow(jerkt,3));
 if(maxyd == 0) velyt = 0;
 else velyt = (yfinal - yinit - 2*interm)/maxyd;
 if(velyt < 0 ){
        printf("\n y constant velocity negative!");
        exit(0);
 }
 interm = (maxtdd/(6*jerkt))*(pow(2*jerkt + acceltt,3) - pow(jerkt+acceltt,3)
                        - pow(jerkt,3));
 if(maxtd == 0) veltt = 0;
 else veltt = (thefin - theinit - 2*interm)/maxtd;
 if(veltt < 0 ){
        printf("\n theta constant velocity negative!");
        exit(0);
 }


printf("\n time for constant x velocity is: %lf",velxt);
printf("\n time for constant y velocity is: %lf",velyt);
printf("\n time for constant theta velocity is: %lf",veltt);
printf("\n time for constant x acceleration is: %lf",accelxt);
printf("\n time for constant y acceleration is: %lf",accelyt);
printf("\n time for constant theta acceleration is: %lf",acceltt);

 atottimex = 4*jerkt + 2*accelxt + velxt;
printf("\n actual move time for x is: %lf",atottimex);
 if(atottimex>tottime) {
  printf("\n Actual x move time too large!");
  exit(0);
 }
 atottimey = 4*jerkt + 2*accelyt + velyt;
printf("\n actual move time for y is: %lf",atottimey);
 if(atottimey>tottime) {
  printf("\n Actual y move time too large!");
  exit(0);
 }
 atottimet = 4*jerkt + 2*acceltt + veltt;
printf("\n actual move time for theta is: %lf",atottimet);
 if(atottimet>tottime) {
  printf("\n Actual theta move time too large!");
  exit(0);
 }

 maxtime = atottimex;
 if(atottimey > maxtime) maxtime = atottimey;
 if(atottimet > maxtime) maxtime = atottimet;
 if(maxtime > tottime){
  printf("\n max time exceeds array length!");
```

```
  exit(0);
 }
}

/* calculates the joint angles from the ee positions (these could be found by
integrating the joint velocities */
void inv_pos_kin(void) {
        int i;
        double t;

  i =0;
        for(t = 0; t<=maxtime;t+=(((double) intgain))/((double) SERVO)) {
                t2[i] = asin((ux[i]+L3*sin(utheta[i]))/L2);
                t3[i] = utheta[i] - t2[i];
                t1[i] = uy[i] + L2*cos(t2[i]) - L3*cos(t2[i]+t3[i]);

                if(t1[i] < JT1NEGLIMIT || t1[i] > JT1POSLIMIT)
                        printf("\n joint 1 limit violation");
                if(t2[i] < JT2NEGLIMIT || t2[i] > JT2POSLIMIT)
                        printf("\n joint 2 limit violation");
                if(t3[i] < JT3NEGLIMIT || t3[i] > JT3POSLIMIT)
                        printf("\n joint 3 limit violation");
                i++;

        }

}


/* calculates the joint velocities and accelerations from the joint angles
end effector velocities and accelerations */
void inv_va_kin(void) {
        double vel[3][1],tvel[1][3], accel[3][1], jvel[3][1], jaccel[3][1];
        double temp1[3][3],temp2[3][3],temp3[3][3];
        double ttemp1[3][3],ttemp2[3][3],ttemp3[3][3];
        double tmp1[1][3],tmp2[1][3],tmp3[1][3];
        double ttmp[3][1];
        double t;
        int i,j;

  i = 0;
  te1[0] = t1[0];
  te2[0] = t2[0];
  te3[0] = t3[0];
  te1d[0] = 0;
  te2d[0] = 0;
  te3d[0] = 0;
        for(t = 0; t<=maxtime;t+=((double) intgain)/((double) SERVO)) {
                fill(i);

        /* compute the joint velocities */
                vel[0][0] = udx[i];
                vel[1][0] = udy[i];
                vel[2][0] = udtheta[i];
                mat_mult31(invJ,vel,jvel);
```

```
                t1d[i] = jvel[0][0];
                t2d[i] = jvel[1][0];
                t3d[i] = jvel[2][0];
                te1[i+1] = te1[i] + (((double) intgain)/((double) SERVO))*t1d[i];
                te2[i+1] = te2[i] + (((double) intgain)/((double) SERVO))*t2d[i];
                te3[i+1] = te3[i] + (((double) intgain)/((double) SERVO))*t3d[i];

        /* compute the joint accelerations */
                accel[0][0] = uddx[i];
                accel[1][0] = uddy[i];
                accel[2][0] = uddtheta[i];
                mat_mult31(invJ,accel,jaccel);
                t1dd[i] = jaccel[0][0];
                t2dd[i] = jaccel[1][0];
                t3dd[i] = jaccel[2][0];
                mat_mult33(H1,invJ,temp1);
                mat_mult33(H2,invJ,temp2);
                mat_mult33(H3,invJ,temp3);
                mat_mult33(TinvJ,temp1,ttemp1);
                mat_mult33(TinvJ,temp2,ttemp2);
                mat_mult33(TinvJ,temp3,ttemp3);
                tvel[0][0] = udx[i];
                tvel[0][1] = udy[i];
                tvel[0][2] = udtheta[i];
                mat_mult13(tvel,ttemp1,tmp1);
                mat_mult13(tvel,ttemp2,tmp2);
                mat_mult13(tvel,ttemp3,tmp3);
                ttmp[0][0] = tmp1[0][0]*vel[0][0] + tmp1[0][1]*vel[1][0] +
                                tmp1[2][0]*vel[0][2];
                ttmp[1][0] = tmp2[0][0]*vel[0][0] + tmp2[0][1]*vel[1][0] +
                                tmp2[2][0]*vel[0][2];
                ttmp[2][0] = tmp3[0][0]*vel[0][0] + tmp3[0][1]*vel[1][0] +
                                tmp3[2][0]*vel[0][2];
                mat_mult31(invJ,ttmp,jaccel);
                t1dd[i] -= jaccel[0][0];
                t2dd[i] -= jaccel[1][0];
                t3dd[i] -= jaccel[2][0];
                te1d[i+1] = te1d[i] + (((double) intgain)/((double) SERVO))*t1dd[i];
                te2d[i+1] = te2d[i] + (((double) intgain)/((double) SERVO))*t2dd[i];
                te3d[i+1] = te3d[i] + (((double) intgain)/((double) SERVO))*t3dd[i];
                i++;

        }
}

/* 3x3 3x3 matrix multiply */
void mat_mult33(double mat1[3][3],double mat2[3][3],double mat[3][3]) {
        int i,j,k;
        double store;

        for(i = 0;i<3;i++) {
                for(j = 0;j<3;j++) {
                        store = 0;
                        for(k = 0;k<3;k++) {
                                store += mat1[i][k]*mat2[k][j];
```

```
                        }
                        mat[i][j] = store;
                }
        }
}

/* 3x3 3x1 matrix multiply */
void mat_mult31(double mat1[3][3],double mat2[3][1],double mat[3][1]) {
        int i,j,k;
        double store;

        for(i = 0;i<3;i++) {
                        store = 0;
                        for(k = 0;k<3;k++) {
                                store += mat1[i][k]*mat2[k][0];
                        }
                        mat[i][0] = store;
        }
}
/* 1x3 3x3 matrix multiply */
void mat_mult13(double mat1[1][3],double mat2[3][3],double mat[1][3]) {
        int i,j,k;
        double store;

                for(j = 0;j<3;j++) {
                        store = 0;
                        for(k = 0;k<3;k++) {
                                store += mat1[0][k]*mat2[k][j];
                        }
                        mat[0][j] = store;
                }
}


/* creates Jacobian and Hessian matrices for each iteration */
void fill(int i) {


        invJ[0][0] = -tan(t2[i]);
        invJ[0][1] = 1;
        invJ[0][2]              =               -((1.0/cos(t2[i]))*(L2*L3*cos(t2[i]+t3[i])*sin(t2[i])-
L2*L3*cos(t2[i])*sin(t2[i]+t3[i]))/L2);
        invJ[1][0] = (1.0/cos(t2[i]))/L2;
        invJ[1][1] = 0;
        invJ[1][2] = (L3*cos(t2[i] + t3[i])*(1.0/cos(t2[i]))/L2);
        invJ[2][0] = -(1.0/cos(t2[i]))/L2;
        invJ[2][1] = 0;
        invJ[2][2] = -((-(L2*cos(t2[i])) + L3*cos(t2[i] + t3[i]))*(1.0/cos(t2[i]))/L2);
        TinvJ[0][0] = invJ[0][0];
        TinvJ[1][0] = invJ[0][1];
        TinvJ[2][0] = invJ[0][2];
        TinvJ[0][1] = invJ[1][0];
        TinvJ[1][1] = invJ[1][1];
        TinvJ[2][1] = invJ[1][2];
        TinvJ[0][2] = invJ[2][0];
```

```
        TinvJ[1][2] = invJ[2][1];
        TinvJ[2][2] = invJ[2][2];


/*      J[0][0] = 0;
        J[0][1] = L2*cos(t2[i]) - L3*cos(t2[i] + t3[i]);
        J[0][2] = -(L3*cos(t2[i] + t3[i]));
        J[1][0] = 1;
        J[1][1] = L2*sin(t2[i]) - L3*sin(t2[i] + t3[i]);
        J[1][2] = -(L3*sin(t2[i] + t3[i]));
        J[2][0] = 0;
        J[2][1] = 1;
        J[2][2] = 1;*/
        H1[0][0] = 0;
        H1[0][1] = 0;
        H1[0][2] = 0;
        H1[1][0] = 0;
        H1[1][1] = -(L2*sin(t2[i])) + L3*sin(t2[i] + t3[i]);
        H1[1][2] = L3*sin(t2[i] + t3[i]);
        H1[2][0] = 0;
        H1[2][1] = L3*sin(t2[i] + t3[i]);
        H1[2][2] = L3*sin(t2[i] + t3[i]);
        H2[0][0] = 0;
        H2[0][1] = 0;
        H2[0][2] = 0;
        H2[1][0] = 0;
        H2[1][1] = L2*cos(t2[i]) - L3*cos(t2[i] + t3[i]);
        H2[1][2] = -(L3*cos(t2[i] + t3[i]));
        H2[2][0] = 0;
        H2[2][1] = -(L3*cos(t2[i] + t3[i]));
        H2[2][2] = -(L3*cos(t2[i] + t3[i]));
        H3[0][0] = 0;
        H3[0][1] = 0;
        H3[0][2] = 0;
        H3[1][0] = 0;
        H3[1][1] = 0;
        H3[1][2] = 0;
        H3[2][0] = 0;
        H3[2][1] = 0;
        H3[2][2] = 0;

}
```

## D.3 Dynamic Simulation Source Code

```
/* Matthew J. Van Doren 12/1/94 */
/* 4th order runge kutta for 6 first order equations
with PD control law implementation */
/* tracks trajectories generated by kin.c */
#include <stdio.h>
#include <math.h>
#define INTERP 40               /* number of interpolations per data point */
#define N              6                /* number of states */
```

```
#define DT              .0001   /* time increment */
#define DATA    40              /* save data at these increments */
#define PI              3.141592654
#define KP1             25000   /* proportional gain for joint 1 */
#define KP2             600             /* proportional gain for joint 2 */
#define KP3             200             /* proportional gain for joint 3 */
#define KD1             1871    /* derivative gain for joint 1 */
#define KD2             25.5    /* derivative gain for joint 2 */
#define KD3             7               /* derivative gain for joint 3 */
#define KACC1   35.2    /* acceleration feedforward gain */
#define KACC2   0.30
#define KACC3   0.0583
#define KVEL1   0       /* velocity feedforward gain */
#define KVEL2   0
#define KVEL3   0
/* SYSTEM CONSTANTS in SI units */
#define M1              11.8    /* carriage mass */
#define M2              22.5    /* column and arm mass */
#define M3              0.7             /* gripper mass */
#define I2              0.21    /* column moment of inertia */
#define I3              0.044   /* gripper moment of inertia */
#define G2              0.0254  /* distance to column center of mass */
#define L2              0.163   /* length of arm */
#define G3              0.04    /* distance to gripper center of mass */
#define N1              1.0             /* joint 1 reduction ratio */
#define N2              1.0             /*144.19*/        /* joint 2 reduction ratio */
#define N3              1.0             /*76.47*/         /* joint 3 reduction ratio */

/* function prototypes */
void kcalc(double k[][N],double (*func) (double s[]),double s[],int j,int i);
void read_data(void);
double ddt1dt(double s[]);
double ddt2dt(double s[]);
double ddt3dt(double s[]);
double dt1dt(double s[]);
double dt2dt(double s[]);
double dt3dt(double s[]);

/* global variables */
double torque[3];                               /* vector of joint torques */
double inttorq[3];                              /* vector of interactive joint torques */
double cs1, cs2, ss1, ss2, cs12, ss12;          /* repeated trig functions */
double accel[3];                                /* vector of estimated joint accelerations */
int pts;                                                        /* number of trajectory data points */
/* trajectory data from kin.c */
double traj1[3][1005], traj2[3][1005],traj3[3][1005];


void main()
{
        int i, j, l, m, n;
        double k[4][N], t;
        double s[N], sold[N];                                   /* states */
        double psetpoint[3], vsetpoint[3];              /* control law setpoints */
        double gain[N];                                                 /* vector of gains */
```

```
        double again[3],vgain[3];
        double tmax;                                        /* total time for simulation
*/
        double ffaccel[3];                                  /* vector of commanded torques */
        FILE *fileptr, *torqptr, *errptr;
        char filename[] = "Data.txt";
        char torqfile[] = "torque.txt";
        char errfile[] = "error.txt";
        char mode[] = "w+";

        fileptr = fopen( filename, mode);
        torqptr = fopen( torqfile, mode);
        errptr = fopen( errfile, mode);


        /* zero all I. C.'s */
        for ( i = 0; i<N; i++)
        {
                s[i] = 0.0;
        }

        gain[0] = KP1;
        gain[1] = KP2;
        gain[2] = KP3;
        gain[3] = KD1;
        gain[4] = KD2;
        gain[5] = KD3;
        again[0] = KACC1;
        again[1] = KACC2;
        again[2] = KACC3;
        vgain[0] = KVEL1;
        vgain[1] = KVEL2;
        vgain[2] = KVEL3;

        read_data();

        tmax = (double) (pts*INTERP*DT);

        s[0] = traj1[0][0];
        s[3] = traj1[1][0];
        s[1] = traj2[0][0];
        s[4] = traj2[1][0];
        s[2] = traj3[0][0];
        s[5] = traj3[1][0];
        psetpoint[0] = traj1[0][0];
        psetpoint[1] = traj2[0][0];
        psetpoint[2] = traj3[0][0];
        vsetpoint[0] = traj1[1][0];
        vsetpoint[1] = traj2[1][0];
        vsetpoint[2] = traj3[1][0];
        ffaccel[0] = traj1[2][0];
        ffaccel[1] = traj2[2][0];
        ffaccel[2] = traj3[2][0];

        /* main loop */
```

```
l = 0;
m = 0;
n = 1;
/* add on an extra 0.25 second to watch system settle */
for ( t = 0; t<(tmax+0.25); t = t + DT)
{
        m++;

        /* repeated trig functions */
        cs1 = cos(s[1]);
        cs2 = cos(s[2]);
        ss1 = sin(s[1]);
        ss2 = sin(s[2]);
        cs12 = cos(s[1]+s[2]);
        ss12 = sin(s[1]+s[2]);

        /* control law implementation */
        for ( i = 0; i<3; i++)
        {
                torque[i] =  gain[i]*(psetpoint[i] - s[i]) +
                gain[i+3]*(vsetpoint[i] - s[i+3]) +
                again[i]*ffaccel[i] + vgain[i]*vsetpoint[i];
        }

        l++;
        /*calculate k's*/
        for ( j = 0; j<4; j++)
        {
                kcalc (k, dt1dt, s, j, 0);
                kcalc (k, dt2dt, s, j, 1);
                kcalc (k, dt3dt, s, j, 2);
                kcalc (k, ddt1dt, s, j, 3);
                kcalc (k, ddt2dt, s, j, 4);
                kcalc (k, ddt3dt, s, j, 5);
        }

        for ( i = 0; i<N; i++)
        {
                sold[i] = s[i];
                s[i] = sold[i] + ((k[0][i] + 2.0*k[1][i] +
                2.0*k[2][i] + k[3][i])/6.0)*DT;

                /*print data*/
                if ( l == DATA )
                        fprintf( fileptr, "%e, ",s[i]);
        }

        for ( i = 3; i<6; i++)
        {
                accel[i] = (s[i] - sold[i])/DT;
        }

        if ( t < tmax) {
                psetpoint[0] += (traj1[0][n]-traj1[0][n-1])/INTERP;
                psetpoint[1] += (traj2[0][n]-traj2[0][n-1])/INTERP;
```

```
                        psetpoint[2] += (traj3[0][n]-traj3[0][n-1])/INTERP;
                        vsetpoint[0] += (traj1[1][n]-traj1[1][n-1])/INTERP;
                        vsetpoint[1] += (traj2[1][n]-traj2[1][n-1])/INTERP;
                        vsetpoint[2] += (traj3[1][n]-traj3[1][n-1])/INTERP;
                        ffaccel[0] += (traj1[2][n]-traj1[2][n-1])/INTERP;
                        ffaccel[1] += (traj2[2][n]-traj2[2][n-1])/INTERP;
                        ffaccel[2] += (traj3[2][n]-traj3[2][n-1])/INTERP;

                        if ( m == INTERP)
                        {
                                psetpoint[0] = traj1[0][n];
                                psetpoint[1] = traj2[0][n];
                                psetpoint[2] = traj3[0][n];
                                vsetpoint[0] = traj1[1][n];
                                vsetpoint[1] = traj2[1][n];
                                vsetpoint[2] = traj3[1][n];
                                ffaccel[0] = traj1[2][n];
                                ffaccel[1] = traj2[2][n];
                                ffaccel[2] = traj3[2][n];
                                n++;
                                m = 0;
                        }
                }
                else
                {
                        vsetpoint[0] = 0;
                        vsetpoint[1] = 0;
                        vsetpoint[2] = 0;
                        ffaccel[0] = 0;
                        ffaccel[1] = 0;
                        ffaccel[2] = 0;
                }


                /* print carriage return/line feed*/
                if ( l == DATA )
                {
                        fprintf( fileptr, "%e", t);
                        fprintf( fileptr, "\n");
                        fprintf(torqptr, "%e, %e, %e, %e, %e, %e \n",
                        torque[0],torque[1],torque[2],inttorq[0],inttorq[1],inttorq[2]);
/*                      fprintf(torqptr, "%e, %e, %e, %e, %e, %e \n",
                        psetpoint[0],psetpoint[1],psetpoint[2],vsetpoint[0],vsetpoint[1],vsetpoint[2]);*/
                        fprintf(errptr,"%e, %e, %e \n",psetpoint[0] - s[0],psetpoint[1] - s[1],
                        psetpoint[2] - s[2]);
                        l = 0;
                }

        }
        fclose (fileptr);
}


/* state equations */
```

```
double ddt1dt(double s[])
{
double temp;

        inttorq[0] = (1/N1)*M2*G2*ss1*accel[1] +
        (1/N1)*M3*L2*ss1*accel[1] + (1/N1)*M3*G3*ss12*accel[2] +
        (1/N1)*M2*G2*cs1*s[4]*s[4] + (1/N1)*M3*L2*cs1*s[4]*s[4] +
        (1/N1)*M3*G3*cs12*(s[5]*s[5] + s[4]*s[5]);
        temp = ((N1*N1)/(M1+M2+M3))*(torque[0] + inttorq[0]);
/*      temp = torque[0]/35.;   */
        return(temp/N1);
}

double ddt2dt(double s[])
{
double temp;

        inttorq[1] = -(1/N2)*I3*accel[2]-M3*G3*G3*accel[2]-
        (1/N2)*M3*L2*G3*cs2*accel[2]+(1/N2)*M2*G2*ss1*accel[0]+
  (1/N2)*M3*L2*ss1*accel[0] + (1/N2)*M3*L2*G3*ss2*s[5]*s[5] +
  (1/N2)*M3*G3*cs12*s[3]*s[5] +(1/N2)*2*M3*L2*G3*ss2*s[4]*s[5];
  temp = ((N2*N2)/(I2+I3+M2*G2*G2+M3*L2*L2+M3*G3*G3+
  2*M3*L2*G3*cs2))*(torque[1] + inttorq[1]);
/*  temp =  torque[1]/.21;  */
        return(temp/N2);
}

double ddt3dt(double s[])
{
double temp;

        inttorq[2] = - (1/N3)*I3*accel[2] - M3*G3*G3*accel[2] -
        (1/N3)*M3*L2*G3*cs2*accel[2] - (1/N3)*M3*L2*G3*ss2*s[4]*s[4] +
        (1/N3)*M3*G3*ss12*accel[0] - (1/N3)*M3*G3*cs12*s[3]*s[5] -
        (1/N3)*M3*L2*G3*ss2*s[4]*s[5];
        temp = ((N3*N3)/(I3+M2*G3*G3))*(torque[2] + inttorq[2]);
/*      temp = torque[2]/.044;  */
        return(temp/N3);
}

double dt1dt(double s[])
{
        return(s[3]);
}

double dt2dt(double s[])
{
        return(s[4]);
}

double dt3dt(double s[])
{
        return(s[5]);
}
```

```
/* calculation of k's */

void kcalc(double k[][N],double (*func) (double s[]),double s[],int j,int i)
{
        int l;
        double ss[N];


        /* which set of k's */

        switch (j)
        {
                case 0:
                        k[j][i] = (*func) (s);
                        break;

                case 1:
                case 2:
                        for ( l = 0; l<N; l++)
                                ss[l] = s[l] + (DT*k[j-1][l])/2;
                        k[j][i] = (*func) (ss);
                        break;

                case 3:
                        for ( l = 0; l<N; l++)
                                ss[l] = s[l] + DT*k[j-1][l];
                        k[j][i] = (*func) (ss);
                        break;
        }
}

/* reads trajectory data files */
void read_data(void){
 char junk[80];
 FILE *theta1, *theta2, *theta3, *points;
 int k;

 if((points = fopen("points.txt","r")) == NULL)
  printf("\nunable to open trajectory data file points for reading\n");
 if((theta1 = fopen("theta1.txt","r")) == NULL)
  printf("\nunable to open trajectory data file theta1 for reading\n");
 if((theta2 = fopen("theta2.txt","r")) == NULL)
  printf("\nunable to open trajectory data file theta2 for reading\n");
 if((theta3 = fopen("theta3.txt","r")) == NULL)
  printf("\nunable to open trajectory data file theta3 for reading\n");

 fgets(junk,80,points);
 sscanf(junk,"%d",&pts);
 printf("\n number of data points: %d",pts);

 fgets(junk,80,theta1);
 for ( k = 0; k<pts; k++)
 {
        fgets(junk,80,theta1);
```

```
        sscanf(junk,"%lf %lf %lf",&traj1[0][k], &traj1[1][k], &traj1[2][k]);
/*printf("\n theta1 data: %lf %lf %lf",traj1[0][k],traj1[1][k],traj1[2][k]);*/
  }

  fgets(junk,80,theta2);
  for ( k = 0; k<pts; k++)
  {
        fgets(junk,80,theta2);
        sscanf(junk,"%lf %lf %lf",&traj2[0][k], &traj2[1][k], &traj2[2][k]);
        traj2[0][k] += PI; /* make theta2 match dynamic model definition */
/*printf("\n theta2 data: %lf %lf %lf",traj2[0][k],traj2[1][k],traj2[2][k]);*/
  }

  fgets(junk,80,theta3);
  for ( k = 0; k<pts; k++)
  {
        fgets(junk,80,theta3);
        sscanf(junk,"%lf %lf %lf",&traj3[0][k], &traj3[1][k], &traj3[2][k]);
        traj3[0][k] += PI; /* make theta3 match dynamic model definition */
/*printf("\n theta3 data: %lf %lf %lf",traj3[0][k],traj3[1][k],traj3[2][k]);*/
  }

  /* duplicate last five set points */
  for ( k = 0; k<5; k++)
  {
   traj1[0][pts+k] = traj1[0][pts-1];
   traj1[1][pts+k] = traj1[1][pts-1];
   traj1[2][pts+k] = traj1[2][pts-1];
   traj2[0][pts+k] = traj2[0][pts-1];
   traj2[1][pts+k] = traj2[1][pts-1];
   traj2[2][pts+k] = traj2[2][pts-1];
   traj3[0][pts+k] = traj3[0][pts-1];
   traj3[1][pts+k] = traj3[1][pts-1];
   traj3[2][pts+k] = traj3[2][pts-1];
   }

}
```

# Appendix E: AHP Selection Matrices

## E.1 Introduction

This appendix contains the analytical hierarchy procedure selection matrices used by the author in the Accipiter design project.

## E.2 Selection Matrices

The AHP was used in four broad areas in the design project. These were:

1. The machine layout concept stage
2. The machine structure concept stage
3. The wafer handling robot concept stage
4. The wafer gripper concept stage.

Each of the selection matrices for the four stages are contained in the following subsections.

### E.2.1 Machine Layout

Table E.1 shows the AHP selection matrix for the machine layout.

**Table E.1** Machine Layout Selection Matrix

| | |
|---|---|
| 1: both criteria of equal importance | 0: no criteria for this position |
| 3: left weakly more important than top | 1/3: top weakly more important than left |
| 5: left moderately more important than top | 1/5: top moderately more important than left |
| 7: left strongly more important than top | 1/7: top strongly more important than left |
| 9: left absolutely more important than top | 1/9: top absolutely more important than left |

**Analytical Hierarchy Selection Spreadsheet for Machine Layout**

| Final Results: | | | | | | |
|---|---|---|---|---|---|---|
| Silo | Wall | SemiC | Box | ModSilo | Rect | |
| **17.8%** | **15.3%** | **15.2%** | **13.4%** | **18.0%** | **20.4%** | 100.0% |

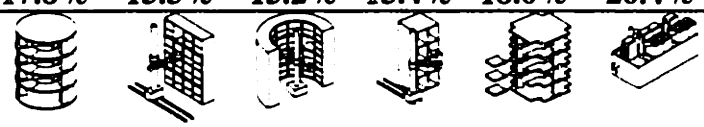

| **Level Two** | Cleanr. | Manufa. | Mainte. | Accur. | Cost | Modula. | |
|---|---|---|---|---|---|---|---|
| Cleanroom | **1.00** | **3.00** | **1.00** | **0.78** | **0.78** | **3.50** | **19.3%** |
| Manufacture | 0.33 | 1.00 | 0.33 | 0.26 | 0.26 | 1.17 | **6.4%** |
| Maintenenc e | 1.00 | 3.00 | 1.00 | 0.78 | 0.78 | 3.50 | **19.3%** |
| Accur/Stabil | 1.29 | 3.86 | 1.29 | 1.00 | 1.00 | 4.50 | **24.8%** |
| Cost | 1.29 | 3.86 | 1.29 | 1.00 | 1.00 | 4.50 | **24.8%** |
| Modularity | 0.29 | 0.86 | 0.29 | 0.22 | 0.22 | 1.00 | **5.5%** |
| | | | | | | | 100.0% |

**Cleanroom Matrix**

| | footpr. | partic. | part. . | robot | |
|---|---|---|---|---|---|
| footprint | **1.00** | **0.44** | **0.33** | **0.56** | **2.4%** |
| particle gen. | 2.25 | 1.00 | 0.75 | 1.25 | **5.4%** |
| part. gen con. | 3.00 | 1.33 | 1.00 | 1.67 | **7.2%** |
| robot | 1.80 | 0.80 | 0.60 | 1.00 | **4.3%** |

**Manufacture Matrix**

| | Compon | Ease | assemb | robot | |
|---|---|---|---|---|---|
| Components | **1.00** | **3.00** | **1.00** | **2.00** | **2.3%** |
| Ease | 0.33 | 1.00 | 0.33 | 0.67 | **0.8%** |
| assembly | 1.00 | 3.00 | 1.00 | 2.00 | **2.3%** |
| robot | 0.50 | 1.50 | 0.50 | 1.00 | **1.1%** |

**Maintenence Matrix**

| | modules | robot | ancill. | |
|---|---|---|---|---|
| modules | **1.00** | **1.50** | **5.00** | **10.3%** |
| robot | 0.67 | 1.00 | 3.33 | **6.9%** |
| ancillary | 0.20 | 0.30 | 1.00 | **2.1%** |

**Accur/Stabil Matrix**

| | module. | layer . | materi. | struc.. | robot | |
|---|---|---|---|---|---|---|
| module pos. | **1.00** | **1.00** | **4.00** | **4.00** | **0.78** | **6.5%** |
| layer | 1.00 | 1.00 | 4.00 | 4.00 | 0.78 | **6.5%** |

| | | | | | | |
|---|---|---|---|---|---|---|
| position material | 0.25 | 0.25 | 1.00 | 1.00 | 0.19 | 1.6% |
| stab. struc. stab. | 0.25 | 0.25 | 1.00 | 1.00 | 0.19 | 1.6% |
| robot | 1.29 | 1.29 | 5.15 | 5.15 | 1.00 | 8.4% |

**Cost Matrix**

| | manufa. | assemb. | mainte. | cleanr. | robot | |
|---|---|---|---|---|---|---|
| manufacture | **1.00** | **1.00** | **0.22** | **0.22** | **0.44** | 1.9% |
| assembly | 1.00 | 1.00 | 0.22 | 0.22 | 0.44 | 1.9% |
| maintenance | 4.50 | 4.50 | 1.00 | 1.00 | 2.00 | 8.4% |
| cleanroom | 4.50 | 4.50 | 1.00 | 1.00 | 2.00 | 8.4% |
| robot | 2.25 | 2.25 | 0.50 | 0.50 | 1.00 | 4.2% |

**Modularity Matrix**

| | config. | expand | interf. | |
|---|---|---|---|---|
| configure | **1.00** | **3.00** | **1.00** | 2.4% |
| expand | 0.33 | 1.00 | 0.33 | 0.8% |
| interface | 1.00 | 3.00 | 1.00 | 2.4% |
| | | | Total | 100.0% |

**Weighting Matrices**

**Cleanroom Matrix**

| | Silo | Wall | SemiC | Box | ModSi | Rect |
|---|---|---|---|---|---|---|
| footpr. | **5** | **4** | **4** | **6** | **5** | **5** |
| partic. | **4** | **5** | **5** | **4** | **4** | **8** |
| part. . | **7** | **5** | **5** | **4** | **7** | **8** |
| robot | **5** | **7** | **6** | **7** | **5** | **7** |

**Manufacture Matrix**

| | Silo | Wall | SemiC | Box | ModSi | Rect |
|---|---|---|---|---|---|---|
| Compon. | **5** | **7** | **5** | **7** | **5** | **5** |
| Ease | **5** | **6** | **5** | **7** | **7** | **7** |
| assemb. | **7** | **6** | **5** | **6** | **7** | **8** |
| robot | **7** | **5** | **6** | **4** | **7** | **7** |

**Maintenence Matrix**

| | Silo | Wall | SemiC | Box | ModSi | Rect |
|---|---|---|---|---|---|---|
| modules | **7** | **7** | **7** | **3** | **7** | **9** |
| robot | **5** | **6** | **6** | **6** | **5** | **8** |
| ancill. | **6** | **6** | **5** | **4** | **9** | **5** |

i

**Accur/Stabil Matrix**

| | | | | | | |
|---|---|---|---|---|---|---|
| module. | 7 | 7 | 7 | 7 | 7 | 8 |
| layer . | 7 | 5 | 4 | 6 | 7 | 8 |
| materi. | 5 | 5 | 5 | 5 | 5 | 5 |
| struc.. | 7 | 6 | 6 | 6 | 7 | 8 |
| robot | 8 | 5 | 6 | 4 | 8 | 8 |
| | Silo | Wall | SemiC | Box | ModS | Rect |

i

**Cost Matrix**

| | | | | | | |
|---|---|---|---|---|---|---|
| manufa. | 5 | 6 | 5 | 7 | 4 | 6 |
| assemb. | 6 | 5 | 5 | 4 | 6 | 6 |
| mainte. | 8 | 5 | 5 | 5 | 8 | 8 |
| cleanr. | 8 | 5 | 6 | 4 | 8 | 8 |
| robot | 7 | 5 | 6 | 3 | 7 | 6 |
| | Silo | Wall | SemiC | Box | ModS | Rect |

i

**Modularity Matrix**

| | | | | | | |
|---|---|---|---|---|---|---|
| config. | 6 | 6 | 6 | 6 | 6 | 6 |
| expand | 6 | 7 | 4 | 5 | 6 | 5 |
| interf. | 5 | 4 | 4 | 4 | 5 | 5 |

## E.2.2 Machine Structure

Table E.2 shows the AHP selection matrix for the machine frame.

**Table E.2** Machine Frame Selection Matrix

**Analytical Hierarchy Selection Spreadsheet for Machine Structure**

| Final Results: | | | |
|---|---|---|---|
| Ibeam | Tube | Spine | |
| 30.9% | 33.3% | 35.8% | 100.0% |

| **Level Two** | Rigidi. | Weight | Manufa. | Modula. | Cost | Assemb. | Access. | |
|---|---|---|---|---|---|---|---|---|
| Rigidity | 1.00 | 5.00 | 3.00 | 3.00 | 1.00 | 3.00 | 1.00 | 23.8% |
| Weight | 0.20 | 1.00 | 0.60 | 0.60 | 0.20 | 0.60 | 0.20 | 4.8% |

| | | | | | | | | |
|---|---|---|---|---|---|---|---|---|
| Manufact | 0.33 | 1.67 | 1.00 | 1.00 | 0.33 | 1.00 | 0.33 | **7.9%** |
| Modular | 0.33 | 1.67 | 1.00 | 1.00 | 0.33 | 1.00 | 0.33 | **7.9%** |
| Cost | 1.00 | 5.00 | 3.00 | 3.00 | 1.00 | 3.00 | 1.00 | **23.8%** |
| Assembly | 0.33 | 1.67 | 1.00 | 1.00 | 0.33 | 1.00 | 0.33 | **7.9%** |
| Access | 1.00 | 5.00 | 3.00 | 3.00 | 1.00 | 3.00 | 1.00 | **23.8%** |
| | | | | | | | | 100.0% |

**Rigidity Matrix**

| | lat. b. | transv. | torsion | |
|---|---|---|---|---|
| lat. bending | **1.00** | **1.00** | **1.00** | **7.9%** |
| transv. bending | 1.00 | 1.00 | 1.00 | **7.9%** |
| torsion | 1.00 | 1.00 | 1.00 | **7.9%** |

**Weight Matrix**

| | System. | |
|---|---|---|
| System weight | **1.00** | **4.8%** |

**Manufacture Matrix**

| | module s | robot | ancill. | |
|---|---|---|---|---|
| modules | **1.00** | **1.50** | **5.00** | **4.3%** |
| robot | 0.67 | 1.00 | 3.33 | **2.8%** |
| ancillary | 0.20 | 0.30 | 1.00 | **0.9%** |

**Modularity Matrix**

| | Tot. A. | Subass. | |
|---|---|---|---|
| Tot. Assembly | **1.00** | **1.00** | **4.0%** |
| Subassembly | 1.00 | 1.00 | **4.0%** |

**Cost Matrix**

| | raw ma. | weld | stress. | machin. | paint | |
|---|---|---|---|---|---|---|
| raw material | **1.00** | **1.00** | **1.00** | **1.00** | **1.00** | **4.8%** |
| welding | 1.00 | 1.00 | 1.00 | 1.00 | 1.00 | **4.8%** |
| stress relief | 1.00 | 1.00 | 1.00 | 1.00 | 1.00 | **4.8%** |
| machine | 1.00 | 1.00 | 1.00 | 1.00 | 1.00 | **4.8%** |
| painting | 1.00 | 1.00 | 1.00 | 1.00 | 1.00 | **4.8%** |

**Assembly Matrix**

| | comple. | part c. | subass. |
|---|---|---|---|

| | | | | |
|---|---|---|---|---|
| complexity | **1.00** | **1.00** | **1.00** | **2.6%** |
| part count | 1.00 | 1.00 | 1.00 | **2.6%** |
| subassembly | 1.00 | 1.00 | 1.00 | **2.6%** |

**Accessability Matrix**

| | storage | plumbi. | electr. | |
|---|---|---|---|---|
| storage | **1.00** | **1.00** | **1.00** | **7.9%** |
| plumbing | 1.00 | 1.00 | 1.00 | **7.9%** |
| electrical | 1.00 | 1.00 | 1.00 | **7.9%** |
| | | | Total | **100.0%** |

**Rigidity Matrix**

| | Ibeam | Tube | Spine |
|---|---|---|---|
| lat. b. | **7** | **8** | **9** |
| transv. | **6** | **7** | **8** |
| torsion | **6** | **9** | **10** |

**Weight Matrix**

| | Ibeam | Tube | Spine |
|---|---|---|---|
| System. | **5** | **7** | **7** |

**Manufacture Matrix**

| | Ibeam | Tube | Spine |
|---|---|---|---|
| modules | **7** | **7** | **7** |
| robot | **5** | **6** | **7** |
| ancill. | **6** | **6** | **8** |

**Modularity Matrix**

| | Ibeam | Tube | Spine |
|---|---|---|---|
| Tot. A. | **7** | **7** | **7** |
| Subass. | **6** | **7** | **6** |

**Cost Matrix**

| | Ibeam | Tube | Spine |
|---|---|---|---|
| raw ma. | **7** | **7** | **7** |
| welding | **7** | **5** | **6** |
| stress. | **7** | **7** | **7** |
| machin. | **7** | **8** | **7** |
| painti. | **7** | **7** | **7** |

**Assembly Matrix**

| | Ibeam | Tube | Spine |
|---|---|---|---|

| | | | |
|---|---|---|---|
| comple. | 6 | 6 | 7 |
| part c. | 8 | 7 | 7 |
| subass. | 7 | 9 | 8 |
| | 0.3333 | 1.6667 | 1 |

**Accessability Matrix**

| | | | |
|---|---|---|---|
| storage | 9 | 7 | 9 |
| plumbi. | 6 | 7 | 8 |
| electr. | 6 | 7 | 8 |

### E.2.3 Wafer Handling Robot

Table E.3 shows the AHP selection matrix for the wafer handling robot.

**Table E.3** Wafer Handler Selection Matrix

**Analytical Hierarchy Selection Spreadsheet for Wafer Handler**

| Final Results: | | | | | | | | | |
|---|---|---|---|---|---|---|---|---|---|
| Winged | Fixed | Tele | Pris | 2 Coup | Redund | 3 Coup | Diver | Teldiver | |
| **12.0%** | **10.0%** | **10.5%** | **9.6%** | **10.0%** | **8.5%** | **8.5%** | **15.4 %** | **15.5 %** | 100.0% |

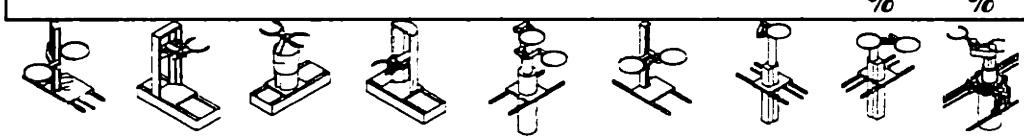

| **Level Two** | Volume | Footpr. | Reach | Comple | Reliab. | Cost | Cleanl. | |
|---|---|---|---|---|---|---|---|---|
| Volume | **1.00** | **0.20** | **1.00** | **1.00** | **0.20** | **0.20** | **0.20** | **4.3%** |
| Footprint | 5.00 | 1.00 | 5.00 | 5.00 | 1.00 | 1.00 | 1.00 | **21.7%** |
| Reach | 1.00 | 0.20 | 1.00 | 1.00 | 0.20 | 0.20 | 0.20 | **4.3%** |
| Complex | 1.00 | 0.20 | 1.00 | 1.00 | 0.20 | 0.20 | 0.20 | **4.3%** |
| Reliable | 5.00 | 1.00 | 5.00 | 5.00 | 1.00 | 1.00 | 1.00 | **21.7%** |
| Cost | 5.00 | 1.00 | 5.00 | 5.00 | 1.00 | 1.00 | 1.00 | **21.7%** |
| Clean | 5.00 | 1.00 | 5.00 | 5.00 | 1.00 | 1.00 | 1.00 | **21.7%** |
| | | | | | | | | 100.0% |

**Volume Matrix**

| | deadsp. | total . | |
|---|---|---|---|
| deadspac | **1.00** | **0.33** | **1.1%** |
| total volume | 3.00 | 1.00 | **3.3%** |

**Footprint Matrix**

alley .

| | | |
|---|---|---|
| alley width | **1.00** | **21.7%** |

**Reach Matrix**

| | reach . | |
|---|---|---|
| reach distance | **1.00** | **4.3%** |

**Complexity Matrix**

| | horiz.. | vert. . | planar. | |
|---|---|---|---|---|
| horiz. axis | **1.00** | **1.00** | **1.00** | **1.4%** |
| vert. axis | 1.00 | 1.00 | 1.00 | **1.4%** |
| planar axes | 1.00 | 1.00 | 1.00 | **1.4%** |

**Reliability Matrix**

| | bearin. | actuat. | cable . | sensor | |
|---|---|---|---|---|---|
| bearings | **1.00** | **1.00** | **0.22** | **0.22** | **2.0%** |
| actuator | 1.00 | 1.00 | 0.22 | 0.22 | **2.0%** |
| cable routing | 4.50 | 4.50 | 1.00 | 1.00 | **8.9%** |
| sensor | 4.50 | 4.50 | 1.00 | 1.00 | **8.9%** |

**Cost Matrix**

| | system. | |
|---|---|---|
| system cost | **1.00** | **21.7%** |

**Cleanliness Matrix**

| | partic. | partic. | |
|---|---|---|---|
| particle gen. | **1.00** | **0.33** | **5.4%** |
| particle cont. | 3.00 | 1.00 | **16.3%** |
| | | Total | 100.0% |

**Volume Matrix**

| | Winged | Fixed | Tele | Pris | 2 Coup | Redund | 3 Coup | Diver | Teldiver |
|---|---|---|---|---|---|---|---|---|---|
| deadsp. | **8** | **8** | **6** | **8** | **5** | **8** | **5** | **5** | **8** |
| total . | **8** | **7** | **7** | **8** | **8** | **8** | **7** | **6** | **9** |

Winged Fixed Tele Pris 2 Coup Redund 3 Coup Diver Teldiver

**Footprint Matrix**

| | Winged | Fixed | Tele | Pris | 2 Coup | Redund | 3 Coup | Diver | Teldiver |
|---|---|---|---|---|---|---|---|---|---|
| alley . | 6 | 5 | 9 | 6 | 8 | 7 | 7 | 9 | 9 |

**Reach Matrix**

| | Winged | Fixed | Tele | Pris | 2 Coup | Redund | 3 Coup | Diver | Teldiver |
|---|---|---|---|---|---|---|---|---|---|
| reach . | 7 | 6 | 8 | 7 | 6 | 8 | 9 | 9 | 9 |

**Complexity Matrix**

| | Winged | Fixed | Tele | Pris | 2 Coup | Redund | 3 Coup | Diver | Teldiver |
|---|---|---|---|---|---|---|---|---|---|
| horiz.. | 8 | 8 | 8 | 8 | 8 | 8 | 8 | 8 | 8 |
| vert. . | 7 | 6 | 5 | 6 | 6 | 6 | 6 | 6 | 5 |
| planar. | 8 | 8 | 8 | 4 | 4 | 4 | 4 | 9 | 9 |

**Reliability Matrix**

| | Winged | Fixed | Tele | Pris | 2 Coup | Redund | 3 Coup | Diver | Teldiver |
|---|---|---|---|---|---|---|---|---|---|
| bearin. | 7 | 6 | 5 | 7 | 7 | 5 | 4 | 8 | 8 |
| actuat. | 6 | 5 | 5 | 4 | 4 | 5 | 4 | 7 | 7 |
| cable . | 8 | 5 | 5 | 5 | 5 | 5 | 5 | 9 | 9 |
| sensor | 8 | 5 | 6 | 4 | 4 | 4 | 4 | 8 | 8 |

**Cost Matrix**

| | Winged | Fixed | Tele | Pris | 2 Coup | Redund | 3 Coup | Diver | Teldiver |
|---|---|---|---|---|---|---|---|---|---|
| system. | 7 | 6 | 3 | 5 | 3 | 2 | 3 | 9 | 8 |

**Cleanliness Matrix**

| | Winged | Fixed | Tele | Pris | 2 Coup | Redund | 3 Coup | Diver | Teldiver |
|---|---|---|---|---|---|---|---|---|---|
| partic. | 6 | 6 | 7 | 6 | 6 | 5 | 5 | 8 | 9 |
| partic. | 4 | 4 | 5 | 4 | 6 | 4 | 3 | 7 | 8 |

## E.2.4 Wafer Gripper

Table E.4 shows the AHP selection matrix for the wafer gripper.

**Table E.4** Wafer Gripper Selection Matrix

**Analytical Hierarchy Selection Spreadsheet for Wafer Gripper**

| Final Results: | | | | |
|---|---|---|---|---|
| Vac. ex. | Passive | Edge1S | Edge2S | |
| 17.3% | 27.6% | 24.5% | 30.6% | 100.0% |

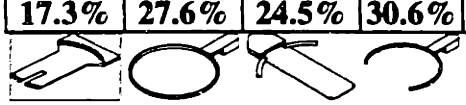

| **Level Two** | Center. | Cleanl. | Comple | Cost | Size | |
|---|---|---|---|---|---|---|
| Centering | **1.00** | **3.00** | **5.00** | **1.00** | **3.00** | **34.9%** |
| Cleanliness | 0.33 | 1.00 | 1.67 | 0.33 | 1.00 | **11.6%** |
| Complexity | 0.20 | 0.60 | 1.00 | 0.20 | 0.60 | **7.0%** |
| Cost | 1.00 | 3.00 | 5.00 | 1.00 | 3.00 | **34.9%** |
| Size | 0.33 | 1.00 | 1.67 | 0.33 | 1.00 | **11.6%** |
| | | | | | | 100.0% |

**Centering Matrix**

| | Accura. | Footpr. | Cycle . | reliab. | |
|---|---|---|---|---|---|
| Accuracy/Rep. | **1.00** | **1.00** | **1.00** | **0.50** | **7.0%** |
| Footprint | 1.00 | 1.00 | 1.00 | 0.50 | **7.0%** |
| Cycle Time | 1.00 | 1.00 | 1.00 | 0.50 | **7.0%** |
| reliability | 2.00 | 2.00 | 2.00 | 1.00 | **14.0%** |

**Cleanliness Matrix**

| | Wafer . | Mech. . | |
|---|---|---|---|
| Wafer Contact | **1.00** | **3.00** | **8.7%** |
| Mech. gen. | 0.33 | 1.00 | **2.9%** |

**Complexity Matrix**

| | mechan | contro. | sensor | |
|---|---|---|---|---|
| mechanical | **1.00** | **1.00** | **1.00** | **2.3%** |
| control sys. | 1.00 | 1.00 | 1.00 | **2.3%** |
| sensor | 1.00 | 1.00 | 1.00 | **2.3%** |

**Cost Matrix**

| | mechan | contro. | sensor | |
|---|---|---|---|---|
| mechanical | **1.00** | **0.33** | **0.33** | **5.0%** |
| control sys. | 3.00 | 1.00 | 0.99 | **14.9%** |
| sensor | 3.03 | 1.01 | 1.00 | **15.0%** |

**Size Matrix**

| | grip v. | grip h. | act. v. | act. h. | | |
|---|---|---|---|---|---|---|
| grip vert | **1.00** | **1.00** | **1.00** | **1.00** | | **2.9%** |
| grip hor | 1.00 | 1.00 | 1.00 | 1.00 | | **2.9%** |
| act. vert | 1.00 | 1.00 | 1.00 | 1.00 | | **2.9%** |
| act. hor. | 1.00 | 1.00 | 1.00 | 1.00 | | **2.9%** |
| | | | | | Total | 100.0% |

**Centering Matrix**

| | Vac. ex. | Passive | Edge1S | Edge2S |
|---|---|---|---|---|
| Accura. | 10 | 5 | 9 | 8 |
| Footpr. | 8 | 7 | 6 | 6 |
| Cycle . | 4 | 10 | 10 | 10 |
| reliab. | 5 | 3 | 6 | 7 |

**Cleanliness Matrix**

| | Vac. ex. | Passive | Edge1S | Edge2S |
|---|---|---|---|---|
| Wafer . | 5 | 6 | 9 | 9 |
| Mech. . | 5 | 6 | 6 | 7 |

**Complexity Matrix**

| | Vac. ex. | Passive | Edge1S | Edge2S |
|---|---|---|---|---|
| mechan. | 7 | 8 | 6 | 5 |
| contro. | 5 | 8 | 7 | 8 |
| sensor | 1 | 10 | 7 | 10 |

**Cost Matrix**

| | Vac. ex. | Passive | Edge1S | Edge2S |
|---|---|---|---|---|
| mechan. | 8 | 8 | 6 | 7 |
| contro. | 1 | 8 | 4 | 7 |
| sensor | 1 | 10 | 5 | 10 |

**Size Matrix**

| | Vac. ex. | Passive | Edge1S | Edge2S |
|---|---|---|---|---|
| grip v. | 6 | 6 | 8 | 8 |
| grip h. | 8 | 5 | 7 | 7 |
| act. v. | 9 | 10 | 8 | 8 |
| act. h. | 9 | 10 | 8 | 8 |

# References


[Abbe '90] Robert Abbe and David Baker, "Rotatry to Linear Motion Robot Arm," U.S. Patent No. 4,897,015, Jan. 30, 1990.

[Bausch '90] John Bausch and Kamal Youcef-Toumi, "Kinematic Methods for Automated Fixture Reconfiguration Planning," *IEEE International Conference on Robotics and Automation*, 1990, pp. 1396-1401.

[Ben '90] Jan I. Ben, "Method and Apparatus for Transporting Semiconductor Wafers," U.S. Patent No. 4,900,214, Feb. 13, 1990.

[Book '84] W. Book, "Recursive Lagrangian Dynamics of Flexible Manipulator Arms," *International Journal of Robotics Research*, Vol. 3, No. 3, 1984.

[Bryan '84] B. Bryan, "The Power of Deterministic Thinking in Machine Tool Accuracy," *First International Machine Tool Engineers Conference*, Tokyo, November 1984. (UCRL preprint 91531)

[Bryan '79] B. Bryan, "The Abbe Principle Revisited-An Updated Interpretation," *Precision Engineering: Journal of the ASPE.* Vol. 1, No. 3, 1979, pp 129-132.

[Bryan '80] B. Bryan, "The Benefits of Brute Strength," *Precision Engineering: Journal of the ASPE.* Vol. 2, No. 4, Oct. 1980, p. 173.

[Bryan '81] B. Bryan, "The Benefits of Brute Strength," *Precision Engineering: Journal of the ASPE.* Vol. 3, No. 1, Jan. 1981, p. 4-6.

[Bullis '93] Murray Bullis and William O'Mara, "Large-diameter Silicon Wafer Trends," *Solid State Technology*, April 1993, pp. 59-65.

[Busch-Vishniac '90] Ilene Busch-Vishniac, "Applications of Magnetic Levitation-Based Micro-Automation in Semiconductor Manufacturing," *IEEE Transactions on Semiconductor Manufacturing*, Vol. 3, No. 3, August 1990. pp. 109-115.

[Carnes '91] Ross Carnes, "Long Term Cost of Ownership: Beyond Purchase Price," *IEEE/SEMI International Semiconductor Manufacturing Science Symposium*, April 1991, pp. 39-43.

[Cheng '89] David Cheng and Wesley Zhang, "System and Method for Detecting the Center of an Integrated Circuit Wafer," U.S. Patent No. 4,819,167, April 4, 1989.

[Chiu '87] L. Chiu, "Control of Redundant Manipulators for Task Compatibility," *Proceedings of the IEEE International Conference on Robotics and Automation*, Rayleigh, North Carolina, March 1987.

[Craig '89] J. Craig, *Introduction to Robotics: Mechanics and Control*, Addison-Wesley Publishing Company, New York, 1989.

[Denavit '55] J. Denavit and R. S. Hartenberg, "A Kinematic Notation for Lower-Pair Mechanisms Based on Matrices," *Journal of Applied Mechanics*, 1955, pp. 215-221.

[de Nijis '88] J. F. C. de Nijis, "Modeling of a Coordinate Measuring Machine for Analysis of Its Dynamic Behavior," *Annals of the CIRP*, Vol 37, No. 1, 1988, pp. 507-510.

[de Smet '90] P. J. de Smet and E. I. Rivin, and Y. Lou, "Robot Performance as Influenced by Mechanical System," *Annals of the CIRP*, Vol. 39, No. 1, 1990, pp. 383-386.

[Dhudshia '93] Vallabh Dhudshia, "Design Practices for Higher Equipment Reliability," SEMATECH, 93041608A-GEN, Austin, TX, 1993.

[Donaldson '72] R. Donaldson, "The Deterministic Approach to Machining Accuracy," *SME Fabrication Symposium*, Golden, CO November 1972. (UCRL preprint 74243)

[Donaldson '80] R. Donaldson, "Error Budgets" in *Technology of Machine Tools*, Vol. 5, Ed. R.J. Hocken, 1980.

[Donmez '86] M. Donmez, D. Blomquist, R. Hocken, C. Liu, and M. Barash, "A General Methodology for Machine Tool Accuracy Enhancement by Error Compensation" *Precision Engineering: Journal of the ASPE*. Vol. 8, No. 4, Oct. 1986, pp. 187-196.

[Dubey '88] V. Dubey and J. Y. S. Luh, "Redundant Robot Control Using Task Based Performance Measures," *Journal of Robotic Systems*, Vol. 6, No. 5, 1988. pp. 411-432.

[Duffy '80] J. Duffy, *Analysis of Mechanisms and Robot Manipulators*, Edward Arnold Ltd., London, 1980.

[Eman '87] K. F. Eman, B. T. Wu, and M. F. DeVries, "A Generalized Geometric Error Model for Multi-Axis Machines," *Annals of the CIRP*, Vol. 36, No. 1, 1987, pp. 253-256.

[Evans '89] Chris Evans, *Precision Engineering: an Evolutionary View*, Cranfield Press, 1989.

[Freeman '88] R. Freeman and D. Tesar, "Dynamic Modeling of Serial and Parallel Mechanisms/Robotic Systems: Part I Methodology, Part II Applications," *Trends and Developments in Mechanisms, Machines, and Robotics*, Proceedings 20th Biennial ASME Mechanisms Conference, Vol. 15-3. 1988. pp 7-27.

[Genov '91A] Genco Genov and James Cameron, "Dual End Effector Robotic Arm," U.S. Patent No. 5,007,784, April 16, 1991.

[Genov '91B] Genco Genov, Lubomir Skrobak, Izya Kremerman, Grzegorz Kielczewski, "Precision Arm Mechanism," U.S. Patent No. 5,064,340, Nov. 12, 1991.

[Gere '84] James Gere and Stephen Timoshenko, *Mechanicss of Materials*, PWS Publishers, 1984.

[Hale '94] Layton Hale and Alexander Slocum, "Design of Anti-backlash Transmissions for Precision Position Control Systems," *Precision Engineering: Journal of the ASPE.* Vol. 16, No. 4, 1994, pp 244-258.

[Harper '84] James Harper and Louis Bailey, "Flexible Material Handling Automation in Wafer Fabrication," *Solid State Technology*, July 1984, pp. 89-98.

[Harper '91] James Harper, "SEMATECH White Paper on Automated Material Handling", SEMATECH, 91040507A-GEN, Austin, TX, April 11, 1991.

[Hayati '83] Samad Hayati, "Robot Arm Geometric Link Parameter Estimation," *Proceedings of the 22nd IEEE Conference on Decision and Control*, 1983, pp. 1477-1483.

[Higuchi '93] Toshiro Higuchi, "Magnetically Suspended Stepping Motors for Clean Room and Vacuum Environments," *2nd International Symposium on Magnetic Suspension Technology*, (Prel. Proceedings), Seattle, Washington, Aug. 11-13, 1993, Vol. II, pp. 11b1-5.

[Hocken '77] R. Hocken, et al. "Three Dimensional Metrology," *Annals of the CIRP*, 1977, Vol. 26, No. 2, pp. 403-408.

[Hollerbach '83] J. M. Hollerbach, "A Recursive Lagrangian Formulation of Manipulator Dynamics and a Comparative Study of Dynamics Formulation Complexity," from *Robot Motion*, M. Brady et al., ed., MIT Press, 1983.

[Iwasawa '90] Y. Iwasawa, et al., "Transporting Robot for Semiconductor Wafers," U.S. Patent No. 4,904,153, Feb. 27, 1990.

[Jacobson '89] Donald Jacobson, "Automated Material Handling in a Class 1 Cleanroom," Society of Manufacturing Engineers. Technical paper MS89-181, 1989.

[Jan '90] C. Jan, C. Chu, and C. Liu, "A Configuration Independent Approach for Modeling Three Dimensional Error Map for Machine Tools Using Hyperpatch Model and Metrology Plate" *Modeling of Machine Tools: Accuracy, Dynamics, and Control.* presented at the Winter Annual Meeting of the ASME. Nov. 25-30, 1990, pp. 75-85.

[Kane '83] T. R. Kane and D. A. Levinson, "The Use of Kane's Dynamic Equations in Robotics," *The International Journal of Robotics Research*, Vol. 2, No. 3, 1983, pp. 3-20.

[Karnopp '90] D. Karnopp, D. Margolis, and R. Rosenberg, *System Dynamics: A Unified Approach*, John Wiley, 1990.

[Klein '87] A. Klein and B. E. Blaho, "Dexterity Measures for the Design and Control of Kinematically Redundant Manipulators," *The International Journal of Robotics Research*, Vol. 6, No. 2. Summer 1987. pp. 72-83.

[Lee '88] J. M. Lee, "A Study on the Dynamic Modeling of Structures with Bolted and Bearing Joints," *Annals of the CIRP*, Vol. 37, No. 1, 1988, pp. 343-346.

[Lee '90] S. Lee, et al., "Transport Device for Wafers of Variable Diameter," U.S. Patent No. 4,971,512, Nov. 20, 1990.

[Love '73] W. J. Love and A. J. Scarr, "The Determination of the Volumetric Accuracy of Multi-Axis Machines," *Proceedings fo the 14th MTDR Conference*, 1973, pp. 307-315.

[Lovell '90] Anthony Lovell, Denise Harris, and Nicholas d'Arbeloff, "Cell Automation: Integrating Manufacturing with Robotics," *Solid State Technology*, Dec. 1990.

[Luh '85] J. Y. S. Luh, "Design of Control Systems for Industrial Robots," from *Handbook of Industrial Robotics*, Shimon Y. Nof, ed., John Wiley and Sons, 1985, pp. 169-202.

[Makino '90] H. Makino, "Clean Room Robots in Semiconductor Manufacturing," *Annals of the CIRP*, 1990, Vol 39, No. 2, pp. 595-598.

[Marsh '93] Eric Marsh, Alex Slocum, and Kevin Otto, "Hierarchical Decision Making in Machine Design," Unpublished paper. MIT, 1993.

[Marsh '94] Eric Marsh, *An Integrated Approach to Structural Damping*, Ph.D. Thesis. MIT, 1994.

[Matsumoto '90] T. Matsumoto, "Apparatus for Detecting and Centering Wafers," U.S. Patent No. 4,944,650, July 31, 1990.

[Meirovitch '67] Leonard Meirovitch, *Analytical Methods in Vibrations*, MacMillan, 1967.

[Narendra '89] K. Narendra and A. Annaswamy, *Stable Adaptive Systems*, Prentice Hall, 1989.

[Nishiyama '92] S. Nishiyama, "Semiconductor Fabricating Apparatus," U.S. Patent No. 5,171,031, Dec. 15, 1992.

[Ogata '70] Katsuhiko Ogata, *Modern Control Engineering*, Prentice-Hall, 1970.

[Ohmi '92] Tadahiro Ohmi, "Break Through for Scientific Semiconductor Manufacturing in 2001," *Break Through*, Vol. 5, No. 71, 1992.

[Pahl '88] G. Pahl and W. Beitz, *Engineering Design: A Systematic Approach*, The Design Council, 1988 (translated from German).

[Papanek '87] Tom Papanek, "Design and Test of a Robot for Class 10 Clean Rooms," *Proceedings of Robots 11/17th International Symposium on Industrial Robots*, Chicago, April 26-30, 1987, p 4-101 to 4-113.

[Paul '81] Richard Paul, *Robot Manipulators: Mathematics, Programming, and Control*, The MIT Press, 1981, pp. 197-220.

[Poduje '92] Noel Poduje and Roy Mallory, "Robot Prealigner," U.S. Patent No. 5,102,280, April 1992.

[Renaud '83] M. Renaud, "An Efficient Iterative Analytical Procedure for Obtaining a Robot Manipulator Dynamic Model," *First International Symposium of Robotics Research*, August, 1983.

[Reshetov '88] N. Reshetov and V. T. Portman, *Accuracy of Machine Tools*, ASME Press, 1988 (translated from Russian).

[Roth '93] N. Roth and B. Schneider, "Clean Room Industrial Robot for Handling and Assembly in Semiconductor Industry," *Annals of the CIRP*, Vol. 42, No. 1, 1993, pp. 21-24.

[Rubin '89] Richard Rubin, Benjamin Petrone, Richard Heim and Scott Pawenski, "Modular Processing Apparatus for Processing Semiconductor Wafers," U.S. Patent No. 4,852,516, Aug. 1, 1989.

[Salisbury '82] Kenneth Salisbury and John Craig, "Articulated Hands: Force Control and Kinematic Issues," *The International Journal of Robotics Research*, Vol. 1, No. 1, 1982, pp. 4-17.

[Schultschik '77] R. Schultschik, "The Components of the Volumetric Accuracy," *Annals of the CIRP*, 1977, Vol. 26, No. 1, pp. 223-226.

[SEMATECH '93] SEMATECH, *Automated Material-Handling Systems User-Needs Analysis and Technology Roadmap*, 93011470A-ENG, Austin, TX, Feb. 22, 1993.

[SEMATECH '92] SEMATECH, *Guidelines for Equipment Reliability*, 92031014A-GEN, Austin, TX, May 1992.

[Sherrington '93] I. Sherrington and E. H. Smith, "Design and Performance Assessment of a Kelvin Clamp for Use in Relocation Analysis of Surface Topography," *Precision Engineering: Journal of the ASPE*, April 1993, Vol. 15, No. 2, pp. 77-85.

[Shin '92] C. Shin and Y. Wei, "A Statistical Analysis of Positional Errors of a Multiaxis Machine Tool" *Precision Engineering: Journal of the ASPE.* Vol. 14, No. 3, July. 1992, pp. 139-146.

[Singer '90] N. Singer and W. Seering, "Preshaping Command Inputs to Reduce System Vibration," *Journal of Dynamic Systems, Measurement and Control*, Vol. 112, March 1990.

[Slocum '92A] A. Slocum, *Precision Machine Design*, Prentice Hall, 1992.

[Slocum '92B] A. Slocum, "Design of Three-Groove Kinematic Couplings," *Precision Engineering: Journal of the ASPE.* Jan. 1992.

[Slocum '88A] A. Slocum, "Kinematic Couplings for Precision Fixturing - Part I: Formulation of Design Parameters," *Precision Engineering: Journal of the ASPE.* Vol. 10, No. 2, April 1988, pp. 85-91.

[Slocum '88B] A. Slocum and M. Donmez, "Kinematic Couplings for Precision Fixturing - Part II: Experimental Determination of Repeatability and Stiffness," *Precision Engineering: Journal of the ASPE.* Vol. 10, No. 3, July 1988, pp. 115-122.

[Slocum '92C] A. Slocum, et al., "Design Review of ProgramMation Incorporated's Products for Automating Handling of Wafer Cassettes Between Process Tools", SEMATECH sponsored design review, Aug. 26, 1992.

[Slocum '92D] A. Slocum, M. Van Doren, and E. Marsh, "Design Review Report: Application of Principles of Precision Engineering to Silicon Valley Group's Process Equipment Designs," Sept. 29, 1992.

[Slocum '92E] A. Slocum, et al., "Design Review Report: Proconics International CMS-200 and WLS-200 Systems," SEMATECH sponsored design review, Dec. 15, 1992.

[Slocum '92F] A. Slocum, et al. "Design Review Report: Precision Robots Incorporated," SEMATECH sponsored design review, Dec. 15, 1992.

[Slocum '93A] A. Slocum, M. Van Doren, and E. Marsh, "Design Review Report: Accu-Fab Incorporated AFS 125 Track and Accubot 600," SEMATECH sponsored design review, Aug. 3, 1993.

[Slocum '93B] A. Slocum, M. Van Doren, and E. Marsh, "Design Review Report: Asyst Technologies SMIF Pod Handling Equipment," SEMATECH sponsored design review, Dec. 15, 1993.

[Slotine '91] Jean Jacques Slotine, *Applied Nonlinear Control*, Prentice Hall, 1991.

[Soons '92] J. Soons, F. Theuws, and P. Schellekens, "Modeling the Errors of Multi-axis Machines: a General Methodology" *Precision Engineering: Journal of the ASPE.* Vol. 14, No. 1, Jan. 1992, pp. 5-18.

[Spencer '89] Robert Spencer and Christopher Lada, "Method and System for Locating and Positioning Circular Workpieces," U.S. Patent No. 4,833,790, May 30, 1989.

[Stevens '87] C. L. Stevens, "The Design of a Clean Room Robot for Wafer Handling," *Proceedings of Robots 11/17th International Symposium on Industrial Robots*, Chicago, April 26-30, 1987, pp 4-59 to 4-89.

[Strang '88] G. Strang, *Linear Algebra and its Applications*, Harcourt Brace Jovanovich, 1988.

[Suh '90] Nam P. Suh, *The Principles of Design*, Oxford University Press, 1990.

[Taguchi '90] Genichi Taguchi and Don Clausing, "Robust Quality," *Harvard Business Review*, January-February, 1990. pp. 65-75.

[Teeuwsen '89] J. W. M. C. Teeuwsen, J. A. Soons, and P. H. J. Schellekens, "A General Method for Error Description of CMMs Using Polynomial Fitting Procedures," *Annals of the CIRP*, Vol. 38, No. 1, 1989, pp. 505-510.

[Thomas '85] M. Thomas and D. Tesar, "Dynamic Modeling of Serial Manipulator Arms," *Journal of Dynamic Systems, Measurements, and Control*, Vol. 107. June 1985. pp. 163-169.

[Tlusty '85] Jiri Tlusty and Elliot Stern, "Use of a Structural Model in Compensating for Robot Deflections," *Annals of the CIRP*, Vol. 34, No. 1, 1985, pp. 357-363.

[Toyama '91] S. Toyama, S. Hatae, S. Haga, "Kinematic Calibration of SCARA Robot with Condition Number and Error Map Method," *Annals of the CIRP*, Vol. 40, No. 1, 1991, pp. 9-12.

[Treib '87] T. Treib, "Error Budgeting – Applied to the Calculation and Optimization of the Volumetric Error Field of Multiaxis Systems," *Annals of the CIRP*, Vol. 36, No. 1, 1987, pp. 365-368.

[Tyra '93] Kevin Tyra, "A Survey of Wafer Transport Automation for Semiconductor Process Tools," Master of Science in the Management of Technology Thesis, Sloan School, Massachusetts Institute of Technology, May 1993.

[Tzes '93] Anthony Tzes and Stephen Yurkovich, "An Adaptive Input Shaping Control Scheme for Vibration Suppression in Slewing Flexible Structures," *IEEE Transactions on Control Systems Technology*, Vol. 1, No. 2, June 1993.

[Vaishnav '87] R. Vaishnav and E. Magrab, "A General Procedure to Evaluate Robot Positioning Errors," *The International Journal of Robotics Research*, Spring 1987, Vol. 6, No. 1, pp. 59-74.

[Van Doren '92] M. Van Doren, *Criteria Development for Redundant Manipulators to Support Decision Making Software*, Master's Thesis, The University of Texas at Austin, May 1992.

[Van Doren '94] M. Van Doren. and A. Slocum, "Design and Implementation of a Precision Material Handling Robot Control System," *International Journal of Machine Tools and Manufacture: Design, Research, and Application*, Vol. 35, No. 7, July 1995.

[Veitschegger '86] W. Veitschegger and Chi-Haur Wu, "Robot Accuracy Analysis Based on Kinematics," *IEEE Journal of Robotics and Automation*, Vol RA-2, No. 3, Sept. 1986, pp. 171-179.

[Veitschegger '88] W. Veitschegger and Chi-Haur Wu, "Robot Calibration and Compensation," *IEEE Transactions on Robotics and Automation*, Vol. 4, No. 6, December 1988, pp. 643-656.

[von Hippel '88] Eric von Hippel, *The Sources of Innovation*, Oxford University Press, 1988.

[Volovich '92] Vladimir Volovich, "Semiconductor Object Pre-aligning Method," U.S. Patent No. 5,125,791, June 30, 1992.

[Vranish '92] John Vranish, "Work Attachment Mechanism/Work Attachment Fixture," U.S. Patent No. 5,174,772, Dec. 29, 1992.

[Wang '91] I. Wang, S. Li, and I. Busch-Vishniac, "A Magnetic Levitation Transport Path," *IEEE Transactions on Semiconductor Manufacturing*, Vol. 4, No. 2, May 1991. pp. 145-154.

[Wang '93] W. Wang, M. Lamb, and I. Busch-Vishniac, "An Automated Loading and Unloading System for a Maglev Wafer and Transport Path," *IEEE Transactions on Semiconductor Manufacturing*, Vol. 6, No. 3, August 1993. pp. 276-279.

[Williams '93] M. E. Williams, D. L. Trumper, and R. Hocken, "Magnetic Bearing Stage for Photolithography," *Annals of the CIRP*, Vol. 42, No. 1, 1993, pp. 607-610.

[Weck '84] Manfred Weck, *Handbook of Machine Tools: Volume 4, Metrological Analysis and Performance Tests*, John Wiley and Sons, 1984 (translated from German).

[Weill '91] R. Weill and B. Shani, "Assessment of Accuracy of Robots in Relation with Geometrical Tolerances," *Annals of the CIRP*, Vol. 40, No. 1, 1991, pp. 395-399.

[Wu '85] Chi-Haur Wu and Chung Lee, "Estimation of the Accuracy of a Robot Manipulator," *IEEE Transactions on Automatic Control*, March, 1985, Vol. AC-30, No. 3, pp. 304-306.

[Wu '93] Hong J. Wu, "Single Semiconductor Wafer Transfer Method and Manufacturing System," U.S. Patent No. 5,256,204, Oct. 26, 1993.

[Zhang '89] G. X. Zhang, "A Study on the Abbe Principle and Abbe Error," *Annals of the CIRP*, Vol. 38, No. 1, 1989, pp. 525-528.

[Ziegert '90] John Ziegert, Daniel Olson, and Philip Datseris, "A Screw Coordinate Model of Machine Tool Errors" *Modeling of Machine Tools: Accuracy, Dynamics, and Control.* presented at the Winter Annual Meeting of the ASME. Nov. 25-30, 1990, pp. 23-31.

# Vita

Matthew J. Van Doren was born on December 11, 1967 in Des Moines, Iowa. He graduated form high school in Stillwater, Oklahoma in May of 1986. Matthew continued his education at The University of Texas at Austin, where he graduated with his Bachelor of Science in mechanical engineering in August of 1990 and his Master's of Science also in mechanical engineering in May of 1992. While studying for his Bachelor's degree, Matthew was employed with Texas Instruments in Dallas, Texas. Following completion of his Master's degree, Matthew enrolled at the Massachusetts Institute of Technology in September, 1992.

Address: 215 Pearl Street, 2nd floor
Braintree, MA 02184

This thesis was written in Microsoft Word (version 6.0a) using the Times New Roman font.